

One-Dimensional Computational Topology

Jeff Erickson

Contents

Foreward^α	1
1 Simple Polygons^β	3
1.1 Definitions	3
1.2 Proof of the Jordan Polygon Theorem	4
1.3 Point-in-Polygon Test	7
1.4 Polygons Can Be Triangulated	8
1.5 Computing a Triangulation	11
1.6 The Dehn-Schönflies Theorem	12
1.7 ... and the aptly named Sir Not Appearing in This Film	12
1.8 References	12
2 Winding Numbers^β	15
2.1 Let me not be pent up, sir; I will fast, being loose.	15
2.2 Shoelaces and Signed Areas	15
2.3 Winding numbers	19
2.4 Homotopy	21
2.5 Vertex moves	21
2.6 Polygon homotopies are sequences of vertex moves	22
2.7 Homotopy Invariant	24
2.8 ... and the Aptly Named Sir Not Appearing in This Film	25
2.9 References	25
3 Homotopy Testing^β	27
3.1 Multiple Obstacles	27
3.2 Crossing Sequences	28
3.3 Reductions	29
3.4 Variations	32
3.5 ... and the Aptly Named Sir Not Appearing in This Film	32
4 Faster Homotopy Testing^β	33
4.1 Trapezoidal decomposition	34
4.2 Vertical and horizontal ranks	35
4.3 Rectification	36
4.4 Reduction	37
4.5 Layered Range Trees	40
4.6 Final Analysis	41

4.7 ... And the Aptly Named Et Cetera Ad Nauseam	42
4.8 References	42
5 Shortest (Homotopic) Paths^β	43
5.1 Shortest Paths in Simple Polygons	43
5.2 Triangulations and Dual Graphs	44
5.3 Crossing Sequences	45
5.4 Sleeves	45
5.5 Growing Funnels	46
5.6 Polygons with Holes	48
5.7 The Universal Cover	49
5.8 Covering Spaces	50
5.9 ...and the Aptly Named Yadda Yadda	50
5.10 References	50
6 Generic Planar Curves^α	53
6.1 Technicalities	54
6.2 Image graphs	54
6.3 Gauss codes and Gauss diagrams	55
6.4 Tracing Faces	56
6.5 Homotopy moves	58
6.6 Planarity testing	60
6.7 ...and the Aptly Named Yadda Yadda	61
6.8 References	61
6.9 Possible reorganization	61
7 Unsigned Gauss codes^β	63
7.1 Winding numbers again	63
7.2 Smoothing	65
7.3 Gauss's parity condition	66
7.4 Dehn's non-crossing condition	67
7.5 Tree-onion figures	68
7.6 Bipartite interlacement	71
7.7 Recrossing	71
7.8 Algorithm summary	72
7.9 Faster! Faster!	73
7.10 ...and the Aptly Named Yadda Yadda	73
7.11 References	73
8 Curve homotopy and curve invariants^α	75
8.1 Steinitz's contraction algorithm	75
8.2 Rotation number	77
8.3 Regular homotopy	78
8.4 Strangeness	79
8.5 Defect	79
8.6 Aptly Yadda Yadda	80
9 Planar Graphs^β	81
9.1 Abstract graphs	81

9.2 Data structures	82
9.3 Topological graphs	83
9.4 Planar graphs and planar maps	84
9.5 Rotation systems	84
9.6 Formalities and Trivialities	86
9.7 Caveat Lector	87
9.8 Duality	88
9.9 Self-dual data structures	89
9.10 Endianity	89
9.11 Other derived maps	90
9.12 Aptly Yadda Yadda	92
9.13 Revision?	92
10 Tree-Cotree Decompositions^β	93
10.1 Important graph definitions (yawn)	93
10.2 Deletion and Contraction	93
10.3 Spanning trees	94
10.4 Deletion and Contraction in Planar Maps	95
10.5 Tree-Cotree Decompositions	97
10.6 Euler's Formula	98
10.7 The Combinatorial Gauss-Bonnet Theorem	99
10.8 Historical Digression	100
10.9 Aptly Named	103
11 Straight-line Planar Maps^β	105
11.1 Simple triangulations	106
11.2 Inner Induction (Hole Filling)	106
11.3 Outer Induction (Canonical Ordering)	107
11.4 Schnyder Woods	109
11.5 Grid embedding	112
11.6 References	113
11.7 Not Appearing	113
12 Tutte's Spring Embedding Theorem^β	115
12.1 Outer Face is Outer	116
12.2 Laplacian linear systems and energy minimization	117
12.3 Slicing with Lines	118
12.4 No Degenerate Vertex Neighborhoods	118
12.5 No Degenerate Faces	120
12.6 Whitney's Uniqueness Theorem	121
12.7 Not Appearing	124
13 Maxwell–Cremona Correspondence^β	125
13.1 Dramatis Personae	126
13.2 Reciprocal diagrams	128
13.3 Polyhedral lifts	129
13.4 A Non-Obvious Example: The “Anticube”	130
13.5 Steinitz's Theorem	131

13.6 Non-3-connected Frameworks	131
13.7 Non-Planar Frameworks	132
13.8 References	134
13.9 Aptly Named	135
14 Circle Packing\oslash	137
15 Multiple-Source Shortest Paths$^\alpha$	139
15.1 Problem Statement	139
15.2 Shortest paths and slacks	140
15.3 Compact Output	140
15.4 Parametric Shortest Paths	141
15.5 Dynamic Forest Data Structures	142
15.6 The Pivoting Algorithm	143
15.7 Applications	143
15.8 Enforcing Unique Shortest Paths	144
15.9 Leftmost shortest paths	146
15.10 References	146
15.11 Sir not appearing	147
16 Multiple-Source Shortest Paths, Revisited$^\alpha$	149
16.1 Problem formulation	150
16.2 Overview	151
16.3 Properly shared edges	152
16.4 Contraction	153
16.5 Distance Queries	155
16.6 Space and Time Analysis	156
16.7 References	158
17 Planar Separators$^\beta$	159
17.1 Tree separators	159
17.2 Fundamental cycle separators	160
17.3 Breadth-first level separators	160
17.4 Cycle separators	161
17.5 Good r -divisions and Subdivision Hierarchies	163
17.6 History	165
17.7 References	165
17.8 Aptly Named Sir Not	166
18 Branch Decompositions\oslash	167
18.1 Branchwidth	167
18.2 Treewidth	167
18.3 Width versus diameter	167
18.4 Local approximation	167
18.5 Aptly Named Sir Not	167
19 Fast Shortest Paths in Planar Graphs$^\beta$	169
19.1 Dense Distance Graphs	169
19.2 Beating Dijkstra	169

19.3 Beating Bellman-Ford: Nested Dissection	170
19.4 Aside: Computing Spring Embeddings	172
19.5 Repricing	173
19.6 Nested Dissection Revisited	173
19.7 Monge arrays and SMAWK	175
19.8 Planar distance matrices are (almost) Monge	176
19.9 Beating Nested Dissection	176
19.10 References	178
19.11 Aptly Named Sir Not	180
20 Minimum Cuts^β	181
20.1 Duality: Shortest essential cycle	181
20.2 Crossing at most once	182
20.3 Slicing along a path	183
20.4 Algorithms	183
20.5 Faster Shortest Paths with Negative Lengths	185
20.6 Faster Minimum Cuts: FR-Dijkstra	187
20.7 References	187
20.8 Aptly Named Sir Not	188
21 Faster Minimum Cuts (FR-Dijkstra)^α	189
21.1 Monge Heaps	189
21.2 Monge structure of nice r -divisions	191
21.3 FR-Dijkstra	192
21.4 Back to minimum cut	193
21.5 Aptly Named Sir Not	195
22 Distributive Flow Lattices[∅]	197
22.1 Pseudoflows and Circulations	197
22.2 Aptly Named Sir Not	197
23 Maximum Flow^{∅/α}	199
23.1 Background	199
23.2 Planar Circulations	201
23.3 Feasible Planar Circulations and Shortest Paths	202
23.4 Our First Planar Max-flow Algorithm	203
23.5 Parametric Shortest Paths	204
23.6 Active Darts	205
23.7 Fast Pivots	205
23.8 Universal Cover Analysis	205
23.9 References	205
23.10 Aptly Not	206
24 Surface Maps^β	207
24.1 Surfaces, Polygonal Schemata, and Cellular Embeddings	207
24.2 Orientability	208
24.3 Band Decompositions	209
24.4 Reflection Systems	210
24.5 Equivalence	211

24.6 Duality	212
24.7 Loops and Isthmuses; Deletion and Contraction	213
24.8 References	215
24.9 Sir Not Appearing	215
25 Surface Classification^β	217
25.1 Tree-Cotree Decompositions and Systems of Loops	217
25.2 Handles	218
25.3 Twists	219
25.4 Dyck's Surface	220
25.5 Canonical Polygonal Schemata	221
25.6 "Oiler's" Formula	221
25.7 References	223
25.8 Aptly Named Sir	223
26 Homotopy in Surface Maps^α	225
26.1 Cut Graphs	225
26.2 Systems of Loops and Homotopy	226
26.3 What's a "curve"?	226
26.4 Spur and Face Moves	227
26.5 Characterizing Homotopy	228
26.6 References	229
26.7 Aptly Named Sir	229
27 Planarization and Separation^{α/β}	231
27.1 Multiple Short Cycles	231
27.2 Slabification	232
27.3 Nice r -divisions	234
27.4 Applications	236
27.5 References	236
27.6 Aptly Named Sir	236
28 Homotopy Testing on Surface Maps^β	237
28.1 Reducing to a System of Loops	237
28.2 Universal Cover	238
28.3 Dehn's Lemma	240
28.4 Dehn's algorithm!	241
28.5 System of quads	241
28.6 Brackets	242
28.7 Reduction algorithm	243
28.8 References	244
28.9 Sir Not	244
29 Systems of Cycles and Homology^α	245
29.1 Cycles and Boundaries	245
29.2 Homology	246
29.3 Relax, it's just linear algebra!	247
29.4 Crossing Numbers	248
29.5 Systems of Cocycles and Cohomology	249

29.6 Homology Signatures	250
29.7 Separating Cycles	250
29.8 References	251
29.9 Aptly Named Sir	251
30 Shortest Interesting Cycles^a	253
30.1 Properties of Shortest Nontrivial Cycles	253
30.2 A polynomial-time algorithm	254
30.3 Near-quadratic time	255
30.4 Multiple-Source Shortest Paths	255
30.5 Shortest Nonseparating Cycles in Near-Linear Time	257
30.6 Shortest Noncontractible Cycles in Near-Linear Time (sketch)	257
30.7 References	258
30.8 Aptly Named Sir	259
31 Surfaces with Boundary^Ø	261
31.1 Arcs and Slicing	261
31.2 Forest-Cotree Decompositions	261
31.3 Cut Graphs and Systems of Arcs	261
31.4 Tree-Coforest Decompositions and Systems of Coarcs	261
31.5 References	261
31.6 Aptly Named Sir	261
32 Minimum Cuts in Surface Graphs^Ø	263
32.1 Duality with Even Subgraphs	263
32.2 \mathbb{Z}_2 -Homology Cover	263
32.3 \mathbb{Z}_2 -Minimal Cycles	263
32.4 \mathbb{Z}_2 -Minimal Even Subgraphs	263
32.5 NP-hardness (??)	263
32.6 References	263
32.7 Aptly Named Sir	264
33 Maximum Flows in Surface Graphs^Ø	265
33.1 Real Homology	265
33.2 Homologous Feasible Flows	265
33.3 Shortest Paths with Negative Edges	265
33.4 Ellipsoid Method (Sketch)	265
33.5 Summary	265
33.6 References	266
33.7 Aptly Named Sir	267
34 Geodesic Embeddings^Ø	269
34.1 Flat Torus	269
34.2 Spring Embeddings on Other Surfaces	269
34.3 Circle Packing on Other Surfaces	269
34.4 References	269
34.5 Named Sir Not	269
35 Closing the Loop^Ø	271

35.1 Simple Polygons	271
35.2 Winding Numbers	272
35.3 Curve Homotopy	272
35.4 Shortest Homotopic Paths and Cycles	272
35.5 Gauss codes	272
35.6 Curve Invariants and Simplification	273
35.7 Geodesic Embeddings	273
35.8 Maxwell–Cremona	273
35.9 References	274

Foreward ^{α}

These are lecture notes from a special-topics class on topological graph algorithms that I have taught several times at the University of Illinois. These lecture notes (and other course materials) are available under a Creative Commons Attribution license (CC BY 4.0).



Figure 1: CC BY 4.0

I drafted most of these notes in Fall 2020 and revised them in Spring 2023; a handful of chapters (13, 16, 26, 27, 29, 30) were first drafted in Spring 2023. Even after a second round of revision, these are all still very rough drafts. Most of the missing chapters either cover material I did not discuss in class, or cover material from my own research papers.

I've attempted, with various degrees of success, to write the first draft of each note to exactly cover one 75-minute lecture, to force myself to prioritize the most fundamental results, sometimes at the expense of technical details, prerequisite material (like point-set topology or dynamic-forest data structures), accurate reflection of the state of the art, and historical anecdotes. Later revisions tend to include more technical details that I don't actually cover in lecture, except to say "You can find more details in the notes." In practice, I can cover at most 5 pages of material in detail in one lecture (and each semester has only 25 lectures).

Similarly, I am writing these notes in Markdown instead of LaTeX, in part to intentionally focus my time on writing instead of typography, and in part to make the final output more accessible by producing HTML and ePub versions. As a result, the notes are typographically rather awkward/ugly. Some day I will figure out how to use Pandoc templates and filters, or better yet, a more modern system like Quarto. (Real Soon Now, Honest.) For similar reasons, many notes are embarrassingly short on figures and/or references.

I think I'm about 2/3 of the way to a complete first draft of an actual book. I'm reasonably happy with the current set of chapters, plus or minus one, but less so about their order, especially in the last third. If I stick to the current outline, the final book should be just over 400 pages long in its current format (or about 600 pages in a more book-friendly format). Depending on their degree of completion, each chapter title has one of the following annotations:¹

- \emptyset : mostly (or completely) unwritten
- α : mostly written, but missing significant details, or only used once
- β : reasonably polished, but possibly missing some minor details

¹I would like to include a section describing related state-of-the-art results at the end of each chapter. These annotations ignore those missing sections.)

- δ : complete and totally polished (so needs only five more rounds of copy editing)
- Nothing: actually done

Once I have a complete draft of the entire book, I plan to make the source files available on Github to attract bug reports, feature requests, and pull requests. Stay tuned!

Chapter 1

Simple Polygons $^\beta$

The Jordan Curve Theorem and its generalizations are the formal foundations of many results, if not *every* result, in two-dimensional topology. In its simplest form, the theorem states that any simple closed curve partitions the plane into two connected subsets, exactly one of which is bounded. Although this statement is intuitively clear, perhaps even obvious, the generality of the term “simple closed curve” makes a formal proof of the theorem incredibly challenging. A complete proof must work not only for sane curves like circles and polygons, but also for more exotic beasts like fractals and space-filling curves. Fortunately, these exotic curves rarely occur in practice, except as counterexamples in point-set topology textbooks.

A full proof of the Jordan Curve Theorem requires machinery that we won’t cover in this class (either point-set topology or singular homology). Here I’ll consider only the important special case of *simple polygons*. Polygons are by far the most common type of closed curve employed in practice, so this special case has immediate practical consequences.

Most published proofs of the full Jordan Curve Theorem both dismiss this special case as trivial and rely on it as a key lemma. Indeed, the proof is ultimately *elementary*. Nevertheless, the Jordan Polygon Theorem and its proof are the foundation of several fundamental algorithmic tools in computational geometry and topology.

1.1 Definitions

A *path* in the plane is an arbitrary continuous function $\pi : [0, 1] \rightarrow \mathbb{R}^2$, where $[0, 1]$ is the unit interval on the real line. The points $\pi(0)$ and $\pi(1)$ are called the *endpoints* of the path. A *closed curve* (or *cycle*) in the plane is a continuous function from the unit circle $S^1 = \{(x, y) \in \mathbb{R}^2 \mid x^2 + y^2 = 1\}$ to the plane.

A path or cycle is *simple* if it is injective, or intuitively, if it does not “self-intersect”. To avoid excessive formality, we do not normally distinguish between a simple path or cycle (formally a function) and its image (formally a subset of the plane).¹

¹Historically, the definition of “simple closed curve” was a point of serious confusion for several decades, starting with Bolzano around 1840s. This confusion was finally resolved only when Jordan defined closed curves as *functions* instead of *subsets of the plane*.

A subset X of the plane is *(path-)connected* if there is a path in X from any point in X to any other point in X . A *(path-)component* of X is a maximal path-connected subset of X .

Theorem (The Jordan Curve Theorem). *The complement $\mathbb{R}^2 \setminus C$ of any simple closed curve C in the plane has exactly two components.*

A *polygonal chain* is a path that passes through a finite sequence of points p_0, p_1, \dots, p_n , such that for each index i , the subpath from p_{i-1} to p_i is the straight line segment $p_{i-1}p_i$. The points p_i are called the *vertices* of the polygonal chain, and the segments $p_{i-1}p_i$ are called its *edges*. We usually assume without loss of generality that no pair of consecutive edges is collinear, and in particular, that no two consecutive vertices coincide.

A polygonal chain is *closed* if it has at least one edge and its first and last vertices coincide (that is, if $p_0 = p_n$) and *open* otherwise. Closed polygonal chains are also called *polygons*; a polygon with n vertices and n edges is also called an n -gon. We can regard any polygon as a closed curve in the plane. Every simple polygon has at least three vertices.

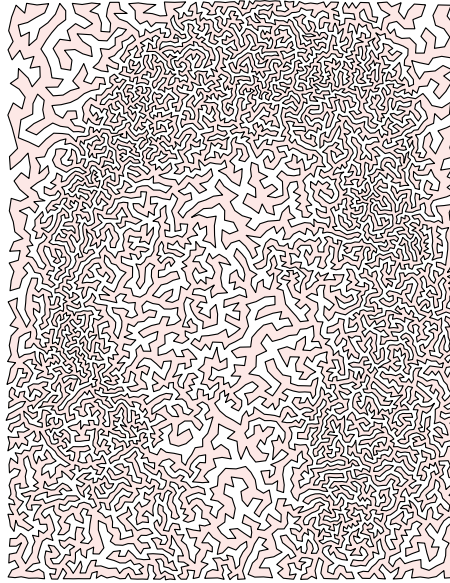


Figure 1.1: A simple 10000-gon, with interior shaded

Theorem (The Jordan Polygon Theorem). *The complement $\mathbb{R}^2 \setminus P$ of any simple polygon P in the plane has exactly two components.*

Let me emphasize that even though this theorem considers only *polygonal* closed curves, the definitions of “connected” and “component” allows for *arbitrary* paths between points.

1.2 Proof of the Jordan Polygon Theorem

Fix a simple polygon P with n vertices. Without loss of generality, assume no two vertices of P have equal x -coordinates. The vertical lines through the vertices partition the plane into $n + 1$ *slabs*, two of which (the leftmost and rightmost) are actually halfplanes. The edges of P subdivide each slab into a finite number of regions we call *trapezoids*, even though some of these regions are actually triangles, and others are unbounded in one or more directions.

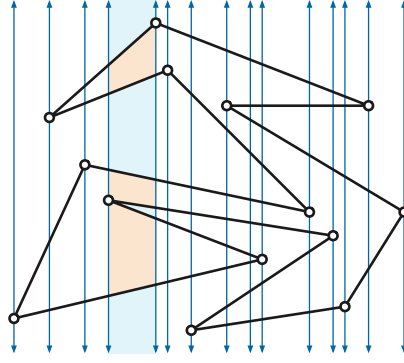


Figure 1.2: A slab decomposition of a simple polygon, with trapezoids in one slab highlighted

The boundary of each trapezoid consists of (at most) four line segments: the *floor* and *ceiling*, which are segments of polygon edges, and the *left* and *right walls*, which are segments of the vertical slab boundaries. The endpoints of each vertical wall (if any) lie on the polygon P .

Formally, we define each trapezoid to include its walls but not its floor, its ceiling, or any vertex on its walls. Thus, each trapezoid is connected, any two trapezoids intersect in a common wall or not at all, and the union of all the trapezoids is $\mathbb{R}^2 \setminus P$. In particular, a trapezoid is a convex (and therefore connected) region in the plane, but it is not a polygon!

Lemma 2. $\mathbb{R}^2 \setminus P$ has at most two components.

Proof: Direct the edges of P in increasing index order (modulo n). Informally, we label every trapezoid *left* or *right* depending on whether a person walking around P would see that trapezoid immediately to their left or immediately to their right. More formally, we label every trapezoid that satisfies at least one of the following conditions *left*:

- The ceiling is directed from right to left.
- The floor is directed from left to right.
- The right wall contains a vertex p_i , and the incoming edge $p_{i-1}p_i$ is below the outgoing edge p_ip_{i+1}
- The left wall contains a vertex p_i , and the incoming edge $p_{i-1}p_i$ is above the outgoing edge p_ip_{i+1}

These conditions apply verbatim to unbounded and degenerate trapezoids. There are four symmetric conditions for labeling a trapezoid *right*. Every trapezoid is labeled left or right or (as far as we know at this point) possibly both.

Now imagine walking once around the polygon, facing directly forward along edges and turning at vertices, and consider the sequence of trapezoids immediately to our left, as suggested by the white arrows in Figure 2 above. Without loss of generality, start at the leftmost vertex p_0 . Whenever we traverse a directed edge $p_{i-1}p_i$ from right to left, our left hand sweeps through all trapezoids immediately below that edge. Whenever we reach a vertex p_i whose neighbors are both to the right of p_i , where the edges make a right (clockwise turn), our hand sweeps through the trapezoid just to the left of p_i . The other cases are symmetric. The resulting sequence of trapezoids contains every left trapezoid at least once (and at most four times); moreover, any adjacent pair of trapezoids in this

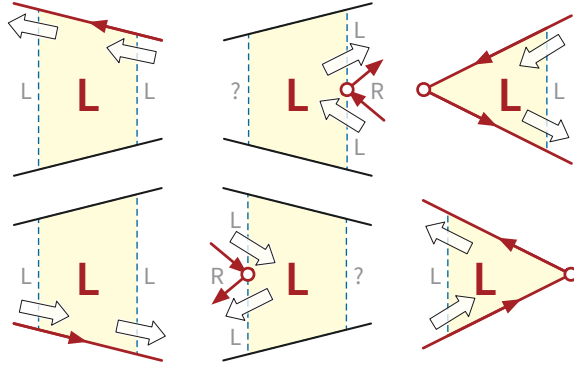


Figure 1.3: Left trapezoids

sequence share a wall and thus have a connected union. So the union of the left trapezoids is connected.

A symmetric argument implies that the union of the right trapezoids is also connected, which completes the proof.

It's worth noting here that Lemma ≤ 2 holds for simple closed curves on arbitrary *surfaces*, including non-orientable surfaces like the Klein bottle, but it can fail for more complex topological spaces.

Lemma ≥ 2 . $\mathbb{R}^2 \setminus P$ has at least two components.

Proof (Jordan): Label each trapezoid *even* or *odd* depending on the parity of the number of polygon edges directly above the trapezoid. Thus, within each slab, the highest trapezoid is even, and the trapezoids alternate between even and odd. For example, in Figure 1, the blue slabs are even, and the orange slabs are odd.

Consider any path π that intersects exactly two trapezoids τ and τ' . If τ and τ' lie in the same slab, this path must intersect at least one edge of P . (I am *not* invoking the Jordan curve theorem here, but rather a much more basic fact called the *plane separation axiom*.²) Otherwise, τ and τ' must lie in adjacent slabs, because π is continuous, and therefore must share a vertical wall.

Suppose this wall lies on the vertical line ℓ through p_i , and without loss of generality, τ lies on the left of ℓ and τ' on the right. If vertices p_{i-1} and p_{i+1} are on opposite sides of ℓ , exactly the same number of polygon edges are above τ and above τ' . Suppose p_{i-1} and p_{i+1} lie to the left of ℓ . If p_i lies below the wall $\tau \cap \tau'$, then τ and τ' are below the same number of edges; otherwise, τ is below two more edges than τ' . Similar cases arise when p_{i-1} and p_{i+1} both lie to the right of ℓ . In all cases, τ and τ' have the same parity.

More generally, consider any two trapezoids τ and τ' in the same component of $\mathbb{R}^2 \setminus P$. There must be a path $\pi: [0, 1] \rightarrow \mathbb{R}^2 \setminus P$ with $\pi(0) \in \tau$ and $\pi(1) \in \tau'$. Let $\tau_0, \tau_1, \dots, \tau_N$ be the sequence of trapezoids that π intersects, sorted in order of their first intersection.

²The plane separation axiom states that the complement $\mathbb{R}^2 \setminus \ell$ of any *straight line* ℓ in the plane has exactly two components. This axiom follows easily from the intermediate value theorem; it is also formally equivalent to *Pasch's axiom*: If a line ℓ does not contain any vertex of a triangle Δ , then ℓ intersects an even number of edges of Δ . In 1882, Moritz Pasch proved that his axiom is independent of Euclid's postulates, but that some theorems in the *Elements* require it. Yes, there is such a thing as non-Paschian geometry. It's weeeeeird.

Thus, $\tau_0 = \tau$ and for each index $i > 0$, the path π enters trapezoid τ_i for the first time from some trapezoid τ_j with $j < i$. Our earlier arguments imply that π must leave τ_j and enter τ_i through a common wall, so these two trapezoids have the same parity. It follows by induction that every trapezoid τ_i has the same parity as τ_0 ; in particular, τ and τ' have the same parity.

We conclude that any two trapezoids in the same component of $\mathbb{R}^2 \setminus P$ have the same parity, which completes the proof.

It's worth noting here that Lemma ≤ 2 holds for more complex planar shapes, such as polygons with holes, but it fails for any surface that is no homeomorphic to a subspace of the sphere.

The Jordan Polygon Theorem now follows immediately from Lemmas ≤ 2 and ≥ 2 . In particular, if the polygon is oriented counterclockwise (the way god intended), then “right” and “even” (and blue) mean “outside”, and “left” and “odd” (and orange) mean “inside”.

In contexts where polygons are assumed to be simple, it is standard practice to use the single word “polygon” (and the same variable names, and the same data structures) to refer *both* to a simple closed polygonal chain *and* to (the closure of) the interior of that polygonal chain, with the precise meaning *hopefully* clear from context. For example, the slab decomposition we used in this section decomposes *the polygon* into trapezoids, and in later lectures we will consider *polygons with holes*. This polysemy is justified by the Jordan Polygon Theorem.

1.3 Point-in-Polygon Test

The parity proof of Lemma ≥ 2 immediately suggests a standard algorithm to test whether a point lies in the interior of a simple polygon in the plane in linear time: Shoot an arbitrary ray from the query point, count the number of times this ray crosses the polygon, and return true if and only if this number is odd. This algorithm appears in Gauss' notes (written around 1830 but only published after his death); it has been rediscovered many times since then.

To make the ray-parity algorithm concrete, we need one numerical primitive from computational geometry. A triple (q, r, s) of points in the plane is *oriented counterclockwise* if walking from q to r and then to s requires a left turn, or *oriented clockwise* if the walk requires a right turn. More explicitly, consider the 3×3 determinant

$$\Delta(q, r, s) = \det \begin{bmatrix} 1 & q.x & q.y \\ 1 & r.x & r.y \\ 1 & s.x & s.y \end{bmatrix} = (r.x - q.x)(s.y - q.y) - (r.y - q.y)(s.x - q.x).$$

The triple (q, r, s) is oriented counterclockwise if $\Delta(q, r, s) > 0$, oriented clockwise if $\Delta(q, r, s) < 0$, and collinear if $\Delta(q, r, s) = 0$. (The absolute value of $\Delta(q, r, s)$ is twice the area of the triangle Δqrs .)

Straightforward case analysis implies that the vertical ray from q crosses the line segment rs if and only if q lies between the vertical lines through r and s , and $\Delta(q, r, s)$ has the same sign as $r.x - s.x$.

Finally, here is the algorithm in (pseudo)Python. The input polygon P is represented by an array of consecutive vertices. The algorithm returns $+1$, -1 , or 0 to indicate that the query point q lies inside, outside, or directly on P , respectively. To correctly handle ties between x -coordinates, the

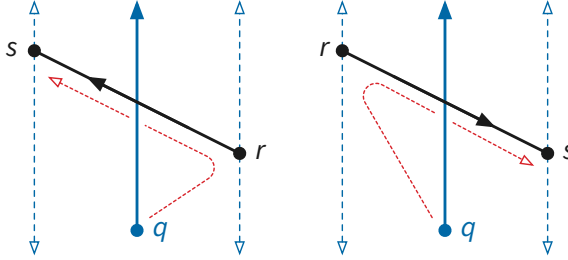


Figure 1.4: Ray-crossing test

algorithm treats any polygon vertex on the vertical line through q (but not actually coincident with q) as though it were slightly to the left. The algorithm clearly runs in $O(n)$ time.

```
def PtInPolygon(P, q):
    sign = -1                                // outside if no crossings
    n = len(P)
    for i in range(n):
        r = P[i]
        s = P[(i+1)% n]
        Delta = (r.x - q.x)*(s.y - q.y) - (r.y - q.y)*(s.x - q.x)
        if s.x <= q.x < r.x                  // positive crossing?
            if Delta > 0:
                sign = -sign
            elif Delta == 0:
                return 0
        elif r.x <= q.x < s.x              // negative crossing?
            if Delta < 0:
                sign = -sign
            elif Delta == 0:
                return 0
    return sign
```

1.4 Polygons Can Be Triangulated

Most algorithms that operate on simple polygons actually require a decomposition of the polygon into simple pieces that are easier to manage. We've already seen one such decomposition, first into vertical slabs, and then into trapezoids. For many geometric and topological algorithms, the most natural decomposition breaks the interior of the polygon into triangles that meet edge-to-edge. More formally, a *triangulation* is a triple of sets (V, E, T) with the following properties.

- T is a finite set of triangles in the plane with disjoint interiors.
- E is the set of edges of triangles in T .
- Any two segments in E have disjoint interiors.
- V is the set of vertices of triangles in T .

The third condition guarantees that the intersection of any two triangles in T is either an edge of both, a vertex of both, or empty.

If the union of the triangles in T is equal to the closure of the interior of a simple polygon P ,

we call (V, E, T) a *triangulation* of P . If moreover V is the set of vertices of P , then (V, E, T) is called a *frugal triangulation* of P . Every edge of a frugal triangulation is either an edge of P or an (*interior*) *diagonal*, meaning a line segment between two vertices of P whose interior lies in the interior of P .

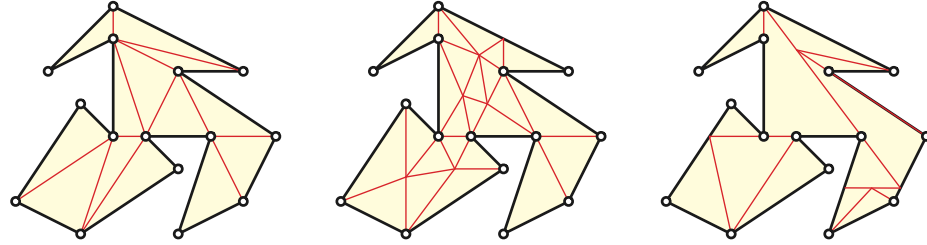


Figure 1.5: A frugal triangulation, a non-frugal triangulation, and a non-triangulation of a simple polygon

After playing with a few examples, it may seem obvious that every simple polygon has a frugal triangulation, but a formal proof of this fact is surprisingly subtle; several incorrect (or at least incomplete) proofs appear in the literature. The first complete, correct, axiomatic proofs were developed by Dehn (1899, unpublished) and Lennes (1911), although some components of their arguments already appear in the Gauss's posthumously published notes.

The following proof is somewhat more complicated (and intentionally *less* formal!) than Dehn's and Lennes's arguments, but it directly motivates a faster algorithm for constructing triangulations.

Diagonal Lemma (Dehn, Lennes): *Every simple polygon with at least four vertices has an interior diagonal.*

Proof: Let P be a simple polygon with vertices p_0, p_1, \dots, p_{n-1} for some $n \geq 4$. As before, we assume without loss of generality that no two vertices of P lie on a common vertical line. We begin by subdividing the closed interior of P into trapezoids with vertical line segments through the vertices. Specifically, for each vertex p_i , we cut along the longest vertical segment through p_i in the closure of the interior of $\sim P$. The resulting subdivision, which is called a *trapezoidal decomposition* of P , can also be obtained from the slab decomposition we used to prove the Jordan polygon theorem by removing every exterior wall and every wall that does not end at a vertex of P .

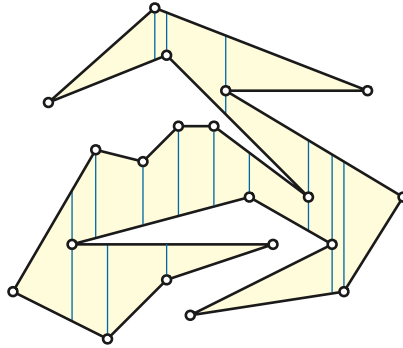


Figure 1.6: A trapezoidal decomposition of a simple polygon

Every trapezoid in the decomposition has exactly two polygon vertices on its boundary. Call a trapezoid *boring* if the line segment between these two vertices cuts through the

interior of the trapezoid, and therefore is a diagonal of P , and *interesting* otherwise. Every interesting trapezoid either has two vertices of P on its ceiling, or two vertices of P on its floor.

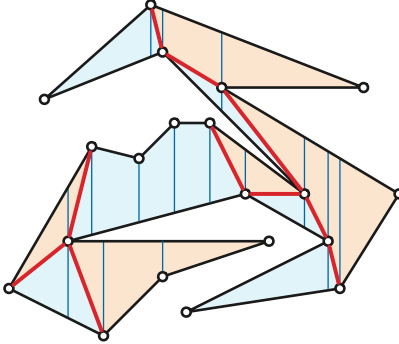


Figure 1.7: Boring diagonals

If any of the trapezoids is boring, we immediately have a diagonal. Yawn.

Any path through the interior of P that starts in a ceiling trapezoid and ends in a floor trapezoid must pass through a boring trapezoid. So if every trapezoid is interesting, then every trapezoid is interesting *the same way*—either every trapezoid has two vertices on its ceiling, or every trapezoid has two vertices on its floor. Thus, P is a special type of polygon we call a *monotone mountain*: any vertical line intersects at most two edges of P , and the leftmost and rightmost vertices of P are connected by a single edge of P .

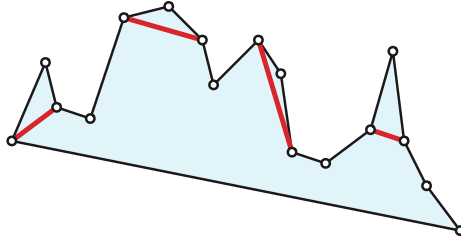


Figure 1.8: Four diagonals in a monotone mountain

Without loss of generality, suppose p_0 is the leftmost vertex, p_{n-1} is the rightmost vertex, and every other vertex is above the edge p_0p_{n-1} (so every trapezoid has two vertices on its ceiling). Call a vertex p_i *convex* if the interior angle at that vertex is less than π , or equivalently, if the triple (p_{i-1}, p_i, p_{i+1}) is oriented *clockwise*. Every monotone mountain has at least one convex vertex p_i other than p_0 and p_{n-1} ; take, for example, the vertex furthest above the floor p_0p_{n-1} . For any such vertex p_i , the line segment $p_{i-1}p_{i+1}$ is a diagonal.

Triangulation Theorem: *Every simple polygon has a frugal triangulation.*

Proof (Dehn, Lennes): The theorem follows by induction from the diagonal lemma. Intuitively, to triangulate any nontrivial polygon, we can split any polygon along a diagonal and then recursively triangulate each of the two resulting smaller polygons.

Let P be a simple polygon with n vertices $p_0, p_1, p_2, \dots, p_{n-1}$. If P is a triangle, it has a trivial triangulation, so assume $n > 3$. Suppose without loss of generality (reindexing the

vertices if necessary) that $d = p_0 p_i$ is a diagonal of P , for some index i . Let P^+ and P^- denote the polygons with vertices $p_0, p_i, p_{i+1}, \dots, p_{n-1}$ and $p_0, p_1, p_2, \dots, p_i$, respectively. The definition of “diagonal” implies that both P^+ and P^- are simple. Color each edge of P red if it is an edge of P^+ and blue otherwise; every blue edge is an edge of P^- .

Now we need to prove that the diagonal d partitions the interior of P into the interiors of P^+ and P^- . Proving this claim is surprisingly subtle.

Let U be any open disk in the interior of P that intersects d ; such a disk exists because d is an *interior* diagonal. (We had to use that fact somewhere!) The set $U \setminus p_0 p_i$ has exactly two components.^[^pasch2] Choose arbitrary points q^+ and q^- , one in each component. Let R^+ and R^- be parallel rays starting at q^+ and q^- , respectively, such that R^+ contains R^- . Then R^+ crosses d but R^- does not, and R^+ and R^- cross exactly the same edges of P .

[^pasch2] We are invoking the plane separation axiom again here.

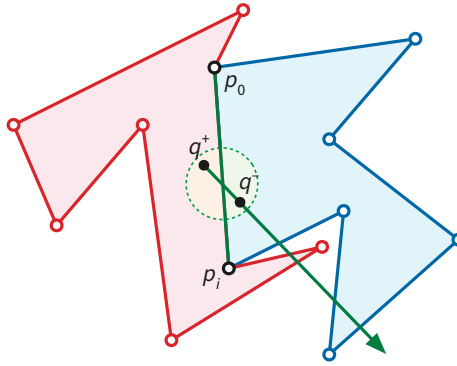


Figure 1.9: Partitioning a polygon with an interior diagonal

As above, R^+ (and therefore R^-) crosses an odd number of edges of P . Without loss of generality, suppose R^+ (and therefore R^-) crosses an even number of red edges and an odd number of blue edges. Then, because R^+ crosses d , the point q^+ lies inside P^+ and outside P^- . Similarly, q^- lies inside P^- and outside P^+ , because R^- does not cross d . We conclude (finally!) that the interiors of P^+ and P^- are disjoint subsets of the interior of P . Whew!

The inductive hypothesis implies that P^+ has a frugal triangulation (V^+, E^+, T^+) and that P^- has a frugal triangulation (V^-, E^-, T^-) . One can now verify mechanically that $(V^+ \cup V^-, E^+ \cup E^-, T^+ \cup T^-)$ is a frugal triangulation of P .

1.5 Computing a Triangulation

The proof of the diagonal lemma implies an efficient algorithm to triangulate any simple polygon. I'll only sketch the algorithm here; for further details, see your favorite computational geometry textbook. First, we construct a trapezoidal decomposition in $O(n \log n)$ time using a *sweepline* algorithm. Intuitively, we sweep a vertical line from left to right across the plane, maintaining its intersection with the polygon in a balanced binary search tree, and inserting a new vertical wall whenever the line touches a vertex. (In fact, we only visit the vertices in order from left to right.) Second, we insert diagonals inside every boring trapezoid; these diagonals decompose P into monotone mountains in $O(n)$ time. Finally, we triangulate each monotone mountain in $O(n)$ time by cutting off convex vertices in order from left to right.

The overall running time is $O(n \log n)$; the running time is dominated by the time to construct the trapezoidal decomposition. Theoretically faster algorithms for that construction are known—in particular, Chazelle described a famously complex $O(n)$ -time algorithm—but it is unclear whether any of these improvements is faster in practice, or indeed if any of them have actually been implemented.

I'll leave the following corollaries of the polygon triangulation theorem as exercises.

Corollary: *Every frugal triangulation of a simple n -gon contains exactly $n - 2$ triangles and exactly $n - 3$ diagonals.*

Corollary: *Every simple polygon with at least four vertices has at least two **ears**, where an ear is an internal diagonal that cuts off a single triangle.*

Corollary: *Let P be a simple polygon with vertices p_0, p_1, \dots, p_{n-1} . Let i, j, k, l be four distinct indices with $i < j$ and $k < l$, such that both $p_i p_j$ and $p_k p_l$ are interior diagonals of P . These two diagonals cross if and only if either $i < k < j < l$ or $k < i < l < j$.*

Corollary: *Any maximal set of non-crossing interior diagonals in a simple polygon P yields a frugal triangulation of P .*

1.6 The Dehn-Schönflies Theorem

The Dehn-Schönflies Theorem: *For any simple polygon P , there is a homeomorphism $H: \mathbb{R}^2 \rightarrow \mathbb{R}^2$ that maps P to a convex polygon Q and maps the interior of P to the interior of Q .*

Proof (Dehn): [to be written]

1.7 ... and the aptly named Sir Not Appearing in This Film

- Basic geometric algorithms:
 - Details of sweepline algorithm
 - Der Dreigroschenalgorithmus
 - Faster decomposition/triangulation algorithms
- Triangulating polygons with holes
- Compatible triangulations
- Weakly simple polygons
- Proof (via Hex and Y) of the full Jordan Curve Theorem
- Geodesic polygons on other surfaces (see exercises)

1.8 References

1. Mark de Berg, Otfried Cheong, Marc van Kreveld, and Mark Overmars. *Computational Geometry: Algorithms and Applications*, 3rd edition. Springer-Verlag, 2008. Your favorite computational geometry textbook.
2. Bernard Bolzano. Anti-Euklid. Unpublished manuscript, c. 1840. Published posthumously in [10].
3. Max Dehn. Beweis des Satzes, daß jedes geradlinige geschlossene Polygon ohne Doppelpunkte ‘die Ebene in zwei Teile teilt’. Unpublished manuscript, c.1899. Max Dehn Papers

- archive, University of Texas at Austin. Cited and described in detail by Guggenheimer [4]. Proof of the Jordan Polygon Theorem.
4. Heinrich W. Guggenheimer. The Jordan curve theorem and an unpublished manuscript of Max Dehn. *Arch. History Exact Sci.* 17:193–200, 1977.
 5. Camille Jordan. Courbes continues. *Cours d'Analyse de l'École Polytechnique*, 1st edition, vol. 3, 587–594, 1887.
 6. Camille Jordan. Lignes continues. *Cours d'Analyse de l'École Polytechnique*, 2nd edition, vol. 1, 90–99, 1893.
 7. Nels Johann Lennes. Theorems on the simple finite polygon and polyhedron. *Amer. J. Math.* 33:37–62, 1911. Read to the AMS in April, 1903. Proof of the Jordan Polygon Theorem.
 8. Joseph O'Rourke. *Computational Geometry in C*, 2nd edition. Cambridge University Press, 1998. Your favorite computational geometry textbook.
 9. Moritz Pasch. *Vorlesung über neuere Geometrie*. Teubner, 1882.
 10. Kazimír Večerka. Bernard Bolzano: Anti-Euklid. *Sborník pro dějiny přírodních věd a techniky / Acta Hist. Rerum Natur. Nec Non Tech.* 11:203–216, 1967. In Czech, with German summary.

Chapter 2

Winding Numbers^β

2.1 Let me not be pent up, sir; I will fast, being loose.

Fast and Loose is the name of a family of magic tricks (or con games) performed with ropes, chains, and belts that have been practiced since at least the 14th century; the con game is mentioned in three different Shakespeare plays. In one such trick, now sometimes called the *Endless Chain*, the con artist arranges a closed loop of chain into a doubled figure-8, and then asks the mark to put their finger on the table inside one of the loops. The con artist then pulls the chain along the table. If the chain catches on the mark's finger, then the chain is *fast* and the mark wins; if the con artist can pull the chain completely off the table, the chain is *loose* and the mark loses.

The con artist shows the mark that there are two different ways for the loops to fall. (Notice how the chain crosses itself in the lower corners.) Because the chain is bright and shiny and bumpy, it's impossible for the mark to tell which way the chain is actually arranged, but because these are the only possibilities, the mark should have a 50-50 chance of winning. Right? *Riiight?*

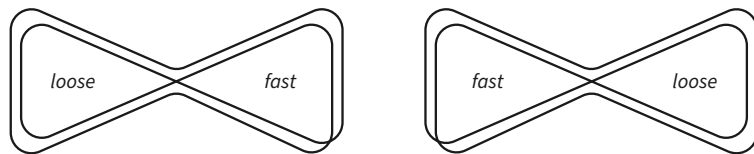


Figure 2.1: Two arrangements of the Endless Chain

Oh, you sweet summer child. Of course not! As soon as the mark places money *on the barrelhead*, the con artist wins every time. The con artists was lying; there is a third arrangement of the chain that is *always* loose, no matter where the mark puts their finger.¹

2.2 Shoelaces and Signed Areas

Swap this section and next? This is historical order, but the narrative is a bit clunky.

¹There is another completely different “Fast and Loose” con game, also known as called “Pricking the Garter”, that’s usually performed with a belt. It’s less self-working, less mathematically interesting (despite seeming to invoke the Jordan curve theorem), and less shiny than the Endless Chain.

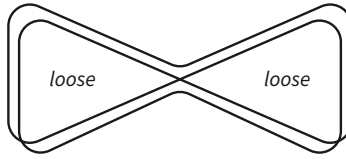


Figure 2.2: The actual arrangement of the Endless Chain

Before discussing the mathematical reasons you just lost all your money, let's consider a basic computational geometry problem: How quickly can we compute the area enclosed by a given polygon P ?

A particularly simple algorithm was described by Albrecht Meister in 1785. In principle, we can calculate the area of P by cutting P into disjoint triangles and then summing the triangle areas, each of which can compute in $O(1)$ time, but it would be more than a century before anyone knew how to cut polygons into triangles. Meister's insight was to consider the *signed* areas of *overlapping* oriented triangles.

The signed area of a triangle depends not only on its vertex coordinates, but on the orientation of its three vertices. By convention, counterclockwise triangles have positive signed area, and clockwise triangles have negative signed area. Recall that a triple of points (q, r, s) is oriented counterclockwise or clockwise if and only if the following determinant is positive or negative, respectively:

$$\Delta(q, r, s) = \det \begin{bmatrix} 1 & q.x & q.y \\ 1 & r.x & r.y \\ 1 & s.x & s.y \end{bmatrix} = (r.x - q.x)(s.y - q.y) - (r.y - q.y)(s.x - q.x).$$

The *signed area* of the triangle Δqrs is $\frac{1}{2}\Delta(q, r, s)$.

Let o be an *arbitrary* point in the plane. Meister observed that the *signed* area of any *oriented* polygon P is the sum of the signed areas of the triangles determined by o and the edges of P :

$$\text{area}(P) = \frac{1}{2} \sum_{i=0}^{n-1} \Delta(o, p_i, p_{i+1})$$

(To simplify notation, I'll omit “mod n ” from all index arithmetic.) In particular, if we take o to be the origin $(0, 0)$, we have

$$\text{area}(P) = \frac{1}{2} \sum_{i=0}^{n-1} (x_i \cdot y_{i+1} - y_i \cdot x_{i+1}) = \frac{1}{2} \sum_{i=0}^{n-1} \det \begin{bmatrix} x_i & y_i \\ x_{i+1} & y_{i+1} \end{bmatrix}$$

where $p_i = (x_i, y_i)$ for each index i . This expression of Meister's algorithm is commonly known as the *shoelace formula*, because the pattern of multiplications resembles the usual method for threading shoelaces:

$$\begin{bmatrix} x_0 & \times & x_1 & \times & x_2 & \times & x_3 & \times & \dots \\ y_0 & & y_1 & & y_2 & & y_3 & & \dots \end{bmatrix}$$

Proving that the shoelace algorithm correctly computes areas is straightforward. First, we

can prove that the formula is correct for *triangles*, either by verifying² the algebraic identity

$$\Delta(q, r, s) = \Delta(o, q, r) + \Delta(o, r, s) + \Delta(o, s, q)$$

or by geometric case analysis, as suggested by the figure below. Areas outside the triangle are either counted once positively and once negatively, or not counted at all; areas inside the triangle are counted exactly once, with the correct sign.

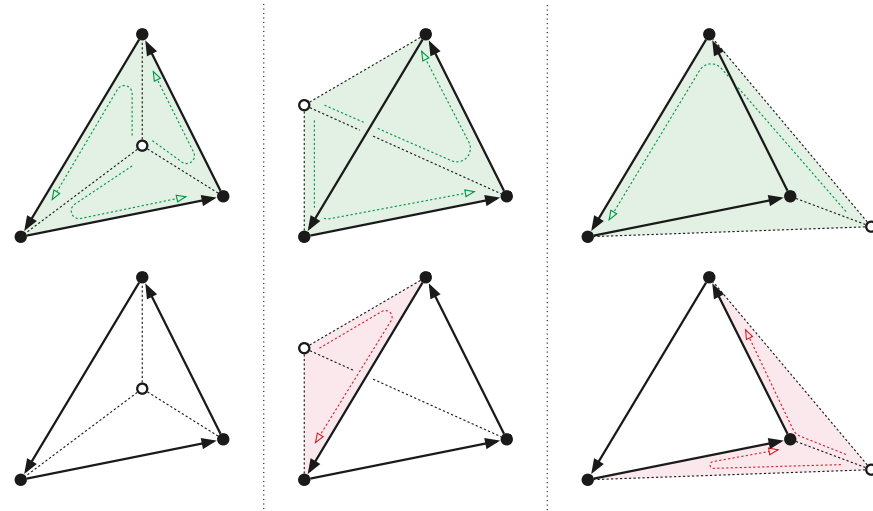


Figure 2.3: Lacing a triangle: Add the green (counterclockwise) triangles and subtract the pink (clockwise) triangles.

Then to prove the shoelace formula correct for any larger polygon P , we can sum the signed areas of all triangles in any frugal triangulation of P and observe that the terms involving diagonals of the triangulation cancel out. As expected, the resulting signed area is positive if P is oriented counterclockwise (that is, with the interior on the left) and negative if P is oriented clockwise.

Meister actually used his shoelace formula to define the signed areas of an *arbitrary* polygon, even if that polygon is not simple. Here it's somewhat less clear that the formula is *correct* for non-convex polygons, but we can verify two facts that suggest that it is at least *sensible*. First, the resulting signed area is still independent of the choice of point o . Second, the formula counts the area of each component of $\mathbb{R}^2 \setminus P$ some integer number of times; in particular, the (infinite) area of the unbounded region is not counted at all. The resulting assignment of integers to the components of $\mathbb{R}^2 \setminus P$ is called the *Alexander numbering* of P .

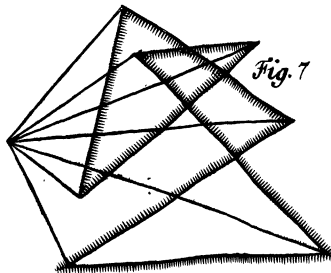


Figure 2.4: Computing the signed area of a polygon, from Meister (1785)

²Hint: cofactor expansion

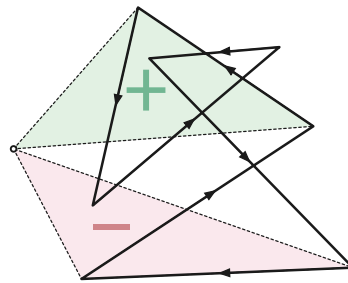


Figure 2.5: One positive triangle and one negative triangle for Meister's polygon

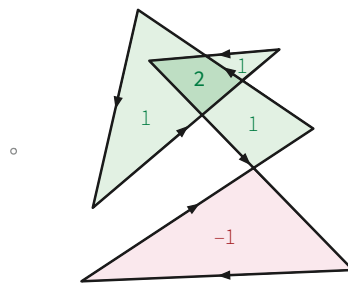


Figure 2.6: The Alexander numbering of Meister's polygon

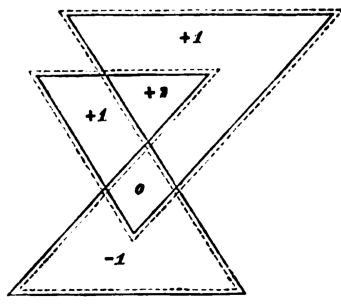


Fig. 5.

Figure 2.7: Another Alexander numbering, from Möbius (1865)

2.3 Winding numbers

The *winding number* of a polygon P around a point o is intuitively (and not surprisingly) the number of times that P winds counterclockwise around o . For example, if P is a *simple* polygon, its winding number around any exterior point is zero, and its winding number around any interior point is either $+1$ or -1 , depending on how the polygon is oriented. If the polygon winds *clockwise* around o , the winding number is negative. Crucially, the winding number is only well defined if the polygon does not contain the point o .

We can define the winding number more formally as follows. Let p_0, p_1, \dots, p_{n-1} denote the vertices of P in order. For each index i , let θ_i denote the interior angle at o in the triangle $\Delta p_i o p_{i+1}$, with positive sign if (o, p_i, p_{i+1}) is oriented counterclockwise, and with negative sign if (o, p_i, p_{i+1}) is oriented clockwise. Assuming angles are measured in *circles*,³ the winding number of P around o is the sum $\sum_i \theta_i$.

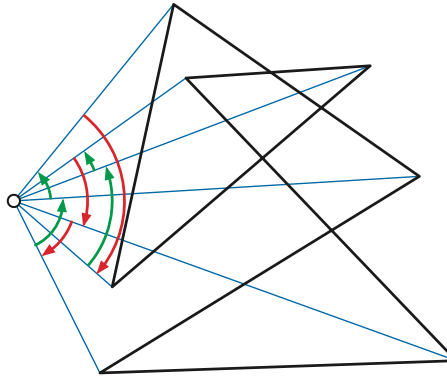


Figure 2.8: Winding number as a sum of angles, after Meister

Actually computing the winding number according to this definition requires inverse trigonometric functions, square roots, and other numerical madness. Fortunately, there is an equivalent definition that builds on our ray-shooting test from the previous lecture. Let R be a vertical ray shooting upward from o . We distinguish two types of crossings between the R and the polygon, depending on the orientation of the crossed edges. Specifically, if the crossed edge is directed from right to left, we have a *positive crossing*; otherwise, we have a *negative crossing*. Equivalently, when R crosses an edge $p_i p_{i+1}$, the sign of the crossing is the sign of the determinant $\Delta(o, p_i, p_{i+1})$.

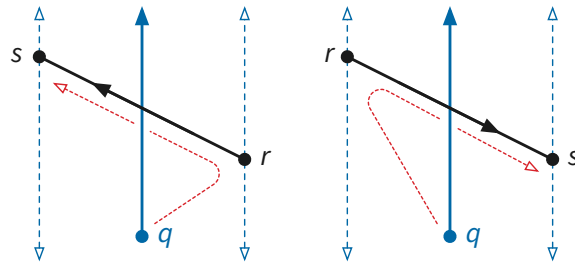


Figure 2.9: A positive crossing (left) and a negative crossing (right)

I'll leave the equivalence of these two definitions as an exercise. (Hint: prove equivalence for

³This is, of course, the only correct way to measure angles, as opposed to radians or degrees or some other heresy.

triangles, and then look at Meister's figure again!)

Here is the ray-shooting algorithm in (pseudo)Python. Any similarities with the point-in-polygon algorithm from the previous lecture are purely intentional.

```
def windingNumber(P, o):
    wind = 0
    n = size(P)
    for i in range(n):
        p = P[i]
        q = P[(i+1)%n]
        Delta = (p.x - o.x)*(q.y - o.y) - (p.y - o.y)*(q.x - o.x)
        if p.x <= o.x < q.x && Delta > 0:
            wind += 1
        elif q.x <= o.x < p.x && Delta < 0:
            wind -= 1
    return wind
```

Winding numbers has a third useful interpretation, which we've already seen in this lecture. Case analysis similar to our proof of Lemma ≤ 2 from the previous lecture implies that if o and o' are two points in the same component of $\mathbb{R}^2 \setminus P$, then P has the same winding number around both points. Moreover, if o and o' are in components of $\mathbb{R}^2 \setminus P$ that share a segment of some polygon edge e on their boundary, then the winding numbers around o and o' differ by 1, with the higher winding number to the left of e .

This assignment of winding numbers to the components of $\mathbb{R}^2 \setminus P$ is identical to the Alexander numbering of P that we defined earlier. That is, the winding number of P around any point $q \notin P$ is precisely the number of times that the area around q is counted by the shoelace formula. Thus, the signed area of any polygon P can expressed in terms of winding numbers as

$$\text{area}(P) = \sum_c \text{wind}(P, c) \cdot \text{area}(c)$$

where the sum is over the components of $\mathbb{R}^2 \setminus P$.

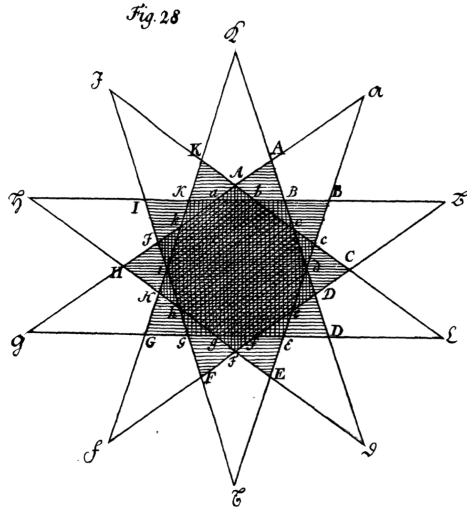


Figure 2.10: Another non-simple polygon from Meister, with winding numbers indicated by shading (1785)

2.4 Homotopy

Now let's go back to the Endless Chain. A bit of case analysis should convince you—or should at least *strongly suggest*—that in all three configurations, the chain is loose around your finger if and only if the winding number of the Chain around your finger is zero.

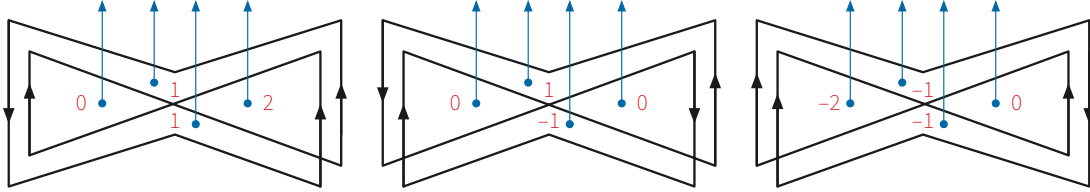


Figure 2.11: Winding numbers of the Endless Chain around various points

But in the actual game, we aren't dealing with a single fixed closed curve. The con man grabs one side of the chain and pulls, causing the chain to move continuously across the barrelhead and around your finger, until it either gets stuck Fast or pulls Loose. Instead of thinking about how a fixed polygon wraps with a changing point, we need a way to reason about how a *continuously changing* curve wraps around a *fixed* point.

A *homotopy* between two closed curves is a continuous deformation—a morph—from one curve to the other. Homotopies can be defined between curves in any topological space, but for purposes of illustration, let's restrict ourselves to curves in the punctured plane $\mathbb{R}^2 \setminus o$, where o is an arbitrary point called the *obstacle*. (In Fast and Loose, the obstacle is your finger.) Without loss of generality, I will assume that o is actually the origin $(0, 0)$.

Formally, a *homotopy* between two closed curves in $\mathbb{R}^2 \setminus o$ is a continuous function $h: [0, 1] \times S^1 \rightarrow \mathbb{R}^2 \setminus o$, such that $h(0, \cdot)$ and $h(1, \cdot)$ are the initial and final closed curves, respectively. For each $0 < t < 1$, the function $h(t, \cdot)$ is the intermediate closed curve at “time” t . Crucially, none of these intermediate curves touches the obstacle point o .

Two closed curves in $\mathbb{R}^2 \setminus o$ are *homotopic*, or in the same *homotopy class*, if there is a homotopy from one to the other in $\mathbb{R}^2 \setminus o$. Homotopy is an equivalence relation.

A closed curve is *contractible* in $\mathbb{R}^2 \setminus o$ if it is homotopic to a single point (or more formally, to a constant curve).

2.5 Vertex moves

Similar to the definition of “connected”, the definition of “homotopy” allows intermediate curves to be arbitrarily wild closed curves even if the initial and final curves are polygons.

Fortunately, there is a general principle that allows us to “tame” homotopies between tame curves like polygons, by decomposing them into a sequence of elementary *moves*. (This principle is similar to the observation that any closed curve can be approximated by a sequence of line segments, otherwise known as a polygon.)

Let P be any polygon. A *vertex move* translates exactly one point p of P along a straight line from its current location to a new location p' , yielding a new polygon P' . As the point p moves, the edges incident to p pivot around their other endpoints. Typically the moving point p is a vertex of the initial polygon P and the final point p' is a vertex of the final polygon P' , but neither of

these restrictions is required by the definition. We are allowed to freely introduce new vertices in the middle of edges, or freely delete “flat” vertices between two collinear edges.

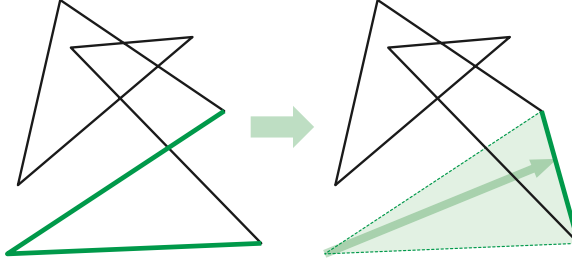


Figure 2.12: A vertex move.

Now suppose the polygon P lives in the punctured place $\mathbb{R}^2 \setminus o$. Let p, q, r be three consecutive vertices of P . The vertex move $q \mapsto q'$ is *safe* if neither of the triangles $\Delta pqq'$ or $\Delta qq'r$ contains the obstacle point o . Equivalently, during a safe vertex move, the continuously changing polygon never touches o .

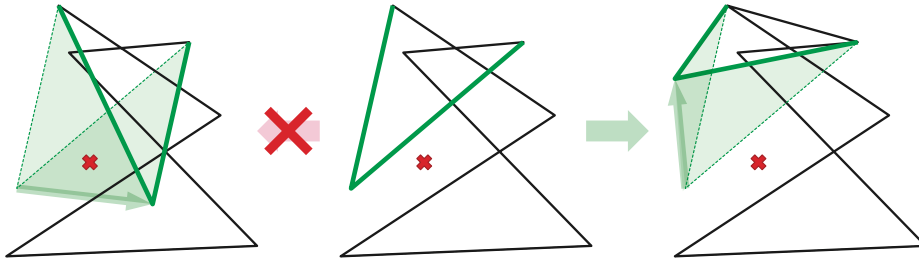


Figure 2.13: An unsafe vertex move and a safe vertex move.

It follows that every safe vertex move is a homotopy in $\mathbb{R}^2 \setminus o$. We can build up more complex homotopies by concatenating several safe vertex moves. In fact, *any* sequence of safe vertex moves describes a homotopy in $\mathbb{R}^2 \setminus o$.

2.6 Polygon homotopies are sequences of vertex moves

Unfortunately, the converse of this observation is false; not every homotopy is a sequence of vertex moves. Consider, for example, a simple translation or rotation of the entire polygon! Nevertheless, every homotopy can be *approximated* by a sequence of safe vertex moves.

Lemma: If two polygons in $\mathbb{R}^2 \setminus o$ are homotopic, then they are homotopic by a sequence of safe vertex moves.

Proof: Fix a homotopy $h: [0, 1] \times S^1 \rightarrow \mathbb{R}^2 \setminus o$ between two polygons $P_0 = h(0, \cdot)$ and $P_1 = h(1, \cdot)$.

For any parameters t and θ , let $d(t, \theta)$ be the Euclidean distance from $h(t, \theta)$ to the origin o , and let $\varepsilon = \min_{t, \theta} d(t, \theta)$. Because the cylinder $[0, 1] \times S^1$ is compact, this minimum is well-defined and positive.

We subdivide the cylinder $[0, 1] \times S^1$ into triangles as follows. First, cut the cylinder into a grid of $\delta \times \delta$ squares $\square(i, j) = [i\delta, (i+1)\delta] \times [j\delta, (j+1)\delta \text{ mod } 1]$, where $\delta > 0$ is chosen so that the diameter of $h(\square(i, j))$ is at most $\varepsilon/2$. (The existence of δ is guaranteed by

continuity.) Then further subdivide each grid square into two right isosceles triangles, as shown in the figure below. Without loss of generality, assume each vertex of P_0 and P_1 the image of some vertex on the boundary of the resulting triangle mesh Δ .

The homotopy h maps any cycle in this mesh to a closed curve, which consists of $O(1/\delta)$ curve segments, each with diameter at most $\epsilon/2$, and each with distance at least ϵ from o . Define a new homotopy $h': [0, 1] \times S^1 \rightarrow \mathbb{R}^2 \setminus o$ that agrees with h at every grid vertex and linearly interpolates within each grid triangle. Changing from h to h' changes the image of any grid cycle by replacing each short curve segment with a straight line segment.

We can easily construct a sequence of $1 + 2/\delta^2$ cycles in Δ that starts with one boundary $0 \times S^1$ and ends with the other boundary $1 \times S^1$, such that the symmetric difference between two adjacent cycles is the boundary of one triangle in Δ . Two adjacent cycles in this sequence are shown on the right in the following figure.

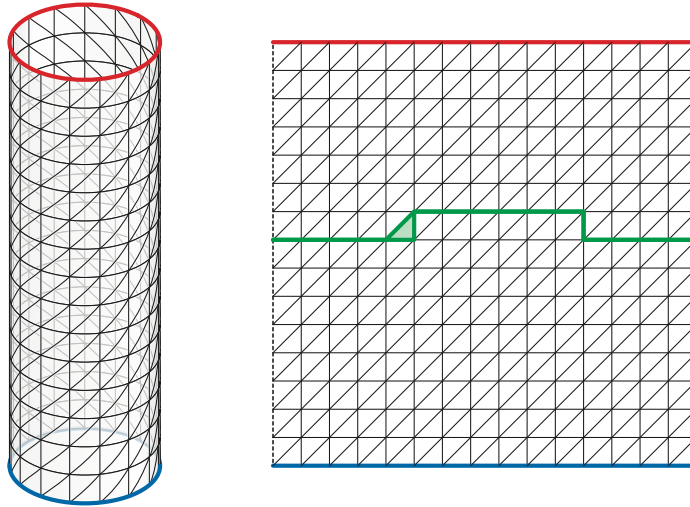


Figure 2.14: A grid on the unit cylinder.

The piecewise-linear homotopy h' maps any two adjacent cycles in this sequence to a pair of polygons P_t and P_{t+1} that differ by a single vertex move. Every vertex of each intermediate polygon has distance at least ϵ from the origin, each edge has length at most $\epsilon/2$, and each vertex move translates its vertex a distance of at most $\epsilon/2$. It follows that every vertex move in this sequence is safe.

We conclude that P_0 can be transformed into P_1 by a sequence of $1 + 2/\delta^2$ safe vertex moves.

This lemma is a special case of a more general *simplicial approximation theorem*, which intuitively states that any continuous map between *nice* topological spaces (formally, geometric simplicial complexes) can be approximated by a *nice* continuous map (formally, simplicial maps between finite subdivisions of the original complexes); moreover, the original map can be continuously deformed to its approximation.

2.7 Homotopy Invariant

Winding numbers are our first example of a *topological invariant*, and specifically a *complete homotopy invariant*. A topological invariant is any property of objects or spaces that is unchanged by some form of topological equivalence. One simple example is the number of components of a subset of the plane; another standard example is the *genus* of a surface. A *homotopy invariant* is any property that is preserved by homotopy; a homotopy invariant is *complete* if it takes on different values for two objects that are not homotopic.

Theorem: Two polygons are homotopic in $\mathbb{R}^2 \setminus o$ if and only if they have the same winding number around the origin o . Thus, winding number is a complete homotopy invariant for polygons in $\mathbb{R}^2 \setminus o$.

Proof: Fix two polygons P_0 and P_1 in $\mathbb{R}^2 \setminus o$. If these two polygons are homotopic, then by the previous lemma, they are connected by a sequence of safe triangle moves. A safe triangle move does not change the winding number of a polygon around the origin. Thus, by induction, P_0 and P_1 have the same winding number.

To prove the converse, I'll describe a sequence of safe triangle moves that transforms any polygon P into a *canonical* polygon \diamond^w with the same winding number w around the origin. (The notation \diamond^w will make sense later, honest.) Thus, if P_0 and P_1 have the same winding number w , we can deform P_0 into P_1 by concatenating the move sequence that takes P_0 to \diamond^w and the reverse of the move sequence that takes P_1 to \diamond^w .

Our homotopy consists of several stages. First let's consider the case where the winding number of P around 0 is not zero.

- Let p_i be any vertex of P , and let p_{i-1} and p_{i+1} be the next and previous vertices. We call q *redundant* if the triangle $\Delta p_{i-1}p_ip_{i+1}$ does not contain the origin. In particular, if the triples (o, p_{i-1}, p_i) and (o, p_i, p_{i+1}) have opposite orientations, one clockwise and the other counterclockwise, then p_i is redundant. In the first phase of our homotopy, we repeatedly remove redundant vertices, by moving each redundant vertex q to one of its neighbors, until none are left. The resulting polygon P' is *angularly monotone*: every triple (o, p_i, p_{i+1}) has the same orientation.

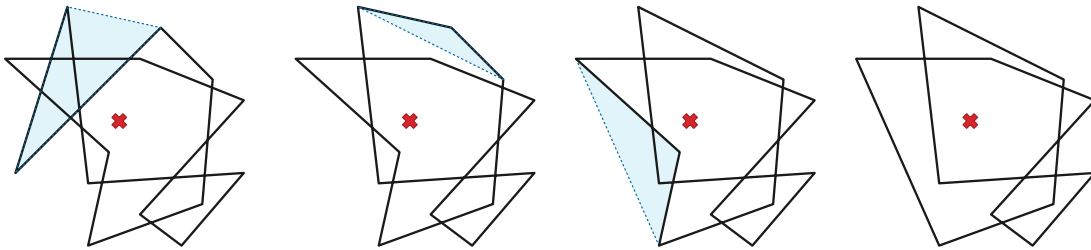


Figure 2.15: Removing three redundant vertices

- Next, we subdivide P' by adding vertices at its intersections with rays pointing up, down, left, and right from the origin o . After this subdivision, any vertex that is *not* on one of these rays is redundant. So in the second phase of the homotopy, we remove all non-ray vertices using safe vertex moves. The resulting polygon P'' is still angularly monotone.
- Finally, we move each vertex so that its distance from the origin is 1; each of these

vertex moves is safe. The resulting polygon \diamond^w has vertices only at the points $(0, 1)$, $(1, 0)$, $(0, -1)$, and $(-1, 0)$; the polygon winds around this diamond $|w|$ times, counterclockwise if $w > 0$ and clockwise if $w < 0$.

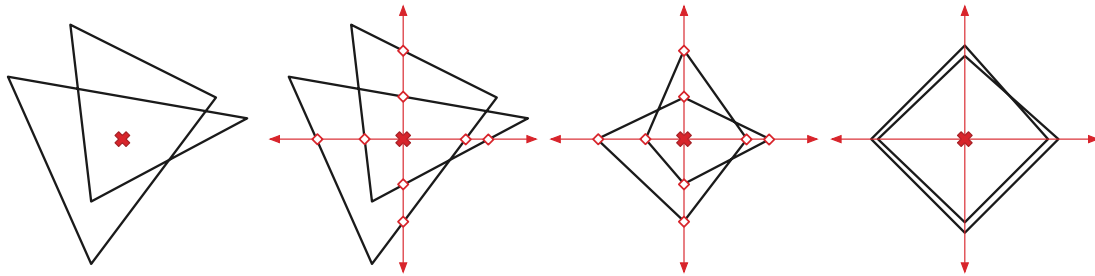


Figure 2.16: Making an angularly monotone polygon canonical

The special case where P has winding number 0 is even simpler. The first phase (removing redundant vertices) actually reduces P to a single point; we can then translate this point to $\diamond^0 = (1, 0)$ using one more safe vertex move.

This theorem immediately implies a linear-time algorithm to decide if two polygons are homotopic in the punctured plane: Count positive and negative crossings between each polygon and an arbitrary ray from the origin.

2.8 ... and the Aptly Named Sir Not Appearing in This Film

- rotation number = total turning angle = smiles – frowns
- regular homotopy = vertex moves without spurs
- rotation number is a regular homotopy invariant
- complex root finding / fundamental theorem of algebra
- signed volumes of self-intersecting polyhedra (hic utres unilaterales nascuntur)

2.9 References

1. James W. Alexander. Topological invariants of knots and links. *Trans. Amer. Math. Soc.* 30(2):275–306, 1928. The reason we call it “Alexander numbering”.
2. Brian Brushwood. Fast and Loose. YouTube, October 19, 2015.
3. Brian Brushwood. Pricking the Garter.. YouTube, June 26, 2017.
4. Albrecht Ludwig Friedrich Meister. Generalia de genesi figurarum planarum, et independentibus earum affectionibus. *Novi Commentarii Soc. Reg. Scient. Gott.* 1:144–180 + 9 plates, 1769/1770. Presented January 6, 1770. The shoelace formula.
5. August F. Möbius. Über der Bestimmung des Inhaltes eines Polyéders. *Ber. Sächs. Akad. Wiss. Leipzig, Math.-Phys. Kl.* 17:31–68, 1865. *Gesammelte Werke* 2:473–512, Liepzig, 1886. An earlier appearance of Alexander numbering.

Chapter 3

Homotopy Testing^β

3.1 Multiple Obstacles

Now let's generalize the homotopy problem from the last lecture to the case of more than one obstacle. Let $O = \{a, b, c, \dots\}$ be an arbitrary finite set of points in the plane. The definitions of homotopy and contractible easily generalize to polygons (and other closed curves) in $\mathbb{R}^2 \setminus O$. How quickly can we tell whether two polygons in $\mathbb{R}^2 \setminus O$ are homotopic?

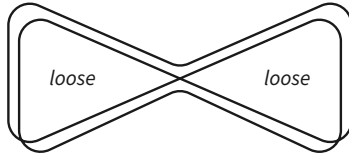


Figure 3.1: The Endless Chain again

The game Fast and Loose shows some of the subtlety of this problem. Let a and b be arbitrarily points in each of the two loops of the curve C that the con artist actually uses. It's not hard to see that $\text{wind}(c, a) = \text{wind}(C, b) = 0$; any ray upward from either a or b has one positive crossing and one negative crossing. Thus, the curve is contractible in the plane with only *one* of these punctures; in other words, the chain is loose if we only use one finger. But the curve C is *not* contractible in $\mathbb{R}^2 \setminus \{a, b\}$; we can hold the chain fast by placing a finger in each loop. Winding numbers are *not* a homotopy invariant when there is more than one obstacle.

Just as in the one-obstacle setting, we can (approximately) decompose any homotopy between two polygons in $\mathbb{R}^2 \setminus O$ into safe vertex moves, where now a vertex move is *safe* if the moving vertex and its incident edges avoids *all* points in O . Essentially the same argument from the previous lecture implies the following:

Theorem: Two polygons in $\mathbb{R}^2 \setminus O$ are homotopic if and only if they are connected by a sequence of safe vertex moves.

3.2 Crossing Sequences

However, we can still define a homotopy invariant by shooting rays out of *every* obstacle, and recording how the polygon intersects these rays. Specifically, we record not only the *number* of times the polygon crosses each ray, but the actual order and directions of these crossings.

As usual, we will assume without loss of generality that the obstacles have distinct x -coordinates. Shoot a vertical ray upward from each obstacle point; I'll call these vertical rays *fences*. The *crossing sequence* of a polygon P in $\mathbb{R}^2 \setminus O$ is the sequence of intersections between the fences and the polygon, in order along the polygon, along with the sign of each crossing (positive if the polygon crosses the fence to the left, negative if the polygon crosses the fence to the right).

Figure 2 shows a polygon in the plane with two obstacle points a and b . If we orient the polygon as indicated by the arrows, starting at the lower left corner, the crossing sequence is **BAabBAabB**, where each upper-case letter denotes a positive crossing through the corresponding fence, and each lower-case letter denotes a negative crossing through the corresponding fence.

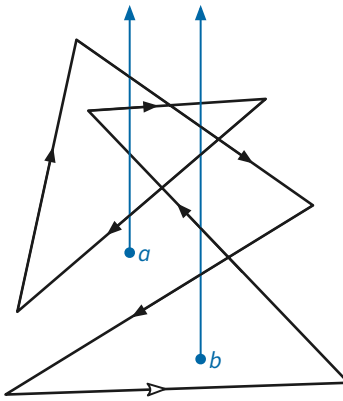


Figure 3.2: A polygon with crossing sequence BAabBAabB

Lemma: Two polygons in $\mathbb{R}^2 \setminus O$ with the same crossing sequence are homotopic.

Proof: I'll describe a homotopy that transforms any polygon P into a *canonical* polygon with the same crossing sequence. (With more care, the homotopy can be described explicitly as a sequence of safe vertex moves.)

First, we define two new *sentinel* points a^\flat and a^\sharp just above and on either side of each obstacle a . These points are close enough to a that no vertex of P , no other obstacle, and no other sentinel point lies on or between the vertical lines through a^\flat and a^\sharp .

Next, we *divert* edges through the sentinel points, by adding two additional vertices near each intersection between P and any fence, and then moving those new vertices to the sentinel points near the corresponding obstacle.

- If the original edge crosses a 's fence from right to left (a positive crossing), the diverted edge passes through sentinel points a^\sharp and a^\flat in that order.
- If the original edge crosses a 's fence from left to right (a negative crossing), the diverted edge passes through sentinel points a^\flat and a^\sharp in that order.

See Figure 3. The resulting polygon P' has the same crossing sequence as the original polygon P .

Finally, we divert the rest of the polygon to a single point far below any obstacle. First we add a new vertex at the midpoint of each edge of P' between two sentinel points of different obstacles. Then we choose a point z sufficiently far below the polygon and the sentinel points that for any polygon vertex p , the segment zp does not cross any of the fences. Finally, we move every vertex of P' that is *not* a sentinel point directly to this new bottom point z . Again, this deformation does not change the polygon's crossing sequence.

The resulting canonical polygon P'' is a concatenation of loops of the form $za^b a^\# z$ (for each negative crossing) or $za^\# a^b z$ (for each positive crossing).

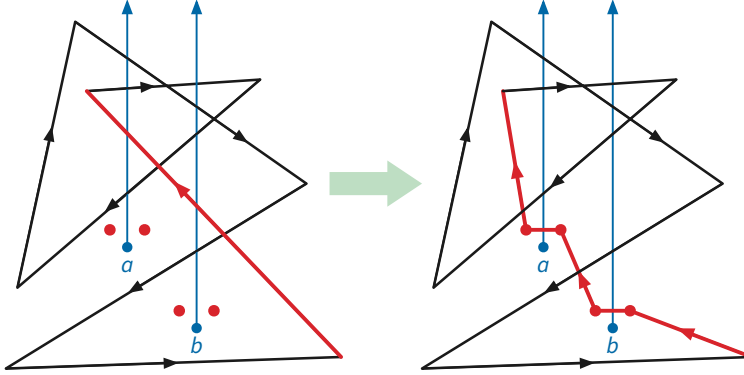


Figure 3.3: Diverting one edge of a polygon

Corollary: Any polygon in $\mathbb{R}^2 \setminus O$ with an empty crossing sequence is contractible.

Unfortunately, the converses of these two results are false; a homotopy that moves one polygon vertex across one fence either inserts or deletes a pair of crossings in the polygon's crossing sequence. Thus, crossing sequences are not homotopy invariants. Fortunately, this is the *only* way that a homotopy can change the crossing sequence.

3.3 Reductions

We regard signed crossing sequences as strings of abstract symbols, where each symbol a has a formal “inverse” \bar{a} . In our earlier example, each upper case letter is the inverse of the corresponding lower-case letter, and vice versa. Let $x \cdot y$ denote the concatenation of strings x and y , and let ε denote the empty string.

An *elementary reduction* is a transformation of the form $x \cdot a\bar{a} \cdot y \mapsto x \cdot y$, where x and y are (possibly empty) strings and a is a single symbol. An *elementary expansion* is the reverse transformation $x \cdot y \mapsto x \cdot a\bar{a} \cdot y$. Two strings are *equivalent* if once can be transformed into the other by a sequence of elementary reductions and expansions. (Check for yourself that equivalence is in fact an equivalence relation!) We call a string *trivial* if it is equivalent to the empty string ε . Finally, a string is *reduced* if no elementary reductions are possible; for example, the empty string ε is trivially reduced, as is any string of length 1.

Crossing sequences of polygons are actually *cyclic* strings. Formally, a cyclic string is an equivalence class of linear strings:

$$(w) := \{y \cdot x \mid x \cdot y = w\}$$

For example, $(ABbA) = \{ABbA, BbAA, bAAB, AABb\}$ and $(\varepsilon) = \{\varepsilon\}$. I'll write $w \sim z$ to denote that w is a cyclic shift of z , or equivalently $w \in (z)$, or equivalently $z \in (w)$. To emphasize that

elementary reductions can “wrap around” cyclic strings, we say that a cyclic string is *cyclically reduced* if no elementary reductions are possible. A (cyclic) string is *trivial* if it is equivalent to the empty (cyclic) string.

For example, the cyclic string (EcaCbaABcEeEeAdbcCBaEdDeADCe) is trivial; two different sequences of elementary reductions are shown below (using interpuncts to represent missing symbols). In the first sequence, each elementary reduction removes the *leftmost* matching pair; the second sequence is more haphazard. In fact, as the following lemma implies, *any* sequence of elementary reductions eventually reduces this string to nothing.

```

EcaCbaABcEeEeAdbcCBaEdDeADCe
EcaCb··BcEeEeAdbcCBaEdDeADCe
EcaC····cEeEeAdbcCBaEdDeADCe
Eca·····EeEeAdbcCBaEdDeADCe
Eca·····EeAdbcCBaEdDeADCe
Eca·····AdbcCBaEdDeADCe
Ec·····dbcCBaEdDeADCe
Ec·····db··BaEdDeADCe
Ec·····d···aEdDeADCe
Ec·····d···aE··eADCe
Ec·····d···a···ADCe
Ec·····d···DCE
Ec·····Ce
E·····e
······
EcaCbaABcEeEeAdbcCBaEdDeADCe
EcaCbaABcEeEeAdb··BaEdDeADCe
EcaCb··BcEeEeAdb··BaEdDeADCe
·caCb··BcEeEeAdb··BaEdDeADC·
·caC···cEeEeAdb··BaEdDeADC·
·caC···cE··eAdb··BaEdDeADC·
·caC···cE··eAdb··BaE··eADC·
·caC···cE··eAdb··Ba···ADC·
·caC···cE··eAd···a···ADC·
··aC···cE··eAd···a···AD··
··aC···c···Ad···D··
··a···Ad···D··
··a···A···
······

```

Lemma: Every cyclic string is equivalent to exactly one cyclically reduced cyclic string.

Proof: Let w be a cyclic string that allows two elementary reductions $w \mapsto x$ and $w \mapsto y$, meaning two different pairs of symbols are deleted. We claim that either $x = y$ or there is another string z such that $x \mapsto z$ and $y \mapsto z$ are elementary reductions.

- If the pairs of symbols deleted by $w \mapsto x$ and $w \mapsto y$ are disjoint, then we can write $w = (a\bar{a} \cdot w_1 \cdot c\bar{c} \cdot w_2)$ for some (possibly empty) linear strings w_1 and w_2 and (possibly equal, possibly inverse) symbols a and c . Without loss of generality we have

$x = (w_1 \cdot c\bar{c} \cdot w_2)$ and $y = (w_2 \cdot a\bar{a} \cdot w_1)$. In this case, we can take $z = (w_1 w_2)$.

- If the pairs of symbols deleted by $w \mapsto x$ and $w \mapsto y$ overlap, then we can write $w = (a\bar{a}a \cdot w')$ for some (possibly empty) linear string w' and some symbol a . In this case we have $x = y = (a \cdot w')$.

It follows that applying *only* elementary reductions leads to a unique reduced string; however, equivalence also allows elementary *expansions*. Consider two equivalent but distinct cyclic strings $x \neq y$, and let $x = w_1 \leftrightarrow w_2 \leftrightarrow \dots \leftrightarrow w_n = y$ be a sequence of strings, each connected to its success by an elementary reduction in one direction $w_i \mapsto w_{i+1}$ or the other $w_{i+1} \mapsto w_i$.

Suppose for some index i , we have reductions $w_i \mapsto w_{i-1}$ and $w_i \mapsto w_{i+1}$. If $w_{i-1} = w_{i+1}$, then we can remove w_{i-1} and w_i to obtain a shorter transformation sequence. Otherwise, there is another string z_i such that $w_{i-1} \mapsto z_i$ and $w_{i+1} \mapsto z_i$. Thus, by induction, we can modify our transformation sequence so that every reduction appears before every expansion.

Let z be the shortest string in this normalized sequence. Both x and y can be reduced to z using only elementary reductions. Because $x \neq y$, either $x \neq z$ or $y \neq z$; we conclude that at most one of x and y is reduced.

Lemma: Any cyclic crossing sequence of length x can be cyclically reduced in $O(x)$ time.

Proof: The following (pseudo-)python code assumes the input X is an array of non-zero integers, with inverses indicated by negation. The algorithm runs in two phases. The first phase reduces the *linear* sequence X by repeatedly removes the leftmost matching pair, using the output array as a stack. The second phase performs any remaining cyclic reductions that “wrap around” the ends of the array.

```
def LeftGreedyReduce(X):
    n = size(X)
    Y = [0] * n                                // reduced sequence = stack
    top = -1                                     // top stack index
    // _____ linear reduction _____
    for i in range(n):
        if top < 0 || (X[i] != -Y[top]):          // empty or no match
            top = top + 1
            Y[top] = X[i]                         // push
        else:
            top = top - 1                         // pop
    // _____ cyclic reduction _____
    bot = 0
    while (bot < top) and (Y[bot] = -Y[top]):
        bot = bot + 1
        top = top - 1
    // _____ done! _____
    return Y[bot:top+1]
```

Lemma: Two polygons are homotopic in $\mathbb{R}^2 \setminus O$ if and only if their crossing sequences are equivalent.

Proof (sketch): A single safe vertex move changes the signed crossing sequence by a finite number of elementary reductions and their inverses, at most one per obstacle.

Conversely, any elementary reduction of the signed crossing sequence can be modeled by a sequence of safe vertex moves, performed either directly on the original polygon or (more easily) on the canonical polygon with the same crossing sequence.

We finally have all the ingredients of our homotopy-testing algorithm.

Theorem: For any set O of k points in \mathbb{R}^2 , and any two n -gons P and Q in $\mathbb{R}^2 \setminus O$, we can determine whether P and Q are homotopic in $\mathbb{R}^2 \setminus O$ in $O(k \log k + kn)$ time.

Proof (sketch): As usual we assume without loss of generality that the obstacles and polygon vertices all have distinct x -coordinates. First we sort the obstacles from left to right in $O(k \log k)$ time. Then we compute the crossing sequence of P and Q , in constant time per crossing, plus constant time per vertex. Each crossing sequence has length $O(nk)$. Then we cyclically reduce the two crossing sequences in $O(nk)$ time. Finally, we check whether the two reduced crossing sequences are equal (as *cyclic* strings) in linear time using Knuth-Morris-Pratt (or any other fast string-matching algorithm).

Let me emphasize here that the algorithm does not construct an explicit homotopy between the two polygons.

3.4 Variations

To be written

- Polygons with holes: Replace each hole with a sentinel point.
- Paths:
 - Paths, concatenation, reversal, loops, path homotopy
 - Two paths π and σ are homotopic if and only if the loop $\pi \cdot \bar{\sigma}$ is contractible.
 - Two polygonal paths P and Q are homotopic if and only if they have the same (**not** cyclically) reduced crossing sequence.

3.5 ... and the Aptly Named Sir Not Appearing in This Film

- alternative fences: vertical lines, spanning tree + ray
- picture hanging puzzles

Chapter 4

Faster Homotopy Testing^β

In the previous lecture, we saw an algorithm to decide if one polygon is contractible, or if two polygons are homotopic, in the plane with several points removed. The algorithm runs in $O(k \log k + nk)$ time, where k is the number of obstacle points; in the worst case, this running time is quadratic in the input size.

A running time of $\Omega(nk)$ is inevitable if we are required to compute an explicit reduced crossing sequence; consider the polygon and obstacles below. But if a polygon is *contractible*—homotopic to a single point—its reduced crossing sequence is empty. Similarly the (non-reduced) crossing sequence of a polygon can have length $\Omega(nk)$, even if the polygon is contractible, but nothing requires us to compute explicit crossing sequences!

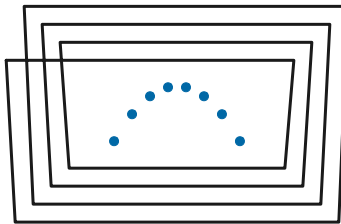


Figure 4.1: A polygon and obstacles with a long reduced crossing sequence

In this lecture, I'll describe another algorithm to test contractibility of polygons in punctured planes, which is faster either when the polygon has few self-intersections or when the number of obstacles is significantly larger than the number of polygon vertices. This algorithm is based on an algorithm of Cabello et al. [1], with some improvements by Efrat et al. [2]. Variations of this algorithm compute reduced crossing sequences *without* explicitly computing non-reduced crossing sequences first.

The key observation is that we are free to modify *both* the polygon *and* the obstacles, as long as our modifications do not change the reduced crossing sequence. In short, we are solving a *topology* problem, so we should feel free to choose whatever *geometry* is most convenient for our purposes.

To make the following discussion concrete, let O be an arbitrary set k of obstacle points in the plane, and let P be an arbitrary n -vertex polygon in $\mathbb{R}^2 \setminus O$. As usual, we assume these objects are in *general position*: no two interesting points (obstacles, polygon vertices, or self-intersection

points) lie on a common vertical line, and no three polygon vertices lie on a common line. In particular, no edge of P is vertical, and every point where P self-intersects is a transverse intersection between two edges. This assumption can be enforced with probability 1 by randomly rotating the coordinate system and randomly perturbing the vertices.

4.1 Trapezoidal decomposition

This first stage of our algorithm, like our earlier polygon triangulation algorithm, first constructs a *trapezoidal decomposition* of the input. We define the decomposition by extending vertical segments, which we call *fences*, upward and downward from each obstacle, from each vertex of P , and from each self-intersection point of P , until they hit edges of P (or escape to infinity). These fences, together with the edges of P , decompose the plane into trapezoids, some of which are unbounded and others degenerate. See Figure 2.

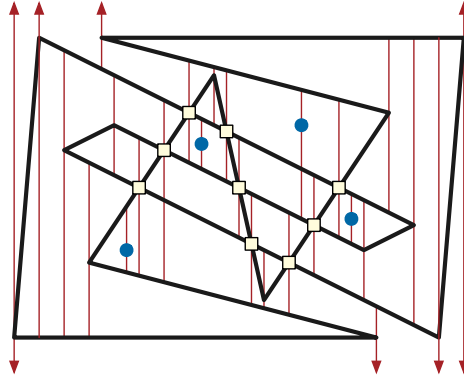


Figure 4.2: A trapezoidal decomposition of a self-intersecting polygon and four obstacles

A classical sweepline algorithm of Bentley and Ottmann constructs this decomposition in $O((n + k + s) \log(n + k))$ time, where s is the number of self-intersection points. (There are several faster algorithms, especially when the number of self-intersections is small, but the Bentley-Ottmann algorithm is much simpler to describe and implement, and using these faster alternatives would not significantly improve the overall running time of our contractibility algorithm.)

Think of the n polygon edges and k obstacle points as $n + k$ line segments (k of which have length zero). Any vertical line intersects t most $n + 1$ of these segments. The Bentley-Ottman algorithm sweeps a vertical line ℓ across the plane, maintaining the sorted sequence of segments intersecting ℓ in a balanced binary search tree, so that segments can be inserted or deleted in $O(\log n)$ time. The x -coordinates where this intersection sequence changes are called *events*; there are two types of events:

- *vertex events*, where ℓ passes through a vertex of P or a point in O , and
- *intersection events*, where ℓ passes through a self-intersection point of P .

The algorithm processes these events in order from left to right.

The vertices and obstacles are all known in advance, so after an initial $O((n + k) \log(n + k))$ sorting phase, it is easy to find the next vertex event. Intersections are *not* known in advance, and computing them by brute force in $O(n^2)$ time would take too long. Instead, we observe that the *next* intersection event must occur at the intersection of two consecutive segments along ℓ .

Thus, for each consecutive pair of segments that intersects to the right of ℓ , we have a *potential* intersection event. We maintain these $O(n)$ potential intersection events in a priority queue, so that we can find the next *actual* intersection event in $O(\log n)$ time.

At each event, we insert a single fence, perform $O(1)$ binary-tree operations to maintain the intersection sequence with ℓ , and then perform $O(1)$ priority-queue operations. There are $O(n+k+s)$ events, each requiring $O(\log n)$ time, so including the initial sort, the overall running time is $O((n+k+s)\log(n+k))$.

As a by-product of the sweep-line algorithm, we obtain the complete list of self-intersection points. We subdivide P by introducing two coincident vertices at each self-intersection point, increasing the number of vertices from n to $n+2s$, and ensuring that the edges of P intersect only at vertices.

4.2 Vertical and horizontal ranks

Next, we replace P and O with a new *orthogonal* polygon \bar{P} and a new set of obstacles \bar{O} that define exactly the same crossing sequence. At a high level, we replace each edge of P with a horizontal line segment and each vertex of P with a vertical line segment.

The y -coordinates of the horizontal segments are determined by the following *vertical ranking* of the polygon edges and obstacle points. Let S be the set of $m = n + 2s + k$ interior-disjoint segments, consisting of the subdivided edges of P and the obstacles O . For any two segments σ and τ in S , write $\sigma \uparrow\!\!\uparrow \tau$ (and say “sigma is above tau”) if there is a vertical segment with positive length whose upper endpoint lies on σ and whose lower endpoint lies on τ .

Lemma: For any set S of interior-disjoint non-vertical line segments, the $\uparrow\!\!\uparrow$ relation is acyclic.

Proof: For the sake of argument, let $\sigma_1 \uparrow\!\!\uparrow \sigma_2 \uparrow\!\!\uparrow \cdots \uparrow\!\!\uparrow \sigma_r \uparrow\!\!\uparrow \sigma_1$ be a minimum-length cycle of segments in S . Obviously $r \geq 2$, because no segment is above itself. Similarly, $r \geq 3$, because $\sigma_1 \uparrow\!\!\uparrow \sigma_2$ and $\sigma_2 \uparrow\!\!\uparrow \sigma_1$ would imply that σ_1 and σ_2 have intersecting interiors.

Rotate the indices if necessary, so that the right endpoint of σ_1 has strictly smaller x -coordinate than the right endpoint of any other segment σ_i in the cycle. In particular, the right endpoints of σ_2 and σ_r are both strictly to the right of σ_1 . Thus, the right endpoint of σ_1 is both directly above some point of σ_2 and directly below some point of σ_r . It follows that $\sigma_r \uparrow\!\!\uparrow \sigma_2$, which contradicts the minimality of the cycle.

Now write $\sigma \uparrow \tau$ (and say “sigma is *immediately* above tau”) of some fence in the trapezoidal decomposition of S touches both σ and τ , and in particular touches σ above the point where it touches τ . Because $\sigma \uparrow \tau$ immediately implies $\sigma \uparrow\!\!\uparrow \tau$, the relation \uparrow is also acyclic; in fact, our earlier relation $\uparrow\!\!\uparrow$ is the transitive closure of \uparrow . We can easily extract a directed acyclic graph G^\uparrow representing the relation \uparrow (and thus its transitive closure $\uparrow\!\!\uparrow$) directly from the trapezoidal decomposition of S .

(Any linear extension of $\uparrow\!\!\uparrow$ is called a *vertical shelling order* of D ; the previous lemma implies that such an order always exists.)

Now index the segments $S = \{\sigma_1, \sigma_2, \dots, \sigma_m\}$ according to an arbitrary topological ordering of the graph G^\uparrow , so that $\sigma_i \uparrow\!\!\uparrow \sigma_j$ implies $i < j$. For any segment σ_i , let $\text{obsbelow}(\sigma_i)$ denote the number of obstacle segments σ_j such that $j < i$. Finally, we define the *vertical rank* $\text{vrank}(\sigma_i)$ as follows:

- If σ_i is a polygon segment, then $\text{vrank}(\sigma_i) = 2 \cdot \text{obsbelow}(\sigma_i)$.
- If σ_i is an obstacle segment, then $\text{vrank}(\sigma_i) = 2 \cdot \text{obsbelow}(\sigma_i) + 1$.

Thus, all vertical ranks are integers between 0 and $2k$, every obstacle has odd vertical rank, and every polygon edge has even vertical rank.

We also define the *horizontal rank* of any polygon vertex or an obstacle point p as follows. Let $\text{obsleft}(p)$ to be the number of obstacles with strictly smaller x -coordinates than p .

- If p is a polygon vertex, then $\text{hrank}(p) = 2 \cdot \text{obsleft}(p)$.
- If p is an obstacle point, then $\text{hrank}(p) = 2 \cdot \text{obsleft}(p) + 1$.

Thus, all horizontal ranks are integers between 0 and $2k$, every obstacle has odd horizontal rank, and every polygon vertex has even horizontal rank.

4.3 Rectification

Now we define a *rectified* polygon \bar{P} and new obstacles \bar{O} as follows:

- Replace each edge pq of P with a horizontal segment between $(\text{hrank}(p), \text{vrank}(pq))$ and $(\text{hrank}(q), \text{vrank}(pq))$. Similarly, replace each vertex q of P , with adjacent edges pq and qr , with a vertical segment between $(\text{hrank}(q), \text{vrank}(pq))$ and $(\text{hrank}(q), \text{vrank}(qr))$. Connecting these horizontal and vertical segments in sequence around P gives us an orthogonal polygon \bar{P} .
- For each obstacle o , let $\bar{o} = (\text{hrank}(o), \text{vrank}(o))$. The set of all such points is our new obstacle set \bar{O} .

By construction, every vertex of \bar{P} has even integer coordinates, and every obstacle in \bar{O} has odd integer coordinates, so \bar{P} is a polygon in $\mathbb{R}^2 \setminus \bar{O}$. Moreover, the crossing sequence of the rectified polygon \bar{P} with respect to the new obstacles \bar{O} is *identical* to the crossing sequence of the original polygon P with respect to the original obstacles O . Thus, P is contractible in $\mathbb{R}^2 \setminus O$ if and only if \bar{P} is contractible in $\mathbb{R}^2 \setminus \bar{O}$.

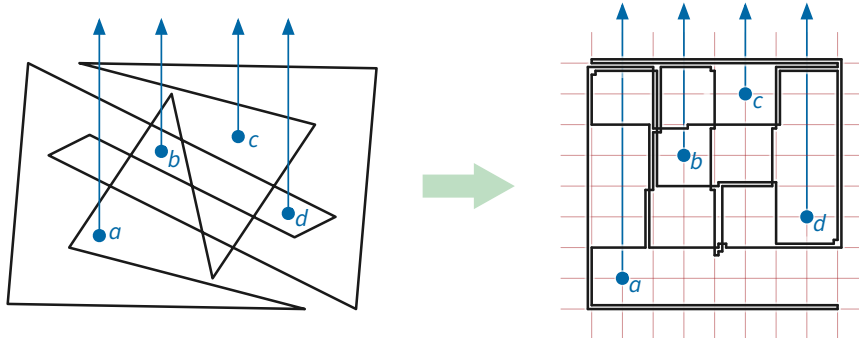


Figure 4.3: A polygon and its rectification (perturbed to show overlapping and zero-length edges) defining the same (trivial) crossing sequence abdDCBAabcdAaDBA

It is actually possible to construct an explicit deformation of P and O into \bar{P} and \bar{O} , as a sequence of elementary moves of two types: safe vertex moves (translate a vertex of P without touching any obstacle) and “safe obstacle moves” (translate one obstacle in O without touching P). Moreover, we can guarantee that throughout the entire deformation, the crossing sequence of the polygon

with respect to the obstacles remains unchanged. Fortunately, we don't actually need an explicit homotopy; the invariance of the crossing sequence is enough.

4.4 Reduction

So why did we go through this madness? We have now reduced our problem from *arbitrary* polygons to particularly well-behaved *orthogonal* polygons. Restricting to orthogonal polygons allows us to represent and manipulate the crossing sequence of \bar{P} *implicitly* using relatively simple data structures.

Let $\bar{n} = 2n + 4s$ denote the number of vertices in the rectified polygon \bar{P} . Without loss of generality, we can assume that the i th edge $\bar{p}_i\bar{p}_{i+1}$ of \bar{P} is horizontal if i is even and vertical if i is odd. Thus, we can represent \bar{P} itself using an alternating sequence of x - and y -coordinates:

$$x_0, y_1, x_2, y_3, \dots, x_{\bar{n}-2}, y_{\bar{n}-1},$$

where $\bar{p}_i = (x_i, y_{i+1})$ if i is even, and $\bar{p}_i = (x_{i+1}, y_i)$ if i is odd. We store these coordinates in any data structure that allows us to change one coordinate or remove any adjacent pair of coordinates $x_i, y_{i\pm 1}$ in $O(1)$ time—for example, a circular doubly-linked list.

We now *reduce* \bar{P} by repeatedly applying two operations, called *eliding* and *sliding*, which simplify the polygon without changing its homotopy class. Each operation requires $O(\log k)$ time, and the reduction requires at most $O(\bar{n})$ of these operations, so the overall reduction time is $O(\bar{n} \log k) = O((n+s) \log k)$. If the reduced polygon is *empty*, we correctly report that P is contractible; otherwise, we correctly report that P is not contractible.

4.4.1 Eliding Zero-Length Edges

This makes the pictures nicer, but it isn't actually necessary; consider removing.

The rectified polygon \bar{P} can contain edges with length zero; we *elide* (that is, remove) all such edges in a preprocessing phase. Geometrically, there are two types of zero-length edges:

- A *bump* is a zero-length edge whose previous and next edges have the same orientation. Removing a bump merges the previous and next edges into a single edge.
- A *spur* is a zero-length edge whose previous and next edges do overlap. Removing a spur replaces those two edges with their *difference*, which could have length zero, making more elisions possible.

However, our representation of \bar{P} as a list of alternating x - and y -coordinates allows us to treat these two cases identically in $O(1)$ time. To remove the zero-length edge edge $\bar{p}_{i-1}\bar{p}_i$, we delete the $(i-1)$ th and i th coordinates from our coordinate list. Specifically:

- if i is odd, so $y_{i-1} = y_{i+1}$ and the zero-length edge is “horizontal”, we delete y_{i-1} and x_i .
- If i is even, so $x_{i-1} = x_{i+1}$ and the zero-length edge is “vertical”, we delete x_{i-1} and y_i .

Equivalently, we can remove any zero-length edge $\bar{p}_{i-1}\bar{p}_i$ using two safe vertex moves:

- First (formally) move \bar{p}_{i-1} to \bar{p}_i , merging those two vertices.
- Then move \bar{p}_i either \bar{p}_{i-2} and \bar{p}_{i+1} , whichever is closer. It follows that removing a zero-length edge does not change the homotopy class of \bar{P} .

We can remove all zero-length edges from \bar{P} in $O(\bar{n})$ time using a “left-greedy” algorithm similar to the crossing-word reduction algorithm in the previous lecture.

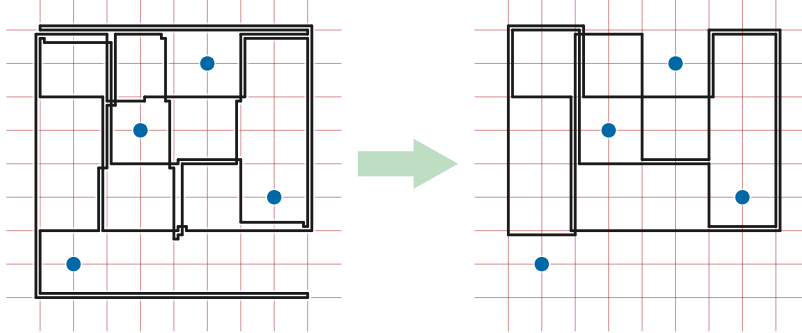


Figure 4.4: Eliding all zero-length edges in the rectified polygon

4.4.2 Sliding Brackets

We call a positive-length edge of \bar{P} a *bracket* if both of its neighboring edges are on the same side of the line through the edge. That is, the edge and its neighbors look like \sqcup , \sqsubset , \sqcap , or \sqsupset . *Sliding* a bracket moves it as far inward as possible, shortening the neighboring edges, until at least one of two conditions is met:

- The bracket has distance 1 from an obstacle inside the bracket; we call such a bracket *frozen*. Sliding a frozen bracket further would change the crossing sequence of \bar{P} by either adding or deleting a *single* crossing, thereby changing the homotopy class.
- At least one of the edges adjacent to the bracket has length zero, which we can safely elide, just as in the previous phase. (If the zero-length edge is a spur, several elisions may be required to ensure that all edges have positive length.)

Sliding a bracket requires changing exactly one coordinate in our alternating coordinate list, and then deleting zero or more pairs of coordinates (to elide zero-length edges created by the slide).

The reduction algorithm ends either when all remaining brackets are frozen (and all edges have positive length), or when no edges are left at all. For example, if \bar{P} is a rectangle that doesn’t contain any obstacles, the first bracket slide creates two zero-length edges; eliding these edges removes every edge from the polygon.

Because each bracket slide (and ensuing elisions) either freezes a bracket or decreases the number of polygon vertices, the reduction ends after at most $O(\bar{n})$ bracket slides. (A bracket slide can *increase* the number of polygon *self-intersections*, but we don’t care about that; we only needed to find self-intersections so that we could compute vertical ranks.) The figure on the next page shows a sequence of bracket slides contracting a rectified cycle.

The correctness of this algorithm rests on the following lemma.

Lemma: The rectified polygon \bar{P} is contractible in $\mathbb{R}^2 \setminus \bar{O}$ if and only if it reduces to a single point.

Proof: One direction is easy: Every sequence of elisions and bracket slides is a homotopy. Thus, if \bar{P} reduced to a single point, it must be contractible.

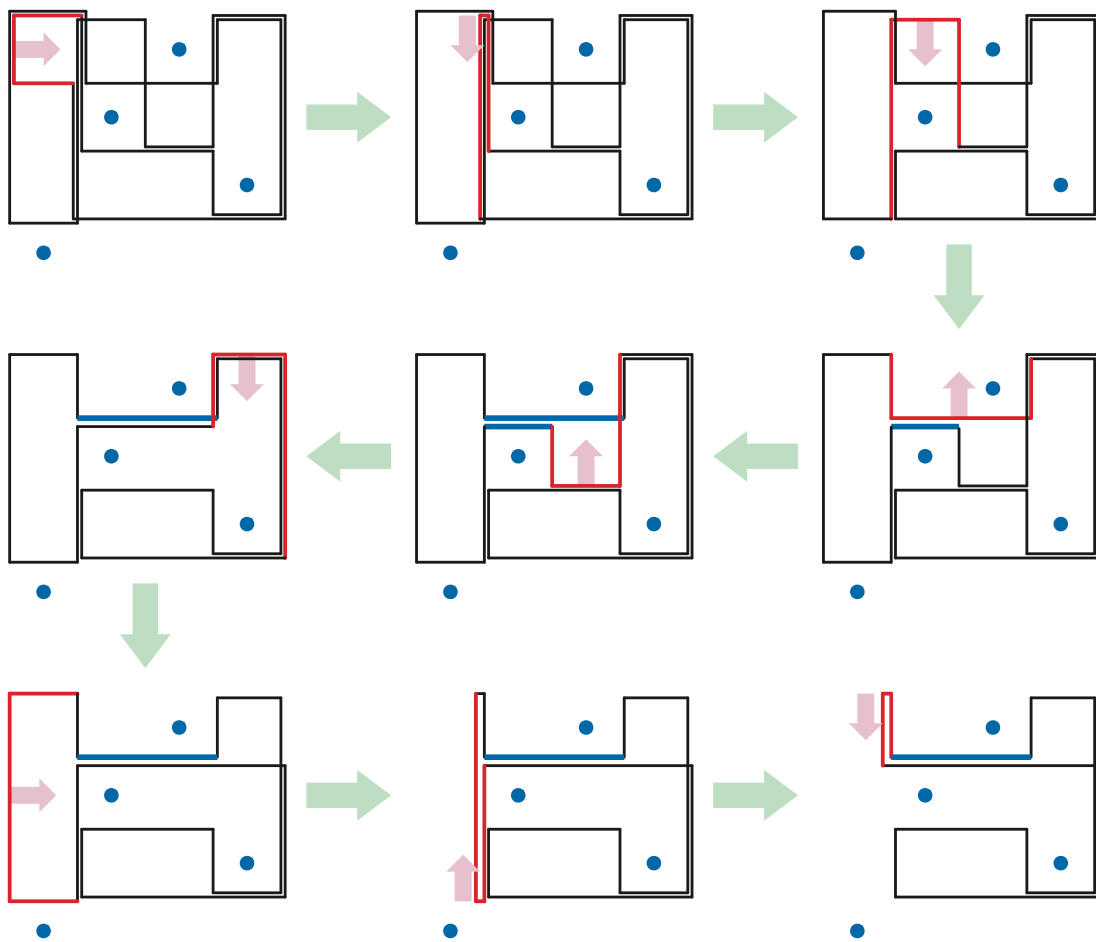


Figure 4.5: A sequence of bracket slides (and spur elisions). Heavy blue edges are frozen.

The other direction is more interesting. We actually need to reason about the crossing sequence defined by both upward *and* downward rays from each obstacle. Suppose \bar{P} is contractible. Then our earlier arguments imply that the mixed crossing sequence of \bar{P} can be reduced to the empty string, using exactly the same algorithm as usual. There are two cases to consider.

First suppose both mixed crossing sequences of \bar{P} is actually empty. Then \bar{P} does not cross the vertical line through any obstacle. It follows that every vertex of \bar{P} has the same even x -coordinate, and thus every “horizontal” edge of \bar{P} has length zero. It follows by induction that \bar{P} can be reduced to a single point by eliding every horizontal edge.

Otherwise, because \bar{P} is contractible, its mixed crossing sequence contains an elementary reduction. So there must be a subpath of \bar{P} that crosses the same obstacle ray twice in a row, without crossing the vertical line through any obstacle in between. (These two crossings would be canceled by an elementary reduction.) Without loss of generality, suppose this subpath crosses some upward obstacle ray from right to left, and then crosses that same ray from left to right. Then the leftmost vertical edge of that subpath forms a bracket, and sliding that bracket reduces the complexity of either the polygon or its crossing sequence. It follows by induction that \bar{P} can be reduced to a polygon with an empty crossing sequence, and thus to a single point.

A close reading of this proof reveals that we only ever need to perform *horizontal* bracket slides; even eliding zero-length edges is unnecessary.

4.5 Layered Range Trees

To implement bracket slides efficiently, we preprocess the rectified obstacles \bar{O} that supports fast queries of the following form: Given a horizontal query segment σ , report the lowest obstacle (if any) that lies directly above σ . Symmetric data structures can report the highest sentinel point below a horizontal segment, or the closest sentinel points to the left and right of a vertical segment.

Lemma: Any set \bar{O} of k points in the plane can be preprocessed in $O(k \log k)$ time into a data structure of size $O(k \log k)$, so that the lowest point (if any) above an arbitrary horizontal query segment can be computed in $O(\log k)$ time.

Proof: We use a data structure called a *layered range tree*, first described by Willard [3]. The layered range tree of \bar{O} consists of a balanced binary search tree T over the x -coordinates of \bar{O} , with additional information stored at each node. To simplify queries, the (odd) x -coordinates of \bar{O} are stored only at the leaves of T ; the search keys for internal nodes are intermediate (even) x -coordinates.

For each node v of T , let l_v and r_v denote the smallest and largest x -coordinates in stored in the subtree rooted at v , and let \bar{O}_v denote the subset of obstacle points with x -coordinates between l_v and r_v . Each node v in T stores the following information, in addition to the search key x_v .

- The x -coordinates l_v and r_v .
- The points \bar{O}_v , sorted by y -coordinate.
- For each point \bar{O}_v , the number of points in $\bar{O}_{\text{left}(v)}$ with larger y -coordinate.

- For each point \bar{O}_v , the number of points in $\bar{O}_{\text{right}(v)}$ with larger y -coordinate.

It is possible to construct a layered range tree for \bar{O} in $O(k \log k)$ time; the total size of the data structure is also $O(k \log k)$.

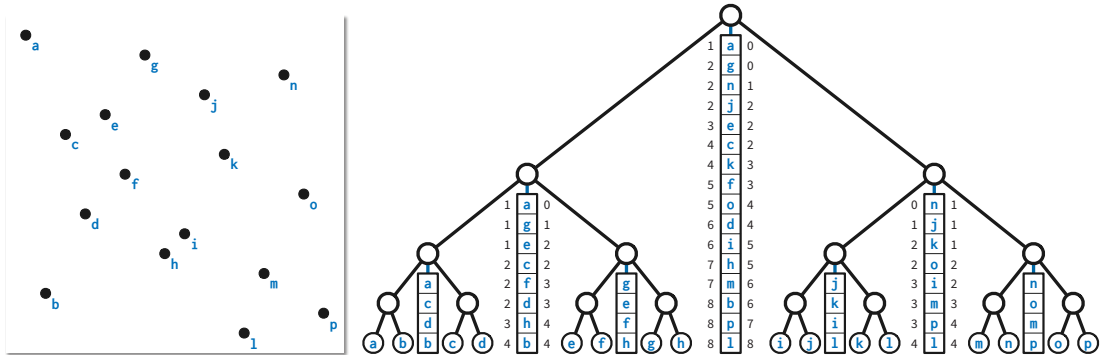


Figure 4.6: A layered range tree for 15 points (with some internal structure omitted).

Now consider a query segment σ with endpoints (l, b) and (r, b) with $l < r$. We call a node v *active* for this segment if $l_v \leq l$ and $r \leq r_v$, but the parent of v is not active. There are at most two active nodes at each level of the tree, so there are $O(\log k)$ active nodes altogether. We can easily find these active nodes in $O(\log h)$ time by searching down from the root.

For any node v , let $\text{lowest}(v, b)$ denote the index of the lowest point in \bar{O}_v that lies above the line $y = b$, or 0 if there is no such point. We can compute $\text{lowest}(\text{root}(T), b)$ in $O(\log h)$ time by binary search; for any other node v , we can compute $\text{lowest}(v, b)$ in $O(1)$ time from $\text{lowest}(\text{parent}(v), b)$ and the left or right ranks stored at $\text{parent}(v)$. Thus, we can compute $\text{lowest}(v, b)$ for every active node v in $O(\log h)$ time. The answer to our query is the lowest of these $O(\log h)$ points.

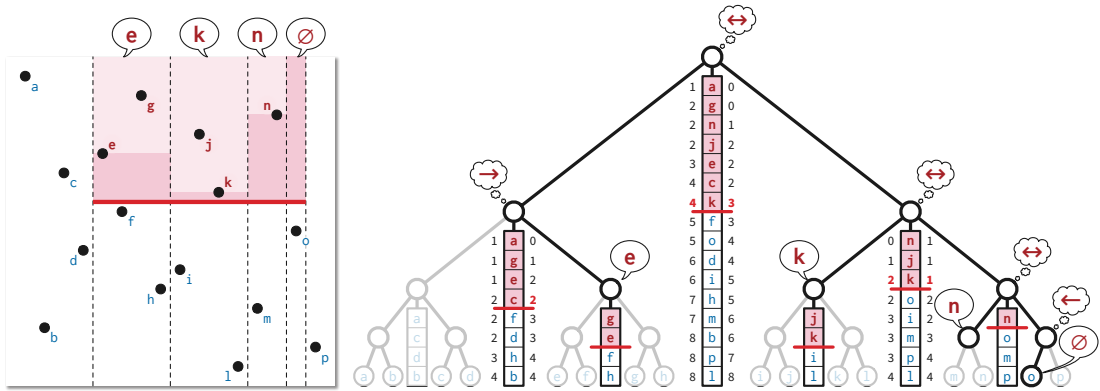


Figure 4.7: Answering a query in a layered range tree (with some details omitted).

4.6 Final Analysis

Now let's put all the ingredients of the algorithm together. Recall that the original input is a set O containing k sentinel points, and a polygon P in $\mathbb{R}^2 \setminus O$.

- First we sort the obstacles in O from left to right in $O(k \log k)$ time.
- Next we compute the trapezoidal decomposition of P and O using the Bentley-Ottmann sweepline algorithm in $O((n + k + s) \log(n + k))$ time, where s is the number of self-intersection points of P . We subdivide the edges of P at its self-intersection points, increasing the number of vertices of P to $m = n + 2s$.
- Then we compute the vertical ranks of the obstacles and the edges of P in $O(m + k) = O(n + k + s)$ time. We also compute the horizontal ranks of the obstacles and the vertices of P in $O(m \log m + k)$ time, by sorting the vertices of P and merging them with the sorted list of obstacles.
- Next we compute the rectified polygon \bar{P} and obstacles \bar{O} in $O(m + k)$ time.
- Then, we reduce \bar{P} as much as possible by eliding zero-length edges and sliding brackets. After an $O(m)$ -time initial pass, each elision takes $O(1)$ time, and each bracket slide takes $O(\log k)$ time. Each operation either freezes a bracket or reduces the complexity of \bar{P} , so after $O(m)$ operations, performed in $O(m \log k)$ time, \bar{P} is reduced as much as possible.
- Finally, we report that P is contractible if and only if the reduced rectified polygon is empty.

Altogether, this algorithm runs in $O((n + k + s) \log(n + k))$ time.

This is faster than the brute-force reduction algorithm from the previous lecture when *either* the polygon has few self-intersections *or* the number of obstacles is significantly larger than the number of polygon vertices. Specifically, the running time of the new algorithm is smaller than the old running time $O(k \log k + nk)$ whenever $s = o(nk / \log(n + k))$. Even in the worst case, when $s = \Theta(n^2)$, the running time of the new algorithm simplifies to $O((k + n^2) \log(n + k))$, which is still smaller than $O(k \log k + nk)$ when $n = o(k / \log n)$.

4.7 ... And the Aptly Named Et Cetera Ad Nauseam

- Extracting reduced crossing sequences from the reduced rectified polygon.
- Testing if a polygon made from two (almost) simple paths is contractible.
- Testing if two polygons, *each* with few self-intersections, are homotopic.
- Faster three-sided range query structures for integer points and ranges.
- Avoiding computing self-intersections (Bespanyatnikh)

4.8 References

1. Sergio Cabello, Yuanxin Liu, Andrea Mantler, and Jack Snoeyink. Testing homotopy for paths in the plane. *Discrete Comput. Geom.* 31(1):61–81, 2004.
2. Alon Efrat, Stephen G. Kobourov, and Anna Lubiw. Computing homotopic shortest paths efficiently. *Comput. Geom. Theory Appl.* 35(3):162–172, 2006. arXiv:cs/0204050.
3. Dan E. Willard. New data structures for orthogonal range queries. *SIAM J. Comput.* 24 14(1):232–253, 1985. Layered range trees.

Chapter 5

Shortest (Homotopic) Paths $^\beta$

In this lecture, we'll consider a problem that combines both geometry and topology that arises in VLSI design (or at least *did* arise in VLSI design in the 1980s). Suppose we have an environment X that can be modeled as a *polygon with holes*; this is the area bounded between a simple outer polygon P_0 and several disjoint simple polygons or “holes” P_1, P_2, \dots, P_h , each of which lies in the interior of P_0 . (Yes, previously we used “polygon” to refer to the boundary, and now we’re using “polygon with holes” to refer to the area. Welcome to mathematical jargon.)

We are also given a polygonal path π in the interior of X . Recall that two *paths* are homotopic if one can be continuously deformed to the other within X while keeping both endpoints fixed at all times. Our problem is to find the shortest path (that is, the path of minimum Euclidean length) that is homotopic in X to the given path π .

Although we could reduce to our earlier notion of homotopy by using the vertices of X as point obstacles, the pictures will be nicer (and the algorithms arguably simpler) if we use X itself as our underlying space. Our earlier formal definition of homotopy extends directly to this setting: A homotopy between two paths α and β in X is a continuous function $h: [0, 1] \times [0, 1] \rightarrow X$ such that the restrictions $h(\cdot, 0)$ and $h(\cdot, 1)$ are constant functions, and the restrictions $h(0, \cdot)$ and $h(1, \cdot)$ are the paths α and β , respectively.

Throughout this section, n denotes the number of vertices of the environment X , and k denotes the number of vertices in the input path π . (Yes, this is reversed from the previous lecture.) Let s (“source”) and t (“target”) denote the first and last vertices of π .

5.1 Shortest Paths in Simple Polygons

Let's start with the topologically trivial case where X is the interior of a simple polygon with no holes. A strengthening of the Jordan Curve Theorem due to Schönflies implies that X is homeomorphic to an open circular disk. It follows that any two paths in X with the same endpoints are homotopic. Thus, we are now looking for the globally shortest path in X between the endpoints of π .

The shortest path between two points s and t in a simple polygon P is a polygonal chain, whose interior vertices lie at concave vertices of P . Imagine a taut rubber band between s to t ; the rubber band will be straight everywhere, except at concave corners that it must wrap around.

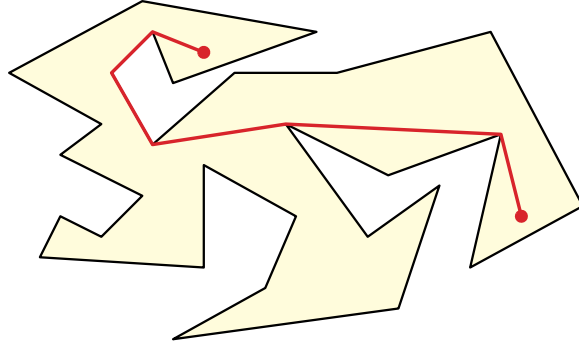


Figure 5.1: The shortest path between two points in a simple polygon

I'll describe an algorithm for this special case *as though* the topology of the problem were non-trivial; in particular, even though the output depends only on the endpoints of the input path π , I will still use the entire input path to guide the algorithm.

5.2 Triangulations and Dual Graphs

The first step of our shortest-path algorithm is to triangulate the polygon X . We saw an algorithm in the first lecture that computes a frugal triangulation of X in $O(n \log n)$ time.

The (*weak*) *dual graph* of a polygon triangulation has a vertex for each triangle and an edge for each diagonal; two vertices are connected by an edge in the dual graph if and only if the corresponding triangles share a diagonal. We can draw the dual graph by placing each vertex at the centroid of its triangle, and drawing each edge as a polygonal path through the midpoint of the corresponding diagonal.

Lemma: *The dual graph of any frugal triangulation of a polygon without holes is a tree.*

Proof: Suppose to the contrary that the dual graph contains a cycle C . The image of C in our drawing is a simple polygon, which I'll also call C (at the risk of confusing the reader). Any diagonal d whose dual edge is in C crosses C exactly once at the midpoint of d . It follows that one endpoint of d is inside C and the other endpoint is outside. So the Jordan curve theorem implies that the polygon X intersects C . But that's impossible, because X does not intersect the dual graph.

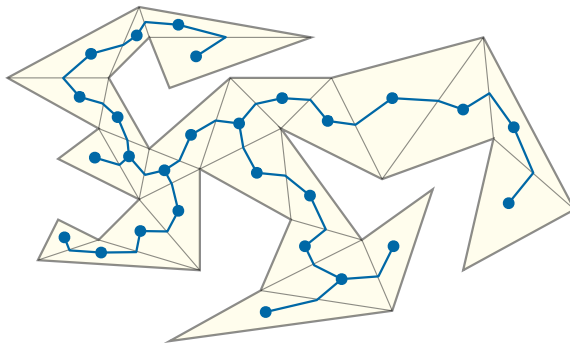


Figure 5.2: The dual graph of a polygon triangulation

5.3 Crossing Sequences

Next we apply the same strategy that we previously used to test contractibility. We compute the *crossing sequence* of π and then *reduce* it as much as possible. (Two paths are homotopic if and only if they have identical reduced crossing sequences.) In this setting, the crossing sequence is the sequence of diagonals crossed by π , in order along π .

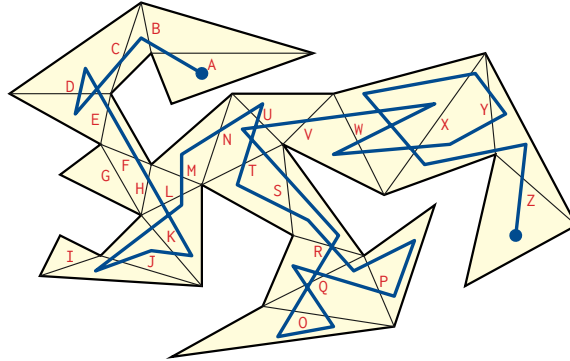


Figure 5.3: A path with crossing sequence ABCDDDEFHLKJJKLMNUUTSRQPPQQOQRSTUVWWWWXYYXXYZ

In our earlier homotopy-testing algorithm, we also recorded the *sign* of each crossing, but that information is actually redundant in our current setting. Recall from our proof of the polygon triangulation theorem that any interior diagonal partitions the interior of a polygon into two disjoint subsets. Thus, if π crosses the same diagonal multiple times, those crossings must alternate between positive and negative. It also follows that we can reduce the crossing sequence by removing arbitrary adjacent pairs of *equal* symbols; for any such pair, the corresponding crossings have opposite signs. For example, the crossing sequence ABCDDDEFHLKJJKLMNUUTSRQPPQQOQRSTUVWWWWXYYXXYZ of the path in the previous figure reduces to ABCDEFHMNUVWXYZ.

We can compute the crossing sequence of π in $O(n + k + x)$ time, where $x = O(kn)$ is the length of the crossing sequence. Specifically, we find the triangle containing s by brute force; then we can repeatedly find the next crossing (if any) along the current edge of π in $O(1)$ time. Finally, we can reduce the crossing sequence in $O(x)$ time using left-greedy cancellation.

(The reduced crossing sequence of π contains precisely the edge labels that appear an odd number of times in the unreduced crossing sequence; moreover, these labels appear in the same order as their first (or last) occurrences in the unreduced crossing sequence.)

5.4 Sleeves

Let \bar{x} denote the length of the reduced crossing sequence. The reduced crossing sequence defines a sequence of $\bar{x} + 1$ triangles in the triangulation of X , starting with the triangle containing the first vertex π_0 of π , and ending with the triangle containing the last vertex π_k of π . The union of these triangles is called the *sleeve* of the reduced crossing sequence.

Any path α in X from s to t that leaves the sleeve must cross a diagonal d on the boundary of the sleeve. The endpoints s to t lie in the same component of $X \setminus d$, so the path must cross d an even number of times. Let p and q be the first and last intersection points along α . The line segment pq is shorter than the subpath of α from p to q , so α cannot be a shortest path.

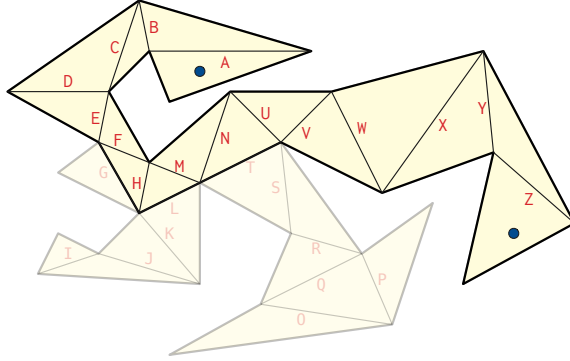


Figure 5.4: The sleeve of the reduced crossing sequence ABCDEFHMNUVWXYZ

Alternatively, the crossing sequence describes a walk in the dual graph of the triangulation, starting at the vertex dual to the triangle containing s . Reducing the crossing sequence removes *spurs* from this walk—subpaths that consist of the same edge twice in a row, necessarily in opposite directions. Thus, the *reduced* crossing sequence describes a *shortest* walk—in fact, the unique simple path between its endpoints—in the dual graph. This path is also the dual graph of the induced triangulation of the sleeve.

Note that we do not actually need to *construct* the sleeve; the sequence of diagonals that the funnel crosses is exactly the reduced crossing sequence of π .

5.5 Growing Funnels

To compute the actual shortest path from s to t , we use an algorithm independently discovered by Tompa (1981), Chazelle (1982), Lee and Preparata (1984), and Leiserson and Maley (1985). (My presentation most closely follows Lee and Preparata's.) The *funnel* of any diagonal d of the sleeve is the union of the shortest paths from the source point s to all points on e .

The funnel consists of a polygonal path, called the *tail*, from s to a point a called the *apex*, plus a simple polygon called the *fan*. The tail may be empty, in which case s is the apex. The fan is bounded by the diagonal d and two concave chains joining the apex to the endpoints of d . The shortest path from s to either endpoint of d consists of the tail plus one of the concave chains bounding the fan. Extending the edges of the concave chains to infinite rays defines a series of *wedges*, which subdivide both the fan and the triangle just beyond d .

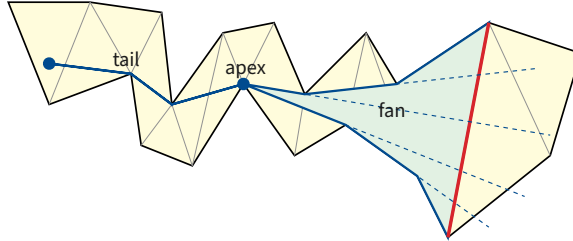


Figure 5.5: A typical funnel

Beginning with a single triangle joining s to the first edge in the reduced crossing sequence, we extend the funnel through the entire sleeve one diagonal at a time. Each diagonal in the

sleeve shares one endpoint with the previous diagonal; suppose we are extending the funnel from diagonal pq to diagonal qr . Let o be the predecessor of p on the shortest path from s to p .

There are two cases to consider, depending on whether q and r lie on the same sides of the line through o and p or on opposite sides. We can actually detect this case in $O(1)$ time with a single orientation test.

- If q and r lie on opposite sides of line op , then the new endpoint r does not lie inside any wedge of the current fan. We can detect this case in $O(1)$ time with a single orientation test, and then extend the tunnel in $O(1)$ time by inserting r as a new fan vertex.

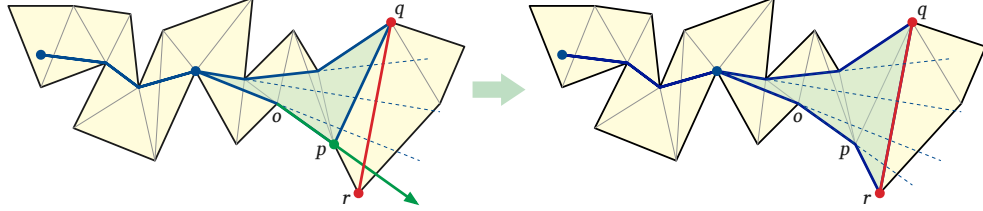


Figure 5.6: Growing the funnel

- If q and r lie on the same side of line op , we *contract* the funnel, intuitively by moving p continuously along the boundary edge pr . Each time the moving point crosses the boundary of a wedge, we remove a vertex from the fan. If the removed vertex is the apex, the next vertex on that side of the fan (on the shortest path from s to r) becomes the new apex. We can detect whether the moving point will cross any wedge boundary in $O(1)$ time using our standard orientation test. Thus, the total time in this case is $O(\delta + 1)$, where δ is the number of vertices deleted from the fan. The total number of deleted vertices cannot exceed the total number of previously inserted vertices, so the *amortized* time for this case is also $O(1)$.

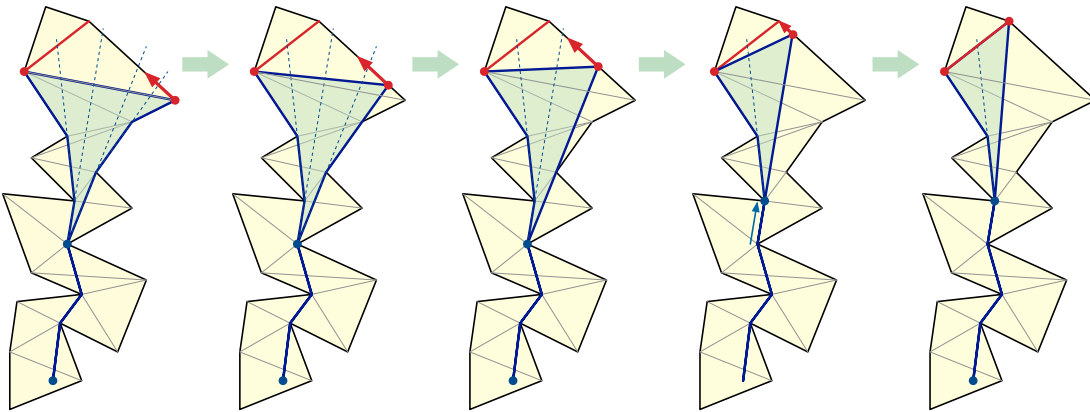


Figure 5.7: Shrinking the funnel

Let yz be the last diagonal in the reduced crossing sequence. To end the algorithm, we treat the line segment tz as another diagonal and extend the funnel one more time. The shortest path homotopic to π then consists of the tail of the funnel plus the concave chain of the fan containing t ; we can extract this shortest path in $O(1)$ time per edge.

Summing up, we spend $O(n \log n)$ time triangulating X , then $O(k + x) = O(nk)$ time computing the crossing sequence of π , then $O(x) = O(nk)$ time reducing the crossing sequence, $O(\bar{x}) =$

$O(nk)$ time growing the funnel, and finally $O(\bar{x}) = O(nk)$ extracting the shortest path from the final funnel.

Theorem: *Given a polygonal path π in a simple polygon X **without holes**, we can compute the shortest path in X homotopic to π in $O(n \log n + nk)$ time.*

5.6 Polygons with Holes

Now let's consider the more general case where X has one or more holes. Perhaps surprisingly, the previous algorithm needs *no modifications whatsoever* to compute the shortest path homotopic to π in $O(n \log n + nk)$ time.

- Triangulate X in $O(n \log n)$ time using the algorithm described in the first lecture. First build a trapezoidal decomposition using a sweep-line algorithm (such as Bentley-Ottmann). Then insert diagonals inside every boring trapezoid in $O(n)$ time, partitioning X into monotone mountains. Finally, triangulate these monotone mountains in $O(n)$ total time.
- Compute the crossing sequence of π with respect to this triangulation in $O(n + k + x)$ time, where x is the number of crossings. Locate the triangle containing s in $O(n)$ time by brute force, then repeatedly find the next crossing (if any) along the current edge in $O(1)$ time.
- Reduce the resulting crossing sequence in $O(x)$ time using the left-greedy reduction algorithm.
- Extend the funnel through the sleeve of the reduced crossing sequence in $O(\bar{x}) = O(nk)$ time using the standard funnel algorithm.
- Finally, extract the shortest homotopic path from the final funnel in $O(1)$ time per edge.

Theorem: *Given a polygonal path π in a simple polygon X **with holes**, we can compute the shortest path in X homotopic to π in $O(n \log n + nk)$ time.*

Same algorithm, same running time, same everything. This strikes many people as counterintuitive. After all, the sleeve can run through the same triangle multiple times, and the funnel can self-intersect; why doesn't this cause any problems?

One way to answer this question is that *the algorithm doesn't look for self-intersections, so its behavior can't be affected by them*. Or said differently: *the algorithm only makes local decisions, but self-intersection is a global property*. Every branch in our algorithm is based on either a comparison between two x -coordinates or an orientation test on some triple of points. As far as the algorithm is concerned, every time the funnel enters a triangle, it is entering that triangle for the very first time, or equivalently, it is entering a *new copy* of that triangle. So the sleeve of the reduced crossing sequence, while not being *geometrically* a triangulated simple polygon, is still *topologically* a triangulated simple polygon: a collection of triangles glued together along common edges into a topological disk.

There is a reasonable analogy here with classical graph traversal algorithms: depth-first search, breadth-first search, and their more complex descendants. All of these algorithms maintain a set of vertices; at each iteration, each algorithm pulls one vertex v out of this set, *marks* that vertex, and then puts the *unmarked* neighbors of v into the set. Without the marking logic, unless the input graph is a tree, these algorithms will visit at least one vertex infinitely many times, each time treating it as a brand-new vertex.

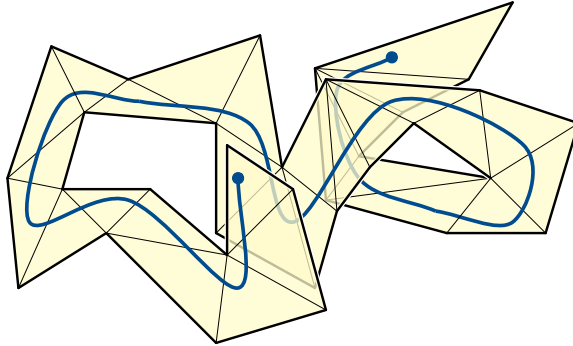


Figure 5.8: The sleeve of a reduced path in a polygon with holes

In fact, even the original shortest-path algorithm does not actually require the environment X to be a simple polygon. We only require that (1) X is assembled from *any* set of Euclidean triangles by identifying disjoint pairs of equal-length edges, (2) all triangle vertices are on the boundary of X , and (3) the dual graph of the triangulation is a tree (equivalently, X is homeomorphic to a disk in the plane). More generally, the shortest-homotopic-path algorithm applies to any triangulated space satisfying conditions (1) and (2); these spaces can reasonably be called *boundary-triangulated flat surfaces*. For example, without modification, our algorithm can compute shortest homotopic paths on a triangulated Möbius band.

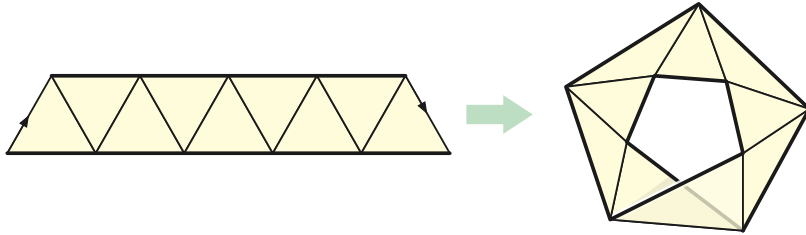


Figure 5.9: A flat Möbius band assembled from nine Euclidean triangles

5.7 The Universal Cover

Another explanation that may be more familiar to topologists is that our algorithm is effectively exploring the *universal cover* of the input polygon. Informally, the universal cover (of *universal covering space*) of X is the infinite topological space constructed by a breadth-first search of X *without memory*.

We can define the universal cover more constructively in terms of a triangulation of X as follows. Fix a starting point s . For every reduced crossing sequence w of a path starting at s , let Δ_w denote an *independent copy* of the triangle containing the final point in that path. For example, Δ_e is a copy of the triangle containing s . Two triangles Δ_w and Δ_x are *neighbors* if $x = wd$ for some diagonal d ; glue every such pair together along their copies of d . For example, if $w = ABCB$ and $x = ABCD$, then we would identify the copies of edge D in Δ_w and Δ_x . We call each triangle Δ_w a *lift* of the corresponding triangle in the triangulation of X , and we call the original triangle a *projection* of Δ_w .

Figure! Polygonal annulus to infinite polygonal parking garage?

The dual graph of the universal cover of X —or equivalently, the universal cover of the dual graph of X —has a vertex for every possible reduced crossing sequence (of a path starting at s), and an edge between two reduced crossing sequences if they differ by exactly one crossing. Unless the input polygon X has no holes, the universal cover of the dual graph is an infinite tree. The crossing sequence describes a walk from some vertex \hat{s} to another vertex \hat{t} in this infinite tree; removing all spurs computes the *unique* path in that tree between \hat{s} and \hat{t} .

Figure?

5.8 Covering Spaces

The universal cover is an example of a *covering space*. We will see several other examples of covering spaces in this course, so let me start here with some formal definitions.

A *covering map* is a continuous surjective function $p: \widehat{X} \rightarrow X$, such that every point $x \in X$ has an open neighborhood U whose preimage $p^{-1}(U)$ is the disjoint union of open sets $\bigsqcup_{i \in I} U_i$, such that the restriction of the function p to each open set U_i is a homeomorphism to U . The open sets U_i are sometimes called *sheets* over U . If there is a covering map from \widehat{X} to X , we call \widehat{X} a *covering space* of X . By convention, we require covering spaces to be connected.

The *universal* covering space \widetilde{X} can be defined in several different ways:

- \widetilde{X} is the unique covering space of X that also covers every covering space of X .
- \widetilde{X} is the unique *simply-connected* covering space of X . (Recall that a space is *simply connected* if every closed curve in that space is contractible.)
- \widetilde{X} is the space of all *homotopy classes* of paths from some fixed basepoint $s \in X$:

$$\widetilde{X} := \{[\pi] \mid \pi: [0, 1] \rightarrow X \text{ and } \pi(0) = s\}$$

The covering map $p: \widetilde{X} \rightarrow X$ maps each homotopy class $[\pi]$ of paths to their common final endpoint $\pi(1)$.

In our construction by gluing labeled triangles, the covering map sends each triangle Δ_w to the corresponding triangle in the triangulation of X .

Concrete examples?

5.9 ...and the Aptly Named Yadda Yadda

- Technicalities for point obstacles
- Bundling homotopic subpaths
- Minimum-link (homotopic) paths
- Thick non-crossing paths
- Shortest non-crossing walks / wire routing

5.10 References

1. Bernard Chazelle. A theorem on polygon cutting with applications. *Proc. 23rd Ann. IEEE Symp. Found. Comput. Sci.*, 339–349, 1982. The funnel algorithm.

2. Shaodi Gao, Mark Jerrum, Michael Kaufmann, Kurt Mehlhorn, and Wolfgang Rülling. On continuous homotopic one layer routing. *Proc. 4th Ann. Symp. Comput. Geom.*, 15:392–402, 1988.
3. John Hershberger and Jack Snoeyink. Computing minimum length paths of a given homotopy class. *Comput. Geom. Theory Appl.* 4:63–98, 1994.
4. Der-Tsai Lee and Franco P. Preparata. Euclidean shortest paths in the presence of rectilinear barriers. *Networks* 14:393–410, 1984. The funnel algorithm.
5. Charles E. Leiserson and F. Miller Maley. Algorithms for routing and testing routability of planar VLSI layouts. *Proc. 17th Ann. ACM Symp. Theory Comput.*, 69–78, 1985. The funnel algorithm.
6. Martin Tompa. An optimal solution to a wire-routing problem. *J. Comput. System Sci.* 23:127–150, 1981. The funnel algorithm.

Chapter 6

Generic Planar Curves^α

Recall that a *closed curve* in the plane is any continuous function from the circle to the plane. Previously we considered a common representation of closed curves as *polygons*: circular sequences of line segments joined at common endpoints. Polygons are convenient for reasoning about intersections with other simple geometric structures like vertical rays, trapezoidal decompositions, and triangulations, but in other ways the geometry of the representation is irrelevant. Starting with this lecture, I'll consider a more abstract representation that records only how the curve intersects *itself*.

A self-intersection $\gamma(t) = \gamma(t')$ of a closed curve γ is *transverse* if, for all sufficiently small $\varepsilon > 0$ the subpaths $\gamma(t-\varepsilon, t+\varepsilon)$ and $\gamma(t'-\varepsilon, t'+\varepsilon)$ are homeomorphic to two orthogonal lines. A closed curve is *generic* if every self-intersection is transverse (in particular, there are no self-tangencies or repeated curve segments) and there are no triple self-intersections $\gamma(t) = \gamma(t') = \gamma(t'')$.

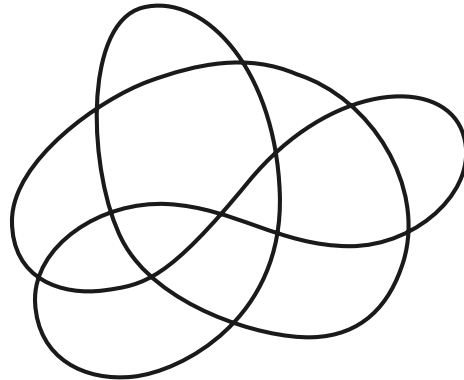


Figure 6.1: A generic closed curve with eleven crossings

Two generic curves are *isotopic* if one can be continuously deformed to the other without ever changing the number of self-intersections. For example, all simple closed curves are isotopic to each other. A homotopy that always preserves the number of self-intersections is called an *isotopy*. In fact, two planar curves γ and γ' are isotopic if and only if there is an orientation-preserving homeomorphism $h: \mathbb{R}^2 \rightarrow \mathbb{R}^2$ such that $\gamma' = h \circ \gamma$. At least in the next few lectures, we really don't care about the *geometry* of these curves, so we won't distinguish between isotopic curves.

6.1 Technicalities

Generic closed curves are sometimes called *immersions* or *regular* curves, but the latter term more commonly refers to closed curves with continuous non-zero derivatives. In fact, the most common word used to describe this class of closed curves is “curve”! The definition of generic curves does *not* require continuous, non-zero, or even well-defined derivatives at *any* point, much less at *every* point. Despite this freedom, the following standard *compactness argument* implies that generic curves are well-behaved.

Lemma: *Every generic closed curve has a finite number of self-intersection points.*

Proof: Call a point $t \in S^1$ *singular* if $\gamma(t) = \gamma(t')$ for some $t' \neq t$, and *regular* otherwise. For each point $t \in S^1$, we define an open interval U_t as follows:

- If t is singular, let $U_t = (t - \varepsilon, t + \varepsilon)$, such that $\gamma(t - \varepsilon, t + \varepsilon)$ and some other arc $\gamma(t' - \varepsilon, t' + \varepsilon)$ are homeomorphic to two orthogonal lines.
- If t is regular, let U_t be any open interval that contains t but no singular points.

The open sets $\mathcal{C} = \{U_t \mid t \in S^1\}$ clearly *cover* the circle, meaning $\bigcup_{t \in S^1} U_t = S^1$. Because S^1 is compact, there must be a finite subset $\mathcal{F} \subset \mathcal{C}$ that also covers S^1 . Let $F \subset S^1$ be the (necessarily finite) index set of the finite subcover \mathcal{F} , meaning $\mathcal{F} = \{U_t \mid t \in F\}$.

The only set in \mathcal{U} that contains a singular point t is its own interval U_t . Thus, the finite set T must contain every singular point.

The adjective “generic” is justified by the observation that *every* closed curve can be approximated arbitrarily closely by a generic closed curve. Previously we argued that every closed curve can be approximated arbitrarily closely by a *polygon*. (This is the *simplicial approximation theorem*.) An arbitrarily small perturbation of any polygon ensures that all vertices are distinct, no vertex lies in the interior of an edge, and no three edges share a common point. Any polygon satisfying these conditions *is* a generic closed curve.

A more careful application of simplicial approximation and compactness implies that any generic closed curve γ can be approximated arbitrarily closely by a polygon that is *isotopic* to γ . Thus, even though generic curves are not polygons *by definition*, they are polygons *without loss of generality*. In fact, results in future lectures imply that each generic curve with n self-intersection points is isotopic to a polygon with only $O(n)$ vertices.

6.2 Image graphs

Any non-simple generic closed curve can be naturally represented by its *image graph*, which is a connected 4-regular plane graph¹ whose vertices are the self-intersection points of the curve, and whose edges are curve segments between vertices. Image graphs are not necessary *simple*; they can contain loops and parallel edges. The image graph of a *simple* closed curve is obviously a simple cycle.

However, not every 4-regular plane graph is the image graph of a generic closed curve. Any generic curve is a particular Euler tour of its image graph. Recall that an *Euler tour* of a graph

¹We’re admittedly getting a little ahead of ourselves here. A *plane graph* is any graph whose vertices are points in the plane, and whose edges are *interior-disjoint* paths between their endpoints.

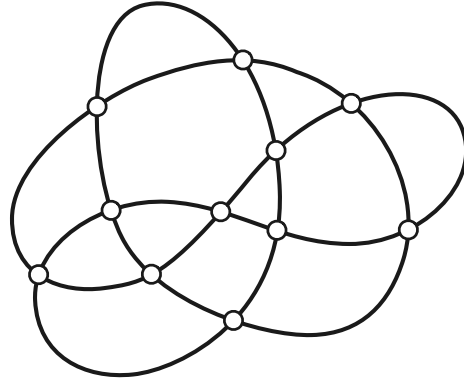


Figure 6.2: The image graph of the curve in Figure 1

G is any closed walk that traverses each edge of G exactly once. A closed walk is *Gaussian* if, whenever the walk visits a vertex v , it enters and exits v along opposing edges. A 4-regular graph is *unicursal* if it contains a Gaussian Euler tour; every *unicursal* 4-regular plane graph is the image of a non-simple generic curve.

Any generic planar curve partitions the plane into regions called the *faces* of the curve. The Jordan-Schönflies theorem implies that every planar curve has one unbounded face that is homeomorphic to the complement of a closed disk, and every other face is homeomorphic to an open disk. The faces of a curve are also the faces of its image graph. A face is called a *monogon* if it has only one edge on its boundary, a *bigon* if it has two boundary edges, and a *triangle* if it has three boundary edges.²

More generally, a *multicurve* is a continuous map of the disjoint union of circles into the plane; a multicurve is *generic* if it has only transverse pairwise self-intersections. The restriction of a multicurve to one of its circles is a generic closed curve called a *constituent* of the multicurve. Every 4-regular plane graph G is the image graph of a generic multicurve, whose constituents are the Gaussian walks in G . Most of the results I'll discuss in this set of lectures extend easily to multicurves, but for ease of exposition I'll discuss only curves explicitly.

6.3 Gauss codes and Gauss diagrams

In the mid-1800s, Gauss developed a symbolic representation of closed curves similar to the crossing sequences that we previously used for homotopy testing.

Assign a unique label to each vertex of the image graph of the curve. The *Gauss code* of a curve is the sequence of labels encountered by a point moving once around the curve, starting at an arbitrary *basepoint* and moving in an arbitrary direction. In other words, a Gauss code is a *self-crossing* sequence. Different choices of basepoint and direction lead to different Gauss codes. Specifically, changing the basepoint cyclically shifts the Gauss code, and changing direction reverses the Gauss code.

A *signed* Gauss code also records *how* the curve crosses itself at each vertex. Imagine a point moving along the curve in the chosen direction, starting at the chosen basepoint. The signed Gauss code records a *positive* crossing whenever the point crosses the curve from right to left,

²Stop trying to make “digon” and “trigon” happen, Gretchen. They’re not going to happen.

and a *negative* crossing whenever the point crosses the curve from left to right. (This is exactly the same sign convention that we used to compute winding number, *from the point of view of the polygon*.) Each vertex of the image graph of a curve appears twice in the curve's signed Gauss code, once with each sign. I'll typically indicate positive and negative crossings using upper- and lower-case letters, respectively. Again, different choices of basepoint and direction lead to different signed Gauss codes.

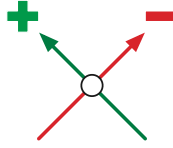


Figure 6.3: Gauss's sign convention for positive and negative crossings.

Figure 4 shows the curve from Figure 1, with a direction indicated by arrows and a basepoint on the far left indicated by a white arrowhead. Each vertex is labeled positive or negative according to the sign of the *first* crossing through that vertex. The resulting signed Gauss code is ABCdeFGChAigDjKHbifEJK; by forgetting the signs, we recover the unsigned Gauss code ABCDEFGCHAIGDJHKHIFEJK.

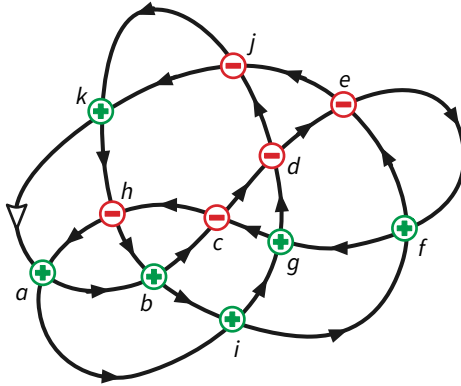


Figure 6.4: A based directed curve with signed Gauss code ABCdeFGChAigDjKHbifEJK.

Gauss diagrams are an equivalent graphical representation of Gauss codes. A Gauss diagram for a curve with n self-intersections consists of an undirected cycle of $2n$ nodes labeled by crossings, in the order they appear along the curve, along with edges joining the two appearances of each crossing point, directed from the negative crossing to the positive crossing. (Using directed edges here is slightly non-standard.)

6.4 Tracing Faces

Perhaps surprisingly, we can completely recover the combinatorial structure of a curve from its signed Gauss code. I'll justify this claim in more generality later, when we've built up more background on planar graphs, but we can already show one example, observed by Carter in the early 1990s [2]: The signed Gauss code implicitly encodes the *faces* of the curve.

Imagine a point moving counterclockwise around the boundary of some face (or clockwise if the face is unbounded); the face always lies just to the left of the moving point. Between vertices,

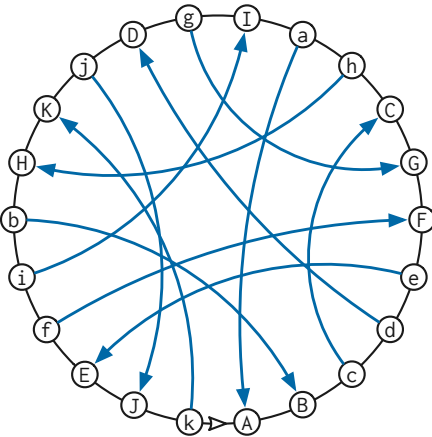


Figure 6.5: A Gauss diagram for the signed Gauss code ABCdeFGChaiDjKHbiFEJK.

the point is either moving forward or backward along some edge of the image graph. At each crossing, the point turns to the *left*, as follows:

- After entering a positive crossing forward, leave the corresponding negative crossing backward.
- After entering a negative crossing forward, leave the corresponding positive crossing forward.
- After entering a positive crossing backward, leave the corresponding negative crossing forward.
- After entering a negative crossing backward, leave the corresponding positive crossing backward.

Similar case analysis allows us to trace a face to the right of a moving point, in clockwise order around the face, by turning right at every vertex.

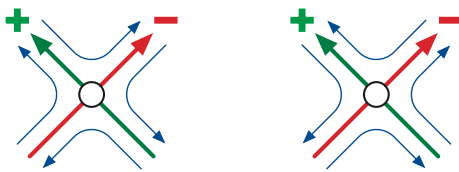


Figure 6.6: Turning left or turning right at a vertex.

(Pseudo)python (pseudo)code for Carter's face-tracing algorithm is shown below. The first function computes the matching between different occurrences of the same crossing point; obviously this matching only needs to be extracted once if we want to trace several faces. With careful bookkeeping, we can extract *all* the faces of the curve directly from the signed Gauss code in $O(n)$ time. Different Gauss codes for the same curve yield the same set of faces (but possibly with the vertices of each face rotated and/or reflected).

```
# extract matching between crossings from a signed Gauss code
#   input:  code = signed Gauss code
#          = permutation of list(range(-n,0)) + list(range(1,n+1))
#   output: array match, defined by code[match[i]] = -code[i]
```

```

def indexCode(code):
    N = len(code)/2
    posindex = [0] * (N/2)
    match = [0] * N
    for i in range(N):
        if code[i] > 0:
            posindex[code[i] - 1] = i
    for i in range(N):
        if code[i] < 0:
            match[i] = posindex[1 - code[i]]
            match[match[i]] = i
    return match

# trace the face to the right of a moving point
#   code = signed Gauss code (integers)
#   start = index of starting edge (basepoint edge = 0)
#   forward = boolean indicating starting direction
def traceFace(code, starti, forward):
    match = matchCode(code)
    N = len(code)
    i = starti
    while True:
        next = forward ? i : (i + N - 1)%N
        print(code[next])
        if code[next] > 0:
            forward = !forward
        i = match[next]
        if i = starti:
            break

```

The clockwise tracing process can be visualized on the Gauss diagram as follows. We start by tracing just inside an arc of the outer circle. Whenever we reach a crossing, we follow the interior edge across the diagram to its partner. If the crossing is positive, we stay on the same side of the interior edge; if the crossing is negative, we switch to the opposite side of the interior edge. Again, we can visualize counterclockwise tracing by a symmetric case analysis.

6.5 Homotopy moves

Every closed curve in the plane is homotopic to a point, and therefore to every other closed curve in the plane. However, it is still useful to study the *structure* of homotopies between generic curves. Recall that the simplicial approximation theorem let us approximate any homotopy between *polygons* as a finite sequence of *vertex moves*. If we make sufficiently small vertex moves that preserve genericity, each move incurs only a small local change in the pattern of self-intersections.

Careful case analysis implies that every homotopy between generic curves can be approximated by a finite sequence of *homotopy moves* of five different types. Each homotopy move modifies the curve only within a small neighborhood containing at most three vertices, leaving the rest of the curve unchanged outside this neighborhood.

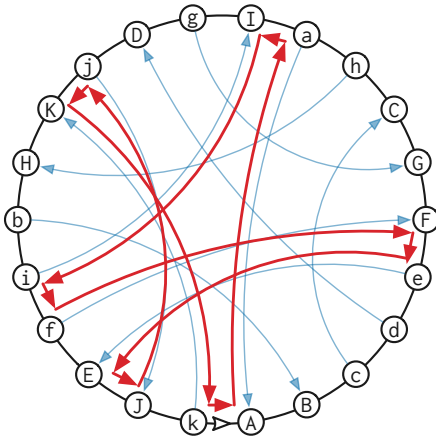


Figure 6.7: Tracing the outer face of our example curve (to the right of the basepoint)

- $1 \rightarrow 0$: remove a monogon
- $0 \rightarrow 1$: create a monogon
- $2 \rightarrow 0$: remove a bigon by separating two subpaths.
- $0 \rightarrow 2$: create a bigon by overlapping two subpaths.
- $3 \rightarrow 3$: flip a triangle by moving one subpath over the opposite crossing.

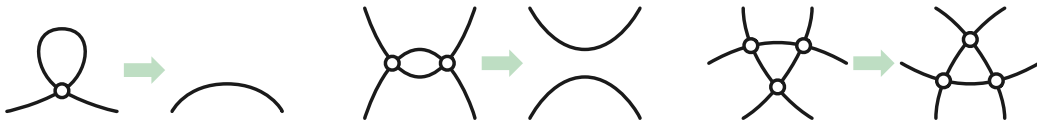


Figure 6.8: $1 \rightarrow 0$, $2 \rightarrow 0$, and $3 \rightarrow 3$ homotopy moves

In particular, we have the following:

Theorem: *Every generic closed curve in the plane can be transformed into a simple closed curve by a finite sequence of homotopy moves.*

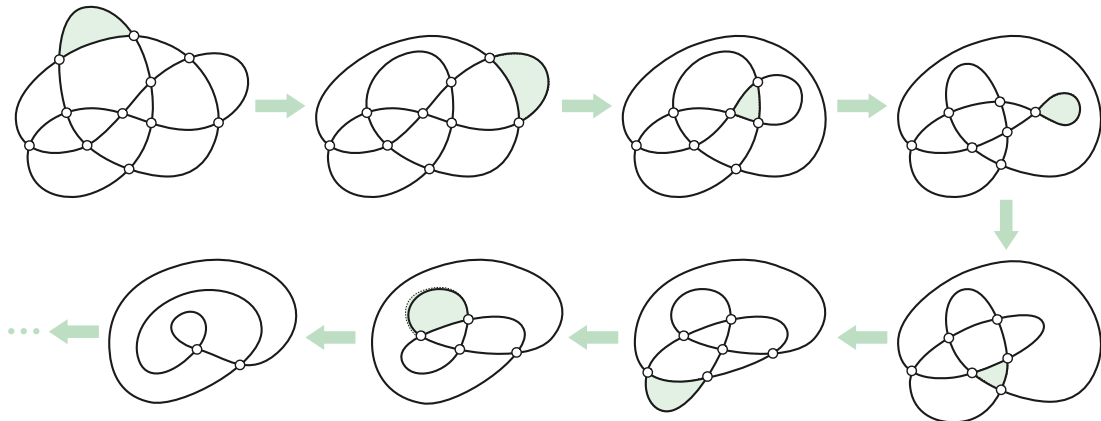


Figure 6.9: A sequence of homotopy moves simplifying the curve in Figure 1

The proof of this theorem (via simplicial approximation) follows from the foundational work of

Alexander and Briggs [1] and Reidemeister [2] on knot diagrams.³ This proof is fundamentally non-constructive; the number of homotopy moves we need depends on the geometric structure of the “given” homotopy. In a future lecture, we will see an *algorithm*, implicit in the work of Steinitz [3,4] a decade before Alexander, Briggs, or Reidemeister, that contracts any closed curve with n vertices using at most $O(n^2)$ homotopy moves.

Each homotopy move can be implemented by locally modifying the Gauss code/diagram, or the equivalent data structures, as follows.

- $1 \rightarrow 0$: remove a consecutive pair of crossings of the same vertex, for example: $\cdots Aa \cdots$
- $2 \rightarrow 0$: remove two consecutive pairs, each with opposing signs, that cover two vertices, for example: $\cdots Ab \cdots Ba \cdots$ or $\cdots aB \cdots Ab \cdots$
- $3 \rightarrow 3$: reverse three consecutive pairs that cover exactly three vertices, for example: $\cdots AB \cdots bc \cdots aC \cdots \mapsto \cdots BA \cdots cb \cdots Ca \cdots$.

6.6 Planarity testing

Every signed Gauss code is a *signed double-permutation*: A string of even length, in which each symbol appears exactly twice, once positive and once negative. However, not every signed double-permutation is the signed Gauss code of a planar curve. For example, no planar curve has the signed Gauss code ABab. (This is in fact the signed Gauss code of a closed curve on the torus!) However, signed Gauss codes of planar curves have a very simple characterization.

Lemma: *Every generic closed curve in the plane with n vertices has exactly $n + 2$ faces.*

Proof (via homotopy): Consider two generic closed curves γ and γ' that differ by one homotopy move. Suppose γ has n vertices and f faces, and γ' has n' vertices and f' faces.

- If the move has type $1 \rightarrow 0$, then $n' = n - 1$ and $f' = f - 1$.
- If the move has type $0 \rightarrow 1$, then $n' = n + 1$ and $f' = f + 1$.
- If the move has type $2 \rightarrow 0$, then $n' = n - 2$ and $f' = f - 2$.
- If the move has type $0 \rightarrow 2$, then $n' = n + 2$ and $f' = f + 2$.
- If the move has type $3 \rightarrow 3$, then $n' = n$ and $f' = f$.

In all five cases, we have $f - n = f' - n'$.

It follows by induction that if γ' is any curve reachable from γ by a finite sequence of homotopy moves, then $f - n = f' - n'$. In particular, if γ' is simple, then $n' = 0$ and (by the Jordan curve theorem!) $f' = 2$, and therefore $f - n = 2$.

Proof (sketch, via smoothing): [[Define smoothing!]] Consider two generic closed curves γ and γ' where γ' is the result of smoothing one vertex of γ . If γ has n vertices and f faces, then γ' has $n - 1$ vertices and $f - 1$ faces. Every simple curve has 0 vertices and 2 faces. The lemma follows immediately by induction on the number of vertices.

In fact, the converse of this lemma is also true, although we don’t yet have the tools to prove it:

³A knot diagram is generic closed curve with additional data at each crossing, indicating which branch of the curve passes in front of the other. Homotopy moves that sensibly preserves this crossing data are called *Reidemeister moves*.

Theorem: *A signed double-permutation is the signed Gauss code of a planar curve if and only if it has two more faces than vertices.*

If you have played with planar graphs before, you might recognize this theorem as an avatar of *Euler's formula* $V - E + F = 2$. Because every vertex in the image graph of any non-simple curve has degree 4, the number of edges is exactly twice the number of vertices.

6.7 ...and the Aptly Named Yadda Yadda

- Knots and knot diagrams
- Carter surfaces of non-planar Gauss codes

6.8 References

1. James W. Alexander and Garland B. Briggs. On types of knotted curves. *Ann. Math.* 28(1/4):562–586, 1926–1927. *Reidemeister moves, with pictures.*
2. J. Scott Carter. Classifying immersed curves. *Proc. Amer. Math. Soc.* 111(1):281–287, 1991. *The face-tracing algorithm to reconstruct curves from signed Gauss codes.*
3. Kurt Reidemeister. Elementare Begründung der Knotentheorie. *Abh. Math. Sem. Hamburg* 5:24–32, 1927. *Reidemeister moves, without pictures.*
4. Ernst Steinitz. Polyeder und Raumeinteilungen. *Enzyklopädie der mathematischen Wissenschaften mit Einschluß ihrer Anwendungen* III.AB(12):1–139, 1916. *Proof of “Steinitz’s theorem” — Every 3-connected planar graph is the 1-skeleton of a convex polyhedron — using 3→3 homotopy moves in the medial graph. I promise those words will eventually make sense.*
5. Ernst Steinitz and Hans Rademacher. *Vorlesungen über die Theorie der Polyeder: unter Einschluß der Elemente der Topologie.* Grundlehren der mathematischen Wissenschaften 41. Springer-Verlag, 1934. Reprinted 1976. *More detailed proof of “Steinitz’s theorem”, with pictures.*

6.9 Possible reorganization

Consider shuffling the topics in lectures 6–8:

- Generic curves intro
 - image graphs
 - oriented and connected smoothing
 - winding numbers
 - signed crossings
 - rotation numbers: smiles and frowns, writhe (via smoothing)
- Gauss codes
 - motivation for studying these things!
 - signed: Gauss diagrams, face tracing, Euler’s formula (via smoothing)
 - unsigned: Nagy graphs, Dehn codes, interlacement
- Homotopy
 - homotopy moves

- Steinitz's contraction
- regular homotopy, Whitney-Graustein, Nowik's algorithm
- defect and strangeness

Chapter 7

Unsigned Gauss codes^β

In the last lecture, we saw a simple algorithm to test whether a signed Gauss code is consistent with a generic curve in the plane: Count the faces (by symbol-chasing) and return true if and only if the number of faces is exactly two more than the number of crossings.

In his unpublished notes, written around 1840, Gauss was asked how to determine whether an *unsigned* Gauss code is consistent with a planar curve [3]. The same question was published about 40 years later by Tait [8]. I regard this as the first problem in computational topology. (Euler's famous Bridges of Königsberg is the *zeroth* problem in computational topology.) Both Gauss and Tait described a *partial* solution to his problem. The first complete solution was proposed by Julius Nagy almost a century later [4].¹

In this lecture, I'll describe an $O(n^2)$ -time *algorithm* originally described by Max Dehn in 1936 [1], with some simplifications suggested by Nagy's solution and more modern graph algorithms, as suggested by Read and Rosenstiehl [11], Rosenstiehl and Tarjan [12], and de Fraysseix and Ossona de Mendez [3].² My presentation of Dehn's algorithm also closely follows Kaufmann.
[[Fix reference numbers]]

7.1 Winding numbers again

Recall that the winding number of a polygon P around a point o can be computed by shooting a vertical ray from o and counting positive and negative crossings with the polygon. The same characterization extends to generic curves, but it's a little unsatisfying, for a couple of reasons. First, we only care about curves *up to isotopy*, but the ray-shooting algorithm requires choosing a specific (arbitrary) curve in the isotopy class. We can soften this objection somewhat by observing that we don't really need to count crossings with a *ray*; any path from o to infinity that crosses the curve a finite number of times will work.

But there's a more serious objection. Our representation of closed curves (signed Gauss codes) doesn't include any geometric information. But how do we represent the point? We can't

¹Nagy's algorithm attempts to construct a *Seifert decomposition* of the encoded curve. I'm afraid I don't understand Nagy's solution well enough to describe it, or even to be confident that it is correct.

²**Dozens** of other combinatorial and algebraic characterizations of planar Gauss codes have been published since Dehn's solution, but as far as I know, none lead to a simpler or more efficient algorithm (except through the use of linear-time algorithms to test graph planarity, which is cheating).

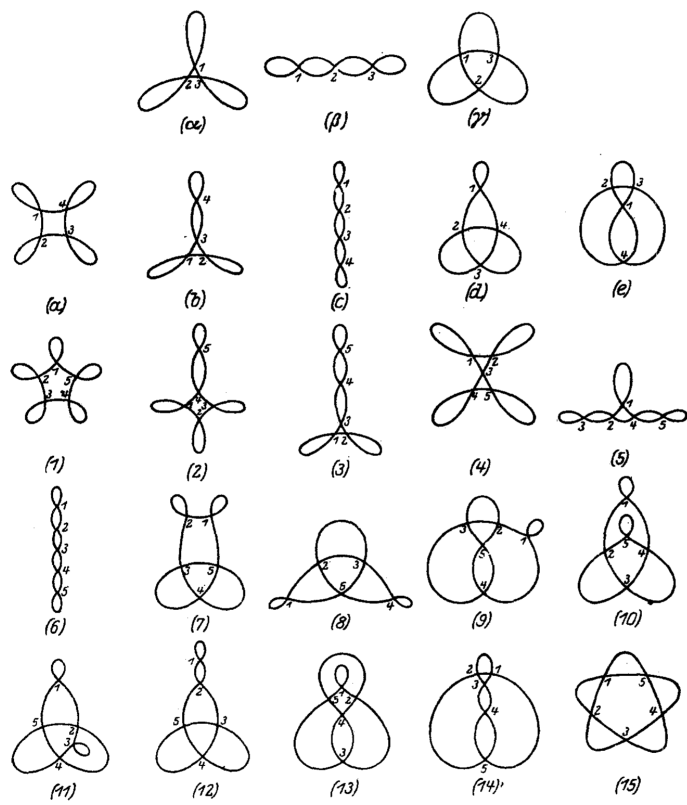


Fig. 1.

Figure 7.1: Nagy's 1927 census of unsigned Gauss codes of lengths 6 through 10

give *coordinates*, because different curves with the same representation have different winding numbers around any *fixed* point!

Instead, we specify the obstacle point o by declaring which *face* of the curve contains it. More cleanly, we define the winding number of a curve γ around each of its *faces* using an *Alexander numbering*, we defined in Lecture 2 for polygons. For any directed edge e of the image graph, let $\text{left}(e)$ and $\text{right}(e)$ denote the faces immediately to the left and right of e (relative to the orientation of e).

- If f is the outer face, then $\text{wind}(\gamma, f) = 0$.
- For every directed edge e , we have $\text{wind}(\text{left}(e)) = \text{wind}(\text{right}(e)) + 1$

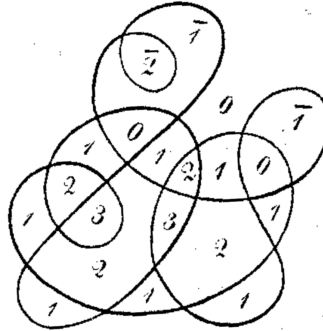


Figure 7.2: The Alexander numbering of a curve; bars indicate negation (Listing 1847)

7.2 Smoothing

Gauss observed that we can also define winding numbers by *smoothing* the curve at each vertex. Smoothing replaces a neighborhood of a single vertex with a pair of disjoint curve segments. In fact there are two different smoothing operations, depending on how the disjoint curve segments are attached. One smoothing operation disconnects the curve (or connects two constituents of a multicurve) but preserves the direction of both subcurves. The other keeps the curve connected, but requires the direction of part of the curve to be reversed.

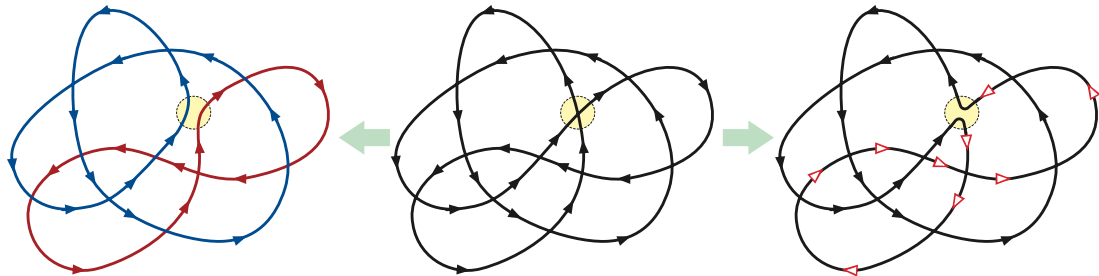


Figure 7.3: Smoothing a curve at a vertex. Left: preserving direction. Right: preserving connection.

Gauss observed that by smoothing *every* vertex of a curve to preserve direction, we can decompose the curve into a finite set of disjoint *simple* curves. This collection of simple curves is called the *Seifert decomposition* of the curve. Each of these simple curves has winding number $+1$ or -1 around its interior, depending whether the curve is oriented counterclockwise or clockwise.

The winding number of a curve γ around any point o (far from the vertices) is equal to the sum

of the winding numbers of the curves in the Seifert decomposition of γ around o . Equivalently, $\text{wind}(\gamma, o)$ is equal to the number of counterclockwise cycles that contain o minus the number of clockwise cycles that contain o .

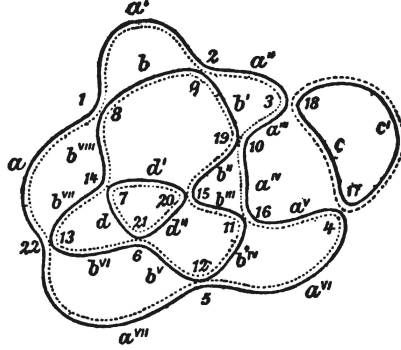


Figure 7.4: Gauss's example of a Seifert decomposition

7.3 Gauss's parity condition

Gauss observed without proof that the unsigned Gauss code of every planar curve satisfies a simple parity condition: Every substring that starts and ends with the same symbol has even length, or equivalently, each symbol appears once at an even index and once at an odd index. This parity condition was first proved necessary by Nagy. The following simpler combinatorial proof is due to Rademacher and Toeplitz.

Lemma: *Every pair of generic closed curves that intersect only transversely intersect at an even number of points.*

Proof: Let α and β be a transverse pair of generic closed curves, directed arbitrarily. Imagine a point moving around α . Each time this point crosses β , the winding number of β around that point changes by 1, and therefore changes from even to odd or vice versa. The moving point starts and ends in the same face of β , so its winding number change parity an even number of times.

Now let X be a string of length $2n$, in which each of the n unique symbols appears twice.

Lemma: *If X is the Gauss code of a planar curve, then every substring of X that starts and ends with the same symbol has even length.*

Proof: Let γ be a planar closed curve. Smoothing γ at any vertex produces two subcurves α and β . Up to a cyclic shift (reflecting a change of basepoint), the Gauss code for γ can be written as $axay$, where a is the label of the vertex, substring x encodes the crossings along α , and string y encodes the crossings along β . Each self-intersection point of α is encoded in x twice, and the other symbols of x encode the intersections between α and β . We conclude that x has even length, which completes the proof.

We can test this parity condition in $O(n^2)$ time by brute force, but in fact, there is a simple linear-time algorithm. Given the Gauss code X , we can define a directed graph $G(X)$, which I'll call the *Nagy graph* of X , as follows:

- The vertices of $G(X)$ correspond to the n distinct symbols in X .

- The edges of $G(x)$ correspond to (cyclic) substrings of X with length 2, alternately directed forward and backward. That is, the Nagy graph contains a forward edge $x_i \rightarrow x_{i+1}$ for every even index i and a backward edge $x_{i+1} \rightarrow x_i$ for every odd index i . For example, the Nagy graph of the string abcdefgchaigdjkhbifejk contains the following edges:

$$a \rightarrow b \leftarrow c \rightarrow d \leftarrow e \rightarrow f \leftarrow g \rightarrow h \rightarrow a \leftarrow i \rightarrow j \leftarrow k \rightarrow h \leftarrow b \rightarrow i \leftarrow f \rightarrow e \leftarrow j \rightarrow k \leftarrow a$$

Let me emphasize (despite the figure below) that the Nagy graph of a string is an *abstract graph*, which may or may not be planar.

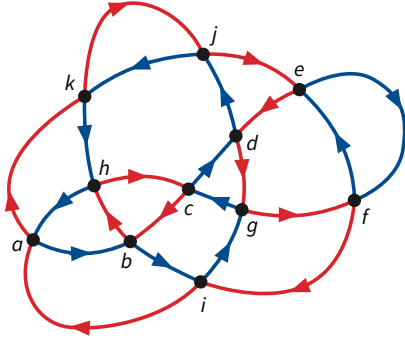


Figure 7.5: The Nagy graph of Gauss code abcdefgchaigdjkhbifejk; compare with Figure 6.

Now imagine a point moving around the Nagy graph $G(X)$, alternately traversing edges forward and backward in the order they appear in X . Whenever the point passes through a vertex of $G(X)$, it either traverses two inward edges $u \rightarrow v \leftarrow w$ (one forward and one backward) or two outward edges $u \leftarrow v \rightarrow w$ (one backward and one forward). The parity condition implies that if we leave any vertex v along a forward edge $v \rightarrow w$, we will next enter v along a backward edge $x \leftarrow v$ and v vice versa. In fact, these two conditions are equivalent.

Lemma: A Gauss code X satisfies the parity condition if and only if every vertex of its Nagy graph $G(X)$ has in-degree 2 and out-degree 2.

If a Gauss code does *not* satisfy the parity condition, then its Nagy graph will contain at least one vertex with in-degree 0 and out-degree 4, and an equal number of vertices with in-degree 4 and out-degree 0.

We can easily construct the Nagy graph and check the degree of each vertex in $O(n)$ time, where X is the length of the given Gauss code. (There are simpler algorithms to check the parity condition in $O(n)$ time, but we'll need the Nagy graph later, so we might as well build it now.)

Gauss also observed that the sequences abcadcedbe and abcabdecde satisfy his parity condition but cannot be realized by planar curves, so the parity condition is not sufficient. Tait later gave a third example abcadebdec.

7.4 Dehn's non-crossing condition

About 100 years after Gauss, Dehn [1] described *das Gaussische Problem der Trakte* and proposed an algorithm to solve it. Dehn observed that smoothing every vertex of a curve to keep the curve connected results in a simple closed curve that touches itself at every vertex. The same closed curve γ can have several different connected smoothings.

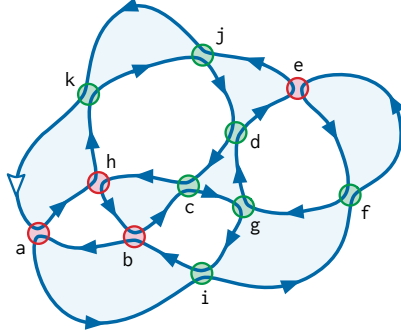


Figure 7.6: A smoothed curve with Dehn code ahkjdcgbcgibaifefgdejk

Lemma: Every connected smoothing of a planar curve γ is an Euler tour of the Nagy graph $G(X(\gamma))$, and vice versa.

Proof: Consider two consecutive edges $u \rightarrow v \rightarrow w$ of γ (not edges of $G(X(\gamma))$). Imagine smoothing the vertices of γ one at a time. Each smoothing reverses one of the subcurves from the smoothed vertex to itself. The edges uv and vw are reversed by all these same smoothing except at their common vertex v . Thus, exactly one of the two subpaths $u \rightarrow v$ or $v \rightarrow w$ is revised in the final Dehn smoothing. It follows that every Dehn smoothing of γ is an Euler tour of $G(X(\gamma))$.

On the other hand, the edges incident to any vertex of $G(X(\gamma))$ alternate in, out, in, out in cyclic order. Thus, every Euler tour of $G(X(\gamma))$ touches itself at every vertex, but never crosses itself. It follows that every Euler tour of $G(X(\gamma))$ is a connected smoothing of γ .

Lemma: A Gauss code X is realized by a planar curve if and only if its Nagy graph $G(X)$ has a planar embedding in which at least one (and therefore every) Euler tour is weakly simple.

Proof: An Euler tour of a planar graph can cross itself only at vertices. If X is the Gauss code of a planar curve γ , the edges incident to any vertex of $G(X)$, embedded on top of γ in the obvious way, alternate in-out-in-out in cyclic order, which makes a crossing at that vertex impossible.

On the other hand, suppose $G(X)$ has a planar embedding with a weakly simple Euler tour. Then the edges incident to each vertex in that embedding must alternate in-out-in-out in cyclic order. The original Gauss code X defines an *undirected* Euler tour U of $G(X)$, which traverses edges of $G(X)$ alternately forward and backward. U crosses itself at every vertex of $G(X)$. It follows immediately that U is a closed curve with Gauss code X .

7.5 Tree-onion figures

Dehn described a symbolic algorithm to test his non-crossing condition in terms of the sequence of *self-touching* points in order along the smoothed curve $\tilde{\gamma}$. Just like Gauss codes, this sequence contains exactly two occurrences of every symbol. To distinguish this sequence from the Gauss code of a curve, I'll refer to this new string as a *Dehn code*. We can similarly define the *Dehn diagram* of $\tilde{\gamma}$ as a cycle of $2n$ vertices, corresponding to the labels in the Dehn code, plus chords connecting identical labels.³

³The terms “Dehn code” and “Dehn diagram” are nonstandard.

Dehn observed that the Dehn diagram of any connected smoothing $\tilde{\gamma}$ of any planar curve γ is a *planar graph*; that is, we can embed some of the chords of the diagram inside the circle and the rest outside the circle, so that no pair of chords intersects. Specifically, if we perturb $\tilde{\gamma}$ slightly into a simple curve, the neighborhood of each vertex either has connected intersection with the interior of $\tilde{\gamma}$ or connected intersection with the exterior of $\tilde{\gamma}$. These vertices correspond to inner and outer chords, respectively.

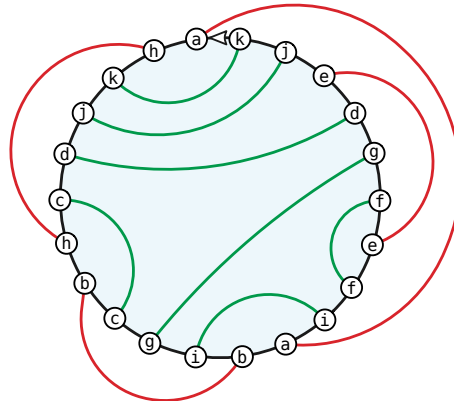


Figure 7.7: A planar Dehn diagram for the Dehn code ahkjjdchbcgibaifefgdejk; compare with the previous figure!

Dehn playfully referred to these planar diagrams as “Baum-Zwiebel Figuren” [“tree-onion diagrams”] and their corresponding Gauss codes as “Baum-Zwiebel Reihen” [“tree-onion strings”]. Tree onions, also known as walking onions or Egyptian onions, are onion cultivars that grow clusters of small bulbs at the top of the stem, where other *Allium* species have flowers. The chords of a tree-onion figure (loosely) resemble clusters of onion layers. Coincidentally(?), the dual graph of the inner chords (or the outer chords) of any tree-onion figure is a tree.⁴

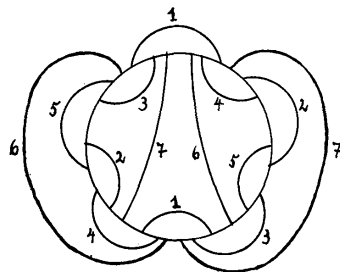


Fig. 15.

Figure 7.8: A tree-onion figure [Dehn 1936]

(Petersen [9] used similar diagrams in 1891 to study abstract regular graphs. Consider a connected 4-regular graph G with n vertices. Petersen defined a “stretched graph” by representing any Euler tour of G as a cycle of length $2n$, with additional edges connecting the two occurrences of each vertex of G . If we alternately color the edges this cycle red and blue, every vertex of G is incident to two edges of each color. Thus, every 4-regular graph can be decomposed into two

⁴Tree-onion figures are also closely related to tree-cotree decompositions of planar maps. Specifically, there is a bijection between tree-cotree decompositions of a planar map Σ and tree-onion figures of non-crossing Euler tours of the medial map Σ^\times . (Don’t worry; those words will make sense soon.) So it’s really tempting to refer to the partition of inner and outer chords in a tree-onion figure as a *coonion-onion decomposition*.



Figure 7.9: Tree onion bulblets. [Kurt Stüber 2004, CC BY-SA 3.0, via Wikimedia Commons]



Figure 7.10: Egyptian tree onion. From *Child's Rare Flowers, Vegetables & Fruits* (1894)

2-factors. Applying Petersen's construction to any curve, as an Euler tour of its image graph, recovers the forward and backward cycles in the curve's Nagy graph.)

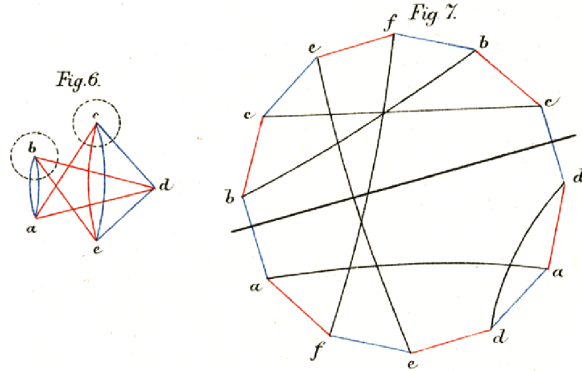


Figure 7.11: Petersen's diagram of an Euler tour (Petersen 1891)

7.6 Bipartite interlacement

Read and Rosenstiehl [6] observed that Dehn's planarity condition can be verified efficiently by constructing yet another graph, called the *interlacement graph* of the Dehn code. The interlacement graph has n vertices, one for each symbol, and an edge between any two symbols x and y whose appearances are interlaced $x \dots y \dots x \dots y$ in the Dehn code. Partitioning the chords of a Dehn diagram into pairwise disjoint inner and outer chords is equivalent to partitioning the vertices of the interlacement graph into two independent sets. In other words, a Dehn diagram is planar if and only if its interlacement graph is bipartite.

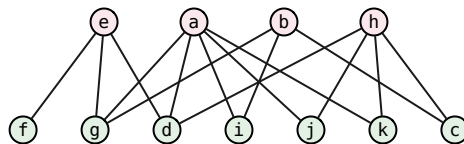


Figure 7.12: The bipartite interlacement graph for the Dehn code ahkjdchbcgibaifefgdejk

7.7 Recrossing

To complete his algorithm, Dehn observed that we can transform the Dehn diagram of any Euler tour of $G(X)$ into a 4-regular graph by replacing each chord with a pair of crossing chords with a crossing, as shown below. Assuming the interlacement graph of the Dehn code is bipartite, the corresponding Dehn diagram is planar, so this recrossing process yields a single closed curve consistent with our original Gauss code X .

Putting all the pieces together, we conclude:

Theorem: A Gauss code X can be realized by a planar closed curve if and only if at least one (and therefore every) Euler tour of $G(X)$ has a bipartite interlacement graph.

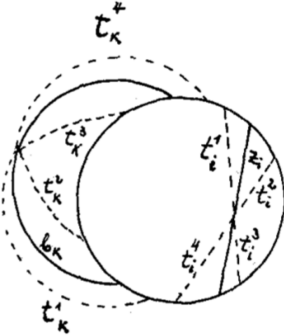


Fig. 18.

Figure 7.13: Building a closed curve from a tree-onion-diagram (Dehn 1936)

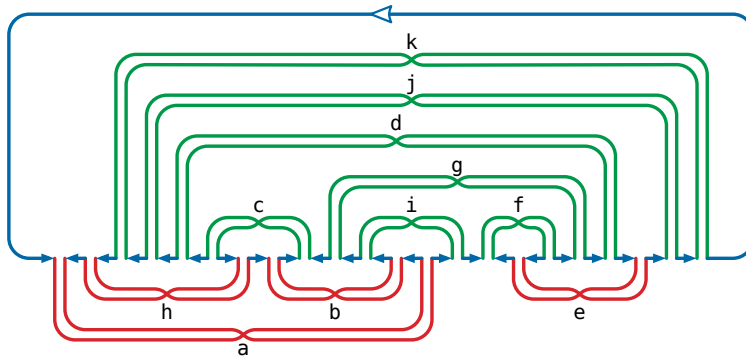


Figure 7.14: A planar curve consistent with the original Gauss code abcdefgchaigdjkhbifejk

7.8 Algorithm summary

Theorem: Given a Gauss code X of length $2n$, we can either construct a planar curve consistent with X or correctly report that no such curve exists, in $O(n^2)$ time.

Proof: The algorithm proceeds as follows:

1. Construct the Nagy graph $G(X)$ of X . This can be done in $O(n)$ time by brute force. If any vertex of $G(X)$ has no outgoing edges, halt and report that X is not realizable. Otherwise, $G(X)$ is Eulerian, and thus X satisfies Gauss's parity condition.
2. Compute any Euler tour of $G(X)$. This can be done in $O(n)$ time using the well-known algorithm of Hierholzer (not Euler!).
3. Construct the Dehn code \tilde{X} of this Euler tour. This can be done in $O(n)$ time by brute force.
4. Construct the interlacement graph $I(\tilde{X})$ of \tilde{X} . This can be done in $O(n^2)$ time by brute force.
5. Verify that the interlacement graph is bipartite. The interlacement graph has n vertices and at most $O(n^2)$ edges, so we can verify bipartiteness in $O(n^2)$ time using whatever-first search. If the interlacement graph is not bipartite, halt and report that X is not realizable.
6. Build a tree-onion figure for \tilde{X} from any partition of nodes in the interlacement graph.

This can be done in $O(n)$ time by brute force.

7. Transform the plane Dehn diagram into a 4-regular plane graph by replacing each chord with a pair of crossing chords, as shown in Figures 13 and 14. This can be done in $O(n)$ time by brute force; the result is a closed curve consistent with our original Gauss code X .

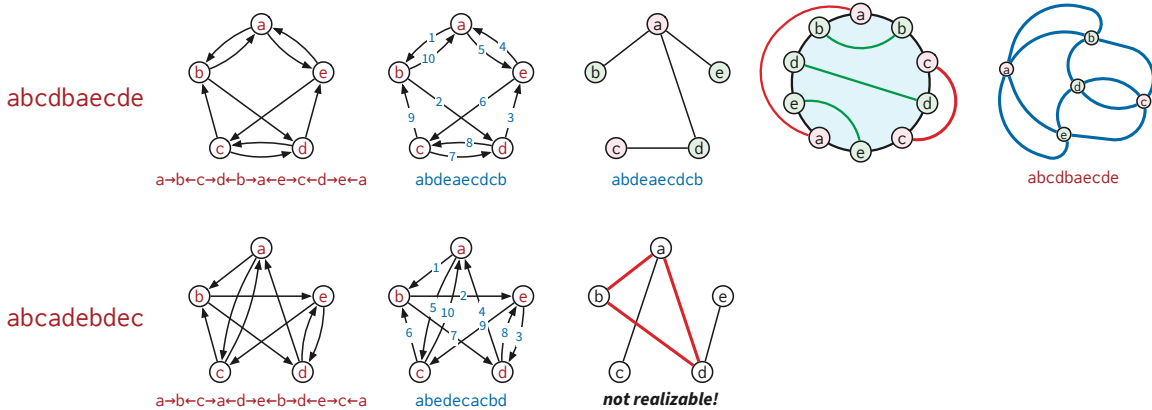


Figure 7.15: Two examples of Dehn's Gauss-code algorithm in action

7.9 Faster! Faster!

There are several linear-time algorithms to test the interlacement condition *without* explicitly constructing the interlacement graph, but we're out of time.

7.10 ...and the Aptly Named Yadda Yadda

- Tait-Dowker-Thistlethwaite codes
- Pile of twin stacks algorithm
- Left-right graph planarity test

7.11 References

1. Max Dehn. Über kombinatorische Topologie. *Acta Math.* 67:123–168, 1936.
2. Clifford H. Dowker and Morwen B. Thistlethwaite. Classification of knot projections. *Topology Appl.* 16(1):19–31, 1983.
3. Hubert de Fraysseix and Patrice Ossona de Mendez. A short proof of a Gauss problem. *Proc. 5th Int. Symp. Graph Drawing*, 230–235, 1997. Lecture Notes Comput. Sci. 1353, Springer.
4. Carl Friedrich Gauß. Nachlass. I. Zur Geometria situs. *Werke*, vol. 8, 271–281, 1900. Teubner. Originally written between 1823 and 1840.
5. Carl Hierholzer. Über die Möglichkeit, einen Linienzug Ohne Wiederholung und ohne Unterbrechung zu umfahren. *Math. Ann.* 6:30–32, 1873.

6. Louis H. Kauffman. Gauss codes, quantum groups and ribbon Hopf algebras. *Rev. Math. Phys.* 5(4):735–773, 1993.
7. Louis H. Kauffman. Virtual knot theory. *Europ. J. Combin.* 20(7):663–691, 1999. arXiv:math/9811028.
8. Julius v. Sz. Nagy. Über ein topologisches Problem von Gauß. *Math. Z.* 26(1):579–592, 1927.
9. Julius Petersen. Die Theorie der regulären graphs. *Acta Math.* 15:193–220, 1891. Yes, really, “graphs” not “Graphen”.
10. Hans Rademacher and Otto Toeplitz. On closed self-intersecting curves. *The Enjoyment of Mathematics: Selections from Mathematics for the Amateur*, chapter 10, 61–66, 1990. Dover Publ. Originally published by Princeton Univ. Press, 1957.
11. Ronald C. Read and Pierre Rosenstiehl. On the Gauss crossing problem. *Combinatorics*, 843–876, 1976. Colloq. Math. Soc. János Bolyai 18, North-Holland. Modern description of Dehn’s solution to the Gauss code problem.
12. Pierre Rosenstiehl and Robert E. Tarjan. Gauss codes, planar Hamiltonian graphs, and stack-sortable permutations. *J. Algorithms* 5(3):375–390, 1984. Linear-time implementation of Dehn’s solution to the Gauss code problem.
13. Peter Guthrie Tait. On knots I. *Trans. Royal Soc. Edinburgh* 28(1):145–190, 1876–7.

Chapter 8

Curve homotopy and curve invariants^α

Caveat Lector: This note is still pretty sketchy!

In an earlier lecture we argued that any generic curve in the plane can be continuously deformed into any other by a finite sequence of homotopy moves. But our earlier argument was unsatisfying for a number of reasons. First, I deliberately glossed over several details; while I claim that these details are ultimately mechanical, you have no reason to believe my assessment, or even that I've worked out the details at all. (I *have* worked out the details, but my mere claim shouldn't be enough to convince you. Proof by Old Tenured White Dude is not a proof at all.) Second, the proof is nonconstructive. Third, the proof gives us no idea *how many* homotopy moves are required.

8.1 Steinitz's contraction algorithm

The following constructive algorithm for contracting a generic curve via homotopy moves is implicit in Steinitz's 1916 proof of the seminal theorem that bears his name: A graph G is the 1-skeleton of a three-dimensional convex polyhedron if and only if G is planar and 3-connected. (I'll explain the connection between this algorithm and Steinitz's theorem later in the course.)

We first define some useful substructures of non-simple generic curves. A *loop* in a curve γ is a simple subpath of γ that starts and ends at the same vertex. A *spindle* is a pair of simple, interior-disjoint subpaths of γ with the same distinct endpoints. A *vertex* of a spindle is an endpoint of the subpaths of γ that defines it. A spindle is *convex* if its interior contains exactly one corner of each vertex. A spindle is *irreducible* if its interior does not contain the interior of another bigon; easy case analysis implies that every irreducible spindle is convex. A *monogon* is a face whose boundary is a loop; a *bigon* is a face whose boundary is a (necessarily convex) spindle.

Lemma (Steinitz): *Let γ be a non-simple curve with no monogons. There is at least one irreducible spindle in γ .*

Proof: Let x be the first vertex encountered twice when traversing γ from an arbitrary basepoint; the subpath of γ between the two occurrences of x is a loop. Thus, γ contains at least one loop. Let ℓ be the loop with the fewest faces in its interior, breaking ties arbitrarily.

We call any maximal subpath of γ in the interior of ℓ a *strand*. There must be at least one

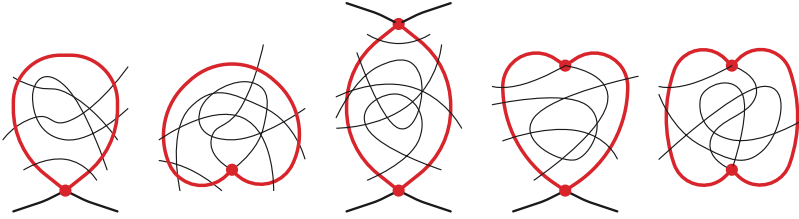


Figure 8.1: Non-minimal loops and spindles; only the first loop and spindle are “convex”.

strand, since otherwise ℓ would be a monogon. The minimality of ℓ implies that each strand is a *simple* path. Each strand in ℓ forms a convex spindle with some subpath of ℓ ; thus, γ contains at least one spindle. Any spindle with the fewest faces in its interior is irreducible.

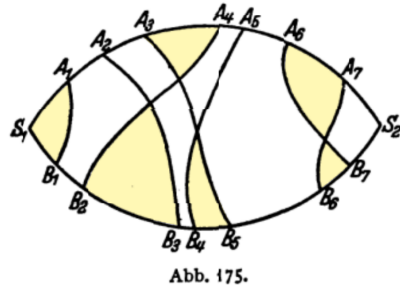


Figure 8.2: An irreducible spindle with six boundary triangles (Steinitz and Rademacher 1934).

Lemma (Steinitz): *Let γ be a non-simple curve with no monogons, and let σ be any irreducible spindle in γ . Either σ is a bigon, or there is a triangular face in the interior of σ that shares an edge with σ .*

Proof: Again, any maximal subpath of γ in the interior of σ a *strand*; there must be at least one strand, since otherwise σ is a bigon. Irreducibility implies that the strands satisfy three conditions:

- Every strand is simple. (Otherwise a strand would contain a loop, and therefore either a monogon or a smaller spindle.)
- Every strand has one endpoint on each subpath defining σ . (Otherwise, that strand would form a smaller spindle with one side of σ .)
- Every pair of strands intersects at most once. (Otherwise, some pair of strands would define a smaller spindle.)

Now there are two cases to consider. If no pair of strands intersect, the faces at both vertices are triangles, each sharing two edges with σ . Otherwise, imagine continuously sweeping a curve through the interior of σ from one boundary subpath to the other, and let x be the first interior vertex that this curve sweeps over. The two strands that intersect at x form a triangular face with one of the boundary curves of σ .

With these two lemmas in hand, we can now describe Steinitz’s algorithm. Let γ be any generic curve with n vertices. If $n = 0$, the curve is simple and there is nothing to do. If γ contains a loop, remove it with a single $1 \rightarrow 0$ move and recursively simplify the remaining curve. Otherwise, let

σ be any irreducible spindle. We empty σ by repeatedly performing $3 \rightarrow 3$ moves, each time moving a triangular face from the interior of σ to the exterior. Once σ becomes a bigon, we remove it with a single $2 \rightarrow 0$ move, and then recursively simplify the remaining curve.

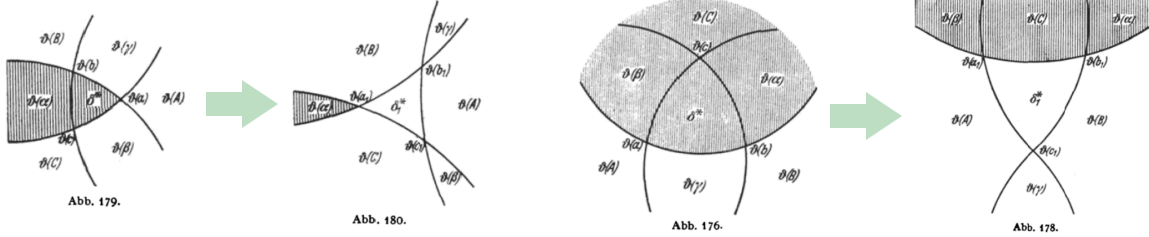


Figure 8.3: Extracting a triangle from a spindle (Steinitz Rademacher 1934).

In the worst case, the algorithm uses $O(n)$ moves to empty and remove each irreducible spindle. Each phase of the algorithm removes either one or two vertices. Thus, the algorithm runs through $\Theta(n)$ phases, each with $O(n)$ moves, so it makes $O(n^2)$ moves altogether. This analysis is tight; Steinitz's algorithm requires $\Omega(n^2)$ moves in the worst case.

This is not the fastest contraction algorithm known; in 2016, Hsien-Chih Chang and I described an algorithm to contract any planar curve Hsien using only $O(n^{3/2})$ homotopy moves; we also proved a matching $\Omega(n^{3/2})$ worst-case upper bound. However, unlike Steinitz's algorithm, our faster algorithm sometimes uses $0 \rightarrow 2$ moves. In 2022, Santiago Aranguri, Hsien-Chih Chang, and Dylan Fridman finally proved that any planar curve can be contracted using a sequence of $O(n^{3/2})$ homotopy moves that never increases the number of vertices; the sequence includes only $1 \rightarrow 0$, $2 \rightarrow 0$, and $3 \rightarrow 3$ moves.

8.2 Rotation number

Definition: winding number of the derivative around the origin. Always an integer. For simple curves, either $+1$ or -1 ; equal to the winding number around any interior point.

For polygons, equal to sum of exterior angles. (Studied by Meister in the 1700s, and arguably by Bradwardine in the 1300s.)

Classify points with rightward tangents as *happy* or *sad*; rotation number = #happy – #sad. [Gauss, possibly Meister]

Gauss: Also equal to sum of rotation numbers of Seifert circles.

But our usual representation doesn't give us access to tangents or curvature; indeed, generic curves need not have well-defined tangents. Instead we use a combinatorial formula known to Gauss in terms of the *writhe* of the curve. The writhe is defined as the sum over all vertices of the sign of the *first* crossing at that vertex; we emphasize that writhe is a function of both the curve and the basepoint.

$$\text{writhe}(\gamma) = \sum_x \text{sgn}(x)$$

To state Gauss's formula succinctly, we also need to extend the definition of winding number to points on the curve. We define the winding number along an edge of the image graph as the average of the winding numbers of its two incident faces; this is always a half-integer. Similarly, we define the winding number of a curve around one of its vertices as the average of the winding

numbers of the four faces incident to that vertex; this is always an integer. (Two of those four faces may be the same face.) We specifically define $\text{wind}_0(\gamma)$ to be the winding number of γ around its basepoint.

Lemma (Gauss): $\text{rot}(\gamma) = 2 \cdot \text{wind}_0(\gamma) + \text{writhe}(\gamma)$

Proof: Moving the basepoint through a positive crossing changes it into a negative crossing (so the writhe decreases by 2), but it also increases the winding number around the basepoint by 1. (So without loss of generality, we could assume that the basepoint is on the outer face and therefore $\text{wind}_0(\gamma) = \pm 1/2$, but this won't be necessary.)

Any continuous deformation of the curve that does not change the number of vertices can only create and destroy happy and sad points in matched pairs. (Deforming the curve also deforms its derivative, and the deformation of the derivative that avoids the origin can only create or destroy crossings with the positive x -axis in matched positive-negative pairs. Think in terms of homotopy moves!) So rotation number is an *isotopy* invariant.

Now we argue by induction over any sequence of homotopy moves that leads to a simple cycle. We assume the basepoint is far away from whatever move we're analyzing, so $\text{wind}_0(\gamma)$ doesn't change.

- 0→1: If the deleted vertex is positive, the loop is oriented counterclockwise, so the move decreases both the rotation number and the writhe by 1. Similarly, deleting a negative vertex increases both rotation number and writhe by 1.
- 2→0: The two vertices have opposite signs, so the writhe doesn't change. But the number of happy and sad points doesn't change either, so the rotation number doesn't change.
- 3→3: Nothing in the formula changes.

Finally, we observe that the formula is trivially correct when the curve is simple.

Would it be easier to argue by induction on the number of vertices via oriented smoothing? By induction we have $\text{rot}(\gamma) = \text{rot}(\gamma^-) + \text{rot}(\gamma^+) = 2 \cdot \text{wind}_0(\gamma^-) + \text{writhe}(\gamma^-) + 2 \cdot \text{wind}_0(\gamma^+) + \text{writhe}(\gamma^+)$. The smoothed vertex vanishes, but it becomes the basepoint of one of the two constituent curves. The number of crossings between the two constituent curves γ^- and γ^+ is even, with exactly half positive and half negative. So we need to relate $\text{wind}_0(\gamma^+)$ to the sign of the smoothed vertex.

8.3 Regular homotopy

No 1→0 or 0→1 moves. So rotation number never changes.

Nowik's algorithm: Without loss of generality the basepoint is on the outer face. Repeat the following until the curve consists of empty loops:

- Find a simple loop.
- Empty the loop (two moves per interior vertex, plus one move for each remaining interior strand)
- Move the loop close to the basepoint
- Boy's trick: Cancel two adjacent loops on opposite sides.

When these iterations end, either all loops are inside or all loops are outside. We can deform one canonical curve to the other using a linear number of moves. Altogether, the algorithm requires $O(n^2)$ moves to canonize a curve with n vertices.

it follows that rotation number is a complete regular homotopy invariant (just like winding number around a point is a homotopy invariant in the once-punctured plane).

8.4 Strangeness

(Cite Arnold, Aicardi, Polyak, *inter alia*)

$$\text{strange}(\gamma) = \text{wind}_0^2(\gamma) - \frac{1}{4} + \sum_x \text{sgn}(x) \cdot \text{wind}(\gamma, x)$$

Basepoint independence: moving the basepoint across a positive vertex x with winding number w changes x to a negative vertex (decreasing the sum by $2w$), but increases wind_0 from $w - 1/2$ to $w + 1/2$ (increasing $\text{wind}_0^2(\gamma)$ by $2w$).

Lemma: *Each $3 \rightarrow 3$ move changes strangeness by exactly 1. $2 \rightarrow 0$ moves do not change strangeness.*

Proof: case analysis

Our outer-canonical curves have strangeness 0, because each vertex has winding number 0. So the strangeness of a curve is a lower bound on the number of moves required to canonize it. A nested counterclockwise loop with rotation number r has $r + 1$ positive vertices and strangeness $r(r + 1)/2$. So Nowik's algorithm is optimal (up to constant factors).

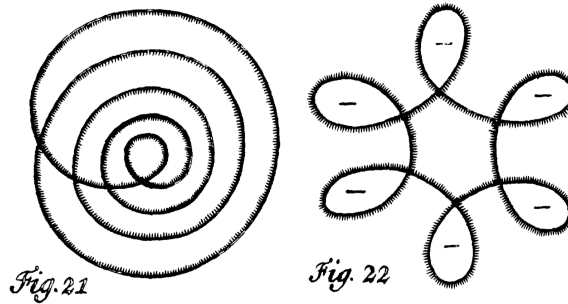


Figure 8.4: Curves with maximum and minimum strangeness (Meister 1769)

8.5 Defect

$$\text{defect}(\gamma) = -2 \sum_{x \neq y} \text{sgn}(x) \cdot \text{sgn}(y)$$

Lemma: *Homotopy moves change defect as follows: $1 \rightarrow 0$ moves do not change the defect. Each $2 \rightarrow 0$ move either decreases the defect 2 or leaves it unchanged. Each $3 \rightarrow 3$ move either increases the defect by 2 or decreases the defect by 2.*

Proof: Case analysis.

The *flat torus knot* $T(p, q)$ is defined as

$$T(p, q)(\theta) = (\cos(q\theta) + 2)\cos(p\theta), (\cos(q\theta) + 2)\sin(p\theta)).$$

This curve has exactly $(p - 1)q$ vertices.

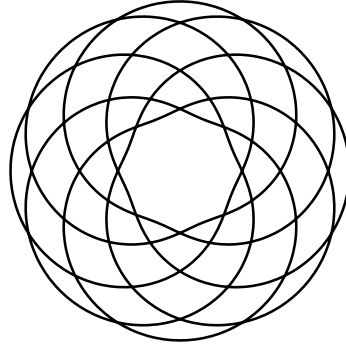


Figure 8.5: The flat torus knot $T(7, 8)$.

Lemma: $\text{defect}(T(p, p + 1)) = 2\binom{p+1}{3} = n^{3/2}/3 - O(n)$

So indeed, there are n -vertex curves that require $\Omega(n^{3/2})$ homotopy moves to simplify, so Hsien-Chih Chang's and my algorithm is worst-case optimal.

8.6 Aptly Yadda Yadda

- Connection to Steinitz's theorem via medial graphs
- Connection to electrical reduction via ΔY -transformations
- Hass and Scott's lemma for curves on orientable surfaces
- Monotone planar homotopy in $O(n^{3/2})$ moves
- Simplifying curves in the annulus or torus in $O(n^2)$ moves
- $\Omega(n^2)$ lower bound for annular curves via winding depth

Chapter 9

Planar Graphs $^\beta$

9.1 Abstract graphs

A graph is an abstract combinatorial structure that models pairwise relationships. You probably have a good intuitive idea what a graph is already. Nevertheless, to avoid subtle but pervasive differences in terminology, notation, and basic assumptions, I will carefully define everything from scratch. In particular, we need a definition that allows parallel edges and loops, so we can't use the standard combinatorialist's definition as a pair of sets (V, E) , and I don't want to wander into the notational quagmire of multisets. So here we go.

An *abstract graph* is a quadruple $G := (V, D, \text{rev}, \text{head})$, where

- V is a non-empty set of abstract objects called *vertices*;
- D is a set of abstract objects called *darts*;
- rev is a permutation of the darts D such that $\text{rev}(\text{rev}(d)) = d \neq \text{rev}(d)$ for every dart $d \in D$;
- head is a function from the darts D to the vertices V .

Darts are also called *half-edges* or *arcs* or *brins* (French for “strands”).

For any dart d , we call the dart $\text{rev}(d)$ the *reversal* of d , and we call the vertex $\text{head}(d)$ the *head* of d . The *tail* of a dart is the head of its reversal: $\text{tail}(d) := \text{head}(\text{rev}(d))$. The head and tail of a dart are its *endpoints*. Intuitively, a dart is a directed path from its tail to its head; in keeping with this intuition, we say that a dart d *leaves* its tail and *enters* its head. I often write $u \rightarrow v$ to denote a dart with tail u and head v , even (at the risk of confusing the reader) when there is more than one such dart.

For any dart $d \in D$, the unordered pair $|d| = \{d, \text{rev}(d)\}$ is called an *edge* of the graph. We often write E to denote the set of edges of a graph. The constituent darts of an edge e are arbitrarily denoted e^+ and e^- . The *endpoints* of an edge $e = \{e^+, e^-\}$ are the endpoints (equivalently, just the heads) of its constituent darts. Intuitively, each dart is an orientation of some edge from one of its endpoints to the other.

A vertex v and an edge e are *incident* if v is an endpoint of e ; two vertices are *neighbors* if they are endpoints of the same edge. We often write uv to denote an edge with endpoints u and v , even (at the risk of confusing the reader) when there is more than one such edge.

A *loop* is an edge e with only one endpoint, that is, $\text{head}(e^+) = \text{tail}(e^+)$. Two edges are *parallel* if

they have the same endpoints. A graph is *simple* if it has no loops or parallel edges, and *non-simple* otherwise. Non-simple graphs are sometimes called “generalized graphs” or “multigraphs”; I will just call them “graphs”.

Let me repeat this louder for the kids in the back: ***Graphs are not necessarily simple.***

The degree of a vertex v , denoted $\deg_G(v)$ (or just $\deg(v)$ if the graph G is clear from context), is the number¹ of darts whose head is v , or equivalently, the number of incident edges plus the number of incident loops. A vertex is *isolated* if it is not incident to any edge.

9.2 Data structures

Here is an equivalent definition that might be clearer to computer scientists: **A (finite) graph is whatever can be stored in a standard graph data structure.**

The canonical textbook graph data structure is the *incidence list*. (For simple graphs, the same data structure is more commonly called an *adjacency list*.) The n vertices of the graph are represented by distinct integers between 1 and n . A standard incidence list consists of an array indexed by the vertices; each array entry in the array points to a linked list of the darts leaving the corresponding vertex. (The order of darts in these linked lists is unimportant; we use linked lists only because they support certain operations quickly.) The record for each dart d contains the index of $\text{head}(d)$ and a pointer to the record for $\text{rev}(d)$. Storing a graph with n vertices and m edges in an incidence list requires $O(n + m)$ space.

If a graph is stored in an incidence list, we can insert a new edge in $O(1)$ time, delete an edge in $O(1)$ time (given a pointer to one of its darts), and visit all the edges incident to any vertex v in $O(1)$ time per edge, or $O(\deg(v))$ time altogether. There are a few standard operations that incidence lists do not support in $O(1)$ time, the most glaring of which is testing whether two vertices are neighbors. Surprisingly, however, most efficient graph algorithms do not require this operation, and for those few that do, we can replace the linked lists with hash tables.

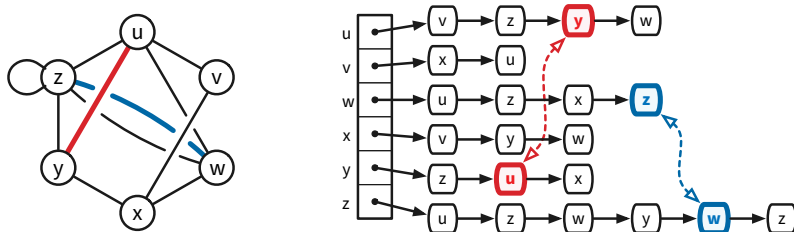


Figure 9.1: An incidence list, with the dart records for two edges emphasized. For clarity, most reversal pointers are omitted.

More generally, “array” and “linked list” can be replaced by any suitable data structures that allow random access and fast iteration, respectively. A particularly simple and efficient implementation keeps *all* data in standard arrays. For a graph with n vertices and m edges, we represent vertices by integers between 0 and $n - 1$, edges by integers from 0 to $m - 1$, and darts by integers between

¹Our definition of graphs allows graphs with infinitely (even uncountably) many vertices and edges, and in particular, vertices with infinite (even uncountable) degree. Most of the graphs we consider in this course are finite, and obviously algorithms can only *explicitly* construct finite graphs. However, we do sometimes implicitly represent infinite graphs with certain symmetries using finite graphs. For example, any triangulation of a polygon with holes (a finite planar map, whose dual is another planar map) is an implicit representation of its universal cover (an infinite planar map whose dual is an infinite tree).

0 and $2m - 1$. Each edge e is composed of darts $e^- = 2e$ and $e^+ = 2e + 1$; thus, the reversal of any dart d is obtained by flipping its least significant bit: $d \oplus 1$. The actual data structure consists of three arrays:

- $\text{first}[0..n - 1]$, where $\text{first}[v]$ is any dart leaving vertex v .
- $\text{head}[0..2m - 1]$, where $\text{head}[d]$ is the head of dart d .
- $\text{next}[0..2m - 1]$, where $\text{next}[d]$ is the successor of d in the list of darts leaving $\text{tail}(d)$.

It is convenient to treat the list of darts leaving each vertex as a *circular* list; then next stores a permutation of the darts, each of whose cycles is the set of darts leaving a vertex. We may also want to store a predecessor array $\text{prev}[0..2m - 1]$ that stores the inverse of this permutation. We do not need a separate tail array, because $\text{tail}(d) = \text{head}[d \oplus 1]$.

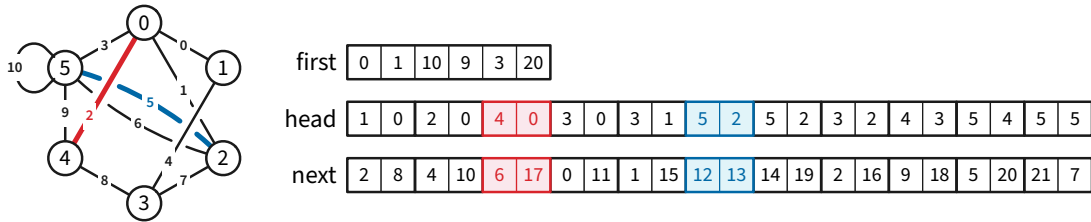


Figure 9.2: An incidence array representation of the same graph as Figure 1.

For algorithms that make frequent changes to the graph (adding and/or deleting vertices and/or edges), we should use dynamic hash tables instead of raw arrays. Finally, we can easily store algorithm-dependent auxiliary data such as vertex coordinates, edge weights, distances, or flow capacities in separate arrays (or hash tables) indexed by vertices, edges, or darts, as appropriate.

9.3 Topological graphs

Graphs can also be formalized as topological structures rather than purely combinatorial structures. Informally, a *topological graph* consists of a set of distinct points called *vertices*, together with a collection of vertex-to-vertex paths called *edges*, which are disjoint and simple, except possibly at their endpoints.

More formally, a topological graph G^\top is the quotient space of a set of disjoint closed intervals, with respect to an equivalence relation over the intervals' endpoints. The projections of the intervals are the *edges* of G^\top ; the projections (or equivalence classes) of interval endpoints are the *vertices* of G^\top . Again, for the kids in the back, topological graphs are not required to be simple; they can contain loops and parallel edges.²

Mechanical definition-chasing implies that any topological graph G^\top can be described by a unique abstract graph G . For example, the darts of G are orientations of the edges of G^\top . Conversely, any abstract graph describes a unique (up to homeomorphism) topological graph G^\top .³

²And again, the definition allows topological graphs with infinitely (even uncountably) many vertices and edges, and infinite (even uncountable) vertex degrees.

³Even worse, graph theorists use the phrase “topological graph” to mean a *generic drawing* or *immersion* of a graph in the plane. In a generic drawing, vertices are represented by distinct points; edges are represented by paths between their endpoints; no edge passes through a vertex except its endpoints; all (self-)intersections between edge interiors are transverse; and all pairwise (self-)intersection points are distinct.

9.4 Planar graphs and planar maps

A *planar embedding* of a graph G represents its vertices as distinct points in the plane (typically drawn as small circles) and its edges as simple interior-disjoint paths between their endpoints. Equivalently, a planar embedding of G is a continuous injective function from the corresponding topological graph G^\top into the plane. A graph is *planar* if it has at least one planar embedding. Somewhat confusingly, the image of a planar embedding of a planar graph is also called a *plane graph*.

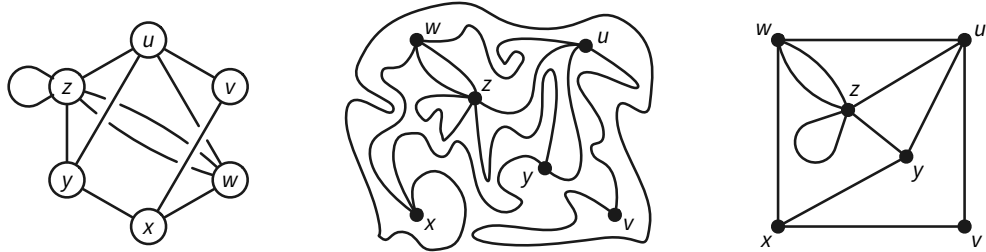


Figure 9.3: A planar graph G and two planar embeddings of G .

The components of the complement of the image of a planar embedding are called the *faces* of the embedding. Assuming the embedded graph is connected, the Jordan curve theorem implies that every bounded face is homeomorphic to an open disk, and the unique unbounded face is homeomorphic to the complement of a closed disk. For disconnected graphs, at least one face is homeomorphic to an open disk with a finite number of closed disks removed.

The faces on either side of an edge of a planar embedding are called the *shores* of that edge. For any dart d , the face just to the left of the image of d in the embedding is the *left shore* of d , denoted $\text{left}(d)$; symmetrically, the face just to the right is the *right shore* $\text{right}(d)$. The left and right shores of a dart can be the same face. An edge e and a face f are *incident* if f is one of the shores of e^+ ; similarly, a vertex v and a face f are incident if v and f have a common incident edge. The *degree* of a face f , denoted $\deg_G(f)$ (or just $\deg(f)$ if G is clear from context), is the number of darts whose right shore is f .

Let F be the set of faces of a planar embedding of a connected graph with vertices V and edges E . The decomposition of the plane into vertices, edges, and faces, typically written as a triple (V, E, F) , is called a *planar map*. Trapezoidal decompositions and triangulations of polygons are both examples of planar maps. A planar map is called a *triangulation* if every face, including the outer face, has degree 3. The underlying graph (V, E) of a planar triangulation is *not necessarily simple*.⁴

9.5 Rotation systems

As usual in topology, we are not really interested in *particular* embeddings or maps, but rather topological equivalence classes of embeddings or maps. Two planar embeddings of the same graph G are considered *equivalent* if there is an orientation-preserving homeomorphism of the plane to itself that carries one embedding to the other, or equivalently, if one embedding can be continuously deformed to the other through a continuous family of embeddings. Fortunately,

⁴For readers familiar with topology, a triangulation is *not* necessarily a simplicial complex, but rather what Hatcher calls a Δ -complex.

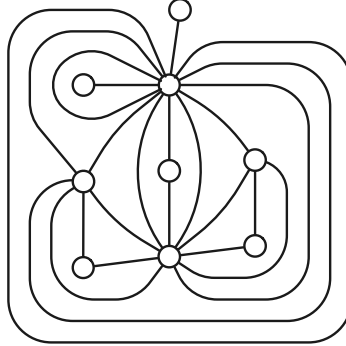


Figure 9.4: A nonsimple planar triangulation.

every equivalence class of embeddings has a concrete combinatorial representation, called a *rotation system*.

Recall that a *permutation* of a finite set X is a bijection $\pi: X \rightarrow X$. For any permutation π and any element $x \in X$, let $\pi^0(x) := x$ and $\pi^k(x) := \pi(\pi^{k-1}(x))$ for any integer $k > 0$. The *orbit* of an element x is the set $\{\pi^k(x) \mid k \in \mathbb{N}\} = \{x, \pi(x), \pi^2(x), \dots\}$. The restriction of π to any of its orbits is a cyclic permutation; the infinite sequence $x, \pi(x), \pi^2(x), \dots$ repeatedly cycles through the elements of the orbit of x . Thus, the orbits of any two elements of X are either identical or disjoint.

The *successor permutation* or an embedding of G is a permutation of the darts of G ; specifically, the successor $\text{succ}(d)$ of any dart d is the successor of d in the *clockwise* sequence of darts entering $\text{head}(d)$.⁵

Finally, the *rotation system* of an embedding is a triple $\Sigma = (D, \text{rev}, \text{succ})$, where

- D is the set of darts,
- rev is the reversal permutation of D , and
- succ is the successor permutation of D .

More generally, a *rotation system* or *combinatorial map* is any triple $(D, \text{rev}, \text{succ})$ where D is a set, rev is a fixed-point-free involution of D , and succ is another permutation of D . The *vertices* of a combinatorial map are the orbits of succ , its *edges* are the orbits of rev , and its *faces* are the orbits of $\text{rev}(\text{succ})$. The vertices and edges define the *1-skeleton* or *underlying graph* of Σ .

In other words, a rotation system is (almost) an incidence list where the order of darts in each list actually matters! The only annoying discrepancy is that rotation systems order darts *into* each vertex, while incidence lists order darts *out of* each vertex, but we can easily translate between these two standards using the identity $\text{next}(d) = \text{rev}(\text{succ}(\text{rev}(d)))$.

The *faces* of any connected graph embedding are also implicitly encoded in its rotation system. Recall that rev is the reversal permutation of the darts of a graph. For any dart d , the *dual successor* $\text{succ}^*(d) := \text{rev}(\text{succ}(d))$ is the next dart after d in *counterclockwise* order around the boundary of $\text{left}(d)$.

⁵Because the edges of a planar embedding can be *arbitrary* paths, it is not immediately obvious that this cyclic order is well-defined. In fact, the existence of a consistent order follows from careful application of the Jordan-Schönflies theorem.

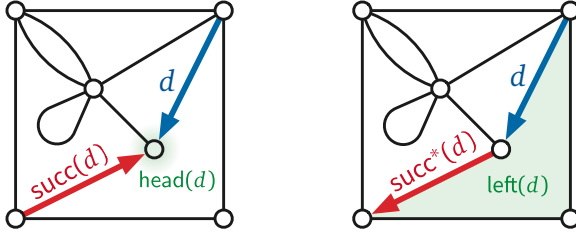


Figure 9.5: The successor and dual successor of a dart in a planar map.

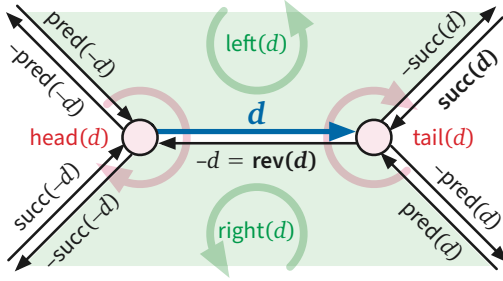


Figure 9.6: Navigating around a dart. To simplify the figure, negation is used to indicate dart reversal.

9.6 Formalities and Trivialities

Formally, rotation systems (and their equivalent incidence lists) describe embeddings onto the sphere $S^2 = \{(x, y, z) \mid x^2 + y^2 + z^2 = 1\}$, not onto the plane. Indeed, for many results about planar graphs, it is actually more natural to consider spherical embeddings on the sphere instead of the plane. Fortunately, we can transfer embeddings back and forth between the sphere and the plane using *stereographic projection*.

Stereographic projection is the function $\text{st}: S^2 \setminus (0, 0, 1) \rightarrow \mathbb{R}^2$ where $\text{st}(x, y, z) := (\frac{x}{1-z}, \frac{y}{1-z})$. The projection $\text{st}(p)$ of any point $p \in S^2 \setminus (0, 0, 1)$ is the intersection of the line through p and the “north pole” $(0, 0, 1)$ with the xy -plane. Points in the northern hemisphere project outside the unit circle; points in the southern hemisphere project inside the unit circle. Given any spherical embedding, if we rotate the sphere so that the embedding avoids $(0, 0, 1)$, stereographic projection gives us a planar embedding; conversely, given any planar embedding, inverse stereographic projection immediately gives us a spherical embedding. Thus, a graph is planar if and only if it has an embedding on the sphere.

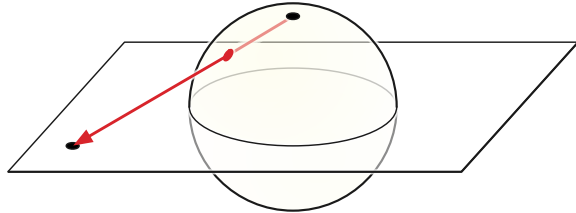


Figure 9.7: Stereographic projection.

To fully specify an embedding on the plane using a rotation system, we must somehow also indicate which face of the embedding is the *outer face*, or equivalently, which face of the corresponding spherical embedding contains the north pole. The outer face can be chosen arbitrarily.

Most of the exposition in these notes implicitly considers only embeddings of graphs with at least one edge. Exactly one map violates this assumption, namely the *trivial map*, which has one vertex, one face, and no edges. The trivial map is represented by the *empty* rotation system $(\emptyset, \emptyset, \emptyset)$.

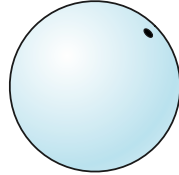


Figure 9.8: The trivial map of the sphere.

9.7 Caveat Lector

“There are dinner jackets and dinner jackets. This is the latter.”

— Vesper Lynd [Eva Green], *Casino Royale* (2006)

It is somewhat confusing standard practice to use the same symbol G (and the same word “graph”) to simultaneously denote at least six formally different structures:

- an abstract planar graph G ,
- the corresponding topological graph G^\top ,
- an embedding of G^\top into the plane,⁶
- the image of that embedding (which by definition is homeomorphic to G^\top),
- the rotation system $(D, \text{rev}, \text{succ})$ of that embedding, and
- the planar map (V, E, F) induced by that embedding.

Even when authors do distinguish between *graphs* and *maps*, it is standard practice to conflate abstract graphs, the corresponding topological graphs, and images of embeddings as “graphs”. In particular, the image of a planar graph embedding is commonly called a *plane graph*. Even the phrases “abstract graph” and “topological graph” are non-standard; the standard names for these objects are “graph” (spoken by a combinatorialist) and “graph” (spoken by a topologist), respectively.⁷ It is also standard practice to use the word “embedding” to mean *both* an injective function from G^\top to the plane *and* the image of such a function, and to use the word “map” to mean *both* the decomposition of the plane induced by an embedding *and* the rotation system of that embedding.

I will *try* to carefully distinguish between these various objects when the distinction matters, but there is a serious tension here between formality and clarity, so I am very likely to slip occasionally.

⁶or into the sphere, or an isotopy/homeomorphism class of such embeddings

⁷Even worse, graph theorists use the phrase “topological graph” to mean a *generic drawing* or *immersion* of a graph in the plane. In a generic drawing, vertices are represented by distinct points; edges are represented by paths between their endpoints; no edge passes through a vertex except its endpoints; all (self-)intersections between edge interiors are transverse; and all pairwise (self-)intersection points are distinct.

9.8 Duality

Recall that a combinatorial map is a triple $\Sigma = (D, \text{rev}, \text{succ})$, where D is a set of darts, rev is an involution of D , and succ is a permutation of D . For any such triple, the triple $\Sigma^* = (D, \text{rev}, \text{rev} \circ \text{succ})$ is also a well-defined combinatorial map, called the *dual map* of Σ .⁸

- The *vertices* of Σ^* are the orbits of $\text{rev} \circ \text{succ}$, which are also the faces of Σ .
- The *edges* of Σ^* are the orbits of rev , which are also the edges of Σ .
- The *faces* of Σ^* are the orbits of $\text{rev} \circ \text{rev} \circ \text{succ} = \text{succ}$, which are also the vertices of Σ !

In other words, each vertex v , edge e , dart d , or face f of the original map Σ corresponds to—or more evocatively, “is dual to”—or more formally, *IS*—a face v^* , edge e^* , dart d^* , or vertex f^* of the dual map Σ^* , respectively.

The endpoints of any primal edge e are dual to the shores of the corresponding dual edge e^* , and vice versa. Specifically, for any dart d , we have $\text{head}(d^*) = \text{left}(d)^*$ and $\text{tail}(d^*) = \text{right}(d)^*$. Intuitively, the dual of a dart is obtained by rotating it a quarter-turn counterclockwise.

Duality is trivially an involution: $(\Sigma^*)^* = \Sigma$, because $\text{rev} \circ \text{rev} \circ \text{succ} = \text{succ}$. It immediately follows that for any dart d , we have $\text{left}(d^*) = \text{head}(d)^*$ and $\text{right}(d^*) = \text{tail}(d)^*$.

We can also directly define the dual of a *topological* map Σ as follows. Choose an arbitrary point f^* in the interior of each face f of Σ . Let F^* denote the collection of all such points. For each edge e of Σ , choose a simple path e^* between the chosen points in the shores of e , such that e^* intersects e once transversely and does not intersect any other edge of Σ . Let E^* denote the collection of all such paths. These paths partition the plane into regions V^* , each of which contains a unique vertex.⁹ The dual map Σ^* is the decomposition of the plane into vertices F^* , edges E^* , and faces V^* .

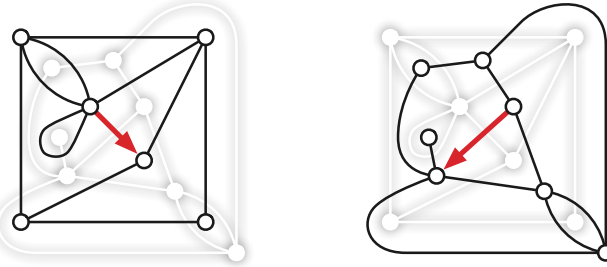


Figure 9.9: A planar map and its dual; one dart and its dual are emphasized.

[[add dual navigation figure]]

When G is an *embedded* graph, it is extremely common to define the *dual graph* G^* as the 1-skeleton of the dual map of the embedding. This habit is a bit misleading, however; duality is a correspondence between *maps* or *embeddings*, not between abstract graphs. An abstract planar graph can have many non-isomorphic planar embeddings, each of which defines a different “dual graph”. Moreover, the dual of a *simple* embedded graph is not necessarily simple; any vertex of degree 2 in G gives rise to parallel edges in G^* , and any bridge in G is dual to a loop in G^* . This is why we don’t want graphs to be simple by definition!

⁸The dual rotation system of a planar map is sometimes also called a *polygonal schema*, because it describes how to construct the map from a collection of disjoint planar polygons (the faces) by identifying pairs of boundary edges.

⁹You should verify this claim!

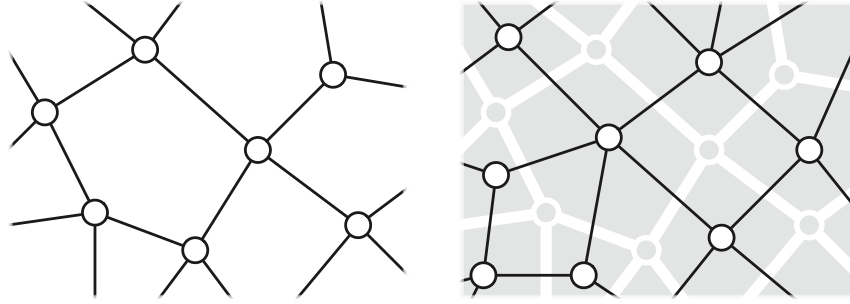


Figure 9.10: A portion of a planar map Σ , and the corresponding portion of the dual map Σ^*

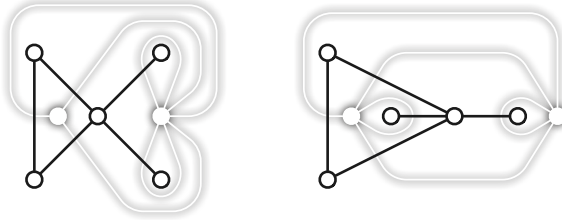


Figure 9.11: Two planar embeddings of a simple planar graph, with non-simple, non-isomorphic dual graphs.

9.9 Self-dual data structures

[[Duality is not a transformation; it's just a type-cast]]

Table 9.1: A (partial) duality dictionary.

Primal Σ	Dual Σ^*	Primal Σ	Dual Σ^*
vertex v	face v^*	head(d)	left(d^*)
dart d	dart d^*	tail(d)	right(d^*)
edge e	edge e^*	left(d)	head(d^*)
face f	vertex f^*	right(d)	tail(d^*)
succ	rev \circ succ	clockwise	counterclockwise
rev	rev		

9.10 Endianity

There are several apparently arbitrary choices to make in the definitions of incidence lists, rotation systems, and duality. Should we store cycles of darts with the same head or the same tail? Should darts be ordered in clockwise or counterclockwise order around vertices? Or around faces? Should $\text{head}(d^*)$ be defined as $\text{left}(d)^*$ or $\text{right}(d)^*$? Different standards are used by different authors, by the same authors in different papers, and sometimes even within the same paper.¹⁰ (Mea culpa!)

¹⁰I can't resist quoting Herodotus' *Histories*, written around 440BCE: "The ordinary [Greek] practice at sea is to make sheets fast to ring-bolts fitted outboard; the Egyptians fit them inboard. The Greeks write and calculate from left to right; the Egyptians do the opposite. Yet they say that their way of writing is toward the right, and the Greek way toward the left." Herodotus was strangely silent on which end of the egg the Egyptians ate first, or whether they preferred to fight a hundred duck-sized horses or one horse-sized duck.

Let me attempt to justify, motivate, or at least provide mnemonics for the specific choices I use in these notes. Some of these rules will only make sense later.

- Dualizing a dart should look (and act?) like multiplying a complex number by the imaginary unit i : a quarter turn *counterclockwise*. Thus, $\text{head}(d^*) = \text{left}(d)^*$ and $\text{tail}(d^*) = \text{right}(d)^*$.
- Duality is an involution, dammit. Thus, $\text{left}(d^*) = \text{head}(d)^*$ and $\text{right}(d^*) = \text{tail}(d)^*$. It follows that primal and dual planes must have opposite orientations!
- Simple *counterclockwise* cycles have winding number +1. So the dual successor function should order darts *counterclockwise* around their *left* shores. Thus, the primal successor function should order darts *clockwise* around their *heads*.
- Derivatives measure how much a function *increases*, so $\delta\omega(d) = \omega(\text{head}(d)) - \omega(\text{tail}(d))$. On the other hand, the directed boundary of a face should be a *counterclockwise* cycle, so $\partial\alpha(d) = \alpha(\text{left}(d)) - \alpha(\text{right}(d))$. Hey, look, consistency!

This standard creates an annoying discrepancy between the mathematical abstraction of a rotation system and its implementation as an incidence list. Rotation systems order darts around their heads because that makes the math cleaner, but incidence lists (typically) order darts around their tails because that better fits our intuition about searching graphs by following directed edges outward. Rather than give up either useful intuition, we'll rely on (and if necessary implement) the identity $\text{next}(d) = \text{rev}(\text{succ}(\text{rev}(d)))$.

9.11 Other derived maps

Let $\Sigma = (V, E, F)$ be an arbitrary planar map. In addition to the dual map Σ^* , there are several other useful maps that can be derived from Σ in terms of two local features.

- A *flag* of Σ is a vertex-edge-face triple (v, e, f) such that v is an endpoint of e and f is a shore of e .
- A *corner* of Σ is a pair of flags that share the same vertex and the same face. Intuitively, a corner is an incidence between a vertex and a face, or if you prefer, a pair of edges whose darts are consecutive around a vertex, or around a face. (Formally, a corner is just a nickname for a dart; for each dart d , the corresponding corner is the incidence between the vertex $\text{head}(d)$ and the face $\text{left}(d)$, or equivalently, between the vertex $\text{tail}(\text{succ}^*(d))$ and the face $\text{right}(\text{succ}(d))$.)

The *medial map* $\Sigma^\times = (E, C, V \cup F)$ is the map whose vertices correspond to the edges of Σ , whose edges correspond to the corners of Σ , and whose faces correspond to vertices and faces of Σ . The medial map of Σ is the image graph of a generic planar multicurve. Specifically, two vertices are connected by an edge in Σ^\times if the corresponding edges in Σ are adjacent in cyclic order around any vertex (or equivalently, around any face). Every map Σ and its dual Σ^* share the same medial map Σ^\times .

The dual of the medial map is called the *radial map* $\Sigma^\diamond = (V \cup F, C, E)$. The radial map can be constructed from Σ by placing a new vertex in the interior of each face f of Σ , connecting each face-vertex f to each vertex incident to f (with the appropriate multiplicity), and then erasing the original edges. Thus, each edge of Σ becomes a quadrilateral face of Σ^\diamond . Again, every map Σ and its dual Σ^* share the same radial map Σ^\diamond .

The *band decomposition* or *ribbon decomposition* of Σ is a map Σ^\square whose vertices correspond to the flags of Σ . Two flags define an edge in Σ^\square if they differ in exactly one component: the

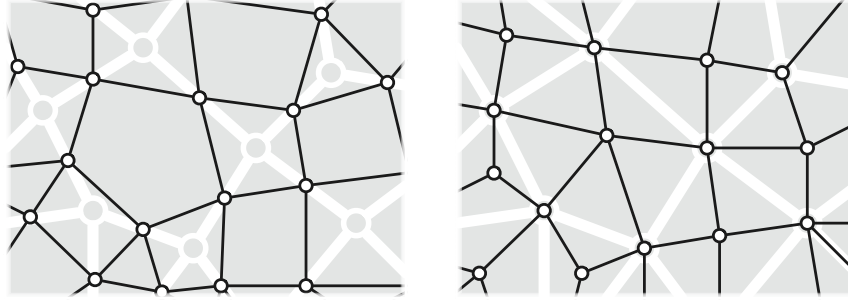


Figure 9.12: Corresponding portions of the medial map Σ^x and radial map Σ° of the planar map in Figure 8.

same vertex and edge but a different face, the same vertex and face but a different edge, or the same edge and face but a different vertex. Every vertex of Σ^\square has degree 3. The faces of Σ^\square correspond to the vertices, edges, and faces of Σ . Every map Σ and its dual Σ^* share the same band decomposition Σ^\square .

The dual of the band decomposition is the *barycentric subdivision* Σ^+ . This map can be constructed by adding a new vertex in the interior of each edge, subdividing it into two edges, adding a new vertex in the interior of every face, and finally connecting each face-vertex to its vertices and edge midpoints. Thus, the vertices of Σ^+ correspond to the vertices, edges, and faces of Σ , and the faces of Σ^+ correspond to the flags of Σ . Every face of Σ^+ is a triangle. Again, every map Σ and its dual Σ^* share the same barycentric subdivision Σ^+ .

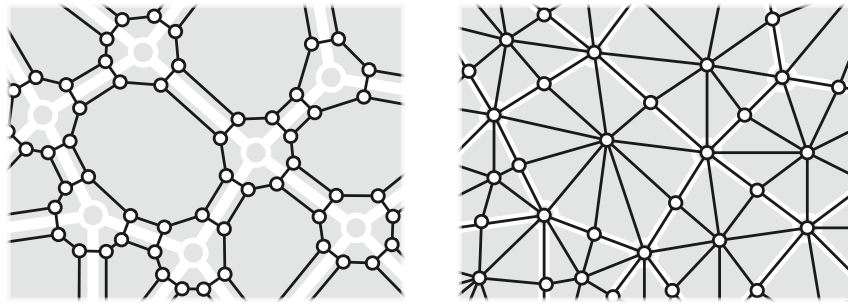


Figure 9.13: Corresponding portions of the band decomposition Σ^\square and the barycentric subdivision Σ^+ of the planar map in Figure 8.

These four derived maps are formally well-defined if and only if the original map Σ has at least one edge. It is sometimes convenient, for example in base cases of inductive arguments, to informally extend the definitions to the trivial map \bullet as follows:

- The trivial medial map \bullet^x and the trivial band decomposition \bullet^\square both consist of a single closed curve on the sphere, with no vertices and two faces, corresponding to the vertex and face of \bullet . I recommend thinking of this object as the result of gluing two flat circular disks together around their boundary.
- The trivial radial map \bullet° and the trivial barycentric subdivision \bullet^+ both consist of a single “edge”, with no faces and two vertices, again corresponding to the vertex and face of \bullet . I recommend thinking of this object as an infinitely thin cylinder with its ends pinched to points.

But let me emphasize that these extensions are informal; the objects I've just described are not maps at all!

9.12 Aptly Yadda Yadda

- References!
 - planar graphs, duality, etc
 - combinatorial maps / rotation systems
 - map data structures (half-edge, winged-edge, quad-edge, gem, etc.)
 - derived maps (Tait, Steinitz, Conway, etc.)
- Directed duality: Acyclic \Leftarrow strongly connected
- Whitney's theorem: Every 3-connected planar graph has a unique planar embedding

9.13 Revision?

Consider using more mnemonic `hnext` instead of `succ`, and similar for other nearby darts:

- $\text{hprev} = \text{hnext}^{-1}$
- $\text{tnext} = \text{rev}(\text{hnext}(\text{rev}))$
- $\text{tprev} = \text{tnext}^{-1} = \text{rev}(\text{hprev}(\text{rev}))$
- $\text{lnext} = \text{rev}(\text{hnext}) = \text{succ}^*$
- $\text{lprev} = \text{lnext}^{-1} = \text{hprev}(\text{rev})$
- $\text{rnext} = \text{rev}(\text{hprev})$
- $\text{rprev} = \text{rnext}^{-1} = \text{hnext}(\text{rev})$

Chapter 10

Tree-Cotree Decompositions^β

10.1 Important graph definitions (yawn)

We need to establish definitions for a few important structures in graphs. Most of these are likely already familiar; I recommend using this list as later reference rather than reading it as text.
Move to end of previous note?

- walk:** A sequence $\langle s, d_1, d_2, \dots, d_k, t \rangle$ where s and t are vertices and each d_i is a dart, such that $\text{tail}(d_1) = s$ and $\text{head}(d_1) = t$ and $\text{head}(d_i) = \text{tail}(d_{i+1})$ for each index i
- length of a walk:** The number of darts in the walk. The walk $\langle s, d_1, \dots, d_k, t \rangle$ has length k .
- trivial walk:** A walk $\langle s, s \rangle$ with length 0.
- closed walk:** A walk $\langle s, d_1, \dots, d_k, t \rangle$ such that $s = t$.
- open walk:** A walk that is either trivial or not closed
- walk from s to t :** A walk with specified initial vertex s and final vertex t
- s can reach t :** There is a walk from s to t . This is an equivalence relation.
- component:** An equivalence class for “can reach”
- connected graph:** A graph with exactly one component
- simple walk:** A walk $\langle s, d_1, \dots, d_k, t \rangle$ such that each vertex is the head of at most one dart d_i .
- path:** A simple open walk, or the subgraph induced by a simple open walk
- even subgraph:** A subgraph in which every vertex has even degree.
- cycle:** A simple non-trivial closed walk, or the subgraph induced by such a walk. A minimal non-empty even subgraph.
- loop:** A cycle with length 1, or an edge whose endpoints coincide.
- cut:** A partition of the vertices V into two non-empty subsets S and $V \setminus S$
- edge cut:** All edges with one endpoint in S and the other in $V \setminus S$, for some subset $S \subseteq V$
- bond:** A minimal nonempty edge cut
- bridge:** An edge cut containing a single edge; that is, a single edge whose deletion disconnects the graph
- acyclic graph:** A graph containing no cycles

10.2 Deletion and Contraction

Let’s begin by discussing two operations for modifying abstract graphs. Let G be an arbitrary connected (but *not* necessarily planar) abstract graph with n vertices and m edges.

Deleting an edge e from G yields a smaller graph $G \setminus e$ with n vertices and $m - 1$ edges. We also write $G \setminus v$ to denote the graph obtained from G by deleting a vertex v and all its incident edges. Deleting a bridge disconnects the graph.

Symmetrically, if e is not a loop, then *contracting* e merges the endpoints of e into a single vertex and destroys the edge, yielding a smaller graph G / e with $n - 1$ vertices and $m - 1$ edges. Contracting a loop is simply forbidden by definition. Contracting a loop is not (yet) defined. If G contains edges parallel to e , those edges survive in G / e as loops.

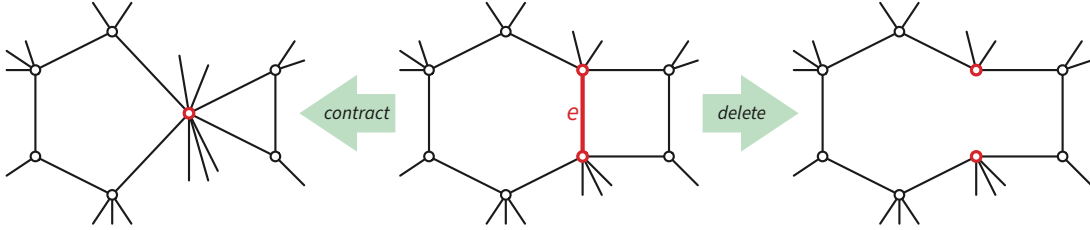


Figure 10.1: Contraction and deletion.

A *subgraph* of a graph G is another graph obtained from G by deleting edges and isolated vertices; a *proper subgraph* of G is any subgraph other than G itself. (We often equate subgraphs of G with subsets of the edges of G .) Deleting any subset of edges $E' \subseteq E$ that does not contain a bond yields a connected proper subgraph $G \setminus E'$.

Symmetrically, contracting any subset of edges $E' \subseteq E$ that does not contain a cycle yields a *proper minor* G / E' . A *minor* of G is any graph obtained from a subgraph of G by contracting edges; a *proper minor* of G is any minor other than G itself.

The inverse of deletion is called *insertion*, and the inverse of contraction is called *expansion*. If G is a (proper) subgraph of another graph H , then H is a (*proper*) *supergraph* of G ; similarly, if G is a (proper) minor of H , then H is a (*proper*) *major* of G .

10.3 Spanning trees

A *spanning tree* of a graph G is a connected, acyclic subgraph of G (more succinctly, a *subtree* of G) that includes every vertex of G . We leave the following lemma as an exercise for the reader.

Lemma: *Let G be a connected graph, and let e be an edge of G .*

- *If e is a loop, then every spanning tree of G excludes e .*
- *If e is not a loop, then for any spanning tree T of G / e , the subgraph $T \cup e$ is a spanning tree of G .*
- *If e is a bridge, then every spanning tree of G includes e .*
- *If e is not a bridge, then every spanning tree of $G \setminus e$ is also a spanning tree of G .*

This lemma immediately suggests the following general strategy to compute a spanning tree of any connected graph: For each edge e , either contract e or delete e . Loops must be deleted and bridges must be contracted; otherwise, the decision to contract or delete is arbitrary. (It is impossible for an edge to be both a bridge and a loop!) The previous lemma implies by induction

that the set of contracted edges is a spanning tree of G , regardless of the order that edges are visited, or which non-loop non-bridge edges are deleted or contracted.

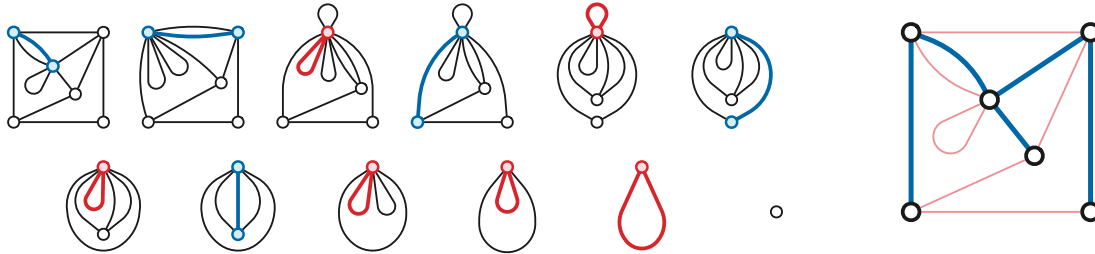


Figure 10.2: Building a spanning tree by contraction and deletion.

In practice, algorithms that compute spanning trees do not *actually* contract or delete edges; rather, they simply label the edges as either belonging to the spanning tree or not. In this context, the previous lemma can be rewritten as follows:

Spanning Tree Lemma: *Let G be a connected graph.*

- *Each spanning tree of G excludes at least one edge from each cycle in G .*
- *For every edge e of every cycle of G , there is a spanning tree of G that excludes e .*
- *Every spanning tree of G includes at least one edge from each bond in G .*
- *For every edge e of every bond of G , there is a spanning tree of G that includes e .*

Corollary: *If the edges of a connected graph G are arbitrarily colored red or blue, so that each cycle in G has at least one red edge and each bond in G has at least one blue edge, then the subgraph of blue edges is a spanning tree of G .*

Given a connected graph with n vertices and m edges, we can compute a spanning tree in $O(n + m)$ time using any number of graph traversal algorithms, the most common of which are *depth-first search* and *breadth-first search*. These algorithms can be seen as variants of the red-blue coloring algorithm, where the order in which edges are colored (or equivalently, the choice of edges to delete or contract) is determined on the fly as the algorithm explores the graph.

10.4 Deletion and Contraction in Planar Maps

Contraction and deletion play complementary roles in planar maps. For example, contracting any (non-loop) edge identifies its two endpoints; deleting any (non-bridge) edge merges its two shores. This resemblance is not merely incidental; in fact, contraction and deletion are *dual* operations. Contracting an edge in any map Σ is equivalent to deleting the corresponding edge in Σ^* and vice versa.

Hopefully this duality is intuitively clear, but we can make it formally trivial by describing how deletion and contraction are *implemented* in planar maps. Let succ denote the successor permutation of a planar map Σ , and let $\text{succ}^* = \text{rev} \circ \text{succ}$ denote its dual successor permutation, which is also the successor permutation of the dual map Σ^* . Fix an arbitrary edge e of Σ .

Deletion: Suppose e is not a bridge. Then $\Sigma \setminus e$ is a planar map that contains every dart in Σ except e^+ and e^- . Let $\text{succ} \setminus e$ and $\text{succ}^* \setminus e$ denote the induced primal and dual successor permutations of $\Sigma \setminus e$. Then for any dart d in $\Sigma \setminus e$, we have

$$(\text{succ} \setminus e)(d) = \begin{cases} \text{succ}(\text{succ}(\text{succ}(d))) & \text{if } \text{succ}(d) \in e \text{ and } \text{succ}(\text{succ}(d)) \in e, \\ \text{succ}(\text{succ}(d)) & \text{if } \text{succ}(d) \in e, \\ \text{succ}(d) & \text{otherwise.} \end{cases}$$

The first case occurs when e is an empty loop based at the head of d . See the figure below. In other words, to find the successor of d in $\Sigma \setminus e$, we repeatedly follow successor pointers until we reach a dart that is not in the deleted edge e .

It follows that the dual successor permutation changes as follows:

$$(\text{succ}^* \setminus e)(d) = \begin{cases} \text{succ}^*(\text{succ}(\text{succ}(d))) & \text{if } \text{succ}(d) \in e \text{ and } \text{succ}(\text{succ}(d)) \in e, \\ \text{succ}^*(\text{succ}(d)) & \text{if } \text{succ}(d) \in e, \\ \text{succ}^*(d) & \text{otherwise.} \end{cases}$$

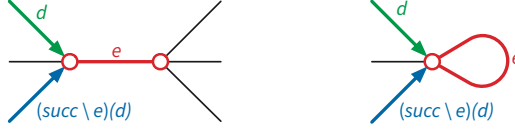


Figure 10.3: Deleting an edge: Default case and empty loop

Contraction: Suppose e is not a loop. Then Σ / e is a planar map that contains every dart in Σ except e^+ and e^- . Let succ / e and succ^* / e respectively denote the induced primal and dual successor permutations of Σ / e . Then for any dart d of Σ / e , we have

$$(\text{succ}^* / e)(d) = \begin{cases} \text{succ}^*(\text{succ}^*(\text{succ}^*(d))) & \text{if } \text{succ}^*(d) \in e \text{ and } \text{succ}^*(\text{succ}^*(d)) \in e, \\ \text{succ}^*(\text{succ}^*(d)) & \text{if } \text{succ}^*(d) \in e, \\ \text{succ}^*(d) & \text{otherwise.} \end{cases}$$

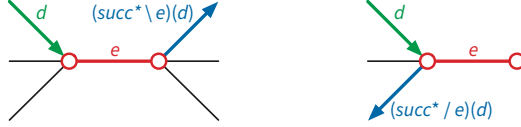
The first case occurs when one endpoint of e has degree 1 and the head of d is the other endpoint of e . See the figure below. In other words, to find the *dual* successor of d in Σ / e , we chase *dual* successor pointers until we reach a dart that is not in the contracted edge e .

It follows that the primal successor permutation changes as follows:

$$(\text{succ} / e)(d) = \begin{cases} \text{succ}(\text{succ}^*(\text{succ}^*(d))) & \text{if } \text{succ}(d) \in e \text{ and } \text{succ}^*(\text{succ}^*(d)) \in e, \\ \text{succ}(\text{succ}^*(d)) & \text{if } \text{succ}(d) \in e, \\ \text{succ}(d) & \text{otherwise.} \end{cases}$$

Both of these formulas are trivially correct when we either delete or contract the only edge in a one-edge map, because the resulting trivial map has no darts. Assuming standard data structures, any edge can be contracted or deleted in $O(1)$ time.

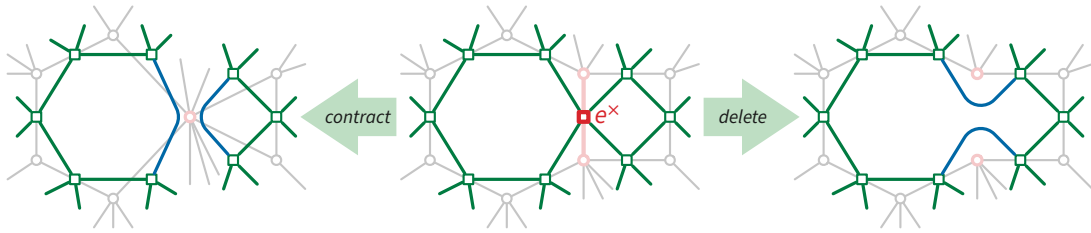
The following lemma is now purely mechanical.

**Figure 10.4:** Contracting an edge: Default case and leaf

Lemma (contraction \Leftarrow deletion): Fix a planar map Σ , and let e be any edge in Σ .

- (a) If e is not a loop, then e^* is not a bridge and $(\Sigma / e)^* = \Sigma^* \setminus e^*$.
- (b) If e is not a bridge, then e^* is not a loop and $(\Sigma \setminus e)^* = \Sigma^* / e^*$.

If we delete a bridge using the formulas above, the components of $G \setminus e$ become embedded independently, each on its own plane/sphere; instead of merging two faces into one, the deletion breaks one face (on either side of the deleted edge) into two. Symmetrically, if we contract a loop using the formula above, instead of merging two vertices into one, we split the single endpoint of the loop into two, splitting the graph into two independent subgraphs, one “inside” the loop and the other “outside”.

**Figure 10.5:** Contraction and deletion in a planar map Σ both induce smoothing in the medial map Σ^* .

10.5 Tree-Cotree Decompositions

Lemma (even subgraph \Leftarrow edge cut): Fix a planar map Σ . A subset H of the edges of Σ is an even subgraph if and only if the corresponding subset H^* of edges in Σ^* is an edge cut.

Proof: Let H be an even subgraph of Σ . Let C_1, C_2, \dots, C_k be edge-disjoint cycles in Σ whose union is H . Color each vertex of Σ^* black if it lies in the interior of an odd number of cycles C_i , and white otherwise. Then H is the subgraph of edges with one white shore and one black shore. It follows that H^* is the subgraph of dual edges with one endpoint of each color; in other words, H^* is an edge cut in Σ^* .

On the other hand, let H^* be an edge cut in Σ^* . Then it is possible to color the vertices of Σ^* black and white, so that H^* is the subset of edges with one white endpoint and one black endpoint. The primal subgraph H contains precisely the edges of Σ with one white shore and one black shore. Every vertex of Σ is incident to an even number of such edges. We conclude that H is an even subgraph of Σ .

Corollary (cycle \Leftarrow bond): A subgraph H of a planar map Σ is a cycle if and only if the corresponding subgraph H^* of Σ^* is a bond.

Proof: A cycle is a minimal non-empty even subgraph; a bond is a minimal non-empty edge cut.

Equivalently, a cycle is a minimal subset of edges that cannot all be contracted, and a bond is a minimal subset of edges that cannot all be deleted.

Corollary (spanning tree \Leftarrow spanning cotree): Fix a planar map $\Sigma = (V, E, F)$, and let $T \sqcup C$ be a partition of E . Then T defines a spanning tree of Σ if and only if $C^* \subset E^*$ defines a spanning tree of Σ^* .

Proof: Let T be an arbitrary spanning tree of G , and let $C^* = E^* \setminus T^*$ be the complementary dual subgraph of Σ^* . The Spanning Tree Lemma implies that every cycle of Σ excludes at least one edge in T , and every bond of Σ contains at least one edge in T . Cycle-bond duality implies that every bond of Σ^* contains at least one edge in C^* , and every cycle of Σ^* excludes at least one edge in C^* . We conclude that C^* is a connected acyclic spanning subgraph of Σ^* , or in other words, a spanning tree of Σ^* .

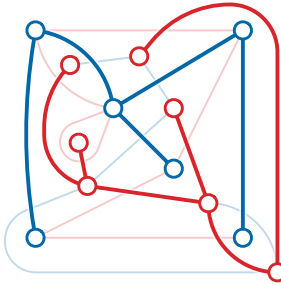


Figure 10.6: A tree-cotree decomposition of a planar map and its dual.

The partition $T \sqcup C$ of edges of a planar map into primal and dual spanning trees is called a *tree-cotree decomposition*. Notice that either the primal spanning tree T or the dual spanning tree C^* can be chosen arbitrarily.

The duality between cycles and bonds was first proved by Hassler Whitney. Whitney also proved the following converse result. An *algebraic dual* of an abstract graph G is another abstract graph G^* with the same set of edges, such that a subset of edges defines a cycle in G if and only if the same subset defines a bond in G^* .

Theorem (Whitney (1932)): A connected abstract graph is planar if and only if it has an algebraic dual.

10.6 Euler's Formula

Arguably the earliest fundamental result in combinatorial topology is a simple formula first published by Leonhard Euler, but described in full generality over a century earlier by René Descartes, and described for the special case of Platonic solids by Francesco Maurolico a century before Descartes. I'll provide two short proofs here, one directly inductive, the other relying on tree-cotree decompositions.

Euler's Formula for Planar Maps. For any connected planar map with n vertices, m edges, and f faces, we have $n - m + f = 2$.

Proof (by induction): Fix an arbitrary planar map Σ with n vertices, m edges, and f faces. If Σ has no edges, it has one vertex and one face. Otherwise, let e be any edge of Σ ; there are two overlapping cases to consider.

- If e is not a bridge, then deleting e yields a planar map $\Sigma \setminus e$ with n vertices, $m - 1$ edges, and $f - 1$ faces. The induction hypothesis implies that $n - (m - 1) + (f - 1) = 2$.
- If e is not a loop, then contracting e yields a planar map Σ / e with $n - 1$ vertices, $m - 1$ edges, and f faces. The induction hypothesis implies that $(n - 1) - (m - 1) + f = 2$.

In all cases, we conclude that $n - m + f = 2$.

Proof (von Staudt 1847): Fix an arbitrary planar map Σ with n vertices, m edges, and f faces. Let T be an arbitrary spanning tree of Σ . Because T has n vertices, it also has $n - 1$ edges. The complementary dual subgraph $C^* = (E \setminus T)^*$ is a spanning tree of Σ^* . Because C^* has f vertices, it also has $f - 1$ edges. Every edge in Σ is either an edge of T or the dual of an edge in C^* , but not both. We conclude that $m = (n - 1) + (f - 1)$.

There are many many other proofs of Euler's formula. David Eppstein has a web page describing more than twenty of them, but even David's list is incomplete. For example, we can leverage our earlier proof of Euler's formula for planar curves, after establishing a few additional definitions.

Recall that the *medial map* Σ^\times of a planar map Σ is another planar map whose vertices correspond to edges of Σ , whose edges correspond to corners of Σ , and whose faces correspond to vertices and faces of Σ . Every medial map Σ^\times is either a simple cycle or 4-regular, and therefore is the image map of a connected planar multicurve. (Steinitz used medial maps ("Θ-Prozeß") to reduce his eponymous theorem about graphs of convex polyhedra to an argument about curves.)

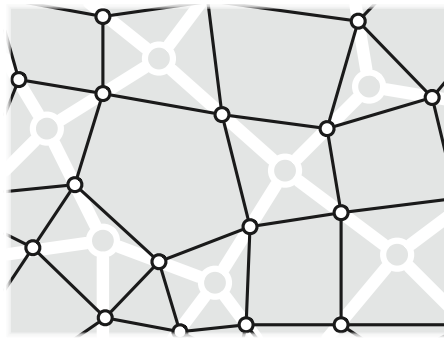


Figure 10.7: The medial map of a planar map.

Proof (via medial homotopy): Fix an arbitrary planar map Σ with n vertices, m edges, and f faces. The medial map Σ^\times is the image map of a connected planar multicurve with $2m$ vertices and $n + f$ faces. We already proved by induction¹ that every connected planar multicurve with N vertices has exactly $N + 2$ faces. We conclude that $n + f = 2m + 2$.

10.7 The Combinatorial Gauss-Bonnet Theorem

I'll close this lecture by proving a powerful reformulation of Euler's formula.

¹Well, okay, we only proved this formula for *curves*, but extending our inductive proof to multicurves requires us to consider only one additional case. Suppose some $2 \rightarrow 0$ move disconnects a multicurve Γ into two smaller connected multicurves Γ^\sharp and Γ^\flat . The original map Γ has $n^\sharp + n^\flat + 2$ vertices and $f^\sharp + f^\flat$ faces (including the deleted bigon and the common outer face), and the induction hypothesis implies that $f^\sharp = n^\sharp + 2$ and $f^\flat = n^\flat + 2$. Later we will see yet another proof of Euler's formula (not on David's list) based on Schnyder woods.

Suppose we assign a value \angle_c to each corner c of a planar map Σ , called the *exterior angle* at c . Intuitively, you should think of \angle_c as the signed angle between the tangent vectors to two darts d and $\text{succ}^*(d)$ at their common endpoint $\text{head}(d)$, but in fact \angle_c can be any real (or complex!) number. As usual, we measure angles in units of circles (or “turns”), as the gods intended.

We can then define the *combinatorial curvature* of a face f or a vertex v , with respect to this angle assignment, as follows:

$$\kappa(f) := 1 - \sum_{c \in f} \angle_c \quad \kappa(v) := 1 - \frac{1}{2} \deg(v) + \sum_{c \in v} \angle_c$$

Or more formally, equating corners with darts:

$$\kappa(f) := 1 - \sum_{d : \text{left}(d)=f} \angle_d \quad \kappa(v) := 1 - \sum_{d : \text{head}(d)=v} \left(\frac{1}{2} - \angle_d \right)$$

For example, suppose every edge of Σ is a line segment, and we actually measure corner angles geometrically. Then every vertex has curvature 0 (because its interior corner angles sum to one circle) and every *bounded* face of Σ has curvature 0 (because its total turning angle is 1). However, the the *outer* face is oriented clockwise instead of counterclockwise, so its total turning angle is -1 , and thus its curvature is 2. That 2 is actually the same as the 2 in Euler’s formula.

Alternatively, suppose Σ is actually embedded on the *unit sphere*, every edge is an arc of a great circle, and angles are again measured geometrically (between tangent vectors). Then every vertex of Σ has curvature zero, because interior angles at any vertex sum to one circle, and a bit of spherical trigonometry implies that every face of Σ has curvature equal to its area divided by 2π . Because the unit sphere has surface area 4π , the sum of all the face curvatures is 2. That 2 is actually the same as the 2 in Euler’s formula! (In fact, this is how Lagrange actually proved Euler’s formula for the first time.)

The Combinatorial Gauss-Bonnet Theorem: *For any planar map $\Sigma = (V, E, F)$ and for any assignment of angles to the corners of Σ , we have $\sum_{v \in V} \kappa(v) + \sum_{f \in F} \kappa(f) = 2$.*

Proof: We immediately have $\sum_f \kappa(f) = |F| - \sum_c \angle_c$ and $\sum_v \kappa(v) = |V| - |E| + \sum_c \angle_c$, which implies that $\sum_v \kappa(v) + \sum_f \kappa(f) = |V| - |E| + |F| = 2$ by Euler’s formula. \square

As a final geometric example, suppose Σ is actually the complex of vertices, edges, and faces of a three-dimensional convex polyhedron (which is homeomorphic to a sphere), and again, angles are measured geometrically. Each face of Σ is a convex planar polygon, and therefore has curvature zero. The interior angles at each vertex of Σ sum to less than a full circle, so every vertex has positive curvature. The Combinatorial Gauss-Bonnet Theorem implies that the sum of the vertex curvatures is exactly 2. In other words, the sum of the *angle defects* at the vertices is two full circles, or eight right angles.

10.8 Historical Digression

Euler’s formula has a long and convoluted history, involving unpublished and lost manuscripts, quack medicine, boat wrecks, priority battles, bad translations, incorrect proofs, and philosophical arguments over the nature of mathematical proof. At the risk of adding to the thousands of gallons of ink, sweat, and blood that have already been spilled over this history, let me briefly mention a few highlights.

The first known statement of Euler's formula is in an unpublished manuscript *Compagationes solidorum regularium* (Combinations of regular solids) written by Francesco Maurolico between 1536 and 1537.

Item manifestum est in unoquoque regularium solidorum, numerum basium coniunctum cum numero cacuminum conflare numerum, qui binario excedit numerum laterum. [It is obvious that in each of the regular solids, the number of bases (faces) combined with the number of peaks (vertices) is a number that exceeds the number of sides (edges) by 2.]

Maurolico only considered the five Platonic solids, for which the formula follows by direct inspection.

René Descartes described the angle defect theorem for convex polyhedra, and derived Euler's formula from it, in his unpublished note *Progymnasmata de solidorum elementis* [*Exercises in the Elements of Solids*], written around 1630.

Ponam semper pro numero angulorum solidorum α & pro numero facirum φ Numerus verorum angulorum planorum est $2\varphi - 2\alpha - 4$. [I always write α for the number of solid angles (vertices) and φ for the number of faces.... The total number of plane angles (corners) is $2\varphi - 2\alpha - 4$.]

It is a matter of surprisingly intense scholarly dispute whether Descartes actually stated Euler's formula, and therefore deserves to share credit with Euler, or only came close, and therefore does not. Descartes did not express his formula using the syntax $V - E + F = 2$, but in my opinion, this is entirely a matter of notational emphasis, not content or understanding. Elsewhere in *Progymnasmata*, Descartes observed that the number of plane angles is exactly twice the number of edges, and he used the numbers of vertices, edges, and faces of the Platonic and several Archimedean solids to derive formulas for corresponding figurate numbers. Had Descartes actually published his *Progymnasmata*, I believe even Euler (who exhibited surprise that the formula was not already known) would have called it "Descartes' formula".

Descartes traveled to Sweden in 1649 at the invitation of then-19-year-old Queen Christina. Due to his poor health, Descartes normally slept late, but after a few months, the young queen required Descartes to give her lessons in philosophy three days a week, lasting five hours per day and beginning at 5am. Within a month, Descartes fell ill. He refused the treatments offered by the Swedish doctors, preferring his own French doctor's prescription of tobacco-infused wine to induce vomiting. The treatment proved ineffective, and Descartes eventually died of pneumonia in February 1650.

After Descartes' death, his possessions were shipped to his friend Claude Clerselier in Paris; upon arrival, a box of manuscripts, including the *Progymnasmata*, fell into the Seine and was not recovered for three days. Clerselier rescued Descartes' manuscripts, and after carefully drying them, made them available to other scholars.

Gottfried Leibniz transcribed several of Descartes' manuscripts, including the *Progymnasmata*, during a trip to Paris in 1676, most likely in an effort to collect evidence against recent charges by English mathematicians that his results were merely elaborations of Descartes' ideas. (Isaac Newton charged Leibniz of plagiarizing his calculus later that same year.) Descartes' original manuscript was then lost forever. Leibniz's hand-written copy vanished into his archives until 1859, when it was rediscovered by Louis Alexandre Foucher de Careil in an uncatalogued pile of

Leibniz's papers.² Foucher de Careil published Leibniz's transcription [?], but his re-transcription introduced several significant errors, rendering it essentially useless. An accurate transcription of the *Progymnasmata* finally appeared in 1908.

Leonhard Euler stated both his eponymous formula and the angle defect theorem for convex polyhedra, expressing surprise that neither was previously known, in a letter to his friend and colleague Christian Goldbach in 1750. Two years later, he proposed an inductive proof to the St. Petersburg Academy of Sciences; unfortunately his proof was flawed. Similarly flawed inductive proofs were published by Karsten in 1768, by Meister in 1785, by L'Huillier in 1811, by Cauchy in 1813, and by Grunert in 1827. One of Cauchy's inductive arguments is presented in numerous textbooks as the first correct proof of Euler's formula, but that claim is incorrect for at least three reasons: The argument is not original to Cauchy; the argument is not a proof; and a correct proof was already known.³

Cauchy argued as follows: Consider a simple planar map Σ whose bounded faces are all triangles and whose outer face is a simple cycle. Let f be any face that has at least one edge on the outer face. If f shares one edge with the outer face, then deleting that edge removes one edge and one face. If f shares two edges with the outer face, then removing those two edges removes one vertex, two edges, and one face. Finally, if all three edges of f are boundary edges, the map has only one bounded face, so $v = e = 3$ and $f = 2$.

Unfortunately, Cauchy (and his predecessors) did not prove that one can always choose a face f so that the outer boundary is still a simple cycle after f is removed. This fact is not hard to prove using a second careful induction argument (which I'll present in the next lecture), but neither Euler, nor Karsten, nor Meister, nor L'Huillier, nor Cauchy, nor Grunert offered such a proof. Lakatos noticed this lacuna in Cauchy's argument and proposed a proof, but his proposed proof was flawed. Most modern presentations of "Cauchy's" "proof"—including Wikipedia's—either ignore this subtlety entirely, or merely *state* that f must be chosen carefully without proving that is always possible.

The first *correct* proof of Euler's formula was given by Legendre in 1794. Legendre projects the vertices and edges of the polyhedron onto the unit sphere from an arbitrary interior point, and then applies the already well-known fact that a spherical triangle with interior angles α , β , and γ has area $\alpha + \beta + \gamma - \pi$. Suppose the original polyhedron has n vertices and f facets, all triangles. The angles at each vertex of the resulting spherical triangulation sum to exactly 2π ; thus, the total area of all f spherical triangles is $2\pi n - \pi f$. We immediately conclude that $f = 2n - 4$, because the surface area of the unit sphere is 4π . The proof for more general polyhedra follows by triangulating the faces.

The first correct *combinatorial* proof of Euler's formula is Von Staudt's 1847 tree-cotree proof. Von Staudt's actual argument is remarkably concise, despite being written in mid-19th-century academic German, especially in comparison to the earlier inductive arguments:

Wenn nämlich der Körper E Eckpunkte hat, so sind $E - 1$ Kanten, von welchen die erste zwei Eckpunkte unter sich, die zweite einen derselben mit einem dritten, die dritte einen der drei vorigen mit einem vierten u.s.w. verbindet, hinreichend um von jedem Eckpunkte auf jeden andern übergehen zu können. Da nun in einem solchen Systeme

²... on display in the bottom of a locked filing cabinet stuck in a disused lavatory with a sign on the door saying 'Beware of the Leonhard'.

³... and the formula isn't Euler's.

von Kanten keine geschlossene Linie enthalten ist, jede der übrigen (noch freien) Kanten aber mit zwei oder mehrern Kanten des Systems eine geschlossene Linie bildet, so sind die übrigen Kanten hinreichend aber auch alle erforderlich, um durch sie von jeder der F Flächen des Körpers auf jede andere übergehen zu können, woraus man schliessen kann, dass die Anzahl der übrigen Kanten $F - 1$, mithin die Anzahl aller Kanten $E + F - 2$ und demnach $E + F = K + 2$ sey.

[When a body has n vertices, then $n - 1$ edges are sufficient—the first connecting two vertices, the second connecting one of those with a third, the third connecting one of the three previous vertices with a fourth, and so on—to be able to go from any vertex to any other. Such a system of edges does not contain a closed line, but each of the remaining edges forms a closed line with two or more edges of the system, so the remaining edges are sufficient, but also necessary, to be able to go through them from any of the f faces of the body to any other. It follows that the number of remaining edges is $f - 1$; hence the number of all edges is $n + f - 2$, and therefore $n + f = m + 2$.]

[More loosely: When a body has n vertices, we can find $n - 1$ edges that define a spanning tree T . Cutting the surface along every edge in T leaves the surface connected, but additionally cutting any other edge disconnects the surface, so that edges not in T are just enough to keep the faces of the body connected. It follows that the number of remaining edges is $f - 1$, so the total number of edges is $n + f - 2$.]

All of these proofs were intended to prove Euler's formula for convex polyhedra, although Cauchy's proof starts by projecting the polyhedron to a *straight-line* planar map. The first proofs that directly consider planar maps are due to Cayley and Listing, both published in 1861. Cayley's argument is a prototype for our first inductive proof; he observed that the quantity $n - m + f$ does not change when one inserts a new vertex in the interior of an edge or inserts a new edge in the interior of a face. Listing repeats (and generalizes) Cauchy's argument, using a global counting argument instead of induction, but again assuming without proof the existence of a shelling order. Both proofs implicitly assume the Jordan curve theorem, so even ignoring shelling issues, they technically only apply to *combinatorial* maps.

10.9 Aptly Named

- Outerplanar graphs/maps
- Easy consequences of Euler's formula:
 - Every simple planar graph has a vertex of degree at most 5.
 - Every planar triangulation has $3n - 6$ edges and $2n - 4$ faces.
 - Every simple planar graph has at most $3n - 6$ edges.
 - Every simple planar bipartite graph has at most $2n - 4$ edges.
 - Every planar map has either a vertex or a face of degree at most 3.
 - $K_{3,3}$ and K_5 are not planar.
 - There are only five Platonic solids.
 - Every loop-free planar graph is 6-colorable.
 - Every planar graph has an independent set of size $\Omega(n)$ in which every vertex has degree $O(1)$.

- Minimum spanning trees:
 - Tarjan's red-blue meta-algorithm
 - Borůvka's algorithm
 - Mareš's algorithm, Matsui's algorithm
 - minimum spanning tree \Leftarrow maximum spanning cotree
- Equivalence of tree-cotree decompositions and tree-onion figures
- Random (but not uniform!) rooted planar maps via random tree-onion figures

Chapter 11

Straight-line Planar Maps^β

So far we have not assumed that planar embeddings are in any way well-behaved geometrically; edges can be embedded as arbitrarily pathological paths. It is not hard to prove using a compactness argument (Similar to the simplicial approximation theorem for homotopy) that every planar graph has a *piecewise-linear* planar embedding, where every edge is embedded as a simple polygonal path.

But in fact, every *simple* planar graph has a *straight-line* embedding, where every edge is represented by a single straight line segment. More strongly, any planar *embedding* is equivalent to (meaning it has the same rotation system as) a straight-line embedding. This result was first proved (indirectly) by Steinitz (1916), and then independently rediscovered by Wagner (1936), [Cairns (1944)], Fáry (1948), Stein (1951), Stojaković (1959), and Tutte (1960), so of course it's usually called “Fáry’s theorem”.

Non-simple planar graphs do not have straight-line embeddings; in any such embedding, parallel edges would coincide and loops would degenerate to points. But every planar map can be transformed into a simple map by subdividing loops into cycles of length 3 and parallel edges into paths of length 2. It (finally!) follows that any generic planar curve with n vertices is equivalent to a planar *polygon* with at most $3n$ vertices.

The existence of straight-line maps for simple planar graphs finally gives us the converse of Euler’s theorem::

- Every rotation system with n vertices, m edges, and f faces is the rotation system of a planar map **if and only if** $n - m + f = 2$.
- A signed Gauss code with n symbols describes a planar curve **if and only if** it induces $n + 2$ faces.

Moreover, all of the proofs described in this note are constructive; in particular, they all imply linear-time algorithms to construct straight-line embeddings from a given planar rotation system.

Theorem: *Given a planar rotation system for a planar graph G with n vertices and m edges, we can compute an equivalent piecewise-linear embedding (or an equivalent straight-line embedding if G is simple) in $O(n + m)$ time.*

11.1 Simple triangulations

Throughout this note, we'll consider the special case of *simple triangulations*: simple planar maps in which every face is bounded by three edges.

Triangulation Lemma (Fáry 1948): *Every simple planar map can be extended to a simple triangulation by adding edges between existing vertices.*

Proof: Fix a simple planar map Σ with a non-triangular face f , and let w, x, y, z be any four consecutive vertices on the boundary of f . I claim that we can add at least one new edge wy or xz inside f without creating any parallel edges. The lemma follows from this claim by induction on the quantity $\sum_f (\deg(f) - 3)$.

For ease of presentation, assume f is bounded. Suppose Σ contains an edge between w and y , necessarily outside f . The vertices w and y subdivide the boundary of f into two paths, one through x and the other through z . Adding the edge wy to those paths creates two cycles. Without loss of generality, x lies in the interior of the cycle C that passes through z ; as shown in Figure 1.

Now suppose for the sake of argument that Σ also contains an edge xz , again necessarily outside f . This edge passes through the exterior of C near z , but it also passes through the interior of C near x . So the Jordan Curve Theorem implies that xz intersects C , contradicting the definition of embedding. \square

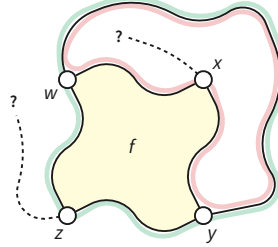


Figure 11.1: Proof of the triangulation lemma.

To compute a straight-line map $\bar{\Sigma}$ equivalent to an arbitrary simple planar map Σ , it suffices to add edges to Σ to obtain a simple planar triangulation T , compute a straight-line map \bar{T} equivalent to T , and then delete the (straightened) added edges.

In the following sections, I'll describe three different constructions of straight-line triangulations equivalent to a given triangulation T .

11.2 Inner Induction (Hole Filling)

Lemma: *Every simple planar triangulation with more than 3 vertices has an interior vertex with degree at most 5.*

Proof: Let T be a simple planar triangulation with $n > 3$ vertices. Every vertex of T has degree at least 3; otherwise, either T is not simple or T has a face with degree greater than 3. Assign angle $\angle c = 1/3$ to every corner of T , so that every face f has discrete curvature $\kappa(f) = 0$. Then each vertex v has curvature $\kappa(v) = 1 - \deg(v)/6 \leq 1/2$; in particular, a vertex has positive curvature if and only if its degree is at most 5. The combinatorial

Gauss-Bonnet theorem implies that $\sum_v \kappa(v) = 2$, so T must have at least four vertices with positive curvature. At least one of these is an interior vertex.

A simple polygon P is *star-shaped* if there is at least one interior point q such that for each vertex p of P , the segment pq does not cross any edge of P . The set of all such points q is called the *kernel* of P .

Lemma (Cairns 1944, Stojaković 1959): *Every simple polygon with at most 5 vertices is star-shaped.*

Proof (sketch): Every convex polygon is trivially star-shaped. Every simple quadrilateral has at most one reflex vertex; every simple pentagon has at most two reflex vertices, which are either adjacent or not. In every case, we can verify by exhaustive case analysis that the kernel is non-empty; see the figure below.

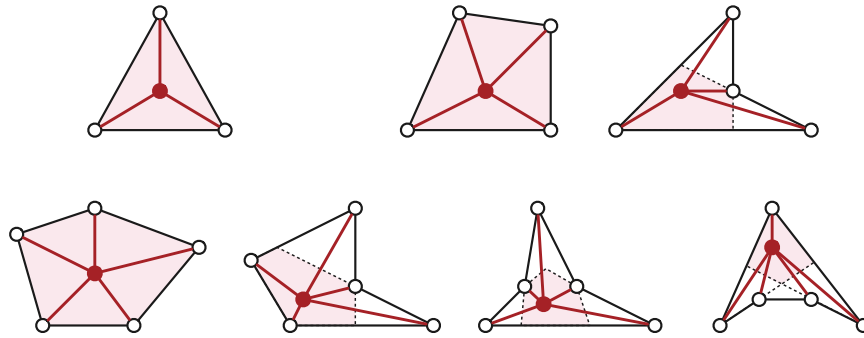


Figure 11.2: Every simple polygon with at most five vertices is star-shaped

Straight-Line Triangulation Theorem: *Every simple planar triangulation is equivalent to a straight-line triangulation.*

Proof (Stojaković 1959): We argue by induction on the number of vertices. Let T be any simple planar triangulation. If T has only 3 vertices, then T is clearly equivalent to any (geometric) triangle \bar{T} . So assume otherwise.

Let v be any interior vertex of T with degree at most 5. Deleting v creates a face f with degree $\deg(v)$. We extend $T \setminus v$ to a simple triangulation T' by adding $\deg(v)-3$ diagonals inside f , following the Triangulation Lemma. The induction hypothesis implies that T' is equivalent to a straight-line triangulation \bar{T}' . Deleting the diagonals yields a simple planar map $T \setminus v$ equivalent to $T \setminus v$. The face \bar{f} of $T \setminus v$ corresponding to f is a simple polygon with $\deg(v) \leq 5$ vertices. Inserting a vertex \bar{v} in the kernel of \bar{f} and connecting \bar{v} to every vertex of \bar{f} yields a straight-line triangulation \bar{T} equivalent to T . \square

11.3 Outer Induction (Canonical Ordering)

Here is a second inductive proof of the Straight-Line Triangulation Theorem that does *not* rely on Euler's formula, roughly following an argument of de Fraysseix, Pach, and Pollack (1988). This proof is close in spirit to early flawed inductive proofs of Euler's formula, including Euler's own flawed proof.

We actually prove the following stronger claim: Let Σ be any simple planar map whose interior faces are triangles and whose outer face is bounded by a simple cycle of length $h \geq 3$. Let

v_1, v_2, \dots, v_h be the vertices of the outer face of Σ in counterclockwise order. Let P be any convex polygon with vertices p_1, p_2, \dots, p_h in counterclockwise order. Then there is a straight-line planar map $\bar{\Sigma}$ that is equivalent to Σ , whose outer face is P , such that each outer vertex v_i corresponds to the polygon vertex p_i .

The proof proceeds by induction on the number of vertices of Σ . If Σ is a single triangle, the claim is trivial, so assume otherwise. There are two nontrivial cases to consider: Either v_1 and v_{h-1} are the only neighbors of v_h on the outer face, or v_h has another neighbor v_j on the outer face.

Case 1: Only two neighbors on the outer face. In this case, we recursively compute a straight-line planar map equivalent to $\Sigma \setminus v_h$ and then embed the edges incident to v_h as line segments.

Specifically, let w_1, w_2, \dots, w_d be the neighbors of v_h , indexed in *clockwise* order around v_h so that $w_1 = v_{h-1}$ and $w_d = v_1$. The vertices w_2, \dots, w_{d-1} all lie in the complement of the outer face, and Σ contains the edge $w_i w_{i+1}$ for every index i . It follows that the outer face of the submap $\Sigma' = \Sigma \setminus v_h$ is bounded by a simple cycle with vertices $v_1, v_2, \dots, v_{h-1} = w_1, w_2, \dots, w_d = v_1$. Every bounded face of Σ' is also a bounded face of Σ and thus has degree 3.

Now let α be a convex arc from p_1 to p_{h-1} inside the triangle $p_1 p_h p_{h-1}$. (For example, α could be a circular arc tangent to $p_1 p_h$ at p_1 and tangent to $p_h p_{h-1}$ at p_{h-1} .) Place d evenly spaced points $q_1, q_2, q_3, \dots, q_d$ along α , with $q_1 = p_{h-1}$ and $q_d = p_1$. Finally, let P' be the convex polygon obtained by replacing the edges $p_{h-1} p_h$ and $p_h p_1$ with the polygonal chain $q_1 q_2 \dots q_d$.

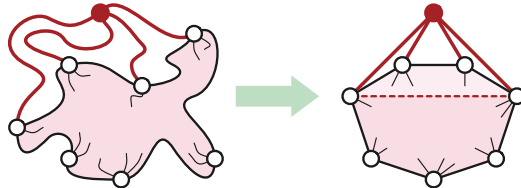


Figure 11.3: Case 1: Remove vertex v_h and recurse

The inductive hypothesis implies that there is a straight-line embedding $\bar{\Sigma}'$ equivalent to Σ' with outer face P' , that maps each vertex v_i (with $i \neq h$) to the corresponding point p_i and each vertex w_i to the corresponding point q_i . Adding the edges $p_h q_i$ gives us a straight-line map $\bar{\Sigma}$ equivalent to Σ with outer face P and the required vertex correspondences.

Case 2: More than two neighbors on the outer face. Now suppose v_h is adjacent to some vertex v_j on the outer face besides v_1 and v_{h-1} . In this case, we split Σ into two submaps along the edge $v_h v_j$, split the polygon P into two smaller polygons along the diagonal $p_h p_j$, and recursively embed each fragment of Σ into the corresponding fragment of P .

Specifically, let Σ^\sharp be the submap of Σ obtained by deleting every vertex outside the simple cycle $(v_h, v_1, v_2, \dots, v_j, v_h)$. (The outside of this cycle is well-defined by the Jordan Curve Theorem.) Similarly, let Σ^\flat be the submap of Σ obtained by deleting every vertex outside the simple cycle $(v_h, v_j, v_{j-1}, \dots, v_{h-1}, v_h)$. Both Σ^\flat and Σ^\sharp satisfy the conditions of our claim.

The line segment $p_h p_j$ partitions the polygon P into two smaller convex polygons P^\flat and

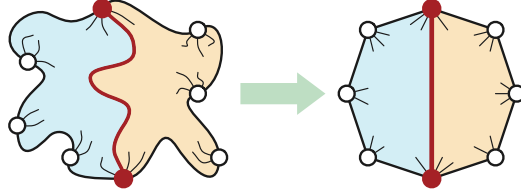


Figure 11.4: Case 2: Split along the diagonal and recurse twice

P^\sharp . The induction hypothesis give us straight-line embeddings $\overline{\Sigma}^b$ and $\overline{\Sigma}^\sharp$, respectively equivalent to Σ^b and Σ^\sharp , with respective outer faces bounded by P^b and P^\sharp , mapping each vertex v_i to the corresponding point p_i . In particular, in both straight-line embeddings, the line segment $p_h p_j$ corresponds to the edge $v_h v_j$. Combining the straight-line embeddings $\overline{\Sigma}^b$ and $\overline{\Sigma}^\sharp$ along $p_h p_j$ gives us the required straight-line embedding $\overline{\Sigma}$.

The second case is actually redundant. A simple recursive argument, similar to the proof that every polygon triangulation has two ears, implies that there are at least two non-adjacent vertices on the outer face with exactly two neighbors on the outer face. It follows that the vertices of Σ can be ordered v_1, v_2, \dots, v_n , so that after deleting any prefix v_1, v_2, \dots, v_i where $i \leq n - 3$, the outer face of the remaining subgraph is bounded by a simple cycle, and the next vertex v_{i+1} lies on the outer face. This sequence of vertices is called a *canonical ordering* (or a *vertex-shelling order*) for Σ .

11.4 Schnyder Woods

In 1989, Walter Schnyder discovered a significant refinement of the previous proof, which implies that any n -vertex planar graph has a straight-line embedding whose vertices lie on an $(n - 1) \times (n - 1)$ integer grid. Again, we consider only simple planar *triangulations*, where all faces have degree 3, including the outer face.

Let T be a simple planar triangulation with n vertices. Schnyder defined two different ways to annotate features of T with the colors red, green, and blue. The first of these is a *Schnyder coloring*, which colors the interior corners subject to two conditions:

- The corners of each face are colored red, green, and blue in counterclockwise order.
- The corners around each internal vertex are colored red, then green, then blue in counterclockwise order. In particular, each internal vertex is incident to at least one corner of each color.

A Schnyder coloring can be constructed in linear time as follows. Color the outer vertices of T red, green, and blue in counterclockwise order. If T has a single bounded face, its three corners inherit the colors of the incident vertices. Otherwise, choose an arbitrary edge from a boundary vertex u to an interior vertex v . There are two cases to consider.

- Suppose v has exactly two common neighbors with u . The contraction T/uv has two pairs of parallel edges; deleting one edge in each pair yields a smaller triangulation T' . Recursively compute a Schnyder coloring for T' , and transfer the corner colors back to T . Finally, there is only one way to consistently color the faces of T on either side of uv ; specifically, the corners incident to the boundary vertex u inherit u 's color.

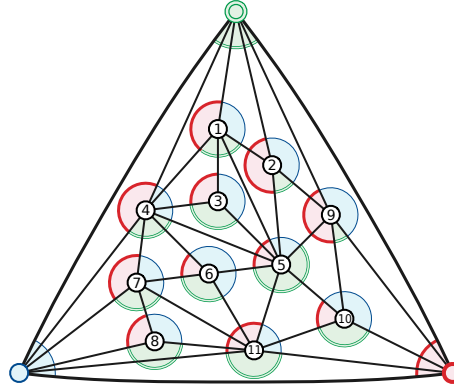


Figure 11.5: A Schnyder coloring of a simple triangulation

- If v has at least three common neighbors with u , there must be a triangle uvw in T containing at least one vertex in its interior. In this case, we recursively compute Schnyder colorings of the subgraphs of G inside uvw and outside uvw . In both recursive subproblems the boundary vertex u retains its originally assigned color, so that the resulting Schnyder colorings are compatible.

In fact, the second case is unnecessary. By expanding the recursion from the second case, we see that the entire construction is carried out by a sequence of contractions; equivalently, an easy induction argument implies that at least one edge from each boundary vertex can be contracted immediately. The Schnyder coloring in the figure above was computed by contracting the interior vertices toward the top (green) vertex in the order indicated by the vertex labels.

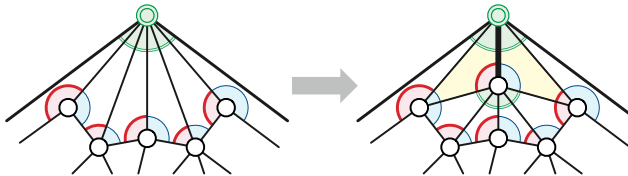


Figure 11.6: Recursively computing a Schnyder coloring

The second annotation, called a *Schnyder wood*, assigns a direction and a color to every internal edge of T . Every internal edge in T is incident to corners with all three colors, with one color appearing twice at one endpoint. Schnyder orients each internal edge e toward the endpoint with the same color twice, and assigns the repeated color to the edge. The resulting coloring and orientation has the following useful properties:

- Each boundary vertex has only incoming internal edges, all with the same color as the vertex itself.
- Every internal vertex has exactly one outgoing edge of each color.
- At every internal vertex, incident edges appear in counterclockwise order as follows: one outgoing red, all incoming blue, one outgoing green, all incoming red, one outgoing blue, all incoming green.

We can also construct Schnyder woods directly using a sequence of edge contractions, just as we constructed Schnyder colorings. Expanding an edge introduces one vertex and three edges; we orient the new edges away from the new vertex, and assign them the only colors consistent

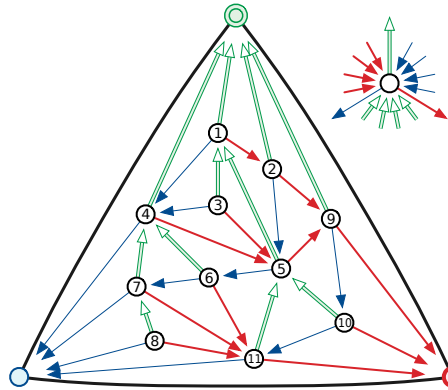


Figure 11.7: The Schnyder wood constructed from the coloring in Figure 5

with the properties listed above. Conversely, *every* Schnyder wood can be constructed using this algorithm, contracting toward any of the outer vertices.

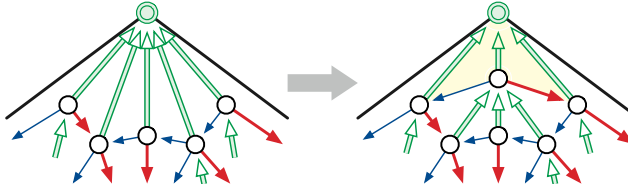


Figure 11.8: Recursively computing a Schnyder wood

Given any Schnyder wood, we can define an equivalent Schnyder coloring as follows. For any interior corner, if the two edges are both leaving the corner vertex, assign the third color to the corner; otherwise, assign the color of the incoming edge(s) to the corner.

Lemma: *In any Schnyder wood, the edges of each color induce a spanning tree of the internal vertices, rooted at the boundary vertex with that color.*

Proof: Without loss of generality, assume the Schnyder wood is constructed by repeatedly contracting to the green boundary vertex. Each interior vertex has exactly one outgoing edge of each color, either leading to another interior vertex or the boundary vertex of that color.

Number the interior vertices by the order in which they are contracted to the green boundary vertex, as shown in the figures. Label the green boundary vertex 0 and the other two boundary vertices ∞ . Call an edge $v \rightarrow w$ *increasing* if the label of w is larger than the label of v and *decreasing* otherwise. Every green edge is decreasing, and every red and blue edge is increasing. Thus, none of the red, green, or blue subgraphs contains a cycle; starting from any interior node, following edges of any fixed color leads to the outer vertex of that color. \square

Hey, look, we have yet another proof of Euler's formula!

Euler's formula: *For any planar map with n vertices, m edges, and f faces, we have $n - m + f = 2$.*

Proof: It suffices to prove the theorem for simple planar triangulations. If Σ is not a simple map, we can make it simple by splitting each edge into a path of three edges, by introducing two new vertices; the resulting simple graph has $n + 2m$ vertices, $3m$ edges, and f faces.

Similarly, if any face of Σ has degree greater than ~ 3 , it must contain a path between two non-adjacent vertices; adding this path to the embedding yields a new planar map with n vertices, $m + 1$ edges, and $f + 1$ faces.

Consider any Schnyder wood of a simple planar triangulation T with n vertices, m edges, and f faces (including the outer face). The edges of each color define a rooted tree with $n - 2$ vertices, and therefore $n - 3$ edges, and every interior edge belongs to exactly one such tree. It immediately follows that $m = 3(n - 3) + 3 = 3n - 6$. Finally, because every face is a triangle, we have $2m = 3f = 6n - 12$, so $f = 2n - 4$. We conclude that $n - m + f = n - (3n - 6) + (2n - 4) = 2$. \square

11.5 Grid embedding

Now we assign integer coordinates to every interior vertex v as follows. There is a unique path of red edges, a unique path of green edges, and a unique path of blue edges from v to the boundary. These three paths partition the triangulation into three regions, which we color red, green, and blue as shown below. Each region contains its clockwise bounding path—for example, the green region includes the blue path, including the blue boundary vertex—but not v itself.

For purposes of defining these regions when v is a boundary vertex, we orient the boundary edges clockwise and color each edge according to its head. Thus, if r, g, b are the red, green, and blue boundary vertices, the green region of g contains every vertex except g and r , the red region of g contains only r , and the blue region of g is empty.

For each vertex v , let $r(v), g(v), b(v)$ respectively denote the number of vertices in the red, green, and blue regions of v . By definition, we have $r(v) + g(v) + b(v) = n - 1$ for every vertex v .

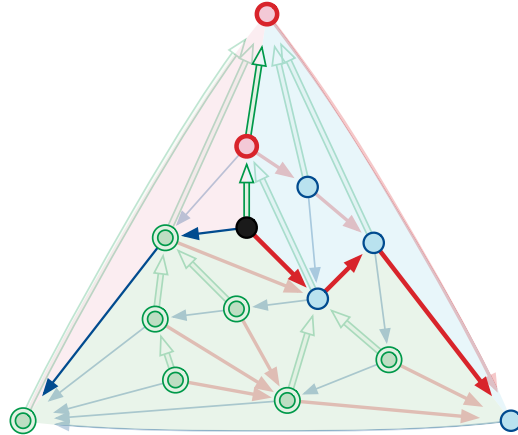


Figure 11.9: Schnyder regions for an interior vertex with coordinates $(r, g, b) = (2, 7, 4)$.

Lemma: *Schnyder's coordinates $(r(v), g(v), b(v))$ satisfy the following conditions:*

- (a) *For every red edge $v \rightarrow w$, we have $r(v) < r(w)$ and $g(v) \geq g(w)$ and $b(v) > b(w)$.*
- (b) *For every green edge $v \rightarrow w$, we have $r(v) > r(w)$ and $g(v) < g(w)$ and $b(v) \geq b(w)$.*
- (c) *For every blue edge $v \rightarrow w$, we have $r(v) \geq r(w)$ and $g(v) > g(w)$ and $b(v) < b(w)$.*

- (d) For every triangle uvw whose corners at u , v , and w are respectively red, green, and blue, we have $r(u) \geq r(v) > r(w)$ and $g(v) \geq g(w) > g(u)$ and $b(w) \geq b(u) > b(v)$.

Proof: Fix an arbitrary reference vertex v , Color v black, and color the other $n - 1$ vertices according to the region that contains it. When we move the reference vertex from v to w along a green edge $v \rightarrow w$, v changes from black to green, w changes from red to black, every green vertex remains green, and no vertex changes from red to blue or vice versa. (Some red or blue vertices might become green, and the set of blue vertices might remain unchanged.) Part (b) now follows immediately; parts (a) and (c) follow from similar arguments.

Finally, part (d) follows by straightforward case analysis. Up to a choice of colors, there are only two cases to consider: either the edges of uvw have distinct colors (and therefore define a directed cycle), or two of the three edges have the same color (so the edges do not define a directed cycle). \square

Theorem: Any planar embedding of a simple planar graph with n vertices is equivalent to a straight-line embedding with vertices on the $(n - 1) \times (n - 1)$ integer grid.

Proof: As usual, it suffices to consider only simple triangulations. Let T be a simple planar triangulation with n vertices. Fix an arbitrary Schnyder coloring of T , and thus an arbitrary Schnyder wood.

Assign each vertex v of T the integer coordinates $(g(v), b(v))$. Let uvw be an arbitrary triangle whose corners at u , v , and w are respectively colored red, green, and blue by the Schnyder coloring. The orientation of the new embedding of uvw is given by the sign of the determinant

$$\begin{vmatrix} 1 & g(u) & b(u) \\ 1 & g(v) & b(v) \\ 1 & g(w) & b(w) \end{vmatrix} = (g(v) - g(u))(b(w) - b(u)) - (g(w) - g(u))(b(v) - b(u)).$$

The previous lemma implies that this expression is positive, which implies that the triangle is oriented counterclockwise. Because every triangle is oriented consistently, no two triangles in the embedding can overlap, and therefore no pair of edges can intersect. (The signed area of the outer triangle is equal to the sum of the signed areas of the interior triangles; if two triangles overlapped, the sum of the *unsigned* areas of the interior triangles would be strictly larger than the unsigned area of the outer triangle!) All vertex coordinates are integers between 0 and $n - 2$. \square

The following figure shows the resulting embedding for our example graph. Instead of embedding on the square grid, I'm using a grid of equilateral triangles, assigning each vertex v *barycentric* coordinates $(r(v), g(v), b(v))$.

11.6 References

Eventually....

11.7 Not Appearing

- Looser grid embedding from canonical ordering or Schnyder face counts

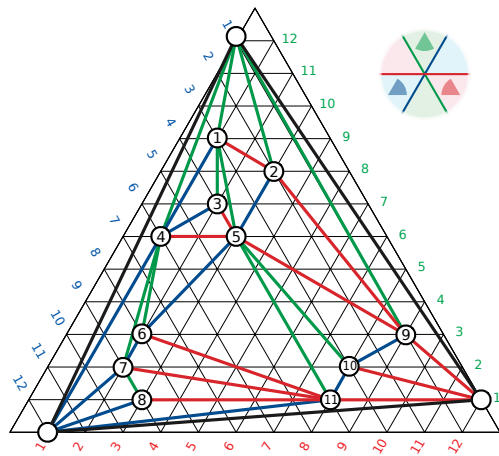


Figure 11.10: Schnyder's barycentric grid embedding.

- Schnyder woods for more general planar graphs (Felsner et al.)
- Weighted Schnyder embeddings
- Morphing between equivalent straight-line embeddings (better via Tutte)
- Convex polyhedral embeddings (Stein, better via Tutte)
- Steinitz's theorem (better via Tutte)
- Distributive lattice of 3-orientations (maybe later)
- Koebe-Andreev circle packing (maybe later)

Chapter 12

Tutte's Spring Embedding Theorem^β

In 1963, William Tutte published a paper ambitiously entitled “How to Draw a Graph”. Let Σ be any planar embedding of any simple planar graph G .

- Nail the vertices of the outer face of Σ to the vertices of an arbitrary strictly convex polygon P in the plane, in cyclic order.
- Build the edges of G out of springs or rubber bands.
- Let go!

Tutte proved that if the input graph G is sufficiently well-connected, then this physical system converges to a *strictly convex* planar embedding of G !

Let me state the parameters of the theorem more precisely, in slightly more generality than Tutte did.¹ A *Tutte drawing* of a planar graph G is described by a *position* function $p: V \rightarrow \mathbb{R}^2$ mapping the vertices to points in the plane, subject to the two conditions:

- (1) The vertices of the outer face f_∞ of some planar embedding of G are mapped to the vertices of a strictly convex polygon in cyclic order. In particular, the boundary of F_∞ must be a simple cycle.
- (2) Each vertex v that is not in f_∞ maps to a point in the interior of the convex hull of its neighbors; that is, we have

$$\sum_{u \rightarrow v} \lambda_{u \rightarrow v} (p_v - p_u) = 0$$

for some positive real coefficients $\lambda_{u \rightarrow v}$ on the darts into v .

(I will use subscript notation p_v instead of function notation $p(v)$ throughout this chapter.) The edges of a Tutte drawing are line segments connecting their endpoints. Let me emphasize that that the *definition* of a Tutte drawing does not require mapping edges to *disjoint* segments, or even mapping vertices to *distinct* points. Moreover, the dart coefficients are not required to be symmetric; it is possible that $\lambda_{u \rightarrow v} \neq \lambda_{v \rightarrow u}$.

A graph G is *3-connected* if we can delete any two vertices without disconnecting the graph, or equivalently (by Menger’s theorem) if every pair of vertices is connected by at least three vertex-disjoint paths.

¹The formulation and proof of Tutte’s theorem that I’m presenting here follows a lecture note by Dan Spielman (2018), which is based on papers by Michael Floater (1997); László Lovász (1999); Steven Gortler, Craig Gotsman, and Dylan Thurston (2006); and Jim Geelen (2012).

Finally, a planar embedding is *strictly convex* if the boundary of every face of the embedding is a convex polygon, and no two edges on any face boundary are collinear.

Tutte's spring-embedding theorem: *Every Tutte drawing of a simple 3-connected planar graph G is a strictly convex straight-line embedding.*

It is not hard to see that 3-connectivity is required. If G has an articulation vertex v , that is, a vertex whose deleting leaves a disconnected subgraph, then a Tutte drawing of G can map an entire component of $G \setminus v$ to the point p_v . Similarly, if G has two vertices v and v' such that $G \setminus \{v, v'\}$ is disconnected, a Tutte drawing of G can map an entire component of $G \setminus \{v, v'\}$ to the line segment $p_v p_{v'}$. In both cases, the Tutte drawing is not even an embedding, much less a strictly convex embedding.

12.1 Outer Face is Outer

Whitney (1932) proved that every simple 3-connected graph G has a unique embedding on the sphere (up to homeomorphism), or equivalently, a unique planar rotation system. I will describe Whitney's proof later in this note. Thus, in every planar embedding of G , the faces are bounded by the same set of cycles; we can reasonably call these cycles the *faces* of G .

The definition of a Tutte drawing requires choosing one of the faces of G to be the outer face f_∞ . We call the vertices of f_∞ *boundary* vertices, and the remaining vertices of G *interior* vertices. Similarly, we call the edges of f_∞ *boundary* edges, and the remaining edges of G *interior* edges. This terminology is justified by the following observation:

Outer face lemma: *In every Tutte drawing of a simple 3-connected planar graph G , every interior vertex maps to a point in the interior of the outer face. In particular, no interior vertex maps to the same point as a boundary vertex.*

Proof: We say that an interior vertex w *directly reaches* a boundary vertex z , or symmetrically that z is *directly reachable* from w , if there is a path from w to z using only interior edges. 3-connectivity implies that every interior vertex of G can directly reach at least three boundary vertices of G .

We prove the lemma by applying Gaussian elimination to the system of linear equations defined by condition (2). Linear system (2) expresses the position p_v of any vertex v as a strict convex combination of the positions of its neighbors in G , that is, a weighted average where every neighbor of v has positive weight. By pivoting on that row, we can remove the variables p_v from the system.

Such a pivot is equivalent to deleting vertex v from the graph and adding new edges between the neighbors of v , with appropriate positive coefficients on their darts.² (Of course the resulting graph may not be planar.) Pivoting out one interior vertex does not change which boundary vertices are directly reachable from any other interior vertex. Thus, if we eliminate all but one interior vertex w , the remaining constraint expresses w as a strict convex combination of at least three boundary vertices.

The same elimination argument implies that *every* assignment of positive dart coefficients

²This modification is called a *star-mesh transformation*; the special case of removing a vertex of degree 3 is called a *Y- Δ transformation*.

$\lambda_{u \rightarrow v} > 0$ defines a *unique* Tutte drawing; the linear system containing the equation

$$\sum_{u \rightarrow v} \lambda_{u \rightarrow v} (p_v - p_u) = 0$$

for every interior vertex v always has full rank.

12.2 Laplacian linear systems and energy minimization

Tutte's original formulation required that every interior vertex lie at the center of mass of its neighbors; this is equivalent to requiring $\lambda_{u \rightarrow v} = 1$ for every dart $u \rightarrow v$.³ More generally, the physical interpretation in terms of springs corresponds to the special case where dart coefficients are symmetric.

Suppose each edge uv is to a (first-order linear) spring with spring constant $\omega_{uv} = \lambda_{u \rightarrow v} = \lambda_{v \rightarrow u}$. For any vertex placement $p \in (\mathbb{R}^2)^V$, the total potential energy in the network of springs is

$$\Phi(p) := \frac{1}{2} \sum_{u,v} \omega_{uv} \|p_u - p_v\|^2.$$

If we fix the positions of the outer vertices, Φ becomes a strictly convex⁴ function of the interior vertex coordinates. If we let the interior vertex positions vary, the network of springs will come to rest at a configuration with locally minimal potential energy. The unique minimum of Φ can be computed by setting the gradient of Φ to the zero vector and solving for the interior coordinates; thus we recover the original linear constraints

$$\sum_v \omega_{uv} (p_u - p_v) = 0$$

for every interior vertex u . The underlying matrix of this linear system is called a weighted *Laplacian* matrix of G . This matrix is positive definite⁵ and therefore non-singular, so a unique equilibrium configuration always exists.

When the dart coefficients are not symmetric, this physical intuition goes out the window; the linear system of balance equations is no longer the gradient of a convex function. Nevertheless, as we've already argued, any choice of positive coefficients $\lambda_{u \rightarrow v}$ corresponds to a unique straight-line drawing of G . None of the actual proof of Tutte's theorem relies on any special properties of the coefficients $\lambda_{u \rightarrow v}$ other than positivity.

Given the graph G , the outer convex polygon, and the dart coefficients, we can compute the corresponding vertex positions in $O(n^3)$ time via Gaussian elimination. (There are faster algorithms to solve this linear system. In particular, a numerically approximate solution can be computed in $O(n \log n)$ time in theory, or in $O(n \text{polylog } n)$ time in practice.)

³It is sometimes more convenient to formalize Tutte's description as $\lambda_{u \rightarrow v} = 1 / \deg(v)$, so that the weights of all darts into each vertex v sum to 1. This formalization is inconsistent with the physical spring analogy, but instead treats weights as transition probabilities of a (backward) random walk. Both formalizations lead to the same Tutte drawing.

⁴The Hessian of Φ is positive definite, meaning all of its eigenvalues are positive.

⁵The Laplacian matrix is just the Hessian of Φ .

12.3 Slicing with Lines

For the rest of this note, fix a simple 3-connected planar graph G and a Tutte drawing p . At the risk of confusing the reader, I will generally not distinguish between features of the abstract graph G (vertices, edges, faces, cycles, paths, and so on) and their images under the Tutte drawing (points, line segments, polygons, polygonal chains, and so on). For example, an *edge* of the Tutte drawing p is the (possibly degenerate) line segment between the images of the endpoints of an edge of H , and a *face* of the Tutte drawing p is the (not necessarily simple) polygon whose vertices are the images of the vertices of a face of G in cyclic order.

Both sides lemma: *For any interior vertex v and any line ℓ through p_v , either all neighbors of v lie on ℓ , or v has neighbors on both sides of ℓ .*

Proof: Suppose all of v 's neighbors lie in one closed halfplane bounded by ℓ . Then the convex hull of v 's neighbors also lies in that halfspace, which implies that v does not lie in the interior of that convex hull, contradicting the definition of a Tutte drawing. \square

Halfplane lemma: *Let H be any halfplane that contains at least one vertex of G . The subgraph of G induced by all vertices in H is connected.*

Proof: Without loss of generality, assume that H is the halfplane above the x -axis. Let t be any vertex with maximum y -coordinate; the outer face lemma implies that t is a boundary vertex. I claim that for any vertex $u \in H$, there is a directed path in G from u to t , where the y -coordinates never decrease. There are two cases to consider:

- If t and u have the same y -coordinate, the outer-face lemma implies that either $t = u$ or tu is an edge of the outer face. In either case the claim is trivial.
- Otherwise, u must lie below t . Let U be the set of all vertices reachable from u along horizontal edges of G . Because G is connected, some vertex $v \in U$ has a neighbor that is not in U . The both-sides lemma implies that v has a neighbor w that has larger y -coordinate than v . The induction hypothesis implies that there is a y -monotone path in G from $w \rightsquigarrow t$. Thus, $u \rightsquigarrow v \rightarrow w \rightsquigarrow t$ is a y -monotone path, which proves the claim. \square

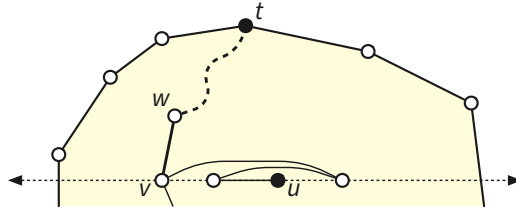


Figure 12.1: The halfplane lemma.

12.4 No Degenerate Vertex Neighborhoods

None of the previous lemmas actually require the planar graph G to be 3-connected. The main technical challenge in proving Tutte's theorem is showing that if G is 3-connected, then every

Tutte drawing of G is non-degenerate. The assumption of 3-connectivity is necessary⁶—if G is 2-connected but not 3-connected, then some subgraphs of G can degenerate to line segments in the Tutte drawing, and if G is connected but not 2-connected, some subgraphs of G will degenerate to single points.

Utility lemma: *The complete bipartite graph $K_{3,3}$ is not planar.*

Proof: $K_{3,3}$ has $n = 6$ vertices and $m = 9$ edges, so by Euler's formula, any planar embedding would have exactly $2 + m - n = 5$ faces. On the other hand, because $K_{3,3}$ is simple and bipartite, every face in any planar embedding would have degree at least 4. Thus, a planar embedding of $K_{3,3}$ would imply $20 = 4f \leq 2m = 18$, which is obviously impossible. \square

Nondegeneracy lemma: *No vertex of G is collinear with all of its neighbors.*

Proof: By definition, no three boundary vertices are collinear, and thus no boundary vertex is collinear with all of its neighbors.

For the sake of argument, suppose some vertex u and all of its neighbors lie on a common line ℓ , which without loss of generality is horizontal. Let V^+ and V^- be the subsets of vertices above and below ℓ , respectively. Let U be the set of all vertices that are reachable from u and whose neighbors all lie on ℓ . The halfplane lemma implies that the induced subgraphs $G[V^+]$ and $G[V^-]$ are connected, and the induced subgraph $G[U]$ is connected by definition. Fix arbitrary vertices $v^+ \in V^+$ and $v^- \in V^-$.

Finally, let W denote the set of all vertices that lie on line ℓ and are adjacent to vertices in U , but are not in U themselves. Every vertex in W has at least one neighbor not in ℓ , so by the both-sides lemma, every vertex in W has neighbors in both V^+ and V^- . Deleting the vertices in W disconnects U from the rest of the graph. Thus, **because G is 3-connected**, W contains at least three vertices w_1, w_2, w_3 .

Now suppose we contract the induced subgraphs $G[V^+]$, $G[V^-]$, and $G[U]$ to the vertices v^+ , v^- , and u , respectively. The resulting minor of G contains the complete bipartite graph $\{v^+, v^-, u\} \times \{w_1, w_2, w_3\} = K_{3,3}$. But this is impossible, **because G is planar** and therefore every minor of G is planar. \square

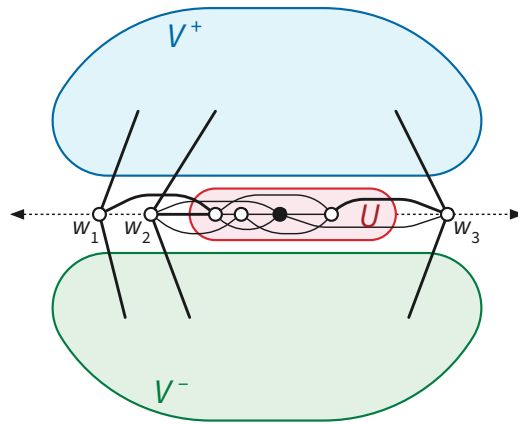


Figure 12.2: A collinear vertex neighborhood implies a $K_{3,3}$ minor.

⁶In fact, we only need the weaker assumption that G is *internally* 3-connected, meaning each interior vertex has three vertex-disjoint paths to the outer face.

Both sides redux: Every interior vertex v has neighbors on both sides of any line through p_v .

12.5 No Degenerate Faces

It remains to prove that the faces of the Tutte drawing are nondegenerate. First we need a combinatorial lemma, similar to Fáry's lemma that any simple planar map can be refined into a simple triangulation.

Geelen's Lemma: Let uv be any edge of G , let f and f' be the faces incident to uv , and let S and S' be the vertices of these two faces other than u and v . Let P be any path that starts at a vertex in S and ends at a vertex of S' . Then every path from u to v in G either consists of the edge uv or contains a vertex of P .

Proof: Fix any planar embedding of G (not necessarily the Tutte drawing!) where uv is an interior edge. The faces incident to uv are disjoint disks on either side of uv . Let s and t be the endpoints of P . Let P' be a path from l to r through the union of the faces incident to uv , crossing the edge uv once. The closed curve $C = P + P'$ separates u from v . Thus, by the Jordan curve theorem, every path Q from u to v crosses C , which implies that either $Q = uv$ or Q contains a vertex of P . \square

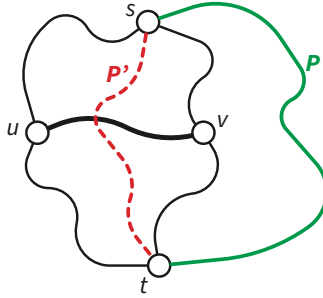


Figure 12.3: Geelen's lemma.

Split Faces Lemma: Let uv be any interior edge of G , let f and f' be the faces incident to uv , and let S and S' be the vertices of these two faces other than u and v . Finally, let ℓ be any line through p_u and p_v . Then S and S' lie on opposite sides of ℓ ; in particular, no vertex in $S \cup S'$ lies on ℓ .

Proof: Without loss of generality, assume ℓ is horizontal. For the sake of argument, suppose both S and S' contain vertices s and t that lie on or below ℓ . If s lies on ℓ , the nondegeneracy lemma implies that s has a neighbor s' strictly below ℓ ; otherwise, let $s' = s$. Similarly, if t lies on ℓ , the nondegeneracy lemma implies that t has a neighbor t' strictly below ℓ ; otherwise, let $t' = t$. The halfspace lemma implies that there is a path P' in G from s' to t' that lies entirely below ℓ . Let P be the path from s to t consisting of the edge ss' (if $s \neq s'$), the path P' , and the edge $t't$ (if $t \neq t'$).

The nondegeneracy lemma also implies that u and v have respective neighbors u' and v' strictly above ℓ , and the halfspace lemma implies that there is a path Q' from u' to v' that lies strictly above ℓ . Let Q be the path from u to v consisting of the edge uu' , the path Q' , and the edge $v'v$.

The edge uv and the path P satisfy the conditions of Geelen's lemma. The path Q clearly

avoids the edge uv , so Q must cross P . But P and Q lie on opposite sides of ℓ . We have reached a contradiction, completing the proof. \square

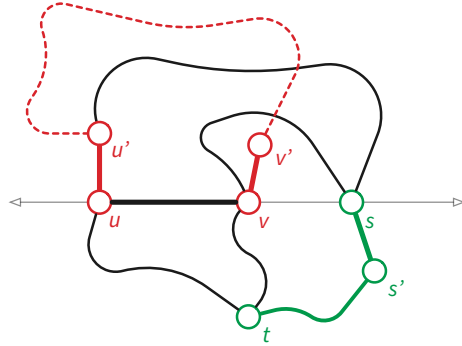


Figure 12.4: The split faces lemma.

Corollary: No edge of G maps to a single point.

Proof: Suppose $p_u = p_v$ for some edge uv . Let ℓ be any line through $p_u = p_v$ and some other vertex on a face incident to uv . We immediately have a contradiction to the previous lemma. \square

Convexity lemma: Every face of G maps to a strictly convex polygon.

Proof: Let f be any face of G , let uv be any edge of f , and let ℓ be the unique line containing p_u and p_v . If uv is a boundary edge, the outer face lemma implies that every vertex of f except u and v lies strictly on one side of ℓ . Similarly, if uv is an interior edge, the split faces lemma implies that every vertex of f except u and v lies strictly on one side of ℓ . In particular, no other vertex of f lies on the line ℓ . It follows that uv is an edge of the convex hull of f . We conclude that f coincides with its convex hull. \square

Now we are finally ready to prove the main theorem.

Proof: Call a point *generic* if it does not lie in the image of the Tutte drawing. Consider any path from a generic point p out to infinity that does not pass through any vertex in the drawing. The split faces lemma implies that whenever the moving point crosses an edge e , it leaves one face and enters another. When the moving point reaches infinity, it is only in the outer face. Thus, every generic point lies in exactly one face.

For the sake of argument, suppose two edges uv and xy intersect in the Tutte drawing. Then any generic point near the intersection $uv \cap xy$ must lie in two different faces, which we just showed is impossible. We conclude that the Tutte drawing is an embedding; in particular, every face is a simple polygon. We already proved that every face in this embedding is strictly convex. \square

12.6 Whitney's Uniqueness Theorem

Tutte's theorem is as strong as possible in the following sense: Every planar graph with a strictly convex embedding is 3-connected. This observation follows from an earlier study of 3-connected planar graphs by Hassler Whitney.

A planar map is *polyhedral* if (1) the boundary of every face is a simple cycle, and (2) the intersection of any two facial cycles is either empty, a single vertex, or a single edge. Every

strictly convex planar map is polyhedral.

Lemma: *Every planar embedding of a 3-connected planar graph is polyhedral.*

Proof: Fix a planar embedding Σ of some graph G .

Suppose the boundary of some face f is not a simple cycle. The boundary of f must have a repeated vertex v . So the radial map Σ^\diamond contains a cycle of length 2 through v and f , which has at least one other vertex of Σ on either side. It follows that $G \setminus v$ must be disconnected.

Suppose two faces f and g have two vertices u and v in common, but not the edge uv . Then the radial map Σ^\diamond contains a simple cycle with vertices f, u, g, v , which has at least one other vertex of G on either side. It follows that $G \setminus \{u, v\}$ is disconnected.

We conclude that if Σ is not polyhedral, then G is not 3-connected. \square

Lemma: *If a graph G has a polyhedral planar embedding, then G is 3-connected.*

Proof: Let G be any graph that is not 3-connected, and let Σ be any planar embedding of G . Again, there are two cases to consider:

- Suppose $G \setminus v$ is disconnected, for some vertex v . Then the same face of Σ must be incident to v twice.
- Suppose $G \setminus \{u, v\}$ is disconnected, for some vertices u and v . We can assume without loss of generality that u and v are not adjacent, since otherwise $G \setminus u$ is already disconnected. Then some pair of faces f and g must have both u and v on their boundaries, but not the edge uv .

In both cases, we conclude that Σ is not polyhedral. \square

Lemma: *The dual Σ^* of any polyhedral planar map Σ is polyhedral.*

Proof: Suppose Σ has a face f whose boundary is not a simple cycle. Then the boundary walk of f encounters some vertex v more than once; in other words, v and f are incident more than once. Thus, in the dual map Σ^* , the dual vertex f^* and the dual face v^* are incident more than once, so the boundary of v^* is not a simple cycle.

On the other hand, suppose Σ has two faces f and g that share two vertices v and w , but there is no dart with endpoints v and w and shores f and g . It follows that the dual faces v^* and w^* in Σ^* share the dual vertices f^* and g^* , but there is no dart with endpoints f^* and g^* and shores v^* and w^* .

We conclude that if Σ is not polyhedral, then neither is Σ^* . \square

Lemma (Whitney): *Every planar graph has at most one polyhedral embedding.*

Proof: Let Σ be a polyhedral planar embedding of some graph G (which must be planar and 3-connected by previous lemmas), and let Σ' be any embedding of G that is not equivalent to Σ . Let succ and succ' be the successor permutations of Σ and Σ' , respectively. Because Σ and Σ' are not equivalent, succ' is not equal to either succ or succ^{-1} .

First, suppose there is a dart d such that $\text{succ}'(d)$ is not equal to either $\text{succ}(d)$ or $\text{succ}^{-1}(d)$. In other words, suppose there is a vertex $v = \text{head}(d)$ where the cyclic orders of darts into v in the two embeddings are different. The darts d and $\text{succ}'(d)$ split the cycle of darts

around v into two non-empty intervals; color the darts in one interval red and the other interval blue. In particular, color $\text{succ}(d)$ red and color $\text{succ}^{-1}(d)$ blue. There must be another dart d' that is red or blue, whose successor $\text{succ}'(d')$ in Σ' is either blue or red, respectively.

Let C be the simple cycle in G that bounds face $f = \text{left}'(d) = \text{right}'(\text{succ}'(d))$ in Σ' . (If the boundary of f is not a simple cycle, then Σ' is not polyhedral and we are done.) Similarly, let C' be the cycle in G that bounds $f' = \text{left}'(d') = \text{right}'(\text{succ}'(d'))$ in Σ' . The images of C and C' in the polyhedral embedding Σ cross each other at v , and therefore (by the Jordan curve theorem) share at least one other vertex w . It follows that faces f and f' in Σ' share vertices v and w , but do not share the edge vw (if that edge exists). We conclude that Σ' is not polyhedral.

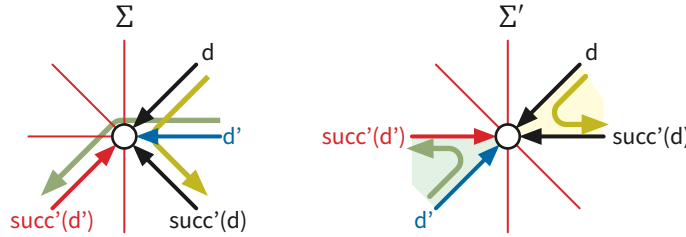


Figure 12.5: If two embeddings disagree at a vertex, at least one embedding is not polyhedral

On the other hand, suppose there are two darts d and d' such that $\text{succ}'(d) = \text{succ}(d)$ and $\text{succ}'(d') = \text{succ}^{-1}(d')$. In other words, suppose the dart order around $v = \text{head}(d)$ is the same in both embeddings, but the dart order around $w = \text{head}(d')$ is reversed from one embedding to the other. Without loss of generality, v and w are adjacent, and we can assume $d = v \rightarrow w$ and $d' = \text{rev}(d) = w \rightarrow v$.

Let C and C' be the cycles in G that bound faces $f = \text{left}'(d) = \text{right}'(\text{succ}'(d))$ and $f' = \text{left}'(d') = \text{right}'(\text{succ}'(d'))$ in Σ' , respectively. After an arbitrarily small perturbation, the images of C and C' in the polyhedral embedding Σ cross each other at the midpoint vw , and therefore share at least one other vertex x . It follows that the faces f and f' in Σ' have disconnected intersection, and therefore Σ' is not polyhedral. \square

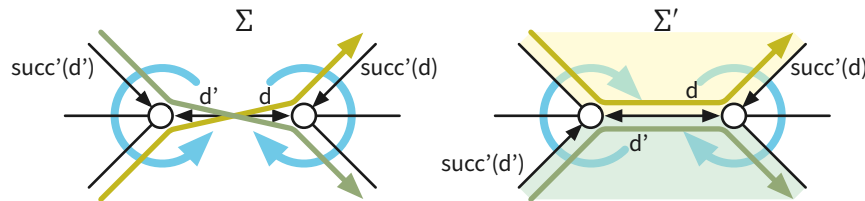


Figure 12.6: If two embeddings disagree along an edge, at least one embedding is not polyhedral

Together, the previous lemmas now imply Whitney's unique-embedding theorem.

Theorem (Whitney): *Every 3-connected planar graph has a unique planar embedding (up to homeomorphism), which is polyhedral.*

In light of Whitney's observation, Tutte's spring-embedding theorem immediately implies the following corollary:

Convex Embedding Theorem: *For every polyhedral planar embedding, there is an equivalent strictly convex embedding.*

12.7 Not Appearing

- Weakly convex faces and internal 3-connectivity
- Directed version allowing zero dart weights via “strong 3-connectivity”
- Colin de Verdière matrices and spherical spectral embeddings
- More spectral graph algorithms!

Chapter 13

Maxwell–Cremona Correspondence^β

The idea of using graphs to model physical networks of springs or ropes under tension does not originate with Tutte, but centuries earlier.

In the late 1500s, the Dutch physicist Simon Stevin published an influential book called *The Art of Weighing*. The 1605 reissue of this book included a supplement where Stevin describes how to calculate the forces imposed by a weight hanging from a tree of ropes. In particular, Stevin correctly observes that as long as every vertex of this tree has degree 3, there is a unique force applied along each rope such that all forces balance out.

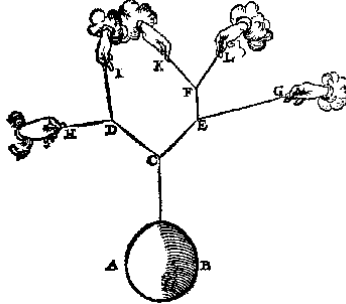


Figure 13.1: A weight hanging from a tree of ropes, from Stevin (1605).

More than a century later, the French engineer Pierre Varignon described a method for visualising the forces acting on a planar tree of ropes under tension. The network of ropes is sometimes called a *funicular polygon*, from the Latin *funiculus* meaning “small rope”, and the Greek *polygonos* meaning “many-angled”. (It would be another 45 years before Meister redefined “polygon” to mean a closed curve composed of line segments.)

Each edge in the funicular polygon is a line segment. We can visualize the forces acting along these edges by drawing a *force polygon* as follows. For each edge e in the funicular polygon, we draw a line segment e^* perpendicular¹ to e whose length is equal to the magnitude of force being applied along e . If the system of ropes is in equilibrium, then the forces vectors into each

¹It may seem more natural to draw each edges of the force diagram *parallel* to the corresponding funicular edge; indeed, many sources define force diagrams this way. The perpendicular formulation makes the *duality* between reciprocal diagrams more apparent. It also simplifies the derivation of polyhedral lifts; in particular, perpendicular reciprocal diagrams have polyhedral lifts that are projective polars through the unit paraboloid $z = (x^2 + y^2)/2$.

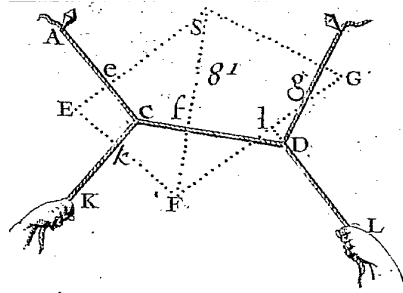


Figure 13.2: A force polygon (dotted) for a funicular polygon of ropes under tension, from Varignon (1725).

vertex of the funicular polygon sum to zero; equivalently, the corresponding edges of the force polygon form a closed figure. In short, the force polygon is the *dual graph* of the funicular polygon. Outside the study of polyhedra (and especially *regular* polyhedra), this may be the oldest example of planar-graph duality.²

Finally, in the mid-1800s, famed Scottish physicist James Clark Maxwell generalized Varignon's force diagrams to arbitrarily complex planar graphs. Maxwell's analysis became a key technique in the new field of *graphical statics* developed by William John Macquorn Rankine, Carl Culmann, Luigi Cremona, and others. One of the early successes of graphical statics was the world's tallest man-made structure (at the time), constructed in the 1880s to celebrate the 100-year anniversary of the French Revolution by Gustave Eiffel.

13.1 Dramatis Personae

13.1.1 Graphs and Frameworks

Let G be a simple 3-connected planar graph. Recall from the previous lecture that G has a unique planar embedding (up to homeomorphism) and therefore has a unique dual graph G^* , which is also simple, 3-connected, and planar.

Let $\langle uv|ab \rangle$ denote the unique dart d in G with tail u and head v , whose dual dart d^* in G^* has tail a and head b . Thus, $\langle uv|ab \rangle^* = \langle ab|uv \rangle$ and $\text{rev} \langle uv|ab \rangle = \langle vu|ba \rangle$. Equivalently, $\langle uv|ab \rangle$ has right shore a^* and left shore b^* in the unique planar embedding of G .

A *position function* for G is a function $p: V(G) \rightarrow \mathbb{R}^2$, or equivalently a matrix $p \in (\mathbb{R}^2)^n = \mathbb{R}^{2 \times n}$, such that $p(u) \neq p(v)$ for every edge uv . For each edge uv of G , we abuse notation by writing $p(uv)$ to denote the straight line segment between $p(u)$ and $p(v)$. The pair (G, p) is called a *planar framework*. The *displacement vector* $\Delta(d)$ of any dart $d = \langle uv|ab \rangle$, with respect to a fixed position function p , is $p(v) - p(u)$.

Let me emphasize that a planar framework (G, p) is a *straight-line drawing* of its underlying planar graph G , but it is not necessarily an *embedding*; images of distinct edges may cross, overlap, or even coincide.

²Computational geometers might see some resemblance between Varignon's figure and the geometric duality between Delaunay triangulations and Voronoi diagrams. That is *not* a coincidence. Neither is the appearance of the unit paraboloid in the previous footnote.

13.1.2 Stresses

A *stress* is a function $\omega: E(G) \rightarrow \mathbb{R}$, or equivalently, a vector $\omega \in \mathbb{R}^m$. A stress is *non-zero* if $\omega(e) \neq 0$ for at least one edge e , and *strict* if $\omega(e) \neq 0$ for every edge e . We frequently abuse notation by defining $\omega(uv) = 0$ when uv is not an edge. We also extend the function ω to the darts of G by defining $\omega(\langle uv|ab \rangle) = \omega(uv)$.

We can interpret each edge e of a planar framework as a (first-order linear) spring with spring constant $|\omega(e)|$, under tension if $\omega(e) > 0$ and under compression if $\omega(e) < 0$. Hooke's Law implies that each edge uv imparts a force of $\omega(uv) \cdot (p(v) - p(u)) = \omega(uv) \cdot \Delta(u \rightarrow v)$ to vertex v .

A stress ω is called an *equilibrium* stress (or a *self-stress*) if the net force on every vertex is zero; that is, for every vertex v we have

$$\sum_u \omega(uv) \cdot (p(v) - p(u)) = \begin{pmatrix} 0 \\ 0 \end{pmatrix}$$

Recall from the previous lecture that this linear system describes the unique critical point of the potential energy function

$$\Phi(p) := \frac{1}{2} \sum_{u,v} \omega(uv) \cdot \|p(u) - p(v)\|^2.$$

Because stress coefficients are allowed to be negative, this unique critical point is no longer a local minimum, as it was in the previous lecture.

13.1.3 1-Forms and Discrete Integration

A *discrete 1-form* (or *1-cochain*, or *voltage assignment*, or *pseudoflow*) on G is an anti-symmetric function $\phi: D(G) \rightarrow R$ from the darts of G to some additive abelian group R , where anti-symmetry means $\phi(d) = -\phi(\text{rev}(d))$ for every dart d . Here we consider only 1-chains over the vector spaces \mathbb{R} and \mathbb{R}^2 . (Let me emphasize here that a stress is not a 1-form!)

A 1-form is *exact* if the sum of the values of the darts in any directed cycle is zero. Exact 1-forms are also called *tensions*; they are also said to obey *Kirchhoff's voltage law*.³

A *vertex potential* (or *price function* or *discrete 0-form*) is any function $\pi: V(G) \rightarrow R$ over the vertices of G . The *derivative* (or *coboundary*) $\delta\pi$ of a 0-form π is the 1-form $\delta\pi(u \rightarrow v) := \pi(v) - \pi(u)$.

Lemma: A 1-form ϕ is exact if and only if ϕ is the derivative of a vertex potential.

Proof: The derivative $\delta\pi$ of any 0-form π is clearly exact. On the other hand, given any exact 1-form ϕ , we can arbitrarily fix the potential $\pi(o)$ of an arbitrary vertex o , and then for any other vertex define $\pi(v)$ by summing (or “integrating”) ϕ along any path from o to v . Exactness of ϕ implies that $\pi(v)$ does not depend on which path we choose to sum along. More generally, for any vertices s and t , we can compute the potential difference $\pi(t) - \pi(s)$ by “integrating” ϕ along any s -to- t path.

³The fact that not all voltage assignments satisfy Kirchhoff's voltage law is an unfortunate byproduct of the term's history. See “red herring principle”.

In particular, for any fixed planar framework (G, p) , the *displacement* function $\Delta: D(G) \rightarrow \mathbb{R}^2$ defined by $\Delta(u \rightarrow v) = p(v) - p(u)$ is an exact 1-form.

A 1-form over a 3-connected planar graph (or more generally, any surface map) is *closed* if the sum of the values of the darts in any *face boundary* of G sum to zero. Exact 1-forms are also called *cocirculations*.

Lemma: *Let G be an arbitrary 3-connected planar graph. A 1-form on G is closed if and only if it is exact.*

Proof: Every face boundary in G is a directed cycle by definition, so every exact 1-form is trivially closed (even if the graph G is not planar). The Jordan curve theorem applied to any planar embedding of G implies that every directed cycle in G is a sum (or symmetric difference) of directed face boundaries. \square

13.2 Reciprocal diagrams

A *reciprocal diagram* for a planar framework (G, p) is another planar framework (G^*, p^*) such that G^* and G are dual and corresponding edges in G and G^* are mapped to orthogonal segments by p and p^* , respectively. Two reciprocal diagrams are *equivalent* if one is a translation of the other. For any vector $v \in \mathbb{R}^2$, let v^\perp denote the result of rotating v a quarter turn counterclockwise: $\begin{pmatrix} x \\ y \end{pmatrix}^\perp = \begin{pmatrix} -y \\ x \end{pmatrix}$.

Theorem [Maxwell, Whiteley]: *There is a bijection between equilibrium stresses ω for (G, p) and equivalence classes of reciprocal diagrams (G^*, p^*) . Moreover, the stress $\omega^*(e) = 1/\omega(e)$ is an equilibrium stress for every reciprocal diagram (G^*, p^*) , and the corresponding equivalence class of reciprocal diagrams of any (G^*, p^*) contains (G, p) .*

Proof: Let ω be any equilibrium stress for (G, p) . Define a 1-form $\Delta^*: D(G^*) \rightarrow \mathbb{R}^2$, which might be called the *dual displacement function*, by setting

$$\Delta^*(d^*) := \omega(d) \cdot \Delta(d)^\perp$$

for every dart d of G . For any face v^* of the dual graph G^* , equilibrium implies that

$$\begin{aligned} \sum_{d^*: v^* = \text{left}(d^*)} \Delta^*(d^*) &= \sum_{d: v = \text{head}(d)} \omega(d) \cdot \Delta(d)^\perp \\ &= \sum_u \omega(uv) \cdot \Delta(u \rightarrow v)^\perp = \begin{pmatrix} 0 \\ 0 \end{pmatrix}^\perp = \begin{pmatrix} 0 \\ 0 \end{pmatrix}. \end{aligned}$$

Thus, the function Δ^* is a closed 1-form in the dual graph G^* . Because G^* is a 3-connected planar graph, it follows that Δ^* is an exact 1-form on G^* . Thus, there is a potential function p^* on the vertices of G^* such that $\Delta^*(a \rightarrow b) = p^*(b) - p^*(a)$ for all dual darts $a \rightarrow b$; moreover, p^* is unique up to translation. By construction, the framework (G^*, p^*) is a reciprocal diagram of (G, p) .

On the other hand, let (G^*, p^*) be any reciprocal diagram for (G, p) . For each dart $d = \langle uv | ab \rangle$, there is a unique real number $\omega(d)$ such that

$$p^*(b) - p^*(a) = \omega(d) \cdot (p(v) - p(u))^\perp.$$

Kirchoff's voltage law in (G^*, p^*) immediately implies that ω is an equilibrium stress for (G, p) . \square

13.3 Polyhedral lifts

A *lift* of a planar framework (G, p) is another *height* function $z: V(G) \rightarrow \mathbb{R}$, or equivalently, a vector $z \in \mathbb{R}^n$. The position and height functions define a three-dimensional position function $\hat{p}: V(G) \rightarrow \mathbb{R}^3$ by concatenation: $\hat{p}(v) = (x(v), y(v), z(v))$, where $(x(v), y(v)) = p(v)$. A lift of (G, p) is *polyhedral* if, for each face f of G , the images $\hat{p}(v)$ of all vertices $v \in f$ are coplanar; a polyhedral lift is *trivial* if all points $\hat{p}(v)$ are coplanar. Finally, two polyhedral lifts z and z' are *equivalent* if their difference is a constant: $z(u) - z'(u) = z(v) - z'(v)$ for all vertices u and v . For example, every trivial lift is equivalent to the zero lift $h \equiv 0$.

Theorem [Maxwell, Whiteley]: *There is a bijection between reciprocal diagrams (G^*, p^*) of (G, p) and equivalence classes of nontrivial polyhedral lifts of (G, p) .*

Proof: The *radial graph* G° of G is a bipartite planar graph whose vertices correspond to the vertices and faces of G , and whose edges correspond to vertex-face incidences or *corners* of G . The radial graph G° inherits a unique planar embedding from the unique embeddings of G and G^* . The faces of this embedding are correspond to the edges of G ; in particular, every face of G° has degree 4.⁴

Let z be any non-trivial polyhedral lift of (G, p) . For each face f of G , let the equation $z = x^*(f) \cdot x + y^*(f) \cdot y - z^*(f)$ denote the plane supporting the lifted face $\hat{p}(f)$, and define $p^*(f) = (x^*(f), y^*(f))$. For every corner (v, f) in G (or equivalently, every edge vf of the radial map G°) we immediately have

$$z(v) + z^*(f) = x^*(f) \cdot x(v) + y^*(f) \cdot y(v) = p(v) \cdot p^*(f)$$

Thus, for every dart $d = \langle uv|ab \rangle$ of G , we have four identities:

$$\begin{aligned} p(u) \cdot p^*(a) &= z(u) + z^*(a) \\ p(u) \cdot p^*(b) &= z(u) + z^*(b) \\ p(v) \cdot p^*(a) &= z(v) + z^*(a) \\ p(v) \cdot p^*(b) &= z(v) + z^*(b) \end{aligned}$$

It follows that $(p(u) - p(v)) \cdot (p^*(a) - p^*(b)) = 0$. We conclude that each edge of (G, p) is orthogonal to its dual edge in (G^*, p^*) .

On the other hand, let (G^*, p^*) be any reciprocal diagram for (G, p) . For each face f of G we interpret the dual position vector $p^*(f)$ as the gradient vector $(x^*(f), y^*(f))$ of the support plane of the lifted face $\hat{p}(f)$. We simultaneously compute vertical offsets $z^*(f)$ for those support planes and heights $z(v)$ for the vertices to obtain a consistent polyhedral lift.

We can assign values $z(v)$ and $z^*(f)$ to the vertices v and faces f of G by integrating a closed 1-form over the darts of the radial map G° . Specifically, we define the 1-form $\phi^\circ: D(G^\circ) \rightarrow \mathbb{R}$ by setting

$$\phi^\circ(f \rightarrow v) := p(v) \cdot p^*(f),$$

and therefore

$$\phi^\circ(v \rightarrow f) = -p(v) \cdot p^*(f),$$

⁴Normally we would consider the faces of the radial map Σ° of a planar map Σ . However, because G is 3-connected, it has only one combinatorial embedding, its radial graph and the faces thereof are well-defined.

for each vertex v and face f of G . For each dart $d = \langle uv|ab \rangle$ of G , reciprocity implies

$$\begin{aligned}\phi^\diamond(a \rightarrow v) + \phi^\diamond(v \rightarrow b) + \phi^\diamond(b \rightarrow u) + \phi^\diamond(u \rightarrow a) \\ = p(v) \cdot p^*(a) - p(v) \cdot p^*(b) + p(u) \cdot p^*(b) - p(u) \cdot p^*(a) \\ = (p(v) - p(u)) \cdot (p^*(a) - p^*(b)) = 0.\end{aligned}$$

Thus, ϕ^\diamond is a closed, and therefore exact, 1-form on the radial graph G^\diamond . It follows that there is a 0-form $\pi^\diamond: V(G^\diamond) \rightarrow \mathbb{R}$, unique up to translation, such that $\phi^\diamond(f \rightarrow v) = \pi^\diamond(v) - \pi^\diamond(f)$. For each vertex v of G , define $z(v) := \pi^\diamond(v)$, and for each face f of G , define $z^*(f) := -\pi^\diamond(f)$. By construction, for any corner (v, f) of G , we have

$$z(v) + z^*(f) = p(v) \cdot p^*(f)$$

and therefore

$$z(v) = x(v) \cdot x^*(f) + y(v) \cdot y^*(f) - z^*(f).$$

Thus, the point $\hat{p}(v) = (x(v), y(v), z(v))$ lies on the supporting plane of $\hat{p}(f)$, which has equation $z = x^*(f) \cdot f + y^*(f) \cdot y - z^*(f)$. We conclude that the vertex heights $z(v)$ and facet-plane offsets $z^*(f)$ are consistent with a polyhedral lift of G . \square

13.4 A Non-Obvious Example: The “Anticube”

Consider the planar framework $\Gamma = (G, p)$ shown below left, whose underlying graph G is the standard cube graph, which is planar and 3-connected. The six faces of the cube have vertices 1243, 1276, 2457, 4365, 3186, and 5687. (Short orthogonal edges have stress coefficient 6; long orthogonal edges have stress coefficient 3; diagonal edges have stress coefficient -4 .)

The resulting reciprocal framework $\Gamma^* = (G^*, p^*)$ is shown on the right, scaled down by a factor of 6, along with its dual equilibrium stress. (Dual vertices A and F actually coincide, but are perturbed apart to better illustrate the framework structure.) The dual graph G^* is the graph of the regular octahedron. I computed this reciprocal framework by solving the system of linear equations $\Delta^*(a \rightarrow b) = p^*(b) - p^*(a)$, one for each dual edge, for the dual position vectors $p^*(a)$.

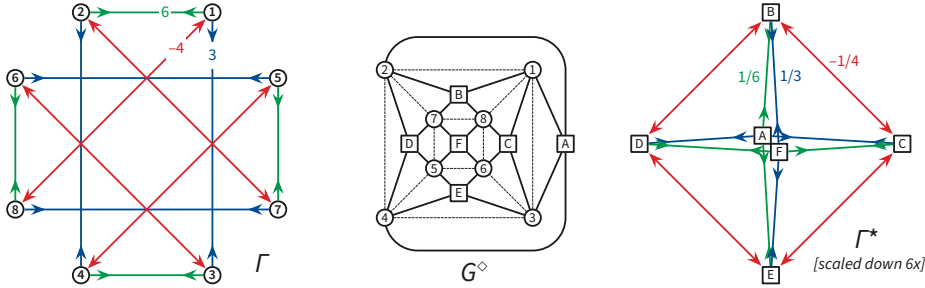


Figure 13.3: The anticube framework with an equilibrium stress, the radial map of the cube, and the corresponding reciprocal framework.

The next figure shows the polyhedral lift of the anticube corresponding to the given equilibrium stress (scaled vertically by a factor of 9). This polyhedron appears to consist of two triangular prisms and a tetrahedron, but in fact it is a self-intersecting embedding of the cube; the corners of the central tetrahedron are not actually vertices of the polyhedron. Four of the six cube faces are embedded as planar but self-intersecting quadrilaterals; opposite pairs of these faces intersect

each other. Again, I computed this polyhedral lift by solving the system of linear equations $\phi^\circ(f \rightarrow v) = \pi^\circ(v) - \pi^\circ(f)$, one for each radial edge, for the radial vertex potentials $z(v) = \pi^\circ(v)$ and $z^*(f^*) = \pi^\circ(f)$.

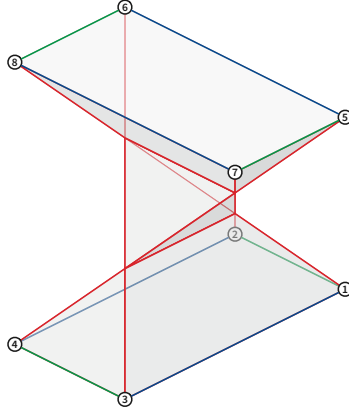


Figure 13.4: The corresponding polyhedral lift of the anticube.

13.5 Steinitz's Theorem

[[Write this!]]

For embedded planar frameworks, positive-stress bars lift to locally convex edges, and negative-stress bars lift to locally concave edges. We can solve for negative boundary stresses that turn any Tutte drawing into an self-stressed planar framework. The Maxwell–Cremona lift of the resulting framework is (the boundary of) a *convex polytope*.

Steinitz's Theorem: *Every 3-connected planar graph is the 1-skeleton of an essentially unique convex polytope in \mathbb{R}^3 .*

(In fact, Steinitz only proved that every *polyhedral planar map* is equivalent to the boundary map of a convex polytope. Steinitz proved this theorem using a direct inductive construction via the medial map. The equivalence of 3-connected planar graphs and polyhedral embeddings was later proved by Whitney.)

Positive interior stresses lift to convex edges; negative interior stresses lift to concave edges.

We can't actually solve for negative boundary stresses for arbitrary outer faces, but we can for triangles. Every simple planar map has either a face or a vertex of degree 3.

13.6 Non-3-connected Frameworks

The definitions of planar framework and equilibrium stress do not actually require the underlying graph to be planar and 3-connected. A planar framework is a pair (G, p) where G is an *arbitrary* graph and $p: V(G) \rightarrow \mathbb{R}^2$ is a position function for the vertices of G . The adjective “planar” refers to the target space of the position function p , not a the underlying graph of the framework. Similarly, the definition of equilibrium stress has nothing to do with the planarity or connectedness of the underlying graph.

If the underlying graph G of a planar framework (G, p) is planar but not 3-connected, we no longer have a bijection between equilibrium stresses and equivalence classes of reciprocal diagrams. Instead, each planar embedding of G yields a *different* bijection between equilibrium stresses and reciprocal diagrams. In short, reciprocal diagrams are defined for *planar embeddings*, not just for abstract graphs.

The following figure shows a planar framework whose underlying graph has two different planar embeddings, obtained by swapping the two “interior” vertices; the shaded green polygons indicate one face of each embedding. Each embedding yields a different reciprocal diagram for the same equilibrium stress. (The arrows indicate the rotation system around the vertex of the reciprocal diagram dual to the shaded green face in the primal framework.)

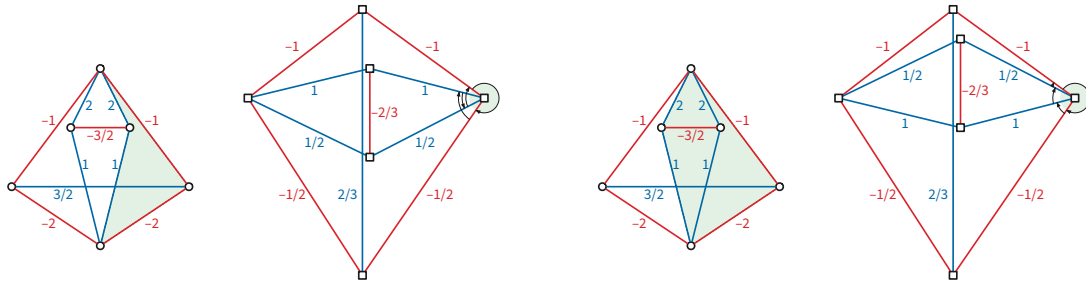


Figure 13.5: Two reciprocal frameworks for the same planar framework

Each embedding similarly yields a different polyhedral lift of the framework (G, p) . One embedding is a tetrahedron with a notch carved out of one edge; the other is a self-intersecting polyhedron with convex faces that looks like two tetrahedra sharing an edge.

13.7 Non-Planar Frameworks

What about non-planar graphs? Every rotation system for a graph G yields a well-defined dual graph G^* . But if the rotation system for G does not define a planar map, we lose the equivalence between *closed* and *exact* 1-forms in the resulting dual graph G^* . The equilibrium stress at each vertex of G still defines (up to translation) a planar polygon of forces for the corresponding face of G^* , but these polygons no longer necessarily fit together consistently in the plane.

The final figures show two examples from Maxwell’s original papers. The first figure shows a framework on the left that has $K_{3,3}$ as a subgraph and is therefore non-planar, together with an attempted reciprocal framework on the right. The framework on the left has two edges e and e' (respectively, h and h') that are dual to the same edge E (respectively H) in the original framework, respectively. We can complete Maxwell’s construction by identifying these edge pairs, but the resulting structure no longer embeds in the plane; instead, we get a well-defined reciprocal framework in the *flat torus*!

On the other hand, sometimes we get lucky. The last figure shows a planar framework (G, p) whose underlying graph G is again not planar, but that has a natural embedding on the torus as a 4×4 toroidal grid. It’s fairly easy to construct an equilibrium stress for this framework by assigning positive stresses to one family of disjoint 4-cycles and negative stresses to the other family of disjoint 4-cycles. Maxwell constructs a reciprocal framework (G^*, p^*) with respect to this toroidal embedding of G and such an equilibrium stress, and the result is a proper planar framework!

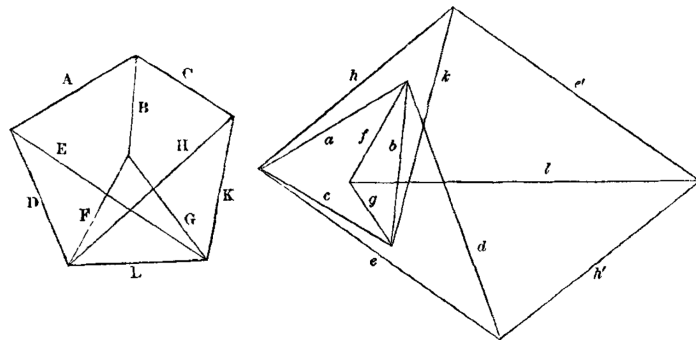


Figure 13.6: A non-planar planar framework with a toroidal reciprocal framework, from Maxwell (1864)

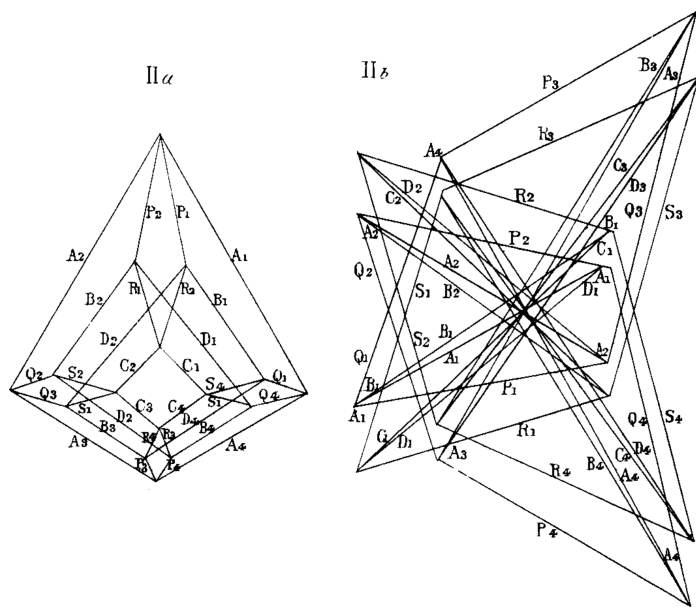


Figure 13.7: A toroidal planar framework with a planar reciprocal framework, from Maxwell (1870)

13.8 References

1. Henry Crapo and Walter Whiteley. Plane self stresses and projected polyhedra I: The basic pattern. *Topologie structurale / Structural Topology* 20:55–77, 1993.
2. Henry Crapo and Walter Whiteley. Spaces of stresses, projections and parallel drawings for spherical polyhedra. *Beitr. Algebra Geom.* 35(2):259–281, 1994.
3. Luigi Cremona. *Le figure reciproche nella statica grafica*. Tipografia di Giuseppe Bernardoni, 1872. English translation in [4].
4. Luigi Cremona. *Graphical Statics*. Oxford Univ. Press, 1890. English translation of [3] by Thomas Hudson Beare.
5. Eduard J. Dijksterhuis, editor. *The Principal Works of Simon Stevin, Volume I*. C. V. Swets & Zeitlinger, 1955. English translation by Carry Dikshoorn.
6. Peter Eades and Patrick Garvan. Drawing stressed planar graphs in three dimensions. *Proc. 2nd Symp. Graph Drawing*, 212–223, 1995. Lecture Notes Comput. Sci. 1027, Springer.
7. John E. Hopcroft and Peter J. Kahn. A paradigm for robust geometric algorithms. *Algorithmica* 7(1–6):339–380, 1992.
8. James Clerk Maxwell. On reciprocal figures and diagrams of forces. *Phil. Mag. (Ser. 4)* 27(182):250–261, 1864.
9. James Clerk Maxwell. On the application of the theory of reciprocal polar figures to the construction of diagrams of forces. *Engineer* 24:402, 1867. Reprinted in [109, pp. 313–316].
10. James Clerk Maxwell. On reciprocal figures, frames, and diagrams of forces. *Trans. Royal Soc. Edinburgh* 26(1):1–40, 1870.
11. James Clerk Maxwell. *The Scientific Letters and Papers of James Clerk Maxwell. Volume 2: 1862–1873*. Cambridge Univ. Press, 2009.
12. Ares Ribó Mor, Günter Rote, and André Schulz. Small grid embeddings of 3-polytopes. *Discrete Comput. Geom.* 45(1):65–87, 2011.
13. Ernst Steinitz. Polyeder und Raumeinteilungen. *Enzyklopädie der mathematischen Wissenschaften mit Einschluß ihrer Anwendungen III.AB(12):1–139*, 1916.
14. Ernst Steinitz and Hans Rademacher. *Vorlesungen über die Theorie der Polyeder: unter Einschluß der Elemente der Topologie*. Grundlehren der mathematischen Wissenschaften 41. Springer-Verlag, 1934. Reprinted 1976.
15. Simon Stevin. *Byvough der Weeghconst [Supplement to the Art of Weighing]*. 1605. Reprinted and translated into English in [5, pp. 525–607].
16. Pierre Varignon. *Nouvelle mechanique ou statique, dont le projet fut donné en M.DC.LXXVII*. Claude Jombert, Paris, 1725.
17. Walter Whiteley. Motion and stresses of projected polyhedra. *Topologie structurale / Structural Topology* 7:13–38, 1982.

13.9 Aptly Named

- Homological constraints for planar reciprocal frameworks
- Impossible figures (cohomology, linear programming)
- Resolving force loads [Rote and Schulz]
- Rigidity (via LP duality)

Chapter 14

Circle Packing \varnothing

Chapter 15

Multiple-Source Shortest Paths^α

15.1 Problem Statement

Let $\Sigma = (V, E, F)$ be a planar map with outer face o , where each edge e is assigned a non-negative weight $w(e)$.¹ Call any vertex incident to o a *boundary* vertex of Σ . The *multiple-source shortest-path* problem asks for an implicit representation of the shortest paths from s to t , for all boundary vertices s and all vertices t . An explicit representation of these shortest paths, for example as a shortest-path tree rooted at every node on the outer face, requires $\Omega(n^2)$ space in the worst case. Nevertheless, the multiple-source shortest-path problem can be solved in only $O(n \log n)$ time, in any of the following forms:

- Given a collection of k vertex pairs (s_i, t_i) , where each s_i is a boundary vertex, we can report all k shortest-path distances $\text{dist}(s_i, t_i)$ in $O(n \log n + k \log n)$ time.
- Assuming the outer face o has k vertices, we can report the $O(k^2)$ shortest-paths distances between every pair of boundary vertices in $O(n \log n + k^2)$ time.
- We can preprocess Σ in $O(n \log n)$ time into a data structure using $O(n \log n)$ space, that can report the shortest-path distance from an arbitrary boundary vertex to an arbitrary vertex in $O(\log n)$ time.

The multiple-source shortest-path problem was first posed and solved by Philip Klein in 2005. Here I'm describing a variant of Klein's algorithm published by Sergio Cabello and Erin Chambers in 2007, which more easily generalizes to graphs on non-planar surface maps. This algorithm plays an essential role in several efficient algorithms for planar maps and surface maps.

To ease presentation, I will make two simplifying assumptions about the input graph:

- (1) The boundary of the outer face o is a simple cycle. This assumption can be enforced if necessary by inserting additional edges with very large weight.
- (2) For every vertex s and every vertex t , there is *exactly one* shortest path from s to t . (Thus, the algorithm I'll describe here cannot be used verbatim on unweighted graphs.) I'll describe two easy methods to enforce this assumption at the end of this note.

¹In fact the algorithm I'm about to describe can be extended to directed graphs, where a dart and its reversal may have different weights, but for ease of exposition, I'll stick to undirected graphs in this lecture.

15.2 Shortest paths and slacks

The MSSP algorithm relies on a characterization of shortest paths developed by Lester Ford in the mid-1950s. Fix a *source* vertex s . For each vertex v , let $\text{dist}(v)$ denote the shortest-path distance from s to v . Let $\text{pred}(v)$ denote the predecessor of vertex v (if any) in the unique shortest path from s to v . Let T_s denote the tree of shortest paths from s to other vertices, defined so that $\text{pred}(v)$ is the parent of v in T_s . Finally, define the *slack* of each dart $u \rightarrow v$ as

$$\text{slack}(u \rightarrow v) := \text{dist}(u) + w(u \rightarrow v) - \text{dist}(v)$$

A dart whose slack is negative is called *tense*.

Ford's generic single-source shortest path algorithm starts by assigning $\text{dist}(s) = 0$ and *tentatively* assigning $\text{dist}(v) = \infty$ for every vertex $v \neq s$. Then as long as the graph contains at least one tense dart, the algorithm *relaxes* one tense dart $u \rightarrow v$ by reassigning $\text{dist}(v) \leftarrow \text{dist}(u) + w(u \rightarrow v)$ and $\text{pred}(v) \leftarrow u$. When no more darts are tense, every value $\text{dist}(v)$ is the correct shortest-path distance, and the predecessor pointers define a correct shortest-path tree T_s .

Lemma (Ford 1956): *The following invariants hold for any shortest-path tree T_s in any edge-weighted graph G :*

- (a) *Every dart in G has non-negative slack.*
- (b) *Every dart in a shortest path tree T_s (directed away from s) has slack zero.*
- (c) *If shortest paths are unique, then every dart that is not in the unique shortest-path tree T_s has positive slack.*

15.3 Compact Output

Disk-tree Lemma: *Let T be any tree embedded on a disk with boundary cycle B ; call any vertex in $T \cap B$ a *boundary vertex*. Let e be any edge of T , and let U and W be the components of $T \setminus e$. Either U contains no vertices, or U contains every boundary vertex, or boundary vertices in U induce a path in B .*

Proof: Let Σ be the planar map induced by $T \cup B$. Trivially, T is a spanning tree of Σ . The complementary dual spanning tree C^* of Σ^* is a star, with the outer face of Σ at the center and other faces of Σ at the leaves.

The dual subgraph C^*/e^* contains a cycle γ of length 2 that separates all vertices in U from all vertices in W . If γ does not intersect B , then U either contains every boundary vertex or none. Otherwise, γ intersects B exactly twice, so U contains an interval of boundary vertices. \square

Now suppose our original planar map Σ has h boundary vertices, indexed $s_0, s_1, s_2, \dots, s_{h-1}$ in cyclic order. For each index i , let T_i denote the shortest-path tree rooted at s_i .

Corollary: *Every directed edge $x \rightarrow y$ is either in every shortest path tree T_i , in no shortest path tree T_i , or in an interval of shortest path trees $T_i, T_{i+1 \bmod h}, \dots, T_{i+j \bmod h}$.*

Proof: Let T be the unique tree of directed shortest paths *into* vertex y , and apply the disk-tree lemma to the components of $T - xy$. \square .

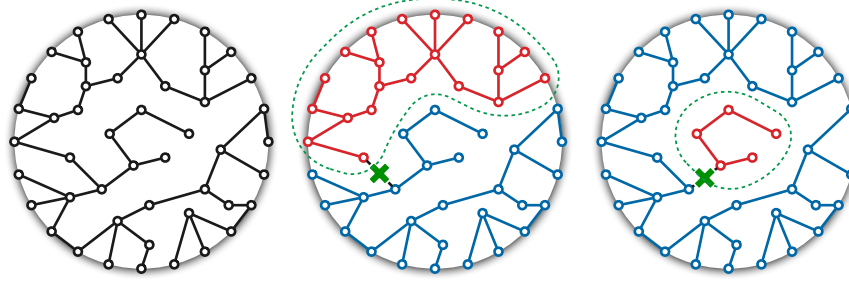


Figure 15.1: The disk-tree lemma.

It follows that we can encode all k shortest paths using only $O(n)$ space, either by recording the first and last trees T_i that contain each directed edge, or by recording the initial tree T_1 followed by the differences $T_2 \setminus T_1, T_3 \setminus T_2 \dots T_h \setminus T_{h-1}$.

15.4 Parametric Shortest Paths

[[Double- and triple-check directions for consistency: Source vertex x moves ccw around boundary. Darts pivoting into T_λ point from new parent to child. Dual dart d^ is right(d) → left(d). But left and right are reversed in the dual plane!]]*

To solve the multiple-source shortest path problem, imagine moving the source vertex s continuously around the outer face and maintaining the shortest-path tree T_s rooted at s . Although the shortest-path distances vary continuously as s moves, the structure of the shortest-path tree changes only at discrete events. (This approach is a variant of the *parametric shortest-path* problem first proposed by Karp and Orlin (1981).)

Now consider a single edge uv on the outer face. Suppose we have already computed the shortest-path tree T_u rooted at u , and we want to maintain the shortest path tree T_s as the source vertex s moves along uv from u to v . We insert s as a new vertex, partitioning uv into two edges us and sv with parametric weights

$$w_\lambda(us) = \lambda \cdot w(uv) \quad \text{and} \quad w_\lambda(sv) = (1 - \lambda)w(uv)$$

Every other edge xy has constant parametric weight $w_\lambda(xy) = xy$. We then maintain the shortest-path tree T_λ rooted at s , with respect to the weight function w_λ , as the parameter λ increases continuously from 0 to 1. The initial shortest-path tree T_0 is equal to T_u , and the final tree T_1 is equal to T_v .

Fix a parameter value $\lambda \in [0, 1]$. For any vertex x , let $\text{dist}_\lambda(x)$ denote the shortest-path distance from s to x with respect to the weight function w_λ . Similarly, for any dart $x \rightarrow y$, let

$$\text{slack}_\lambda(x \rightarrow y) = \text{dist}_\lambda(x) + w_\lambda(x \rightarrow y) - \text{dist}_\lambda(y).$$

Color each vertex x *red* if $\text{dist}_\lambda(x)$ is an increasing function of λ (with derivative 1), and *blue* if $\text{dist}_\lambda(x)$ is an decreasing function of λ (with derivative -1). For generic values of λ , every vertex except s is either red or blue. Finally, call a dart $x \rightarrow y$ *active* if $\text{slack}_\lambda(x \rightarrow y)$ is a decreasing function of λ .

Lemma: *The following invariants hold for all $\lambda \in [0, 1]$:*

- (a) If $s \rightarrow v \notin T_\lambda$, then every vertex except s is red, and the only active dart is $s \rightarrow v$.
- (a) If $s \rightarrow u \notin T_\lambda$, then every vertex except s is blue, and there are no active darts.
- (a) Otherwise, every descendant of u is red, every descendant of v is blue, and $x \rightarrow y$ is active if and only if x is blue and y is red.

Without loss of generality, assume $o = \text{right}(u \rightarrow v)$ is the outer face of Σ . Let $p = \text{left}(u \rightarrow v)$ be the other face incident to uv . Let $C_\lambda^* = (E \setminus T_\lambda)^*$ denote the spanning tree of Σ^* complementary to T_λ . Finally, let π_λ denote the unique directed path in C_λ^* from o^* to p^* .

Lemma: *If T_λ has both red and blue vertices, then a dart is active if and only if its dual is in the directed path π_λ .*

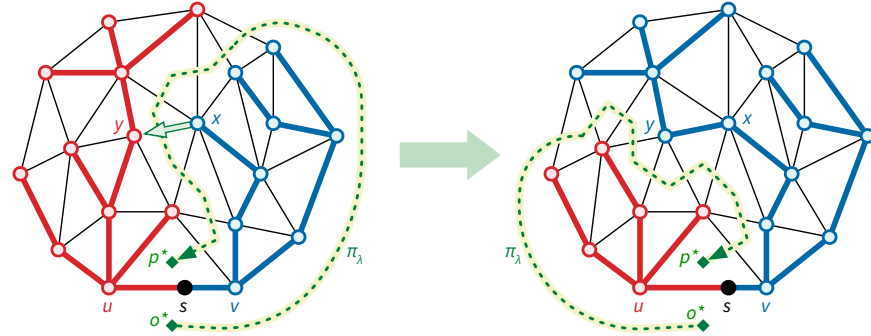


Figure 15.2: A single pivot in a planar shortest-path tree.

Corollary: *If T_λ has both red and blue vertices, the next dart to become tense (if any) is the dart with minimum slack whose dual is in the directed path π_λ .*

Thus, we can execute a single phase of the MSSP algorithm as follows. Initially, we set $s = u$. We repeatedly find the tensest active dart $d = x \rightarrow y$, move s distance $\text{slack}(d)/2$ along uv , increase all red distances and decrease all blue distances by $\text{slack}(d)/2$, decrease the slacks of all active darts and increase the slacks of their reversals by $\text{slack}(d)$, and finally pivot d into the tree by assigning $\text{pred}(y) \leftarrow x$. The loop ends either when there are no more active darts, or when the source vertex s reaches v .

Each pivot changes at least one node y from red to blue, and no pivot changes any node from blue to red. Thus, once a dart is pivoted into the shortest-path tree, it is not pivoted out during that phase. Thus, the darts that are pivoted into the tree are precisely the darts in $T_v \setminus T_u$. The disk-tree lemma now immediately implies that the total number of pivots over all phases is only linear.

Lemma: *The MSSP algorithm performs a total of $O(n)$ pivots.*

15.5 Dynamic Forest Data Structures

To achieve a running time of $O(n \log n)$, we need to perform each pivot quickly. We maintain both the shortest-path tree T_λ and the complementary dual spanning tree C_λ^* in data *dynamic forest* data structures that implicitly maintain dart values (slacks) or vertex values (distances) under edge insertions, edge deletions, and updates to the values in certain substructures.

We maintain the shortest path tree T_λ as a directed tree rooted at s , with dist values associated with each vertex, in a data structure that supports the following operations:

- Cut($x \rightarrow y$): Remove the edge $x \rightarrow y$ from T_λ , breaking it into two rooted trees. The component containing x is still rooted at s ; the other component is rooted at y .
- Link(x, y): Add a directed edge from x to y . This operation assumes that y a root. We always call Link immediately after Cut so that T_λ remains a single spanning tree.
- GetDist(x): Return the distance value associated with vertex x .
- AddSubtreeDist(x): For every descendant y of x , add Δ to dist(y).

Similarly, we maintain the complementary dual spanning tree C_λ^* as an undirected unrooted tree, with slack values associated with every dart, in a data structure that supports the following operations.

- Cut(xy): Remove the edge xy from C_λ^* , breaking it into two trees.
- Link(x, y, α, β): Add the edge xy and assign slack($x \rightarrow y$) = α and slack($y \rightarrow x$) = β . We always call Link immediately after Cut so that C_λ^* remains a single dual spanning tree.
- GetSlack($x \rightarrow y$): Return the slack value associated with dart $x \rightarrow y$.
- MinPathSlack(Δ, x, y): Return the d on the directed path from x to y such that slack(d) is minimized.
- AddPathSlack(Δ, x, y): For each dart d on the directed path from x to y , add Δ to slack(d) and subtract Δ from slack($\text{rev}(d)$).

There are several dynamic-forest data structures that support the operations we need in $O(\log n)$ amortized time each; my favorite is Tarjan and Werneck's *self-adjusting top tree*. (Most of the others also have Tarjan's name on them.) A description of self-adjusting top trees (or the *splay trees* they use under the hood) is unfortunately beyond the scope of this note (or this course).

15.6 The Pivoting Algorithm

With these data structures in hand, we can identify the tensest active dart and perform the necessary updates to pivot it into T_λ in $O(\log n)$ amortised time. The following figure shows the algorithm to perform the next pivot, with all data structure operations in place.

As we already argued, the total number of pivots is $O(n)$, so the overall MSSP algorithm runs in $O(n \log n)$ time, as claimed.

15.7 Applications

Computing all k^2 boundary-to-boundary distances $O((n + k^2) \log n)$ time is straightforward.

[[More detail. Reduce time to $O(n \log n + k^2)$. Say anything at all about persistence?]]

NEXTPIVOT: if $\text{pred}(u) \neq s$ return 1 if $\text{pred}(v) \neq s$ $d \leftarrow s \rightarrow v$ $\Delta \leftarrow \text{GETSLACK}(d^*)$ else $d^* \leftarrow \text{MINPATHSLACK}(o^*, p^*)$ $\Delta \leftarrow \text{GETSLACK}(d^*)/2$ if $\lambda + \Delta/w(uv) < 1$ PIVOT(d, Δ) return $\lambda + \Delta/w(uv)$ else return 1	PIVOT($x \rightarrow y, \Delta$): <i>«Update distances»</i> if $\text{pred}(u) = s$ then $\text{ADDSUBTREEDIST}(\Delta, u)$ if $\text{pred}(v) = s$ then $\text{ADDSUBTREEDIST}(-\Delta, v)$ <i>«Update slacks»</i> $\text{ADDPATHSLACK}(-\Delta, o^*, p^*)$ <i>«Update primal and dual trees»</i> $z \leftarrow \text{pred}(y)$ $\text{pred}(y) \leftarrow x$ $\text{CUT}(zy)$ $\text{JOIN}(x, y)$ $\text{CUT}((xy)^*)$ $\text{JOIN}((z \rightarrow y)^*, 0, w(yz))$
---	---

Figure 15.3: The MSSP pivoting algorithm.

15.8 Enforcing Unique Shortest Paths

So far our presentation has assumed that there is a *unique* shortest path between any two vertices of Σ ; in particular, for any source vertex s , there is a *unique* shortest-path tree T_s . More subtly, we have also assumed that there is always a unique tensest active dart. These assumption obviously do not hold in general, but we can enforce them if necessary using any of several standard *perturbation* techniques. I'll describe two such techniques here, but there are other possibilities.

Standard perturbation methods either explicitly or implicitly define a secondary weight $w'(u \rightarrow v)$ for each each dart $u \rightarrow v$ in Σ . The *perturbed weight* of a dart d is then defined as

$$\tilde{w}(d) := w(d) + w'(d) \cdot \varepsilon$$

for some sufficiently small real number $\varepsilon > 0$. Rather than computing a particular value of ε , we consider the limiting behavior as ε approaches zero. Thus, we can consider each perturbed weight $\tilde{w}(d)$ to be an ordered pair or vector

$$\tilde{w}(d) := (w(d), w'(d)).$$

We compute lengths of paths by summing these vectors normally, but we compare path lengths *lexicographically*. That is, we consider one path π to be shorter than another path π' if either of the following conditions holds:

- (a) $w(\pi) < w(\pi')$
- (b) $w(\pi) = w(\pi')$ and $w'(\pi) < w'(\pi')$

15.8.1 Random Perturbation

The simplest perturbation method chooses *random* secondary weights for each edge. For example, if we choose each secondary weight $w'(e)$ uniformly at random from the real interval $[0, 1]$, then the lengths of all simple paths (indeed, the lengths of all finite walks) are distinct with probability 1.

Somewhat more realistically, the following lemma implies that we can choose small random integers for the secondary weights.

Isolation Lemma (Mulmuley, Vazirani, and Vazirani 1987): Let \mathcal{F} be any family of subsets of $[n]$. For each index $i \in [n]$, let $w'(i)$ be chosen independently and uniformly at random from $[N]$. Define the weight $w'(S)$ of any subset $S \subseteq [n]$ as $w'(S) = \sum_{i \in S} w'(i)$. With probability at least $1 - n/N$, the minimum-weight set in \mathcal{F} is unique.

[[Include the proof, which is relatively straightforward]]

Corollary: If each perturbation weight $w'(e)$ is chosen independently and uniformly at random from $[n^4]$, then with probability $1 - 1/O(n)$, all shortest paths with respect to the perturbed weight function (w, w') are unique.

Let me emphasize that the Isolation Lemma *only* implies that *shortest* paths are distinct; other pairs of paths may still have equal length, even after perturbation.

[[We also need unique tensest darts!!]]

15.8.2 Cotree Perturbation

Let $T \sqcup C$ be a tree-cotree decomposition of Σ . Root the dual spanning tree C^* at the dual of the outer face o^* , and direct all edges of C^* away from the root. We define the weight $w'(d)$ of each dart d of Σ as follows:

- If $d^* \in C^*$, let $w'(d)$ be the number of descendants of $\text{head}(d^*) = \text{left}(d)^*$ in C^* .
- If $\text{rev}(d^*) \in C^*$, let $w'(d) = -w'(\text{rev}(d))$.
- Otherwise, let $w'(d) = 0$.

Equivalently, for any dart $d \notin T$, let $\text{cycle}_T(d)$ be the unique directed cycle in $T + d$. Then $w'(d)$ is the number of faces of Σ inside $\text{cycle}_T(d)$ if that cycle is oriented counterclockwise, the negation of the number of interior cycles if the cycle is clockwise, and zero if d is in T .

Winding Lemma: For any closed walk W in Σ , we have $\sum_{d \in W} w'(d) = \sum_{f \in F} \text{wind}(W, f)$.

Proof: This is essentially the shoelace algorithm. We can compute the winding number of W around f by traversing the path in C^* from f^* to o^* and counting crossings. We can write W as the sum of the fundamental directed cycles determined by the non-tree edges of W .
[[Incomplete]]

The previous lemma implies that although the secondary weights w' depend on the choice of tree-cotree decomposition, the resulting shortest paths do not!

Corollary: For any two paths π and π' with the same endpoints, and any two spanning trees T and T' , we have $w'_T(\pi) < w'_T(\pi')$ if and only if $w'_{T'}(\pi) < w'_{T'}(\pi')$. Thus, shortest paths with respect to w'_T and $w'_{T'}$ coincide.

[[Figure!]]

Theorem: Cotree perturbation makes shortest paths unique.

Proof: Let π and π' be two shortest paths from some vertex s to some other vertex t . By definition, we have $w(\pi) = w(\pi')$ and $w'(\pi) = w'(\pi')$. The latter condition implies that $\sum_{f \in F} \text{wind}(\pi - \pi', f) = 0$. There are two cases to consider.

First, suppose π and π' do not cross. Then the closed walk $\pi - \pi'$ is a weakly simple closed curve, which implies that the non-zero winding numbers $\text{wind}(\pi - \pi', f)$ are either all 1

or all -1 . It follows that $\text{wind}(\pi - \pi', f) = 0$ for every face f , which is only possible if π and π' use the same subset of edges. In other words, $\pi = \pi'$.

Now suppose π and π' cross at some vertex x . The prefixes $\alpha = \pi[s, x]$ and $\alpha' = \pi'[s, x]$ must be shortest paths, otherwise we could shorten one of π and π' . Similarly, the suffixes $\beta = \pi[x, t]$ and $\beta' = \pi'[x, t]$ must be shortest paths. The inductive hypothesis now implies that $\alpha = \alpha'$ and $\beta = \beta'$. Again, we conclude that $\pi = \pi'$. \square

[[We also need unique tensest darts!!]]

15.9 Leftmost shortest paths

In fact, we can implement cotree perturbation without explicit secondary weights. Suppose π and π' are two paths with the same endpoints. We say that π is *to the left* of π' if the closed walk $\pi - \pi'$ winds negatively (clockwise) around at least one face, but does not wind positively (counterclockwise) around any face. If π is to the left of π' , we immediately have $w'(\pi) < w'(\pi')$.

It is not hard to show that for any two paths π and π' with the same endpoints, either one path is the left of the other, or a third path is to the left of both of them. Thus, shortest paths with respect to cotree perturbation are always *leftmost* shortest paths.

We can simulate cotree perturbation by always breaking ties to the left. In the MSSP algorithm, we always pivot the *leafmost* tensest active dart.

[[Need more details here]]

15.9.1 Caveat Emptor!

Cotree perturbation is attractive both because it is deterministic and because it can often be implemented implicitly, but its asymmetry can be a disadvantage. Unless shortest paths are already unique, cotree perturbation yields shortest paths that are not symmetric, even when the original graph is undirected. The reversal of the *leftmost* shortest path from s to t is the *rightmost* shortest path from t to s . Thus, algorithms that rely on the usual behavior of undirected shortest paths cannot automatically use this technique.

As a simple example, consider the *non-crossing* shortest paths problem. Given an undirected planar map Σ with weighted edges and several pairs of vertices $(s_1, t_1), \dots, (s_k, t_k)$ on the outer face, we want to compute shortest paths between each pair s_i and t_i that are pairwise non-crossing. If shortest paths in Σ are already unique, then it suffices to independently compute the shortest path in Σ from s_i to t_i for each index i . But suppose the terminals appear in order s_1, t_1, s_2, t_2 on the outer face, and we use cotree perturbation to *enforce* uniqueness. Then the shortest path from s_1 to t_1 might cross the shortest path from s_2 to t_2 .

15.10 References

1. Sergio Cabello and Erin W. Chambers. Multiple source shortest paths in a genus g graph. *Proc. 18th Ann. ACM-SIAM Symp. Discrete Algorithms*, 89–97, 2007.
2. Sergio Cabello, Erin W. Chambers, and Jeff Erickson. Multiple-source shortest paths in embedded graphs. *SIAM J. Comput.* 42(4):1542–1571, 2013. arXiv:1202.0314.

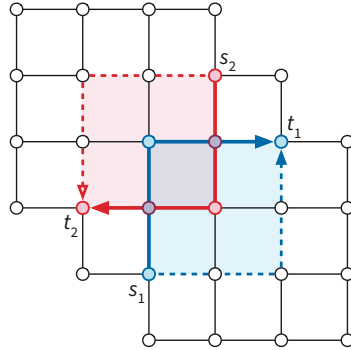


Figure 15.4: Leftmost shortest paths in undirected planar graphs can cross

3. David Eisenstat and Philip N. Klein. Linear-time algorithms for maxflow and multiple-source shortest paths in unit-weight planar graphs. *Proc. 45th Ann. ACM Symp. Theory Comput.*, 735–744, 2013.
4. Lester R. Ford. Network flow theory. Paper P-923, The RAND Corporation, Santa Monica, California, August 14, 1956.
5. Richard M. Karp and James B. Orlin. Parametric shortest path algorithms with an application to cyclic staffing. *Discrete Appl. Math.* 3:37–45, 1981.
6. Philip N. Klein. Multiple-source shortest paths in planar graphs. *Proc. 16th Ann. ACM-SIAM Symp. Discrete Algorithms*, 146–155, 2005.
7. Yaowei Long and Seth Pettie. Planar distance oracles with better time-space tradeoffs. *Proc. 32nd Ann. ACM-SIAM Symp. Discrete Algorithms*, 2517–2537, 2021. arXiv:2007.08585.
8. Ketan Mulmuley, Umesh Vazirani, and Vijay Vazirani. Matching is as easy as matrix inversion. *Combinatorica* 7:105–113, 1987.
9. Robert E. Tarjan and Renato F. Werneck. Self-adjusting top trees. *Proc. 16th Ann. ACM-SIAM Symp. Discrete Algorithms*, 813–822, 2005.

15.11 Sir not appearing

- Subtleties for directed graphs and/or graphs with negative edge lengths.
- Post-hoc distance and path queries via persistence
- Klein’s leafmost pivot strategy
- Unweighted MSSP in linear time [Eisenstat Klein]
- $\Omega(n \log n)$ lower bound [Eisenstat Klein]
- Space-time tradeoff for Klein’s algorithm (but *not* CCE) using different dynamic-forest data structures: $O(kn^{1+1/k})$ preprocessing time and $O(k \log \log n)$ query time. [Long Pettie 2021]

Chapter 16

Multiple-Source Shortest Paths, Revisited^α

In a recent breakthrough, Das, Kipouridis, Probst Gutenberg, and Wulff-Nilsen described an alternative algorithm that solves the planar multiple-source shortest path problem using a relatively simple divide-and-conquer strategy. Their algorithm theoretically runs in $O(n \log h)$ time, where h is the number of vertices on the outer face, which improves the $O(n \log n)$ time of Klein's algorithm when h is small. Moreover, this running time is worst-case optimal as a function of both n and h .

A better expression for the running time is $O(S(n) \log h)$, where $S(n)$ is the time to compute a single-source shortest path tree.

- If we use Dijkstra's algorithm off the shelf, the running time is $O(n \log n \log h)$.
- If we use the $O(n \log \log n)$ -time algorithm that we will see in Lecture 15,¹ the running time is $O(n \log h \log \log n)$.
- If we use the $O(n)$ -time algorithm of Henzinger et al.,² the running time is the optimal $O(n \log h)$.

The new algorithm is simpler in the sense that it uses only black-box shortest-path algorithms, completely avoiding complex dynamic forest data structures that are inefficient in practice, at least for small graphs.³ On the other hand, the new algorithm requires a subtle divide-and-conquer algorithm with weighted r -divisions, which is *also* inefficient in practice, to achieve its best possible running time $O(n \log h)$. On the gripping hand, Klein's algorithm has been observed to require a sublinear number of pivots for many inputs, so the $O(n \log n)$ time bound, while tight in the worst case, is usually conservative; whereas, the $O(n \log h)$ time bound for the new algorithm is tight for *all* inputs. It would be interesting to experimentally compare Klein (or

¹The $O(n \log \log n)$ -time shortest-path algorithm from Lecture 15 uses the *parametric* MSSP algorithm from the previous lecture as a subroutine. If we instead recursively apply the recursive MSSP strategy described in this lecture, the resulting doubly-recursive MSSP algorithm runs in $O(n \log h \log \log n \log \log \log n \log \log \log \log n \dots)$ time.

²This $O(n)$ -time shortest-path algorithm does *not* use MSSP as a subroutine.

³David Eisenstat [2] implemented Chambers, Cabello, and Erickson's MSSP algorithm using both efficient dynamic trees and brute-force to find pivots. His experimental evaluation showed that the brute-force implementation was faster in practice for graphs with up to 200000 vertices. More generally, in a large-scale experimental comparison of several dynamic-forest data structures by Tarjan and Werneck [6, 7], brute-force implementation beat all other data structures for trees with depth less than 1000.

CCE) using linear-time dynamic trees against the new algorithm using Dijkstra as a black box.

16.1 Problem formulation

It will be convenient to describe the inputs and outputs of the MSSP problem slightly differently than in the previous lecture.

The input consists primarily of a *directed* planar map $\Sigma = (V, E, F)$ with a distinguished outer face o and a non-negative weight $\ell(u \rightarrow v)$ for every directed edge/dart $u \rightarrow v$, which could be infinite (to indicate that a directed edge is missing from the graph). The weights are not necessarily symmetric; we allow $\ell(u \rightarrow v) \neq \ell(v \rightarrow u)$.

Let s_0, s_1, \dots, s_{h-1} be any subsequence of h vertices in counterclockwise order around the outer face, and let $S = \{s_0, s_1, \dots, s_{h-1}\}$. Our goal is to compute an implicit representation of the shortest paths from each source vertex s_i to every original vertex of Σ . See Figure 1.

For ease of presentation, I will make a few minor technical assumptions:

- Every source vertex $s_i \in S$ has out-degree 1 and in-degree 0. We can enforce this assumption if necessary by adding a new artificial source vertex s'_i and a single directed edge $s'_i \rightarrow s_i$ with weight 0.
- Σ is simple. We can enforce this condition if necessary by resolving parallel edges and deleting loops in $O(n)$ time using hashing.⁴
- The graph of $\Sigma \setminus S$ is strongly connected. Thus, the shortest path tree rooted at each source vertex s_i includes every non-source vertex. We can enforce this assumption if necessary by adding new infinite-weight edges.
- All shortest paths are unique. If necessary, we can enforce this assumption either by randomly perturbing the edge weights or by choosing leftmost shortest paths, just as in the previous lecture.

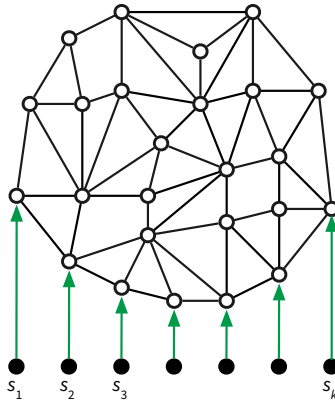


Figure 16.1: Setup for the recursive MSSP algorithm.

For any index j and any vertex v , let $path_j(v)$ denote the shortest path in Σ from s_j to v , let $dist_j(v)$ denote the length of this shortest path, and let $pred_j(v)$ denote the predecessor of v in this shortest path.

⁴The algorithms I describe in this note use hashing in multiple places. It is possible to achieve the same running time without hashing, at the expense of simplicity (and probably some efficiency).

The main recursive algorithm MSSP-Prep preprocesses the map Σ into a data structure that implicitly encodes the single-source shortest path trees rooted at every source s_j . A separate query algorithm $\text{MSSP-Query}(s_j, v)$ returns $dist_j(v)$.

16.2 Overview

The preprocessing algorithm uses a divide-and conquer-strategy. The input to each recursive call $\text{MSSP-Prep}(H, i, k)$ consists of the following:

- A planar map H , which is a simple weighted minor of the top-level input map Σ .
- Two indices i and k . To simplify presentation, we implicitly assume that s_i, s_{i+1}, \dots, s_k are the only source vertices in H .

For each index j , let T_j denote the tree of shortest paths in H from s_j to every other vertex of H . The recursive call $\text{MSSP-Prep}(H, i, k)$ computes an implicit representation of all $k - i + 1$ shortest path trees T_1, T_{i+1}, \dots, T_k . The top-level call is $\text{MSSP-Prep}(\Sigma, 0, h - 1)$.

MSSP-Prep invokes a subroutine $\text{Filter}(H, i, k)$ that behaves as follows:

- Compute the shortest path trees T_i and T_k rooted at s_i and s_k .
- Identify directed edges that are shared by all shortest path trees T_j with $i \leq j \leq k$.
- Contract shared edges and update nearby weights to maintain shortest path distances.
- Return the resulting contracted planar map.

Finally, ignoring base cases for now, $\text{MSSP-Prep}(H, i, k)$ has four steps:

- Set $H' \leftarrow \text{Filter}(H, i, k)$.
- Set $j \leftarrow \lfloor (i + k)/2 \rfloor$.
- Recursively call $\text{MSSP-Prep}(H', i, j)$.
- Recursively call $\text{MSSP-Prep}(H', j, k)$.

Finally, $\text{MSSP-Prep}(H, i, k)$ returns a record storing the following information:

- the indices i and k
- data about each vertex in H computed by Filter
- pointers to the records returned by the recursive calls

Said differently, MSSP-Prep returns a data structure that mirrors its binary recursion tree; every record in this data structure stores information computed by one invocation of Filter .

The time and space analysis of MSSP-Prep hinges on the observation that the total size of all minors H at each level of the resulting recursion tree is only $O(n)$. The depth of the recursion tree is $O(\log h)$, so the total size of the data structure is $O(n \log h)$. Similarly, aside from recursive calls, the time for each subproblem with m vertices is $O(S(m))$, so the overall running time is $O(S(n) \log h)$.

Finally, the query algorithm recovers the shortest-path distance from any source s_j to any vertex v by traversing the recursion tree of MSSP-Prep in $O(\log h)$ time.

In the rest of this note, I'll consider each of the component algorithms in more detail.

16.3 Properly shared edges

Now I'll describe the filtering algorithm $\text{Filter}(H, i, k)$ in more detail. For any index j and any vertex v , define the following:

- T_j is the shortest-path tree in H rooted at source vertex s_j .
- $\text{dist}_j(v)$ is the shortest-path distance in H from s_j to v .
- $\text{pred}_j(v)$ is the predecessor of v on the shortest path in H from s_j to v .

Our filtering algorithm $\text{Filter}(H, i, k)$ begins by computing the distances $\text{dist}_i(v)$ and $\text{dist}_k(v)$ and predecessors $\text{pred}_i(v)$ and $\text{pred}_k(v)$ for every vertex v , using two invocations of your favorite shortest-path algorithm. The algorithm also initializes two variables for every vertex v , which will eventually be used by the query algorithm:

- A *representative* vertex $\text{rep}(v)$, initially equal to v .
- A non-negative real *offset* $\text{off}(v)$, initially equal to 0.

Call any directed edge $u \rightarrow v$ *properly shared* by T_i and T_k if it satisfies the following recursive conditions:

- $\text{pred}_i(v) = \text{pred}_k(v) = u$; in other words, $u \rightarrow v$ is an edge in both T_i and T_k .
- If $\text{pred}_i(u) = \text{pred}_k(u)$, then the edge $\text{pred}_i(u) \rightarrow u$ is properly shared.
- Otherwise, vertices $\text{pred}_i(u), v, \text{pred}_k(u)$ are ordered clockwise around u .

We say that a properly shared edge $u \rightarrow v$ is *exposed* if $\text{pred}_i(u) \neq \text{pred}_k(u)$. For example, in Figure 2, both heavy black edges on the left are properly shared, but only the lower edge is exposed; the heavy black edges on the right are not properly shared.

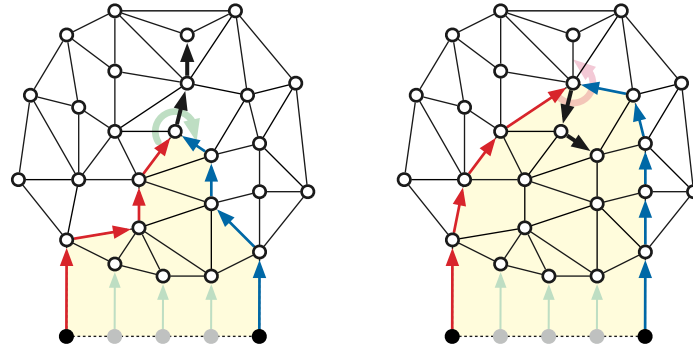


Figure 16.2: Shortest paths that share two edges. Left: Properly shared. Right: Improperly shared.

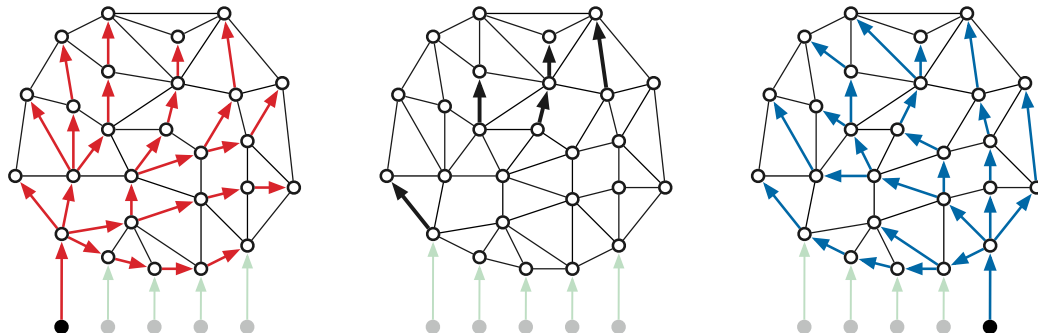


Figure 16.3: Two shortest path trees with five properly shared edges, four of which are exposed.

Lemma: If $u \rightarrow v$ is properly shared by T_i and T_k , then $\text{pred}_j(v) = u$ for all $i \leq j \leq k$.

Proof: First suppose $u \rightarrow v$ is properly shared and exposed. Let γ be a simple closed curve obtained by concatenating $\text{path}_k(u)$, the reversal of $\text{path}_i(u)$, and a simple path from s_i to s_k through the outer face. (The shaded yellow region Figure 2 is the interior of γ .) Each source vertex s_j is inside γ , and v is outside γ . So the Jordan curve theorem implies that $\text{path}_j(v)$ must cross γ . Uniqueness of shortest paths implies that $\text{path}_j(v)$ cannot cross either $\text{path}_i(v)$ or $\text{path}_k(v)$. It follows that $\text{path}_j(v)$ must contain u , and thus $\text{pred}_j(v) = u$.

Now suppose $u \rightarrow v$ is properly shared but not exposed. Let p be the first vertex on $\text{path}_i(v)$ that is also in $\text{path}_k(v)$, and let $p \rightarrow q$ be the first edge on the shortest path from p to v in H . Our recursive definitions imply that $p \rightarrow q$ is properly shared and exposed, so by the previous paragraph, for any index j , we have $\text{pred}_j(q) = p$ for all $i \leq j \leq k$. It follows that T_j contains the entire shortest path from p to v , and in particular, the edge $u \rightarrow v$. \square

The converse of the previous lemma is not necessarily true; it is possible for $\text{pred}_j(v) = u$ for every index j even though $u \rightarrow v$ is not properly shared. Consider the reversed shortest path tree \bar{T}_v rooted at v . Let s_l and s_r be the leftmost and rightmost source vertices in the subtree of \bar{T}_v rooted at u . If this subtree contains every source vertex s_j , then $l = r + 1 \bmod h$; intuitively, the subtree wraps around $u \rightarrow v$ and meets itself at the boundary. See Figure 4 for an example. Edges of this form are *not* detected by the filtering algorithm.

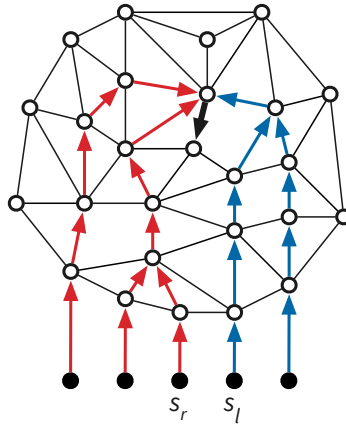


Figure 16.4: The black edge is shared by all shortest-path trees, but not properly shared by T_i and T_k .

Let m denote the number of vertices in H . We can identify all properly shared edges in H in $O(m)$ time using a preorder traversal of either T_i or T_k . In particular, we can find all *exposed* edges leaving vertex u in $\deg(u)$ time by visiting the darts into u in clockwise order—following the successor permutation—from $\text{pred}_i(u) \rightarrow u$ to $\text{pred}_k(u) \rightarrow u$.

16.4 Contraction

The main work of the filtering algorithm is *contracting* properly shared edges so that they need not be passed to recursive subproblems. Intuitively, we contract the edge $u \rightarrow v$ into its tail u , changing the tail of each directed edge $v \rightarrow w$ from v to u . Here are the steps in detail:

- Set $\text{rep}(v) \leftarrow u$
- Set $\text{off}(v) \leftarrow \ell(u \rightarrow v)$

- For every edge $w \rightarrow v$:
 - Set $\ell(w \rightarrow v) \leftarrow \infty$
- For every edge $v \rightarrow w$:
 - Set $\ell(v \rightarrow w) \leftarrow off(v) + \ell(v \rightarrow w)$
 - If $pred_i(w) = v$, set $pred_i(w) \leftarrow u$
 - If $pred_k(w) = v$, set $pred_k(w) \leftarrow u$
- Contract uv to u

The actual edge-contraction (in the second-to-last step) merges the successor permutations of u and v in $O(1)$ time, as described in Lecture 10.

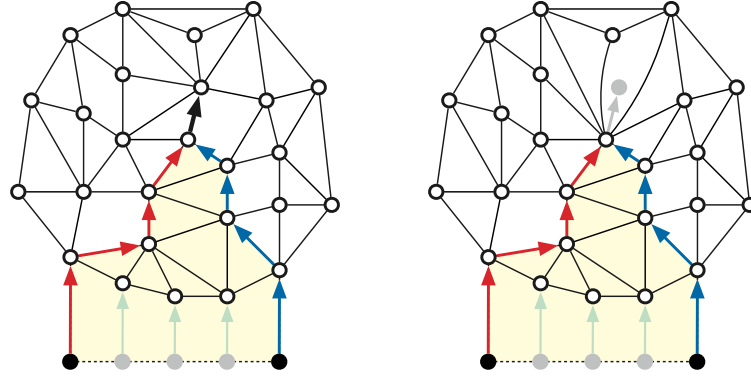


Figure 16.5: Contracting an exposed properly shared dart.

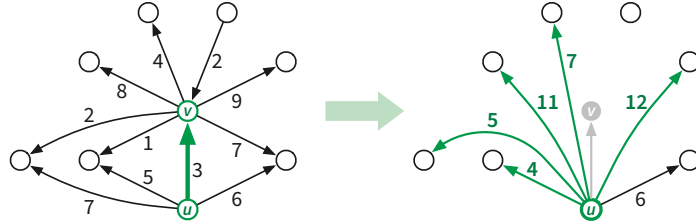


Figure 16.6: Edge weights before and after contraction and cleanup

If u and v have any common neighbors, contracting v into u creates parallel edges, which we must resolve before passing the contracted map to MSSP-prep. After all properly shared edges are contracted, we perform a global cleanup that identifies and resolves all families of parallel edges. Specifically, for each pair of neighboring vertices u and v in the contracted map, we choose one edge e between u and v , change the dart weights of e to match the lightest darts $u \rightarrow v$ and $v \rightarrow u$, and then delete all other edges between u and v . If we use hashing to recognize and collect parallel edges, the entire cleanup phase takes linear time.⁵

Contracting $u \rightarrow v$ preserves the shortest-path distance from every source s_j to every other vertex (except the contracted vertex v). Moreover, for every source vertex s_j and every vertex w in the original map H *including* v , contraction also maintains the following invariant, which allows us to recover shortest-path distances during the query algorithm. Let $dist_j(w)$ denote the shortest-path

⁵Efficiently maintaining a *simple* planar graph under arbitrary edge contractions is surprisingly subtle; see Holm et al [2] and Kammer and Meintrup [3]. For this MSSP algorithm, it suffices to resolve only *adjacent* parallel edges and delete *empty* loops immediately after each contraction in $O(1)$ time per deleted edge using only standard graph data structures. The resulting planar map is no longer necessarily simple, but every face has degree at least 3, which is good enough.

distance from s_j to w in the original map H , and let $dist'_j(w)$ denote the corresponding distance in the current contracted map.

Key Invariant: For every vertex w of H and for every index j such that $i \leq j \leq k$, we have $dist_j(w) = dist'_j(rep(w)) + off(w)$.

When Filter begins, we have $dist_j(w) = dist'_j(w)$ and $rep(w) = w$ and $off(w) = 0$, so the Key Invariant holds trivially.

We contract properly shared edges in the same order they were discovered, following a preorder traversal of T_i . This contraction order conveniently guarantees that we only contract *exposed* edges; contracting one exposed edge $u \rightarrow v$ transforms each properly shared edge leaving v into an *exposed* properly shared edge leaving u . This contraction order also guarantees that after contracting $u \rightarrow v$, no edge into u will ever be contracted. It follows that we change the tail of each edge (and therefore the predecessors of each vertex) at most once, and the Key Invariant is maintained. We conclude:

Lemma: $\text{Filter}(H, i, k)$ identifies and contracts all properly shared edges in H in $O(S(m) + m)$ time, where $m = |V(H)|$. Moreover, after $\text{Filter}(H, i, k)$ ends, the Key Invariant holds.

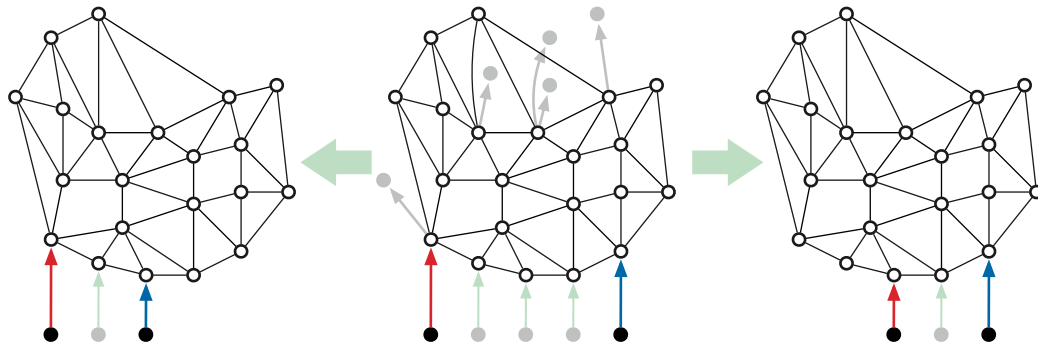


Figure 16.7: Contracting all properly shared directed edges and recursing.

16.5 Distance Queries

Each call to $\text{Filter}(H, i, k)$ creates a record storing the following information:

- indices i and k
- for each vertex v of the input map H :⁶
 - shortest-path distances $dist_i(v)$ and $dist_k(v)$
 - the representative vertex $rep(v)$
 - the offset $off(v)$.

The recursive calls to MSSP-Prep assemble these records into a binary tree, mirroring the tree of recursive calls, connected by *left* and *right* pointers.

The query algorithm $\text{MSSP-query}(Rec, j, v)$ takes as input a recursive-call record Rec , a source index j , and a vertex v , satisfying two conditions:

⁶To keep the space usage low, we store this vertex information in four hash tables, each of size linear in the number of vertices of H . Alternatively, we can avoid hash tables by compacting the incidence-list structure of H' during the cleanup phase of Filter, and storing the index in the filtered map H' of each vertex of the input map H .

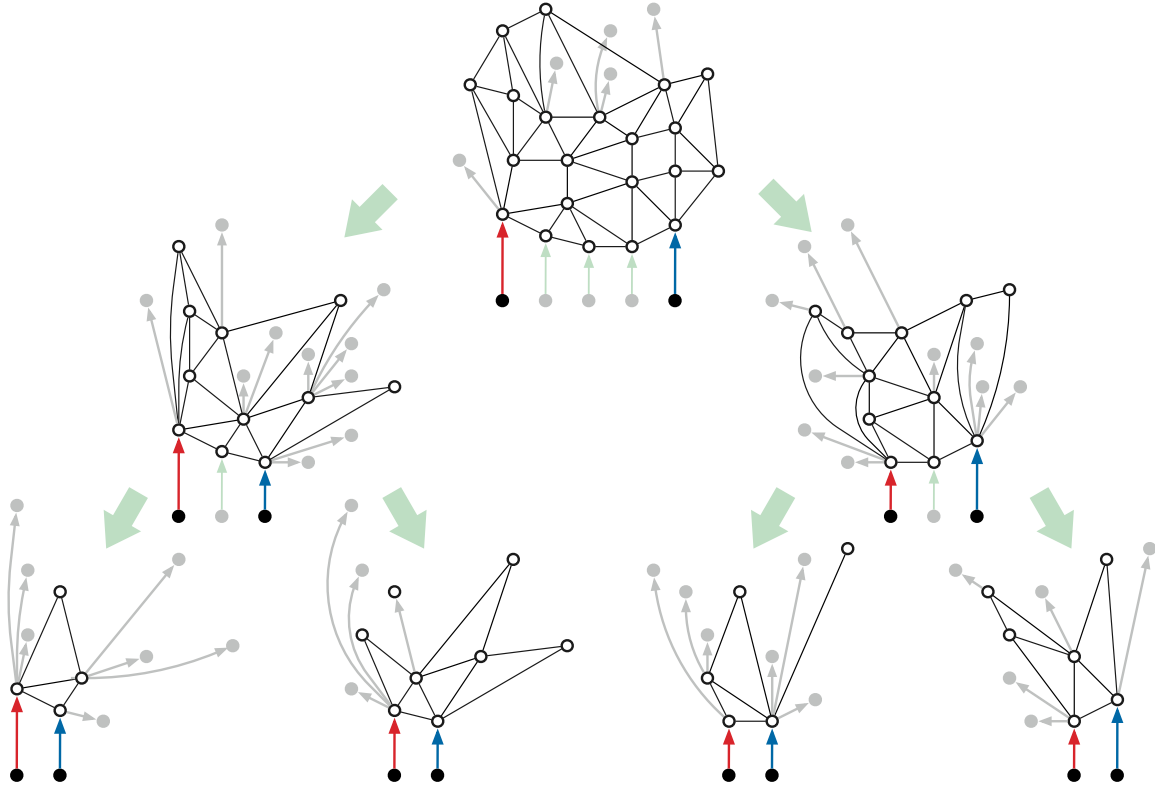


Figure 16.8: Recursive subproblems after contraction become more and more birdlike.

- $Rec.i \leq j \leq Rec.k$
- v is a vertex of the input map H to the recursive call to MSSP-Prep that created Rec .

The output of $MSSP\text{-query}(Rec, j, v)$ is the shortest-path distance from s_j to v in Σ . The query algorithm follows straightforwardly from the Key Invariant:

- if $j = i$, return $Rec.dist_i[v]$
- else if $j = k$, return $Rec.dist_k[v]$
- else if $j \leq Rec.left.k$, return $MSSP\text{-query}(Rec.left, j, Rec.rep[v]) + Rec.off[v]$
- else return $MSSP\text{-query}(Rec.right, j, Rec.rep[v]) + Rec.off[v]$

Because the recursion tree has depth $O(\log h)$, the query algorithm runs in $O(\log h)$ time.

16.6 Space and Time Analysis

It remains only to bound the size of our data structure and the running time of $MSSP\text{-Prep}$. The key claim is that the total size of all input maps at any level of the recursion tree is $O(n)$.

Contraction sharing lemma: *Contracting one properly shared edge neither creates nor destroys other properly shared edges.*

Proof: Fix a map H and source indices i and k . Let $u \rightarrow v$ be an edge in H that is properly shared by T_i and T_k . Let $H' = H/u \rightarrow v$, with dart weights adjusted as described above, and let T'_i and T'_k denote the shortest path trees rooted at s_i and s_k in H' .

First, because contraction preserves shortest paths, we can easily verify that $T'_i = T_i/u \rightarrow v$ and $T'_k = T_k/u \rightarrow v$. It follows that an edge in H is shared by T_i and T_k if and only if the corresponding edge in H' is shared by T'_i and T'_k .

Now consider any edge $x \rightarrow y \in T_i \cap T_k$ that is not $u \rightarrow v$. We must have $y \neq v$, because each vertex has only one predecessor in any shortest-path tree. Let w be the first node on the shortest path from s_i to x in H that is also on the shortest path from s_k to x , so the entire shortest path from w to y is shared by T_i and T_k . Consider three paths:

- α = the shortest path from s_i to w
- β = the reverse of the shortest path from w to y
- γ = the shortest path from s_k to w

Then $x \rightarrow y$ is properly shared if and only if (the last edges of) α , β , and γ are incident to w in clockwise order. The definition of properly shared implies $v = w$, so w is also a vertex in H' . Contracting $u \rightarrow v$ might shorten one of the three paths to w , but it cannot change their cyclic order around w . We conclude that $x \rightarrow y$ is properly shared in H if and only if $x \rightarrow y$ (or $u \rightarrow y$ if $x = v$) is properly shared in H' . \square

The contraction sharing lemma implies by induction that every call to $\text{Filter}(H, i, k)$ outputs the same contracted map as $\text{Filter}(\Sigma, i, k)$. In particular, an edge $u \rightarrow v$ in H is properly shared by two shortest-oath trees in H if and only if the corresponding edge in Σ (which may have a different tail vertex) is properly shared by the corresponding trees in Σ . So from now on, “properly shared” always implies “in the top level map Σ ”.

Corollary: *For all indices $i \leq i' < k' \leq k$, if $u \rightarrow v$ is properly shared by T_i and T_k , then $u \rightarrow v$ is properly shared by $T_{i'}$ and $T_{k'}$.*

Corollary: *The vertices of $\text{Filter}(\Sigma, i, k)$ are precisely the vertices v such that no edge into v is properly shared by T_i and T_k .*

Fix any vertex v of Σ . We call an index j *interesting* if $\text{pred}_j(v) \rightarrow v$ is not properly shared by T_j and T_{j+1} .

Lemma: *Every vertex v of Σ has at most $\deg(v)$ indices.*

Proof: Equivalently, j is interesting to v if either of the following conditions holds:

- $\text{pred}_j(v) \neq \text{pred}_{j+1}(v)$.
- $\text{pred}_0(v) = \text{pred}_1(v) = \dots = \text{pred}_{h-1}(v) = u$ and the paths $\text{path}_j(u)$ and $\text{path}_{j+1}(u)$ “wrap around” $u \rightarrow v$.

The Disk-Tree Lemma implies that the first condition holds for at most $\deg(v)$ indices j . If the first condition never holds (that is, if $\text{pred}_j(v)$ is the same for index j), then the second condition holds for exactly one index j ; otherwise the second condition never holds. \square

Lemma: *Each vertex v appears in at most $2\deg(v)$ subproblems at each level of the recursion tree.*

Proof: The children Rec.left and Rec.right of any recursion record Rec store information about v and if and only if at least one index j such that $\text{Rec}.i \leq j \leq \text{Rec}.k$ is interesting to v . \square

Theorem: *MSSP-Prep($\Sigma, 0, h - 1$) builds a data structure of size $O(n \log h)$ in $O(S(n) \log h)$ time.*

Proof: The total number of vertices in all subproblems at the same level of the recursion tree is at most $\sum_v 2 \deg(v) \leq 4 \cdot |E(\Sigma)| \leq 4(3n - 6) = 12n - 24$ by Euler's formula, since Σ is a simple planar map. Each recursion record uses $O(1)$ space per vertex, so the total space used at any level is $O(n)$. Similarly, the time spent in any subproblem is at most $O(S(n)/n)$ per vertex, so the total time spent in each level of the recursion tree is $O(S(n))$.

Finally, the recursion tree has $O(\log h)$ levels. \square

16.7 References

1. Debarati Das, Evangelos Kipouridis, Maximilian Probst Gutenberg, and Christian Wulff-Nilsen. A simple algorithm for multiple-source shortest paths in planar digraphs. *Proc. 5th Symp. Simplicity in Algorithms*, 1–11, 2022.
2. David Eisenstat. *Toward Practical Planar Graph Algorithms*. Ph.D. thesis, Comput. Sci. Dept., Brown Univ., May 2014.
3. Jacob Holm, Giuseppe F. Italiano, Adam Karczmarz, Jakub Łącki, Eva Rotenberg, and Piotr Sankowski. Contracting a planar graph efficiently. *Proc. 25th Ann. Europ. Symp. Algorithms*, 50:1–50:15, 2017. Leibniz Int. Proc. Informatics 87, Schloss Dagstuhl–Leibniz-Zentrum für Informatik. arXiv:1706.10228.
4. Frank Kammer and Johannes Meintrup. Succinct planar encoding with minor operations. Preprint, January 2023. arXiv:2301.10564.
5. Robert E. Tarjan and Renato F. Werneck. Dynamic trees in practice. *J. Exper. Algorithmics* 14:5:1–5:21, 2009.
6. Renato Werneck. *Design and Analysis of Data Structures for Dynamic Trees*. Ph.D. thesis, Dept. Comput. Sci., Princeton Univ., April 2006. Tech. Rep. TR-750-06.

Chapter 17

Planar Separators^β

Let Σ be an arbitrary planar map, with non-negative weights on its vertices, edges, and/or faces that sum to W . A simple cycle C in a planar map Σ is a *balanced cycle separator* if the total weight of all vertices, edges, and faces on either side of C is at most $3W/4$. As long as each vertex, edge, or face of Σ has weight at most $W/4$, there is a balanced cycle separator with at most $O(\sqrt{n})$ vertices; moreover, we can compute such a cycle in $O(n)$ time.

17.1 Tree separators

Before we consider separators in planar graphs, let's consider the simpler case of trees. Here a balanced separator is a single edge that splits the tree into two subtrees of roughly equal weight. Tree separators were first studied by Camille Jordan

Let $T = (V, E)$ be an unrooted tree in which every vertex has degree at most 3. Intuitively, T is a “binary” tree, but without a root and without a distinction between left and right children. (This bounded-degree assumption is necessary.) Assign each vertex v a non-negative weight $w(v)$ and let $W := \sum_v w(v)$.

Tree-separator lemma: *If every vertex has weight at most $W/4$, there is an edge e in T such that the total weight in either component of $T \setminus e$ is at most $3W/4$.*

Proof: Pick an arbitrary leaf r of T as the root, and direct all edges away from r , so every vertex in T has at most two children. By attaching leaves with weight zero, we can assume without loss of generality that every non-leaf vertex has exactly two children.

For any vertex v , let $W(v)$ denote the total weight of v and its descendants; for example, $W(r) = W$. For any non-leaf vertex v , label its children $\text{heft}(v)$ and $\text{lite}(v)$ so that $W(\text{heft}(v)) \geq W(\text{lite}(v))$ (breaking ties arbitrarily).

Starting at the root r , follow heft pointers down to the first vertex x such that $W(\text{heft}(x)) \leq W/4$. Then we immediately have

$$\begin{aligned} W/4 &< W(x) \\ &= W(\text{heft}(x)) + W(\text{lite}(x)) + w(x) \\ &\leq 2 \cdot W(\text{heft}(x)) + w(x) \\ &\leq 3W/4. \end{aligned}$$

Let e be the edge between x and its parent. The two components of $T \setminus e$ have total weight $W(x) \leq 3W - 4$ and $W - W(x) < 3W/4$. \square .

It's easy to see that the upper bounds on vertex degree and vertex weight are both necessary. This separator lemma has several variants; I'll mention just a few without proof:

Unweighted tree-separator lemma: *For any n -vertex tree T with maximum degree 3, there is an edge e such that each component of $T \setminus e$ has at most $2n/3$ vertices.*

Edge-weight tree-separator lemma: *For any tree T with maximum degree 3 and any weights on the edges of T that sum to W , there is an edge e such that both components of $T \setminus e$ have total edge weight at most $2W/3$.*

Vertex tree-separator lemma: *For any tree T and any weights on the vertices of T that sum to W , there is a vertex v such that every component of $T \setminus v$ has total weight at most $W/2$.*

17.2 Fundamental cycle separators

Now let Σ be a planar triangulation. Assign each face f a non-negative weight $w(f) \leq W/4$, where $W := \sum_f w(f)$. (Again, the upper bounds on face degree and face weight are both necessary.) A cycle C in Σ is a *balanced separator* if the total weight on either side of C is at most $3W/4$.

Let T be an arbitrary spanning tree of Σ . For any non-tree edge e , the *fundamental cycle* $\text{cycle}(T, e)$ is the unique cycle in $T + e$, consisting of e and the unique path in T between the endpoints of e .

Lemma: *At least one fundamental cycle $\text{cycle}(T, e)$ is a balanced separator for Σ .*

Proof: Let C^* be the spanning tree of Σ^* complementary to T . Because Σ is a triangulation, every vertex of C^* has degree at most 3. Suppose each vertex of C^* inherits its weight from the corresponding face of Σ . The tree-separator lemma implies that there is some edge e such that each component of $C^* \setminus e^*$ has at most $3/4$ the total weight of the vertices of C^* . It follows that $\text{cycle}(T, e)$ is a balanced separator. \square

We can extend this lemma to the setting where vertices and edges also have weights, in addition to faces. Let $w: V \cup E \cup F \rightarrow \mathbb{R}_+$ be the given weight function. Define a new face-weight function $w': F \rightarrow \mathbb{R}_+$ by moving the weight of each vertex and edge to some incident face.

Unfortunately, fundamental cycles can be quite long. For any particular map Σ , we can minimize the maximum length of all fundamental cycles using a *breadth-first search* tree from the correct root vertex as our spanning tree T , but in the worst case, every *balanced* fundamental cycle separator has length $\Omega(n)$.

For most applications of balanced separators, breadth-first fundamental cycles are usually the best choice *in practice*; see the detailed experimental analysis by Fox-Epstein et al. [1].

17.3 Breadth-first level separators

A second easy method for computing separators is to consider the levels of a breadth-first search tree. For the moment, let's assume that the *vertices* of Σ are weighted. For each integer ℓ , let V_ℓ denote the vertices ℓ steps away from the root vertex of T . By computing a weighted median, we can find a level V_m such that the total vertex weight in any component of $\Sigma \setminus V_m$ is at most $W/2$.

There are two obvious problems with this separator construction. The less serious problem is that the medial level V_m is not a cycle; it's just a cloud of vertices. Many applications of planar separators don't actually require *cycle* separators, but most of the applications we'll see in this class do. The more serious problem is size; in the worst case, the set V_m could contain a constant fraction of the vertices.

When Richard Lipton and Robert Tarjan introduced planar separators in 1979, they did not consider cycle separators. Rather, they proved that there is always a subset S of $O(\sqrt{n})$ vertices such that any component of $\Sigma \setminus S$ has at most $2n/3$ vertices. Lipton and Tarjan's construction combines fundamental cycle separators and BFS-level separators. I will not describe their construction in detail, partly because we really do need cycles, and partly because most of their ideas show up in the next section.

17.4 Cycle separators

Gary Miller was the first to prove that small balanced cycle separators exist, in 1986. The following refinement of Miller's algorithm is based on later proofs by Philip Klein, Shay Mozes, and Christian Sommer (2013) and Sariel Har-Peled and Amir Nayyeri (2018). Miller's key idea was to generalize our notion of "level" from vertices to faces.¹

As in our earlier setup, Let Σ be a simple planar triangulation with weighted faces, where no individual face weight is too large. Let T_0 be a breadth-first search tree, and suppose the fundamental cycle $\text{cycle}(T_0, xy)$ is a balanced separator. If this cycle has length $O(\sqrt{n})$, we are done, so assume otherwise.

Let r denote the least common ancestor of x and y , and let T be a breadth-first search tree rooted at r . The cycle $\text{cycle}(T, xy) = \text{cycle}(T_0, xy)$ is still a balanced separator.

For any vertex v , let $\text{level}(v)$ denote the breadth-first distance from r to v . Without loss of generality, assume $\text{level}(x) \leq \text{level}(y)$. Then for any face f , let $\text{level}(f)$ denote the maximum level among the three vertices of f . A face at level ℓ has vertices only at levels ℓ and $\ell - 1$. Let o denote the outer face of Σ , and without loss of generality, assume that $L = \text{level}(o) = \max_f \text{level}(f)$.

For any integer ℓ , let $U_{\leq \ell}$ denote the union of all faces with level at most ℓ , and let C_ℓ be the outer boundary of $U_{\leq \ell}$. Trivially $U_{\leq 0} = \emptyset$ and therefore $C_0 = \emptyset$. Similarly, for any $\ell \geq L$, we have $U_{\leq \ell} = \mathbb{R}^2$ and therefore $C_\ell = \emptyset$.

Lemma:

- (a) Every vertex in C_ℓ has level ℓ .
- (b) Every non-empty subgraph C_ℓ is a simple cycle.
- (c) The cycles C_ℓ are pairwise vertex-disjoint.
- (d) The fundamental cycle $\text{cycle}(T, xy)$ intersects C_ℓ in at most two vertices

Proof: Part (a) follows directly from the definitions.

By construction C_ℓ consists of one or more simple cycles, any two of which share at most one vertex. Let C be the simple cycle in C_ℓ that contains r in its interior. and let v be any

¹Fox-Eppstein et al. [1] describe an arguably simpler algorithm that uses a dual breadth-first search rooted at the outer face to define face levels, instead of a primal breadth-first search tree.

vertex of $C_\ell \setminus C$. Let u be the second-to-last vertex on the shortest path from r to v . Vertex u has level $\ell - 1$ and therefore does not lie on C ; moreover, because $v \notin C$, vertex u cannot lie in the interior of C . The Jordan curve theorem implies that the shortest path from u to r crosses C , but this is impossible, because levels decrease monotonically along that path. We conclude that $C_\ell = C$, proving part (b).

Part (c) follows immediately from part (a).

Finally, the vertices of $\text{cycle}(T, xy)$ lie on two shortest paths from r , one to x and the other to y . Levels increase monotonically along any shortest path from r . Thus, by part (a), the shortest paths from r to x and y each share at most one vertex with C_ℓ . \square

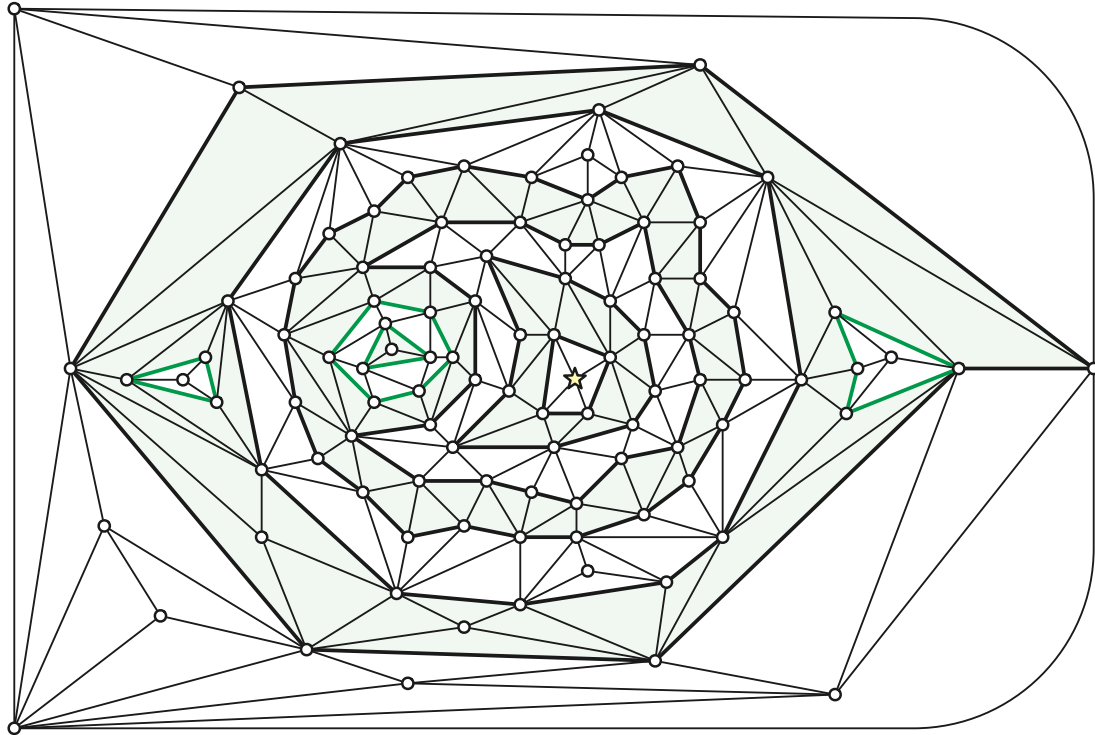


Figure 17.1: Depth contours in a plane triangulation. The starred vertex is the root r . Faces with even depth are shaded. Cycles C_ℓ are black. Green cycles are other portions of the boundary of sublevel sets U_ℓ .

Let m be the largest integer such that the total weight of all faces inside C_m is at most $W/2$. Then the total weight of the faces outside C_{m+1} is also at most $W/2$. If either of these cycles is a balanced cycle separator of length $O(\sqrt{n})$, we are done, so assume otherwise. We choose two level cycles C^- and C^+ as follows.²

- Consider the set of cycles $\mathcal{C}^- = \{C_\ell \mid m - \sqrt{n} < \ell \leq m\}$. These \sqrt{n} cycles contain at most n vertices, and therefore some cycle C^- in this set must have length less than \sqrt{n} . By construction, the total weight of all faces inside C^- is at most $W/2$.
- Similarly, consider the set $\mathcal{C}^+ = \{C_\ell \mid m < \ell \leq m + \sqrt{n}\}$. These \sqrt{n} cycles contain at most n vertices, and therefore some cycle C^+ in this set must have length less than \sqrt{n} . By construction, the total weight of all faces outside C^+ is at most $W/2$.

²I am ignoring two extreme cases. First, if $m < \sqrt{n}$, we define $C^- = \emptyset$; similarly, if $m > \text{level}(y) - \sqrt{n}$, we define $C^+ = \emptyset$. Handling these special cases in the rest of the construction is straightforward.

Let π_x denote the portion of the shortest path from r to x with levels between a and b , and define π_y similarly. By construction, each of these paths has length at most $2\sqrt{n}$. Let Θ denote the graph $C^- \cup C^+ \cup \pi_x \cup \pi_y$, as shown in the figure below. This subgraph of Θ has at most $4\sqrt{n}$ vertices and edges. We label the four faces of Θ as follows:

- A is the interior of C^- .
- B is the exterior of C^+ .
- C is the region between C^+ and C^- and outside cycle(T, xy).
- D is the region between C^+ and C^- and inside cycle(T, xy).

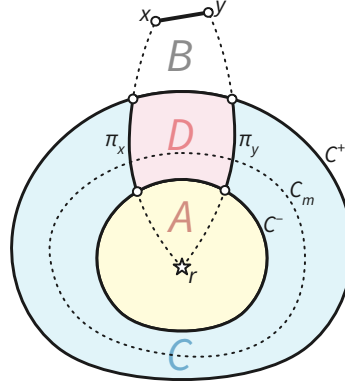


Figure 17.2: Regions in the cycle-separator algorithm.

Let $W(S)$ denote the total weight of the set of faces S . By construction we have

$$W(A) \leq W/2, \quad W(B) \leq W/2, \quad W(C) \leq 3W/4, \quad W(D) \leq 3W/4.$$

At least one of these four regions contains total weight at least $W/4$; the boundary of that region is a balanced cycle separator of length $O(\sqrt{n})$.

Most divide-and-conquer algorithms that use cycle separators do not delete the separator vertices to obtain smaller subgraphs. Rather, the algorithms *slice* the planar map along the cycle separator to obtain smaller *maps*, called *pieces* of the original map, one containing the faces inside the cycle and the other containing the faces outside. Both pieces contain a copy of the $O(\sqrt{n})$ vertices and edges of the separator. Thus, the total size of all subproblems is larger at deeper levels of the recursion tree, but because that increase is sublinear, we can ignore it when solving the resulting divide-and-conquer recurrences.

17.5 Good r -divisions and Subdivision Hierarchies

An r -division is a decomposition of a planar map into n/r pieces, each of which has $O(r)$ vertices and $O(\sqrt{r})$ boundary vertices (shared with other pieces). An r -division is *good* if each piece is a disk with $O(1)$ holes. For any r , we can construct a good r -division by recursively slicing the input triangulation along balanced cycle separators. In fact, this subdivision strategy computes a *subdivision hierarchy* that includes good r -divisions for arbitrary values of r .

In each recursive call, we are given a region R , which is a connected subcomplex of the original triangulation Σ . Any face of the region R that is not a face of Σ is called a *hole*; any vertex of R that is incident to a hole is a *boundary vertex* of R . To split R into two smaller regions, we

first triangulate R by inserting an artificial vertex v_h inside each hole h , along with artificial edges connecting v_h to each corner of h . We then compute a cycle separator in the resulting triangulation R' , splitting it into two smaller triangulated regions R'_0 and R'_1 . Finally, we delete the artificial vertices and edges from R'_0 and R'_1 to get the final regions R_0 and R_1 .

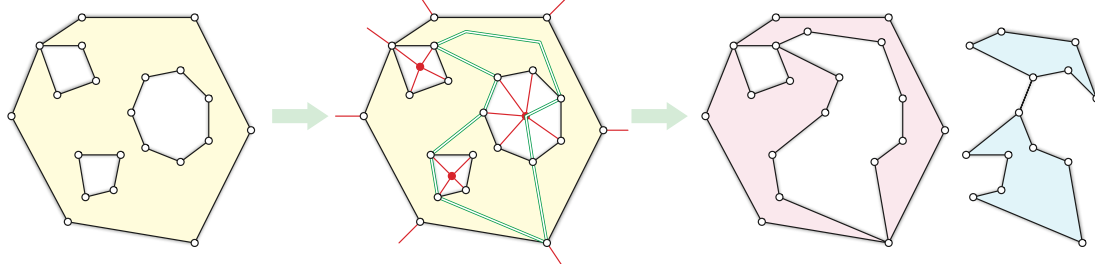


Figure 17.3: A region with three holes, a cycle separator for the triangulated region, and the resulting smaller regions.

To simultaneously bound the number of vertices, the number of boundary vertices, and the number of holes in the final regions, we cycle through three different vertex weights at different levels of recursion. Specifically, at recursion depth l , we weight the vertices as follows:

- If $l \bmod 3 = 0$, we give natural vertices weight 1 and artificial vertices weight 0, so that the separator splits natural vertices evenly.
- If $l \bmod 3 = 1$, we give boundary vertices weight 1 and all other vertices weight 0, so that the separator splits boundary vertices evenly.
- If $l \bmod 3 = 2$, we give artificial vertices weight 1 and natural vertices weight 0, so that the separator splits holes evenly.

Let $T_r(n, b, h)$ denote the time to compute a good r -division for a region with n vertices, b boundary vertices, and h holes. Expanding out three levels of recursion, we have

$$T_r(n, b, h) = O(n + h) + \sum_{i=1}^8 T_r(n_i, b_i, h_i),$$

where

$$\begin{aligned} \sum_{i=1}^8 n_i &\leq n + O(\sqrt{n}) & \sum_{i=1}^8 b_i &\leq b + O(\sqrt{n}) & \sum_{i=1}^8 h_i &\leq h + O(1) \\ \max_i n_i &\leq 3n/4 + O(\sqrt{n}) & \max_i b_i &\leq 3b/4 + O(\sqrt{n}) & \max_i h_i &\leq 3h/4 + O(1) \end{aligned}$$

for suitable absolute big-Oh constants. The recursion stops when the number of vertices in each piece is $O(r)$. Every leaf in the recursion tree has depth at most $O(\log(n/r))$, and there are at most $O(n/r)$ such leaves. One can prove by induction that in every recursive subproblem, the number of boundary vertices is at most $O(\sqrt{r})$ and the number of holes is at most $O(1)$, so we end with a good r -division. We perform $O(n)$ work at every level of recursion, so the overall running time of the algorithm is $T_r(n, 0, 0) = O(n \log(n/r))$. In particular, if $r = O(1)$, the entire algorithm runs in $O(n \log n)$ time.

Theorem: *Given a planar triangulation Σ with n vertices, we can compute a recursive subdivision of Σ , containing good r -divisions of Σ for every $r \geq r_0$, in $O(n \log(n/r_0))$ time.*

Corollary: *Given a planar triangulation Σ with n vertices and an integer r , we can compute a good r -division of Σ in $O(n \log(n/r))$ time.*

Some applications of separators actually require a nested sequence of good r -divisions with exponentially decreasing values of r . For any vector $\vec{r} = (r_1, r_2, \dots, r_t)$ where $r_i < r_{i-1}/\alpha$ for some suitable constant α , a *good \vec{r} -division* of a planar map Σ consists of a good r_1 -division \mathcal{R}_1 of Σ and (unless $t = 1$) a good (r_2, \dots, r_t) -division of each piece of \mathcal{R}_1 . We can easily extract a good \vec{r} -division from any good subdivision hierarchy in $O(n)$ time.

Corollary: *Given a planar triangulation Σ with n vertices, and any exponentially decreasing vector $\vec{r} = (r_1, r_2, \dots, r_t)$, we can construct a good \vec{r} -division of Σ in $O(n \log(n/r_t))$ time.*

17.6 History

Greg Frederickson introduced r -divisions (based on non-cycle separators) in 1989. The current definition of good r -division was proposed by Philip Klein and Sairam Subramanian in 1998. The three-phase algorithm I've just described was first proposed by Jittat Fakcharoenphol and Satish Rao in 2006, and extended to \vec{r} -divisions by Philip Klein, Shay Mozes, and Christian Sommer in 2013.

This is not the fastest algorithm known for computing good r -divisions. A different algorithm for constructing a good r -division in $O(n \log r + O(n/\sqrt{r}) \log n)$ time was described by Giuseppe Italiano, Yahav Nussbaum, Piotr Sankowski, and Christian Wulff-Nilsen in 2011.

In 1996, Lyudmil Aleksandrov and Hristo Djidjev described an $O(n)$ -time algorithm to construct r -divisions based on Lipton-Tarjan separators, for any given r . In 2013, Lars Arge, Freek van Walderveen, and Norbert Zeh described an algorithm to construct a single good r -division in $O(n)$ time. *[[[How do these algorithms work?]]]*

The first linear-time algorithm for building a subdivision *hierarchy* containing r -divisions for every r was described by Michael Goodrich in 1996. Klein, Mozes, and Sommer described a similar algorithm to compute a good subdivision hierarchy in $O(n)$ time.³ Both of these algorithms use dynamic forest data structures (to maintain tree-cotree decompositions of the pieces, identify fundamental cycle separators, compute least common ancestors, and compute the weight enclosed by short cycles), along with several other data structures.

In the next lecture we'll see how to use good r -divisions to compute shortest paths quickly.

17.7 References

1. Lyudmil Aleksandrov and Hristo Djidjev. Linear algorithms for partitioning embedded graphs of bounded genus. *SIAM J. Discrete Math.* 9(1):129–150, 1996.
2. Lars Arge, Freek van Walderveen, and Norbert Zeh. Multiway simple cycle separators and {I/O}-efficient algorithms for planar graphs. *Proc. 24th Ann. ACM-SIAM Symp. Discrete Algorithms*, 901–918, 2013.
3. Jittat Fakcharoenphol and Satish Rao. Planar graphs, negative weight edges, shortest paths, and near linear time. *J. Comput. Syst. Sci.* 72(5):868–889, 2006.
4. Eli Fox-Epstein, Shay Mozes, Phitchaya Mangpo Phothilimthana, and Christian Sommer. Short and simple cycle separators in planar graphs. *ACM J. Exp. Algorithms*

³The two 1996 results are completely independent; so are the two 2013 results.

- 21(1):2.2:1–2.2:24, 2016.
5. Greg N. Frederickson. Fast algorithms for shortest paths in planar graphs with applications. *SIAM J. Comput.* 16(8):1004–1004, 1987.
 6. Michael T. Goodrich. Planar separators and parallel polygon triangulation. *J. Comput. Syst. Sci.* 51(3):374–389, 1995.
 7. Sariel Har-Peled and Amir Nayyeri. A simple algorithm for computing a cycle separator. Preprint, September 2017. arXiv:1709.08122.
 8. Giuseppe F. Italiano, Yahav Nussbaum, Piotr Sankowski, and Christian Wulff-Nilsen. Improved algorithms for min cut and max flow in undirected planar graphs. *Proc. 43rd Ann. ACM Symp. Theory Comput.*, 313–322, 2011.
 9. Camille Jordan. Sur les assemblages de lignes. *J. Reine Angew. Math.* 70:185–190, 1869.
 10. Philip N. Klein, Shay Mozes, and Christian Sommer. Structured recursive separator decompositions for planar graphs in linear time. *Proc. 45th Ann. ACM Symp. Theory Comput.*, 505–514, 2013. arXiv:1208.2223.
 11. Philip N. Klein and Sairam Subramanian. A fully dynamic approximation scheme for shortest paths in planar graphs. *Algorithmica* 22(3):235–249, 1998.
 12. Richard J. Lipton and Robert E. Tarjan. A separator theorem for planar graphs. *SIAM J. Applied Math.* 36(2):177–189, 1979.
 13. Richard J. Lipton and Robert Endre Tarjan. Applications of a planar separator theorem. *SIAM J. Comput.* 9:615–627, 1980.
 14. Gary L. Miller. Finding small simple cycle separators for 2-connected planar graphs. *J. Comput. System Sci.* 32(3):265–279, 1986.

17.8 Aptly Named Sir Not

- Cycle separators via Koebe-Andreev circle packing
- Details of r divisions (and recursive r -divisions) in $O(n)$ time.

Chapter 18

Branch Decompositions \varnothing

18.1 Branchwidth

18.2 Treewidth

18.3 Width versus diameter

18.4 Local approximation

18.5 Aptly Named Sir Not

Chapter 19

Fast Shortest Paths in Planar Graphs^β

19.1 Dense Distance Graphs

One of the most important applications of separators and r -divisions in planar graphs is faster algorithms to compute shortest paths. Most of these faster algorithms rely on an implicit representation of shortest-path distances called the *dense distance graph*, first explicitly described by Jittat Fakcharoenphol and Satish Rao in 2001, but already implicit in Lipton, Rose, and Tarjan's 1979 nested dissection algorithm, which we will discuss shortly.

Let Σ be a simple planar map with weighted darts; for now we'll assume that all edge weights are non-negative. If necessary, add infinite-weight edges so that Σ is a simple triangulation. Recall that a *good r -division* of Σ is a subdivision of Σ into $O(n/r)$ pieces R_1, R_2, \dots satisfying three conditions:

- Each piece has $O(r)$ vertices.
- Each piece has $O(\sqrt{r})$ boundary vertices (that is, vertices that are shared with other pieces).
- Each piece has $O(1)$ holes (faces of the piece that are not faces of Σ).

Fix a good r -division \mathcal{R} . For each piece $R_i \in \mathcal{R}$, let X_i be a complete directed graph over the boundary vertices of R_i , where each dart $u \rightarrow v$ is weighted by the shortest-path distance in R_i from its tail u to its head v . The dense distance graph is the union of these $O(n/r)$ weighted cliques. Altogether, the dense distance graph has $n' = O(n/\sqrt{r})$ vertices—only the boundary vertices of the pieces of the r -division—and $m' = O(n)$ weighted darts.

Assuming all dart weights are non-negative, we can compute all $O(r)$ boundary-to-boundary shortest-path distances in each piece R_i in $O(r \log r)$ time, by running the multiple-source shortest-path algorithm once for each hole in R_i , using Dijkstra's algorithm to compute the initial shortest-path tree. Thus, the overall time to compute the dense-distance graph is $O(n \log r)$.

19.2 Beating Dijkstra

Theorem: *Given any planar map Σ with non-negative lengths on its edges, we can compute the shortest path from any vertex s to every other vertex of Σ in $O(n \log \log n)$ time.*

Proof: We begin by triangulating Σ in $O(n)$ time, building a good r -division for the resulting triangulation in $O(n)$ time, and building the dense distance graph for the r -division in

$O(n \log r)$ time, for some parameter r to be determined. In the top-level recursive call to build the good r -division, we artificially declare s to be a boundary vertex, so that it survives as a vertex in the dense-distance graph.

Next we compute the shortest-path distance from s to every boundary vertex of the r -division by running Dijkstra's algorithm in the dense distance graph. If we implement Dijkstra's algorithm using Fibonacci heaps, this step takes $O(n' \log n' + m') = O((n/\sqrt{r}) \log n + n)$ time.

Finally, for each piece P , we attach an artificial course s' to each boundary vertex u with an edge with length $\text{dist}(s, u)$, and compute a shortest path tree in P from s' using Dijkstra's algorithm. This step takes $O(r \log r)$ time per piece, or $O(n \log r)$ time overall.

The overall running time of our algorithm is $O(n \log r + (n/\sqrt{r}) \log n)$. In particular, if we set $r = O(\log^2 n)$, the running time is $O(n \log \log n)$. \square

Let me reiterate that this analysis assumes that we are using the *parametric* multiple-source shortest path algorithm to construct the dense-distance graph. If we try to use the more recent *contraction-based* MSSP algorithm of Das et al. instead, we end up with two mutually recursive algorithms, one computing single-course shortest paths, the other computing multiple-source shortest paths. The running time of the resulting single-source shortest-path algorithm is $O(n \log \log n \log \log \log n \log \log \log \log n \dots)$.

The idea to use r -divisions to speed up planar shortest paths is due to Greg Frederickson, who described an algorithm that runs in $O(n\sqrt{\log n})$ time in 1987. Ten years later, Monika Henzinger, Philip Klein, Satish Rao, and Sairam Subramanian described an algorithm that runs in $O(n)$ time. Both of these algorithms predate both good r -divisions and Klein's multiple-source shortest-path algorithm. Instead, these algorithms are variants of Dijkstra's algorithm that recursively relax pieces of a carefully chosen recursive separator decomposition, instead of relaxing individual edges. Unlike the $O(n \log \log n)$ algorithm I've described above, which relies on *good* r -divisions and planarity, the $O(n)$ -time algorithm of Henzinger et al. generalizes directly to any minor-closed family of graphs with bounded vertex degrees; the bounded-degree restriction was later removed by Tazari and Müller-Hannemann.

19.3 Beating Bellman-Ford: Nested Dissection

Depending on which textbook you read, Dijkstra's algorithm is either no longer correct or no longer efficient when some darts of the input graph have negative weight. In particular, if Σ contains negative darts, we can no longer solve the multiple-source shortest-path problem in $O(n \log n)$ time, because we don't know how to compute the initial shortest-path trees that quickly.¹

The standard shortest-paths algorithm for graphs with negative edges is *Bellman-Ford*, which runs in $O(mn)$ time; in particular, for simple planar graphs with n vertices, Bellman-Ford runs in $O(n^2)$ time. But just as we beat Dijkstra's algorithm, we can beat Bellman-Ford when the underlying graph is planar.

The following *generalized nested dissection* algorithm, proposed by Richard Lipton, Donald Rose, and Robert Tarjan in 1979, was one of the earliest applications of planar separators. (The original

¹If we are given the shortest-path tree rooted at any boundary vertex, the remainder of the parametric MSSP algorithm runs correctly, without modification, in $O(n \log n)$ time.

nested dissection algorithm, proposed by Alan George in 1973, applied only to square grid graphs.) Although their algorithm was originally designed for abstract planar *graphs* rather than planar *maps*, the presentation and analysis are simpler if we use good r -divisions, which require a planar embedding.

We are given a simple planar graph (sic) G with asymmetrically weighted darts, where some of the darts weights may be negative, and a source vertex s . At a very high level, our strategy is to delete one vertex of G using a *star-mesh transformation*, compute shortest-path distances from s to every remaining vertex of G , and finally compute the shortest-path distance from s to v . A star-mesh transformation adds or reweights edges between the neighbors of the deleted vertex v to restore shortest-path distances. Specifically, if there is no edge uw between two neighbors u and w , we add one with dart weights

$$\begin{aligned}\ell(u \rightarrow w) &\leftarrow \ell(u \rightarrow v) + \ell(v \rightarrow w) \\ \ell(w \rightarrow u) &\leftarrow \ell(w \rightarrow v) + \ell(v \rightarrow u);\end{aligned}$$

on the other hand, if edge uw already exists, we change its dart weights as follows:

$$\begin{aligned}\ell(u \rightarrow w) &\leftarrow \min \{\ell(u \rightarrow w), \ell(u \rightarrow v) + \ell(v \rightarrow w)\} \\ \ell(w \rightarrow u) &\leftarrow \min \{\ell(w \rightarrow u), \ell(w \rightarrow v) + \ell(v \rightarrow u)\}\end{aligned}$$

These changes preserve shortest-path distances from any vertex except v to any other vertex except v .² With the appropriate graph data structures, deleting v takes $O(\deg(v)^2)$ time.

After the Recursion Fairy computes distances from s to all other vertices, we can recover the distance from s to v by brute force in $O(\deg(v))$ time:

$$\text{dist}(v) \leftarrow \min_{u \rightarrow v} \{\text{dist}(u) + \ell(u \rightarrow v)\}$$

In both running times, $\deg(v)$ refers to the degree of v when v is eliminated, not in the original graph G . Different elimination orders can lead to different vertex degrees and therefore different running times. Star-mesh transformations do not preserve planarity, but this elimination process works for arbitrary graphs.

Lipton, Rose, and Tarjan recursively construct an elimination order for *planar* graphs as follows. Let S be a balanced separator that contains the source vertex s , and let A and B be a partition of the vertices $V \setminus S$ so that there is no edge directly from A to B . We first recursively eliminate all vertices in A , then recursively eliminate all vertices in B , and finally eliminate all vertices in S except s in arbitrary order. Opening up the recursive calls, the algorithm constructs a complete separator hierarchy, and then eliminates vertices using a postorder traversal of the decomposition tree.

If we only eliminate the interior vertices of each piece of a fixed r -division in this hierarchy, the result is precisely the dense-distance graph defined by Fakcharoenphol and Rao!

Suppose we build a *good* separator hierarchy using the algorithm of Klein, Mozes, and Sommer. Let $T_{\downarrow}(r)$ denote the worst-case time to eliminate all *interior* vertices in a piece with r vertices, and let $T_{\uparrow}(r)$ denote the time to compute distances to the interior vertices in a piece with r vertices after distances to the boundary vertices are known. The separation algorithm guarantees

²In particular, the original graph G contains a negative cycle if and only if, at after eliminating some subset of vertices, G contains an edge xy such that $\ell(x \rightarrow y) + \ell(y \rightarrow x) < 0$.

that each piece of size r has $O(\sqrt{r})$ boundary vertices and a separator of size $O(\sqrt{r})$. Thus, after recursively eliminating the interior vertices of the subpieces, each interior vertex on the separator has degree $O(\sqrt{r})$. It follows that the functions T_{\downarrow} and T_{\uparrow} satisfy the recurrences

$$\begin{aligned} T_{\downarrow}(r) &= T_{\downarrow}(r_L) + T_{\downarrow}(r_R) + O(r^{3/2}) \\ T_{\uparrow}(r) &= T_{\uparrow}(r_L) + T_{\uparrow}(r_R) + O(r) \end{aligned}$$

where $r_L + r_R < r$ and $\max\{r_L, r_R\} \leq 3r/4$.³ These recurrences solve to $T_{\downarrow}(r) = O(r^{3/2})$ and $T_{\uparrow}(r) = O(r \log r)$.

Theorem: *Given a planar graph G with weighted darts, some of which may be negative, and a source vertex s , we can compute the shortest path from s to every other vertex of G in $O(n^{3/2})$ time.*

19.4 Aside: Computing Spring Embeddings

Almost exactly the same nested-dissection algorithm can be used to solve any $n \times n$ system of linear equations whose support matrix is the adjacency matrix of a planar graph, in $O(n^{3/2})$ time. The only differences are that we use stress coefficients instead of lengths, addition instead of minimization, and multiplication instead of addition.

In particular, we can compute Tutte spring embeddings in $O(n^{3/2})$ time as follows. Recall that the input consists of a planar graph G , where every dart $u \rightarrow v$ has a positive weight $\lambda(u \rightarrow v)$. Without loss of generality, suppose $\sum_{x \rightarrow y} \lambda(x \rightarrow y) = 1$ for every vertex y . When we eliminate any vertex v , we adjust the stress coefficients between neighbors of v by setting

$$\lambda(u \rightarrow w) \leftarrow \lambda(u \rightarrow w) + \lambda(u \rightarrow v) \cdot \lambda(v \rightarrow w)$$

for every pair of neighbors u and w , and setting $\lambda(v \rightarrow w) \leftarrow 0$ for every neighbor w . (These adjustments preserve the invariant $\sum_{x \rightarrow y} \lambda(x \rightarrow y) = 1$ at every vertex y .) On the way back up, we can recover the position of vertex v using the equilibrium equation

$$p(v) \leftarrow \sum_{u \rightarrow v} \lambda(u \rightarrow v) \cdot p(u).$$

This elimination and recovery procedure is normally called *Gaussian elimination*.⁴ Precisely the same analysis as the previous theorem immediately implies:

Theorem: *Given a planar graph G with positively weighted darts, with one face identified with a convex polygon, we can compute the Tutte embedding of G in $O(n^{3/2})$ time.*

The running time of generalized nested dissection can be further improved to $O(n^{\omega/2})$ using a fast-matrix multiplication algorithm in place of eliminating separator vertices. On the other hand, Lipton, Rose, and Tarjan's algorithm cannot solve arbitrary planar linear systems over arbitrary fields; the underlying matrix must satisfy some subtle algebraic restrictions, and the field must

³I'm playing a little fast and loose here. Recall that the Klein-Mozes-Sommer separator hierarchy does not necessarily evenly partition vertices at every level of recursion, but only at every third level. So formalizing this analysis requires considering eight recursive subproblems, not just two.

⁴The formulation of optimal path problems as solving linear systems over $(\min, +)$ - and $(\max, +)$ -algebras dates back to at least the 1960s. For example, in 1971 Bernard Carré observed that different formulations of Bellman-Ford are $(\min, +)$ -variants of Jacobi and Gauss-Seidel iteration, and the Floyd-Warshall all-pairs shortest-path algorithm is a $(\min, +)$ -variant of Jordan elimination.

have characteristic zero (\mathbb{Q} , \mathbb{R} , or \mathbb{C}).⁵ In 2010 Noga Alon and Raphael Yuster described a more complex variant that avoids these restrictions.

19.5 Repricing

More recent planar shortest-path algorithms improve Lipton, Rose, and Tarjan's $O(n^{3/2})$ time bound to near-linear. One of the key components of these faster algorithms is a standard *repricing* technique first⁶ proposed independently for minimum-cost flows by Nobuaki Tomizawa in 1971, and Jack Edmonds and Richard Karp in 1972, but first applied specifically to shortest paths by Donald Johnson in 1973.

Suppose each vertex v has an associate *price* $\pi(v)$. We can assign a new edge-length function ℓ' as follows:

$$\ell'(u \rightarrow v) := \pi(u) + \ell(u \rightarrow v) - \pi(v).$$

Then for any path $s \rightsquigarrow t$ in G , we have a telescoping sum

$$\ell'(s \rightsquigarrow t) := \pi(s) + \ell(s \rightsquigarrow t) - \pi(t).$$

Because the length of every path from s to t changes by the same amount, the shortest paths from s to t with respect to ℓ and ℓ' coincide! Thus, if we can find a pricing function that makes all new edge lengths $\ell'(u \rightarrow v)$ non-negative, we can compute shortest-path distances with respect to ℓ' using Dijkstra's algorithm in $O(n \log n)$ time, or its more efficient planar replacement in $O(n \log \log n)$ time, and then recover distances with respect to ℓ as follows:

$$\text{dist}(s, t) := \text{dist}'(s, t) - \pi(s) + \pi(t).$$

For example, suppose $\pi(v) = \text{dist}(s, v)$ for some fixed source vertex s , where dist denotes shortest-path distance with respect to ℓ . Then we have

$$\ell'(u \rightarrow v) := \text{dist}(s, u) + \ell(u \rightarrow v) - \text{dist}(s, v).$$

Ford's formulation of shortest paths implies that the expression on the right is non-negative. Thus, once we've computed shortest paths from *one* source, we can efficiently compute shortest paths from any other source in near-linear time.

19.6 Nested Dissection Revisited

Now let's consider a different shortest-path algorithm based on nested dissection, based on a 1983 algorithm of Kurt Mehlhorn and Bernd Schmidt, but with some optimizations proposed by later authors.

As before, we are given a simple n -vertex planar triangulation Σ with asymmetrically (and possibly negatively) weighted darts and a source vertex s , and we want to compute the shortest-path distance from s to every other vertex in Σ . To simplify presentation, I'll assume that no cycle in Σ has negative total length, so that shortest-path distances are well-defined.

⁵Specifically, Lipton, Rose, and Tarjan's elimination algorithm assumes that when a row is eliminated, its diagonal entry is nonzero. (Recall that the algorithm chooses the elimination order before doing any elimination.) This condition is automatically satisfied for symmetric positive-definition linear systems over \mathbb{R} , but is not satisfied in general.

⁶At least, first *explicitly* proposed. Arguably the repricing technique is already implicit in Jacobi's mid-19th-century description of the "Hungarian" algorithm for the assignment problem.

I will use the notation $\text{dist}_P(X, Y)$ to denote the set of all shortest-path distances in subgraph P from vertices in X to vertices in Y ; our goal is to compute $\text{dist}(s, \Sigma)$.

The algorithm starts by computing a balanced cycle separator S for Σ . Let A and B be the pieces of Σ obtained by slicing along S , and let r be any vertex in S . The algorithm has five stages.

1. Recursively compute $\text{dist}_A(r, A)$ and $\text{dist}_B(r, B)$. How the Recursion Fairy does this is none of your business.
2. Compute $\text{dist}_A(S, S)$ and $\text{dist}_B(S, S)$. Because S is a simple cycle, we can compute all separator-to-separator distances within each piece time using either of our multiple-source shortest-path algorithms. There are $O(n)$ vertices in each piece, and we want to compute $k = |S|^2 = O(n)$ boundary-to-boundary distances within each piece, so our MSSP algorithms run in $O(n \log n + k \log n) = O(n \log n)$ time.⁷
3. Compute $\text{dist}_\Sigma(r, S)$. Build a complete directed graph $\hat{\Sigma}$ with vertices S , where each dart $u \rightarrow v$ has length $\min\{\text{dist}_A(u, v), \text{dist}_B(u, v)\}$. The graph $\hat{\Sigma}$ has $O(\sqrt{n})$ vertices and $O(n)$ edges, so we can compute $\text{dist}_\Sigma(r, S) = \text{dist}_{\hat{\Sigma}}(r, S)$ using Bellman-Ford in $O(r^{3/2})$ time.
4. Compute $\text{dist}_\Sigma(r, \Sigma)$ using Johnson's repricing trick. We construct a graph H from the disjoint union $A \sqcup B$ as follows. First we add an artificial source vertex \hat{r} . Then for each separator vertex $v \in S$, we add directed edges $\hat{r} \rightarrow v_A$ and $\hat{r} \rightarrow v_B$ to the copies of v in A and B , both with length $\text{dist}_\Sigma(r, v)$, which we computed in step 3. For any target vertex t , we have $\text{dist}_\Sigma(r, t) = \text{dist}_H(\hat{r}, t)$. Now we define prices for the vertices of H using the distances we computed in step 2:

$$\pi(v) = \begin{cases} \text{dist}_A(r, v) & \text{if } v \text{ is a vertex of } A \\ \text{dist}_B(r, v) & \text{if } v \text{ is a vertex of } B \\ \infty & \text{if } v = \hat{r}. \end{cases}$$

Here ∞ is a symbolic placeholder for some sufficiently large value.⁸ Straightforward calculation implies that all darts in H have non-negative repriced length. H is a planar graph with $O(n)$ vertices and edges, so we can compute shortest paths in H in $O(n \log n)$ time via Dijkstra's algorithm, or in $O(n \log \log n)$ time using our faster algorithm based on r -divisions.⁹

5. Finally, compute $\text{dist}_\Sigma(s, \Sigma)$ using Johnson's repricing trick, this time using the prices $\pi(v) = \text{dist}_\Sigma(r, v)$. Again, it is not hard to verify that every dart in Σ has non-negative length after repricing. Thus, we can compute $\text{dist}_\Sigma(s, \Sigma)$ in $O(n \log n)$ time using Dijkstra's algorithm, or in $O(n \log \log n)$ time using our faster algorithm based on r -divisions.

The overall running time $O(n^{3/2})$ is dominated by the application of Bellman-Ford in stage 3. Any further improvements require speeding up Bellman-Ford, which is exactly what we're going to do next!

⁷Mehlhorn and Schmidt's algorithm reprices the vertices in each piece, and then runs Dijkstra's algorithm from each separator vertex, in $O(n^{3/2} \log n)$ total time.

⁸If you're uncomfortable with symbolic infinities, it suffices to set

$$\pi(\hat{r}) = \max \{ \text{dist}_A(r, u) - \text{dist}_\Sigma(r, u), \text{dist}_B(r, u) - \text{dist}_\Sigma(r, u) \mid u \in S \}$$

⁹Mehlhorn and Schmidt compute $\text{dist}_\Sigma(r, \Sigma)$ by brute force in $O(n^{3/2})$ time, by observing that $\text{dist}_\Sigma(r, v) = \min_{u \in S} \{ \text{dist}_\Sigma(r, u) + \text{dist}_A(u, v) \}$ for every vertex $v \in A$, and similarly for B .

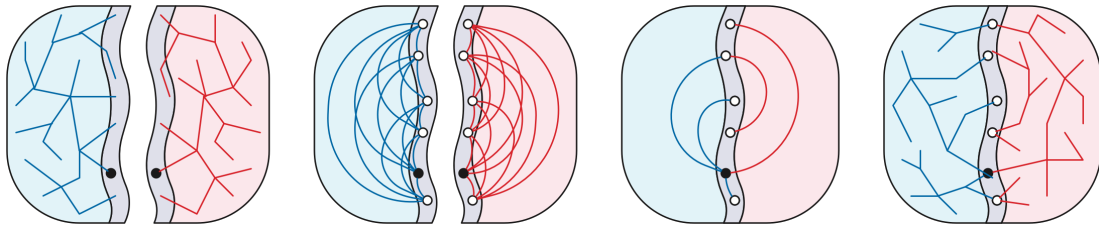


Figure 19.1: Computing planar shortest paths by nested dissection

19.7 Monge arrays and SMAWK

A two-dimensional array M is *Monge* if

$$M[i, j] + M[i', j'] \leq M[i, j'] + M[i', j]$$

for all array indices $i < i'$ and $j < j'$. Monge arrays are named after the French geometer and civil engineer Gaspard Monge, who described an equivalent geometric condition in his 1781 *Mémoire sur la Théorie des Déblais et des Remblais*. Monge observed that if A, B, b, a are the vertices of a convex quadrilateral in cyclic order, the triangle inequality implies that $|Aa| + |Bb| < |Ab| + |aB|$.

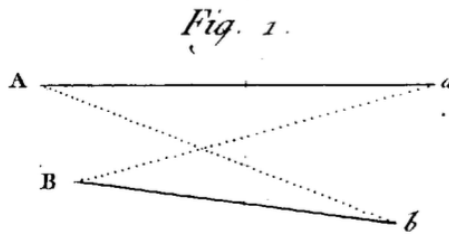


Figure 19.2: Monge's observation: Non-crossing paths are shorter

Monge Structure Lemma: *The following arrays are Monge:*

- (a) Any array with constant rows.
- (b) Any array with constant columns.
- (c) Any array that is all 0s except for an upper-right rectangular block of 1s.
- (d) Any array that is all 0s except for an lower-left rectangular block of 1s.
- (e) Any positive multiple of any Monge array.
- (f) The sum of any two Monge arrays.
- (g) The transpose of any Monge array.

In 1987, Alok Aggarwal, Maria Klawe, Shlomo Moran, Peter Shor, and Robert Wilber described an elegant recursive algorithm that finds the minimum element in every row of an $n \times n$ Monge array in $O(n)$ time, now usually called the *SMAWK* algorithm after the suitably-permuted initials of its authors. In 1990, Maria Klawe and Daniel Kleitman described an extension to the SMAWK algorithm that finds row-minima in *partial* Monge matrices, where some entries are undefined, but the Monge inequality holds whenever all four entries are defined. Klawe and Kleitman's algorithm runs in $O(n \alpha(n))$ time, where $\alpha(n)$ is the slowly-growing inverse Ackermann function.

Very recently, Timothy Chan described a randomized algorithm that find all row-minima in a staircase-Monge matrix in $O(n)$ expected time.

A description of these algorithms is beyond the scope of this class, but you can find a complete description and analysis of the basic SMAWK algorithm in my algorithms lecture notes.

19.8 Planar distance matrices are (almost) Monge

In the same 2001 paper where they defined dense distance graphs, Fakcharoenphol and Rao described how to use SMAWK to compute shortest paths in planar maps more quickly.

Let Σ be a planar map with weighted edges. Let s_1, s_2, \dots, s_k be the sequence of vertices on the boundary of the outer face of Σ , in cyclic order. (If the outer face boundary is not a simple cycle, the same vertex may appear multiple times in this list.) Let D be the $k \times k$ array where $D[i, j] = \text{dist}_\Sigma(s_i, s_j)$.

Lemma: *The distance array D can be decomposed into two partial Monge matrices.*

Proof: Fix four vertices u, v, w, x in cyclic order around the boundary of the outer face of Σ .

The Jordan curve theorem implies that the shortest paths from u to w and from v to x must cross; let z be any vertex in the intersection of these two shortest paths. The triangle inequality implies

$$\begin{aligned} \text{dist}(u, w) + \text{dist}(v, x) &= (\text{dist}(u, z) + \text{dist}(z, w)) + (\text{dist}(v, z) + \text{dist}(z, x)) \\ &= (\text{dist}(u, z) + \text{dist}(z, x)) + (\text{dist}(v, z) + \text{dist}(z, w)) \\ &\leq \text{dist}(u, x) + \text{dist}(v, w) \end{aligned}$$

(omitting subscript Σ 's everywhere).

It follows that the Monge inequality

$$M[i, j] + M[i', j'] \leq M[i, j'] + M[i', j];$$

holds for any indices i, i', j, j' that appear in that cyclic order (possibly with ties) modulo k . In particular, the Monge inequality holds whenever $i \leq i' \leq j \leq j'$, which implies that the portion of M on or below the main diagonal is Monge. Symmetrically, the portion of M on or above the main diagonal is Monge. These two partial Monge matrices cover M . \square

Perhaps a better way to express this analysis is that the $k \times 2k$ partial array defined by

$$D[i, j] := \begin{cases} \text{dist}_G(s_i, s_{j \bmod k}) & \text{if } i \leq j \leq i + k \\ \text{undefined} & \text{otherwise} \end{cases}$$

is a single partial Monge array.

19.9 Beating Nested Dissection

Now recall that the third phase of our nested-dissection algorithm computes the distances $\text{dist}_\Sigma(r, S)$ by running Bellman-Ford on a weighted directed clique \hat{S} over the vertices in S . Let s_1, s_2, \dots, s_k denote the vertices of the cycle separator S , in order around the cycle. It will be

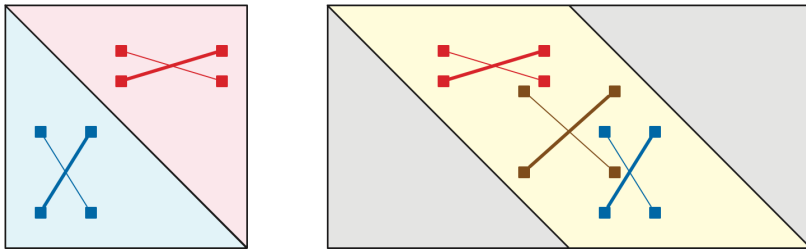


Figure 19.3: For any planar map, the array of boundary-to-boundary distances both splits into two partial Monge arrays (left) and unrolls into a single partial Monge array (right)

more convenient to think of \hat{S} as the overlay of two directed cliques \hat{S}_A and \hat{S}_B , in which each edge $s_i \rightarrow s_j$ has lengths $\ell_A(s_i \rightarrow s_j) = \text{dist}_A(s_i, s_j)$ and $\ell_B(s_i \rightarrow s_j) = \text{dist}_B(s_i, s_j)$, respectively.

The Bellman-Ford algorithm has the following simple structure. After initializing $\text{dist}[r] = 0$ and $\text{dist}[v] = \infty$ for all $v \neq r$, the algorithm repeatedly identifies and then relaxes all tense edges in \hat{S} . The algorithm terminates after $O(k)$ relaxation phases, where $k = O(\sqrt{n})$ is the number of vertices in S .

Here is some pseudo-Python for a single relaxation phase:

```
for i in range(k):
    for j in range(k):
        if dist[j] < dist[i] + l[i,j]
            dist[j] = dist[i] + l[i,j]
```

As written, this block of code runs in $O(k^2)$ time. Because the order that we scan the edges doesn't matter, let's first scan all edges in \hat{S}_A and then all edges in \hat{S}_B :

```
for i in range(k):
    for j in range(k):
        if dist[j] < dist[i] + lA[i,j]
            dist[j] = dist[i] + lA[i,j]
for i in range(k):
    for j in range(k):
        if dist[j] < dist[i] + lB[i,j]
            dist[j] = dist[i] + lB[i,j]
```

Now I'm going to do something a little weird to the first block of code. For each vertex v , I'll first figure out the minimum value of $\text{dist}[i] + lA[i,j]$ and only compare that minimum value to $\text{dist}[j]$ at the end.

```
for j in range(k):
    bestcost = math.inf
    for i in range(k):
        if dist[i] + lA[i,j] < bestcost:
            best[j] = i
            bestcost = dist[i] + lA[i,j]
for j in range(k):
    if dist[j] < bestcost:
        dist[j] = bestcost
```

The first (outer) for-loop is choosing the minimum element in every *column* of a $k \times k$ matrix M , where

$$M[i, j] := \text{dist}(s_i) + \text{dist}_A(s_i, s_j)$$

M is the sum of a matrix with constant columns (which is Monge) and the boundary-to-boundary distance matrix in A . Thus, M can be split into two partial Monge arrays, and therefore so can its transpose. It follows that we can compute $\text{best}[j]$ (and therefore $\text{dist}[j]$) for all j in $O(k\alpha(k))$ time using Klawe and Kleitman's algorithm, or in $O(k)$ expected time using Chan's algorithm.

The same modification relaxes every tense edge in \hat{S}_B in $O(k\alpha(k))$ time, or $O(k)$ expected time.

With this optimization in place, Bellman-Ford computes all shortest-path distances $\text{dist}_\Sigma(r, S)$ in $O(k) \cdot O(k\alpha(k)) = O(n\alpha(n))$ time, or in $O(n)$ expected time. This accelerated version of Bellman-Ford is now commonly called “FR-Bellman-Ford” after Fakcharoenphol and Rao, who described a similar but slightly slower reduction to the original SMAWK algorithm.[`fr]

With all these improvements in place, we obtain a shortest-path algorithm described by Philip Klein, Shay Mozes, and Oren Weimann in 2009.

1. Recursively compute $\text{dist}_A(r, A)$ and $\text{dist}_B(r, B)$
2. Compute $\text{dist}_A(S, S)$ and $\text{dist}_B(S, S)$ using MSSP in $O(n \log n)$ time.
3. Compute $\text{dist}_\Sigma(r, S)$ using FR-Bellman-Ford in $O(n\alpha(n))$ time.
4. Compute $\text{dist}_\Sigma(r, \Sigma)$ using reweighting and r -divisions in $O(n \log \log n)$ time.
5. Compute $\text{dist}_\Sigma(s, \Sigma)$ using reweighting and r -divisions in $O(n \log \log n)$ time.

The overall running time satisfies the recurrence

$$T(n) \leq T(n_A) + T(n_B) + O(n \log n)$$

where (after a suitable domain transformation) $n_A + n_B = n$ and $\max\{n_A, n_B\} \leq 3n/4$. We conclude that the algorithm runs in $O(n \log^2 n)$ time; our invocation of MSSP in stage 2 is (just barely) the bottleneck.

In 2010, Shay Mozes and Christian Wulff-Nilsen improved this algorithm even further by using a good r -division at each level of recursion (with $r \approx n/\log n$) instead of just one separator cycle; their improved algorithm runs in $O(n \log^2 n/\log \log n)$. I will describe their improvement at the end of the next lecture note.

19.10 References

1. Alok Aggarwal, Maria M. Klawe, Shlomo Moran, Peter Shor, and Robert Wilber. Geometric applications of a matrix-searching algorithm. *Algorithmica* 2(1–4):195–208, 1987. The SMAWK algorithm.
2. Noga Alon and Raphael Yuster. Solving linear systems through nested dissection. *Proc. 51st IEEE Symp. Found. Comput. Sci.*, 225–234, 2010.
3. Bernard A. Carré. An algebra for network routing problems. *IMA J. Appl. Math.* 7(3):273–294, 1971.
4. Timothy M. Chan. (Near-)linear-time randomized algorithms for row minima in Monge partial matrices and related problems. *Proc. 32nd Ann. ACM-SIAM Symp. Discrete Algorithms*, 1465–1482, 2021.

5. Jack Edmonds and Richard M. Karp. Theoretical improvements in algorithmic efficiency of network flow problems. *J. Assoc. Comput. Mach.* 19(2):248–264, 1972.
6. Jittat Fakcharoenphol and Satish Rao. Planar graphs, negative weight edges, shortest paths, and near linear time. *J. Comput. Syst. Sci.* 72(5):868–889, 2006.
7. Greg N. Frederickson. Fast algorithms for shortest paths in planar graphs with applications. *SIAM J. Comput.* 16(8):1004–1004, 1987.
8. Alan George. Nested dissection of a regular finite element mesh. *SIAM J. Numer. Anal.* 10(2):345–363, 1973.
9. Monika R. Henzinger, Philip Klein, Satish Rao, and Sairam Subramanian. Faster shortest-path algorithms for planar graphs. *J. Comput. Syst. Sci.* 55(1):3–23, 1997.
10. Carl Gustav Jacob Jacobi. De aequationum differentialium systemate non normali ad formam normalem revocando (Ex Ill. C. G. J. Jacobi manuscriptis posthumis in medium protulit A. Clebsch). *C. G. J. Jacobi's gesammelte Werke, fünfter Band*, 485–513, 1890. Bruck und Verlag von Georg Reimer. English translation in [8].
11. Carl Gustav Jacob Jacobi and François Ollivier (translator). The reduction to normal form of a non-normal system of differential equations. *Appl. Algebra Eng. Commun. Comput.* 20(1):33–64, 2009. English translation of [7].
12. Donald B. Johnson. Efficient algorithms for shortest paths in sparse networks. *J. Assoc. Comput. Mach.* 24(1):1–13, 1977.
13. Maria M. Klawe and Daniel J. Kleitman. An almost linear time algorithm for generalized matrix searching. *SIAM J. Discrete Math.* 3(1):81–97, 1990.
14. Philip Klein, Shay Mozes, and Oren Weimann. Shortest paths in directed planar graphs with negative lengths: A linear-space $O(n \log^2 n)$ -time algorithm. *ACM Trans. Algorithms* 6(2):30:1–30:18, 2010.
15. Richard J. Lipton, Donald J. Rose, and Robert Endre Tarjan. Generalized nested dissection. *SIAM J. Numer. Anal.* 16:346–358, 1979.
16. Kurt Mehlhorn and Bernd H. Schmidt. A single shortest path algorithm for graphs with separators. *Proc. 4th Int. Conf. Foundations of Computation Theory*, 302–309, 1983. Lecture Notes Comput. Sci. 158, Springer.
17. Gaspard Monge. Mémoire sur la théorie des déblais et des remblais. *Histoire de l'Académie royale des sciences* 666–705, 1781.
18. Shay Mozes and Christian Wulff-Nilsen. Shortest paths in planar graphs with real lengths in $O(n \log^2 n / \log \log n)$ time. *Proc. 18th Ann. Europ. Symp. Algorithms*, 206–217, 2010. Lecture Notes Comput. Sci. 6347, Springer-Verlag. arXiv:0911.4963.
19. Siamak Tazari and Matthias Müller-Hannemann. Shortest paths in linear time on minor-closed graph classes, with an application to Steiner tree approximation. *Discrete Appl. Math.* 157(4):673–684, 2009.
20. Nobuaki Tomizawa. On some techniques useful for solution of transportation network problems. *Networks* 1:173–194, 1971.

19.11 Aptly Named Sir Not

- Shortest paths in $O(n)$ time.

Chapter 20

Minimum Cuts^β

Let G be an arbitrary graph, and let s and t be two vertices of G . An (s, t) -cut (or more formally, an (s, t) -edge-cut) is a subset X of the edges of G that intersects every path from s to t in G . A *minimum* (s, t) -cut is an (s, t) -cut of minimum size, or of minimum total weight if the edges of G are weighted. (In this context, edge weights are normally called *capacities*.)

The fastest method to compute minimum (s, t) -cuts in *arbitrary* graphs is to compute a maximum (s, t) -flow and then exploit the classical proof of the maxflow-mincut theorem. In undirected *planar* graphs, however, this dependency is reversed; the fastest method to compute maximum flows actually computes minimum cuts first.

20.1 Duality: Shortest essential cycle

Let Σ be an undirected planar *map*, each of whose edges e has a non-negative capacity $c(e)$, and let s and t be vertices of Σ . The first step in our fast minimum-cut algorithm is to view the problem through the lens of duality. It is helpful to think of the source vertex s and the target vertex t as *punctures* or *obstacles* — points that are missing from the plane — and similarly to think of the corresponding faces s^* and t^* as *holes* in the dual map Σ^* . In other words, we should think of the dual map Σ^* as a decomposition of the *annulus* $A = \mathbb{R}^2 \setminus (s^* \cup t^*)$ rather than a map on the plane or a disk. Without loss of generality, assume that t^* is the outer face of Σ^* .

A simple cycle γ in Σ^* is *essential* if it satisfies any of the following equivalent conditions:

- γ separates s^* from t^* .
- γ has winding number ± 1 around s^* .
- γ is homotopic in A to the boundary of s^* .
- γ is homotopic in A to the boundary of t^* .

Each edge e^* in the dual map Σ^* has a *cost* or *length* $c^*(e^*)$ equal to the capacity of the corresponding primal edge e . Whitney's duality between simple cycles in Σ and minimal cuts (bonds) in Σ^* immediately implies the following:

Lemma: *A subset X of edges is a minimum (s, t) -cut in Σ if and only if the corresponding set X^* of dual edges is a minimum-cost essential cycle in Σ^* .*

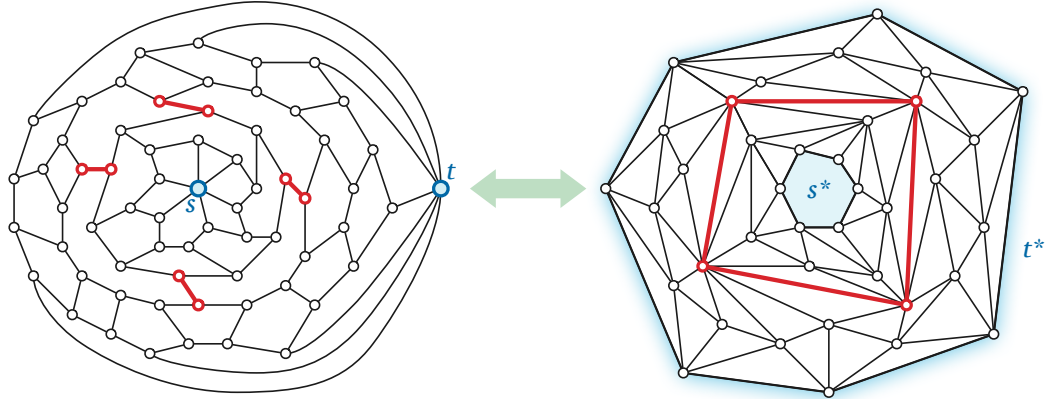


Figure 20.1: A minimum (s, t) -cut in a planar graph is dual to a shortest essential cycle in the annular dual map.

20.2 Crossing at most once

Now let π be a shortest path in Σ^* from any vertex of s^* to any vertex of t^* . We can measure the winding number of any directed cycle γ in Σ^* by counting the number of times γ crosses π in either direction. We have to define “crossing” carefully here, because γ and π could share edges.

Suppose $\pi = p_0 \rightarrow p_1 \rightarrow \dots \rightarrow p_k$, where p_0 lies on s^* and p_k lies on t^* . To simplify the following definition, we add two “ghost” darts $p_{-1} \rightarrow p_0$ and $p_k \rightarrow p_{k+1}$, where p_{-1} lies inside s^* and p_{k+1} lies inside t^* . We say that a dart $q \rightarrow p_i$ enters π from the left (resp. from the right) if the darts $p_{i-1} \rightarrow p_i$, $q \rightarrow p_i$, and $p_{i+1} \rightarrow p_i$ are ordered clockwise (resp. counterclockwise) around p_i . Symmetrically, we say that a dart leaves π to the left (resp. to the right) if its reversal enters π from the left (resp. from the right). The same dart can leave π to the right and enter π to the left, or vice versa.

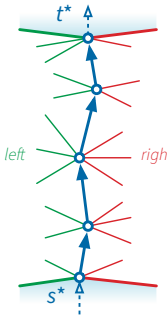


Figure 20.2: Edges incident to both sides of π .

A *positive crossing* between π and γ is a subpath of γ that starts with a dart entering π from the right and ends with a dart leaving π to the left, and a *negative crossing* is defined similarly. Intuitively, for purposes of defining crossings, we are shifting the path π very slightly to the left, so that it intersects the edges of Σ^* transversely. It follows that the winding number $\text{wind}(\gamma, s^*)$ is the number of darts in γ that leave π to the left, minus the number of darts in γ that enter π from the left.

Crossing Lemma [Itai and Shiloach (1979)]: *The shortest essential cycle in Σ^* crosses π exactly once.*

Proof: We follow the same intuition that we used for shortest homotopic paths in the plane. Let γ be any essential cycle in Σ^* , directed so that $\text{wind}(\gamma, s^*) = 1$, that crosses π more

than once. Then somewhere γ must have been a negative crossing followed immediately by a positive crossing. It follows that γ has a subpath $p_i \rightarrow q \rightarrow \dots \rightarrow r \rightarrow p_j$, where $p_i \rightarrow q$ leaves π to the right, $r \rightarrow p_j$ enters π from the right. Let γ' be the cycle obtained from γ by replacing this subpath with the subpath of π from p_i to p_j . Because π is a shortest path, γ' must be shorter than γ . We conclude that γ' is not the *shortest* essential cycle in Σ^* . \square

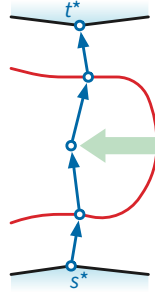


Figure 20.3: Any essential cycle that crosses π more than once can be shortened.

20.3 Slicing along a path

Now let $\Delta := \Sigma^* \setminus \pi$ denote the planar map obtained by *slicing* the annular map Σ^* along path π . The slicing operation replaces π with two copies π^+ and π^- . Then for every vertex p_i of π , all edges incident to p_i on the left are redirected to p_i^+ , and all edges incident to p_i on the right are redirected to p_i^- . The channel between two paths π^+ and π^- joins s^* and t^* into a single outer face. Thus, we should think of Δ as being embedded on a disk. Every face of Σ^* except s^* and t^* appears as a face in Δ .

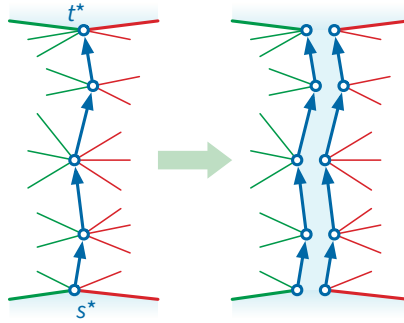


Figure 20.4: Slicing along π .

For any index i , let σ_i denote the shortest path in Δ from p_i^+ to p_i^- . The shortest essential cycle γ in Σ^* appears in Δ as one of the shortest paths σ_i . Thus, to compute the minimum (s, t) -cut in our original planar map Σ , it suffices to compute the length of *every* shortest path σ_i in Δ .

20.4 Algorithms

The simplest way to compute these k shortest-path distances is to run Dijkstra's algorithm at each vertex p_i^+ . Assuming π has k edges, so there are $k + 1$ terminal pairs p_i^\pm , this algorithm runs in $O(kn \log n)$ time, which is $O(n^2 \log n)$ time in the worst case. We can reduce the running time

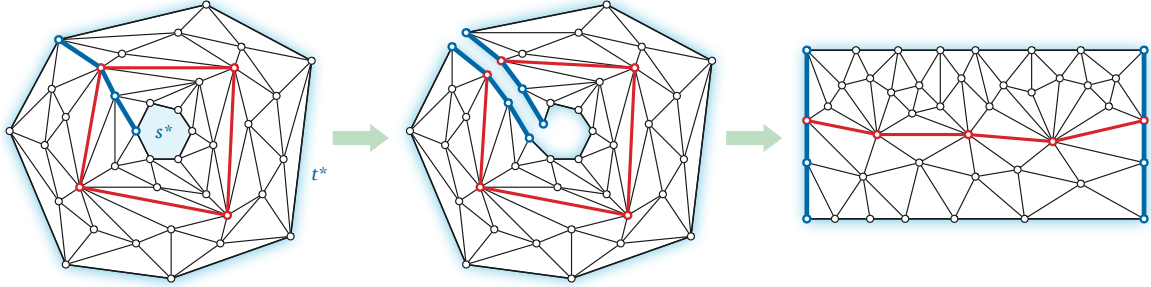


Figure 20.5: Slicing along π transforms the shortest essential cycle into a shortest path between clones of some vertex of π .

to $O(kn \log \log n)$ using the faster shortest-path algorithm we described in the previous lecture note, or even to $O(kn)$ using a linear-time shortest-path algorithm.

Alternatively, we can compute all k of these shortest paths using a multiple-source shortest-paths algorithm. The parametric MSSP algorithms of Klein and Cabello et al. both require $O(n \log n)$ time, which is faster in the worst case than $O(kn)$, but slower when k is small. In particular, even when $k = 2$, that algorithm could require $\Omega(n)$ pivots. The more recent recursive contraction algorithm runs in $O(n \log n \log k)$ time if we use Dijkstra's algorithm to compute shortest paths, or in $O(n \log k)$ time if we use a linear-time shortest-path algorithm.

An older and simpler divide-and-conquer algorithm, proposed by John Reif in 1983, exactly matches the recursive contraction MSSP algorithm. Reif's algorithm computes the median shortest path σ_m , where $m = \lfloor k/2 \rfloor$, and then recurses in each component of the sliced map $\Delta \setminus \sigma_m$. One of these components contains the terminal pairs $p_0^\pm, p_1^\pm, \dots, p_m^\pm$; the other contains the terminal pairs $p_m^\pm, p_{m+1}^\pm, \dots, p_k^\pm$.

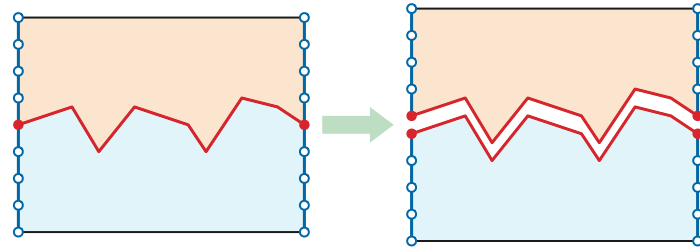


Figure 20.6: Reif's algorithm: Slice along the median shortest path and recurse.

Reif's algorithm falls back on Dijkstra's algorithm in two base cases. First, if $k \leq 2$, we can obviously compute each of the k shortest paths directly. A more subtle base case happens when the “floor” and “ceiling” paths collide. Let α denote the boundary path from p_0^+ to p_0^- , and let β denote the boundary path from p_k^+ to p_k^- . If α and β share a vertex x , then for every index i we have $\text{dist}(p_i^+, p_i^-) = \text{dist}(p_i^+, x) + \text{dist}(x, p_i^-)$; thus, instead of recursing, we can compute all k shortest-path distances by computing a single shortest-path tree rooted at x . (This second base case is not necessary for the correctness of Reif's algorithm, but it is necessary for efficiency.)

Let $T(n, k)$ denote the running time of Reif's algorithm, where $k + 1$ is the number of terminal pairs and n is the total number of vertices in the map Δ . This function obeys the recurrence

$$T(n, k) = T(n_1, \lfloor k/2 \rfloor) + T(n_2, \lceil k/2 \rceil) + O(n \log n).$$

where n_1 and n_2 are the number of vertices in the two components of $\Delta \setminus \sigma_m$. The second base

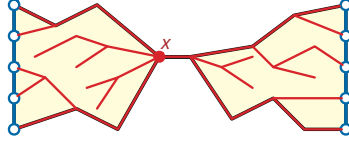


Figure 20.7: Base case of Reif's algorithm.

case ensures that each vertex and edge of Δ appears in at most $O(1)$ subproblems at any level of the recursion tree.¹ Thus, the total work at any level of recursion is $O(n \log n)$. The recursion tree has depth at most $O(\log k)$, so the overall algorithm runs in $O(n \log n \log k)$ time.

If we use a linear-time shortest-path algorithm instead of Dijkstra, the running time improves to $O(n \log k)$. This improvement was first described by Greg Frederickson in 1987, as one of the earliest applications of r -divisions.

20.5 Faster Shortest Paths with Negative Lengths

[[[This is still really sketchy!]]]

In the previous lecture note, we described a 2009 algorithm by Klein, Mozes, and Weimann to compute shortest paths in directed planar maps, possibly with negative dart lengths, in $O(n \log^2 n)$ time. In 2010, Shay Mozes and Christian Wulff-Nilsen improved this algorithm even further by using a good r -division at each level of recursion (with $r \approx n / \log n$) instead of just one separator cycle; their improved algorithm runs in $O(n \log^2 n / \log \log n)$.

Recall the high-level description of the Klein-Mozes-Weimann algorithm:

0. Split the map Σ into two smaller maps A and B along a single cycle separator S .
1. Recursively compute $\text{dist}_A(r, A)$ and $\text{dist}_B(r, B)$
2. Compute $\text{dist}_A(S, S)$ and $\text{dist}_B(S, S)$ using MSSP in $O(n \log n)$ time.
3. Compute $\text{dist}_{\Sigma}(r, S)$ using FR-Bellman-Ford in $O(n\alpha(n))$ time.
4. Compute $\text{dist}_{\Sigma}(r, \Sigma)$ using reweighting and r -divisions in $O(n \log \log n)$ time.
5. Compute $\text{dist}_{\Sigma}(s, \Sigma)$ using reweighting and r -divisions in $O(n \log \log n)$ time.

Steps 1, 4, and 5 of Mozes and Wulff-Nilsen's faster algorithm are identical. In step 2, the only minor difference is that we need to run MSSP around the boundary of each hole of each piece, instead of just once around the sole cycle separator. The total time for each piece is $O(r \log r)$, so the total time for this step across the entire r -division is $O(n/r) \cdot O(r \log r) = O(n \log r)$.

The only major change to the algorithm is in step 3; we need to modify FR-Bellman-Ford to deal with holes in each piece of the r -division.

In step 2, we compute all boundary-to-boundary distances within each piece of the r -division using MSSP. Specifically, within each piece P , we run MSSP around each of the $O(1)$ boundary cycles of P . The total time for each piece is $O(r \log r)$, so the total time for this step across the entire r -division is $O(n/r) \cdot O(r \log r) = O(n \log r)$.

Modifying step 3 is more interesting. Recall that a good r -division \mathcal{R} breaks Σ into $O(n/r)$ pieces, each with $O(r)$ vertices, $O(\sqrt{r})$ boundary vertices, and $O(1)$ holes; thus, overall, \mathcal{R} has $O(n/\sqrt{r})$

¹Without the second base case, it is possible for a constant fraction of the vertices to appear in a constant fraction of the recursive subproblems, leading to a running time of $O(kn \log n)$.

boundary vertices, organized into $O(n/r)$ cycles. We construct a complete directed multigraph \hat{R} over the boundary vertices of the r -division, with an edge $u \rightarrow v$ with weight $\text{dist}_P(u, v)$ for every piece P containing both u and v .

Bellman-Ford computes shortest-path distances in \hat{R} in $O(n/\sqrt{r})$ phases; in each phase, we find and relax all tense edges. Our modification of FR-Bellman-Ford breaks each relaxation phase into subphases:

```

for each piece P:
    for each boundary cycle S of P:
        for each boundary cycle T of P:
            relax every edge within P from S to T

```

We already described how to relax every edge in P from a boundary cycle *to itself* in $O(k\alpha(k))$ time (or $O(k)$ expected time). It remains to show how to relax all edges from one boundary cycle S to a different boundary cycle T .

Without loss of generality, let's assume that S and T are the only two boundary cycles in P ; we'll treat any other boundary cycles as faces of P . Thus, P is a map of an *annulus*. Let s_1, s_2, \dots, s_k and t_1, t_2, \dots, t_l denote the sequences of vertices of S and T , respectively.

Let π be the shortest path in P from s_1 to t_1 , and let $\Delta = P \setminus \pi$ be the map obtained by slicing Σ along the path π . As before, the slicing operation duplicates the path π and merges the faces S and T into a single outer face.

Let Δ' be a duplicate of Δ , and let Δ^2 denote the map obtained by gluing the “right” copy of π in Δ to the “left” copy of π in Δ' .

Lemma: *For all indices i and j , we have*

$$\text{dist}_P(s_i, t_j) = \min \{ \text{dist}_{\Delta^2}(s_i, t_j), \text{dist}_{\Delta^2}(s'_i, t_j), \text{dist}_{\Delta^2}(a_i, b'_j) \}$$

[[[This is already claimed, but without proof, in the next lecture note.]]]

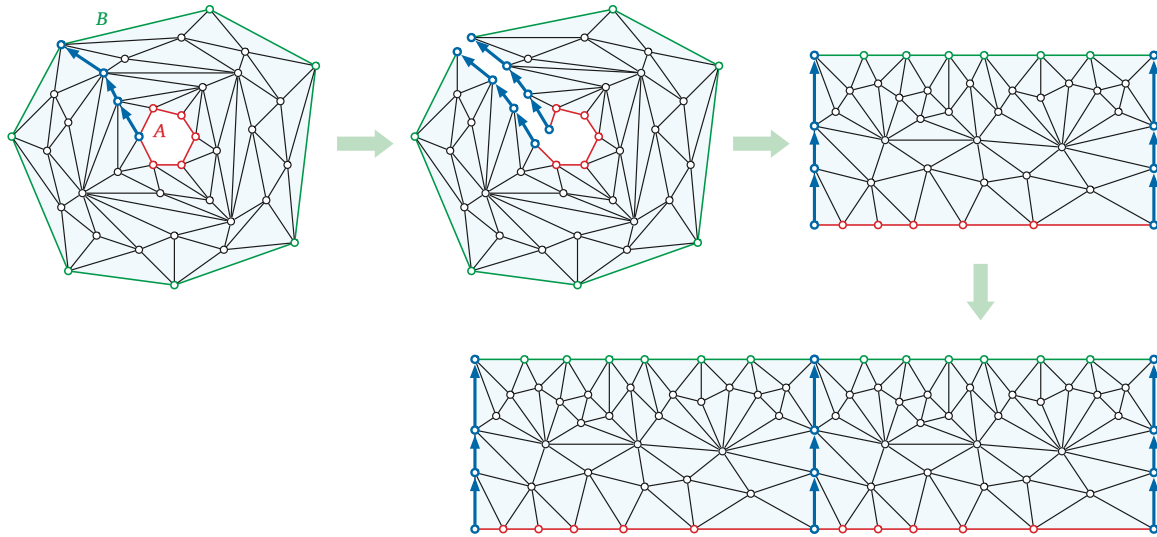


Figure 20.8: Reducing the boundary-to-boundary distance array of an annulus to a Monge array; compare with Figure 5.

The matrix of distances from the “top edge” of Δ^2 to the “bottom edge” of Δ^2 is Monge! So we can relax all the edges from A to B in $O(k + l)$ time with one invocation of SMAWK.

Suppose P has $h = O(1)$ holes, with k_1, k_2, \dots, k_h boundary vertices; recall that $k = \sum_i k_i = O(\sqrt{r})$. Then the total time to relax all boundary-to-boundary edges in P is

$$\sum_{i=1}^h O(k_i \alpha(k_i)) + \sum_{i=1}^h \sum_{j=1}^h O(k_i + k_j) = O(k\alpha(k) + kh) = O(\sqrt{r} \alpha(r)).$$

It follows that the time to relax *all* edges of \mathcal{R} is $O((n/\sqrt{r})\alpha(r)) = o(n)$

20.6 Faster Minimum Cuts: FR-Dijkstra

Frederickson held the record for fastest planar minimum-cut algorithm for almost two and a half decades; the record was finally broken in 2011 by two independent pairs of researchers, who ultimately published their result jointly: Giuseppe Italiano, Yahav Nussbaum, Piotr Sankowski, and Christian Wulff-Nilsen. Their $O(n \log \log n)$ -time algorithm relies on an improvement to Dijkstra’s algorithm in dense distance graphs, proposed by Jittat Fakcharoenphol and Satish Rao in 2001, and now usually called *FR-Dijkstra*.

Recall from the previous lecture on shortest paths that we can compute a dense distance graph for a nice r -division in $O(n \log r)$ time. The dense distance graph has $O(n/\sqrt{r})$ vertices—the boundary vertices of the pieces of the r -division—and $O(n)$ edges. So Dijkstra’s algorithm with a Fibonacci heap runs in $O(E + V \log V) = O(n + (n/\sqrt{r}) \log n)$ time.

FR-Dijkstra removes the $O(n)$ term from this running time. Specifically, within each piece of the r -division, the algorithm exploits the Monge structure in the boundary-to-boundary distances to avoid looking at every pair of boundary vertices. This is the same high-level strategy that we previously used with FR-Bellman-Ford, but with one significant difference: We do not know the relevant Monge arrays in advance. Instead, portions of each Monge array are revealed each time the Dijkstra wavefront touches the corresponding piece of the r -division.

I’ll discuss FR-Dijkstra in detail, along with the faster planar minimum-cut algorithm, in the next lecture.

20.7 References

1. Greg N. Frederickson. Fast algorithms for shortest paths in planar graphs with applications. *SIAM J. Comput.* 16(8):1004–1004, 1987.
2. Alon Itai and Yossi Shiloach. Maximum flow in planar networks. *SIAM J. Comput.* 8:135–150, 1979.
3. Giuseppe F. Italiano, Yahav Nussbaum, Piotr Sankowski, and Christian Wulff-Nilsen. Improved algorithms for min cut and max flow in undirected planar graphs. *Proc. 43rd Ann. ACM Symp. Theory Comput.*, 313–322, 2011.
4. Shay Mozes and Christian Wulff-Nilsen. Shortest paths in planar graphs with real lengths in $O(n \log^2 n / \log \log n)$ time. *Proc. 18th Ann. Europ. Symp. Algorithms*, 206–217, 2010. Lecture Notes Comput. Sci. 6347, Springer-Verlag. arXiv:0911.4963.

5. John Reif. Minimum s - t cut of a planar undirected network in $O(n \log^2 n)$ time. *SIAM J. Comput.* 12(1):71–81, 1983.
6. Hassler Whitney. Non-separable and planar graphs. *Trans. Amer. Math. Soc.* 34:339–362, 1932.
7. Hassler Whitney. Planar graphs. *Fund. Math.* 21:73–84, 1933.

20.8 Aptly Named Sir Not

- Maximum cuts (or minimum cuts with negative capacities) [Hadlock 1975]
- Deriving maximum flows from minimum cuts [Hassin Johnson 1985]
- $O(n)$ time for unweighted graphs [Weihe 1997, Eisenstat Klein 2013, Balzotti Franciosa 2022]
- Global minimum cuts (dual to shortest weighted cycle) [Łącki Sankowski 2011]
- Minimum cuts in directed planar graphs, via double cover [Janiga Koubek 1992 but fixed, Erickson 2011, Fox 2013]
- Faster directed planar minimum cuts [Mozes Nikolaev Nussbaum Weimann SODA 2018]

Chapter 21

Faster Minimum Cuts (FR-Dijkstra) $^\alpha$

21.1 Monge Heaps

Recall that a two-dimensional array M is *Monge* if the inequality $M[i, j] + M[i', j'] \leq M[i', j] + M[i, j']$ holds for all indices $i < i'$ and $j < j'$. Any array where the columns are constant is Monge, and the sum of any two Monge arrays is Monge.

Suppose we are given a $k \times k$ Monge array D , and we are *promised* that there is a k -dimensional vector c . Then no matter what values c contains, the array M defined by $M[i, j] = D[i, j] + c[j]$ is Monge.

A *Monge heap* is a data structure that allows us to extract information from the array M as the coefficients of c are revealed. Specifically, a Monge heap supports the following three operations:

- $\text{Reveal}(j, x)$: Declare that $c[j] = x$, thereby revealing the j th column of M .
- $\text{FindMin}()$: Return the smallest visible element in M . We are guaranteed that this element is the smallest element in its row of M , not just the smallest *visible* element of that row.
- $\text{Hide}(i)$: Hide the row i of M , which must contain the smallest visible element of M (which is also the smallest element of its row of M)

Over the lifetime of the data structure, we will Reveal at most k columns and Hide at most k rows.

An element of M is *visible* if its column has been Revealed but its row has not been Hidden. We call an element of M *active* if it is the smallest visible element in a visible row. Each visible column of M contains zero or more contiguous intervals of M , which we call *active intervals*. Each active interval is specified by a triple of indices (j, i_{\min}, i_{\max}) .

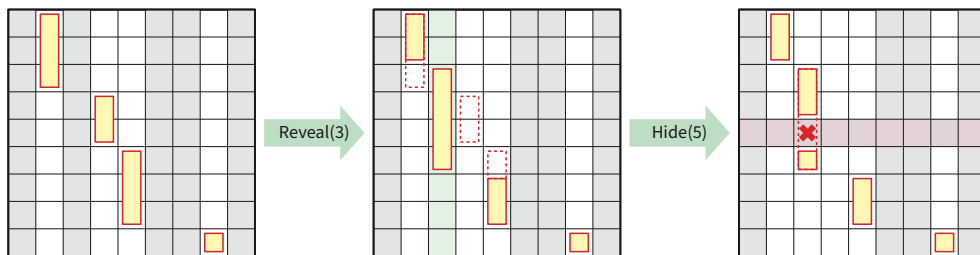


Figure 21.1: Operations on a Monge heap, initially with four visible columns and no hidden rows.

A Monge heap consists of three component data structures (described in more detail below):

- A priority queue storing all live intervals within the visible columns of M
- A balanced binary search tree storing the live intervals in lexicographic order
- A range-minimum query structure for each column of D (sic)

These data structures support each `Reveal` in $O(\log k)$ amortized time, `FindMin` in $O(1)$ time, and `Hide` in $O(\log k)$ time. Over the lifetime of the data structure, we call each of these operations at most k times, thereby finding the minimum elements in some subset of the rows of M in $O(k \log k)$ time. (This is slower than the $O(k)$ running time of SMAWK, but that algorithm requires the entire array M to be visible from the beginning.)

21.1.1 The main priority queue

At all times, the submatrix (or minor) of visible elements in M is Monge. This implies that the minimum *visible* elements in the *visible* rows of M are *monotone*: The index of the row minimum is a non-decreasing function of the row index. More explicitly: For any indices $i < i'$ of visible rows, if $M[i, j]$ is the minimum (visible) element of row i , and $M[i', j']$ is the minimum (visible) element of row i' , then $j \leq j'$.

Thus, each visible column j of M contains the smallest elements of a interval of visible rows, which may be broken into smaller intervals by hidden rows. Each *live interval* can be described by a triple of indices (j, i_{\min}, i_{\max}) , indicating that $M[i, j]$ is the minimum element in every row i such that $i_{\min} \leq i \leq i_{\max}$, and moreover none of those rows has been hidden. The live intervals partition the visible rows of M , so there are at most k of them at any time.

We maintain the live intervals (j, i_{\min}, i_{\max}) in a priority queue, implemented as a standard binary min-heap, where the priority of any interval is its smallest element. In particular, the smallest visible element in M is the priority of the live interval at the root of the heap, so we can support `FindMin` in $O(1)$ time.

21.1.2 Range-minimum queries

The smallest element in any live interval (j, i_{\min}, i_{\max}) depends only on the known Monge matrix D . To compute these minimum elements quickly, we preprocess each column $D[:, j]$ into a data structure that supports *range-minimum queries* of the following form:

- $\text{RMQ}(j, i_{\min}, i_{\max})$: Return the index $i_{\min} \leq i \leq i_{\max}$ that minimizes $D[i, j]$.

The range-minimum data structure consists of a static balanced binary search tree with k leaves. The i th leaf stores $D[i, j]$, and every internal node stores the minimum value of its two children, along with the index of the leaf storing that value. This data structure is constructed once at the start of the algorithm, in $O(k)$ time, and it answers any range-minimum query in $O(\log k)$ time.

Whenever we `Insert` a new live interval (j, i_{\min}, i_{\max}) into the priority queue, we perform a range-minimum query to determine the priority of that interval. Thus, the overall `Insert`ion time is $O(\log k)$. The other priority queue operations `ExtractMin` and `Delete` also take $O(\log k)$ time.

21.1.3 Revealing a column

`Reveal`(j, x) is implemented in $O(\log k)$ amortized time as follows:

- Find the live intervals $I^- = (j^-, i_{\min}^-, i_{\min}^-)$ and $I^+ = (j^+, i_{\min}^+, i_{\min}^+)$ immediately before and after (j, \cdot, \cdot) in lexicographic order, in $O(\log k)$ time, by querying the balanced binary search tree.
- While $M[i_{\min}^-, j] < M[i_{\min}^-, j^-]$, replace I^- with its predecessor in lexicographic order. Then binary search for the smallest index i_{\min} such that $M[i_{\min}, j] < M[i_{\min}, j^-]$.
- While $M[i_{\min}^+, j] < M[i_{\min}^+, j^+]$, replace I^+ with its successor in lexicographic order. Then binary search for the smallest index i_{\max} such that $M[i_{\max}, j] < M[i_{\min}, j^+]$.
- Delete any live intervals (j^\pm, \cdot, \cdot) that overlap (j, i_{\min}, i_{\max}) from the priority queue.
- Insert the new live intervals (j, i_{\min}, i_{\max}) , $(j^-, \cdot, i_{\min} - 1)$, and $(j^+, i_{\max} + 1, \cdot)$ into the priority queue.

To obtain the claimed $O(\log k)$ amortized time bound, we charge the time to delete any interval from the priority queue to its earlier insertion. The requirement that we only Hide rows when their minimum elements are visible implies that there is exactly one live interval in the Revealed column.

21.1.4 Hiding a row

Finally, $\text{Hide}(i)$ is implemented in $O(\log k)$ time as follows:

- Extract the live interval (j, i_{\min}, i_{\max}) from the root of the priority queue. Because row i contains the smallest visible element in M , that smallest element is $M[i, j]$ and $i_{\min} \leq i \leq i_{\max}$.
- Find the smallest element $M[i, j]$ in that interval using a range-minimum query.
- Insert the live intervals $(j, i_{\min}, i - 1)$ and $(j, i + 1, i_{\max})$ into the priority queue.

21.2 Monge structure of nice r -divisions

Suppose we are given a planar map Σ (called Δ in the previous lecture) with non-negatively weighted edges. Recall that a nice r -division partitions S into $O(n/r)$ pieces, each with $O(r)$ vertices and $O(\sqrt{r})$ boundary vertices, and each with the topology of a disk with $O(1)$ holes.

Let D denote the array of boundary-to-boundary distances for a single piece R of this r -division. I claim that we can represent D using a small number of Monge arrays. We need to consider two types of boundary-to-boundary distances, depending on whether the two vertices lie on the same hole of R or on different holes.

First, consider two holes in R , with boundaries α and β . Think of R as a map on the annulus, with boundary cycles α and β . Let π be the shortest path from any vertex $a_1 \in \alpha$ to any vertex $b_1 \in \beta$. For any vertices $a_i \in \alpha$ and $b_j \in \beta$, the shortest path in R from s to t either does not cross π at all, crosses π positively once, or crosses π negatively once. Let $\Delta = R \setminus \pi$, and let Δ^2 be the map obtained by gluing two copies of Δ together along π , as shown in the figure below. Then we have

$$\text{dist}_R(a_i, b_j) = \min \left\{ \begin{array}{l} \text{dist}_\Delta(a_i, b_j) \\ \text{dist}_{\Delta^2}(a_i^+, b_j^-) \\ \text{dist}_{\Delta^2}(a_i^-, b_j^+) \end{array} \right\}$$

where v^+ and v^- denote the two copies of vertex v in Δ^2 . Thus, the array $D(\alpha, \beta)$ of pairwise distances between vertices of α and vertices of β is the element-wise minimum of three Monge arrays.

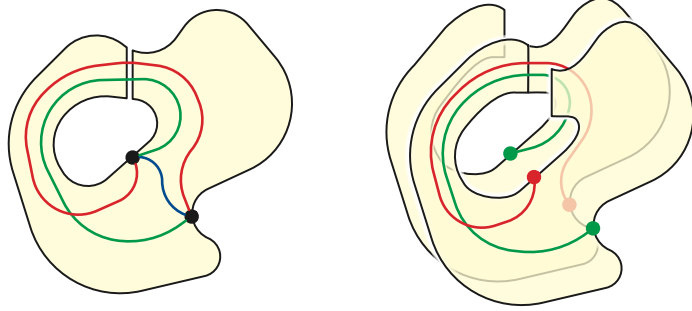


Figure 21.2: Three types of boundary-to-boundary shortest paths in an annulus.

Next consider a single hole in R with boundary α ; by construction α has at most $O(\sqrt{r})$ vertices. As we saw two lectures ago, the array $D(\alpha)$ of pairwise distances in R between vertices in α is *almost* Monge. Instead of splitting this array into *partial* Monge arrays, we recursively partition it into $O(\sqrt{r})$ square Monge subarrays. Specifically, the upper right and lower left quadrants of $D(\alpha)$ are both Monge, and we recursively subdivide the lower left and upper right quadrants. Every row or column of $D(\alpha)$ intersects at most $O(\log r)$ of these square subarrays. The total perimeter of these Monge arrays is $O(\sqrt{r} \log r)$.

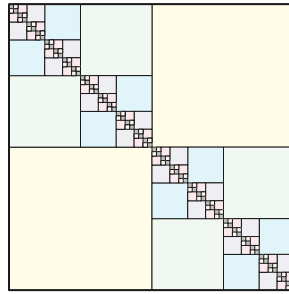


Figure 21.3: Recursive partition of a circular Monge array into square Monge subarrays.

Putting these two cases together, we can represent the boundary-to-boundary distances within each piece R using $O(\sqrt{r})$ Monge arrays, with total area $O(r)$ and total perimeter $O(\sqrt{r} \log r)$. Altogether there are $O(n/\sqrt{r})$ Monge arrays associated with the entire r -division, with total area $O(n)$ and total perimeter $O((n/\sqrt{r}) \log r)$.

Finally, suppose we associate a Monge heap with every Monge array in every piece of our r -division. Then the total number of Reveal and Hide operations we can perform is $O((n/\sqrt{r}) \log r)$, and each of those operations takes $O(\log r)$ amortized time. Thus, the total time spent constructing and maintaining all Monge heaps, over their entire lifetimes, over the entire r -division, is $O((n/\sqrt{r}) \log^2 r)$.

21.3 FR-Dijkstra

Fakcharoenphol and Rao implement their improvement to Dijkstra's algorithm as follows. We begin by computing a nice r -division for Σ and the dense-distance graph for that r -division in

$O(n \log r)$ time, for some value of r to be determined later.

The query phase of FR-Dijkstra solves the single-source shortest path problem in the dense distance graph: Given a boundary vertex s in our r -division, compute the shortest-path distance to every other boundary vertex in the r -division. The algorithm mirrors the Dijkstra's algorithm, but using a nested collection of heaps instead of a standard priority queue:

- $O(\sqrt{r})$ Monge heaps for each piece of the r -division, once for each Monge array in the decomposition described above.
- A standard priority queue, called a *piece heap*, for each piece of the r -division, containing the minimum elements of every Monge heap associated with that piece. We automatically update the piece heap whenever the minimum element of a Monge heap changes.
- A standard priority queue, called the *global heap*, containing the minimum elements of the piece heaps. We automatically update the global heap whenever the minimum element of a piece heap changes.

To begin the algorithm, we initialize all the component heaps to empty, call $\text{Reveal}(s, 0)$ and $\text{Hide}(s)$ inside every Monge heap containing the source vertex s . In alter iterations, whenever we extract the next closest vertex v from the global priority queue, we call $\text{Reveal}(v, \text{dist}(v))$ and $\text{Hide}(v)$ in every Monge heap containing vertex v . By induction, the vertex at the top of the global heap is always the closest boundary vertex beyond the current Dijkstra waveform.

The running time of the algorithm is dominated by the time spent maintain the three different levels of heaps.

- As we argued above, the total time spent managing all Monge heaps is $O((n/\sqrt{r}) \log^2 r)$.
- For each piece R , we perform $O(\log r)$ operations in R 's piece heap for each boundary vertex of R . Thus, the number of piece-heap operations across the entire r -division is $O((n/\sqrt{r}) \log r)$; each piece-heap operation takes $O(\log r)$ time.
- Finally, each iteration of Dijkstra's algorithm removes one vertex v from the global heap and performs at most one deletion and one insertion for each piece containing v . Said differently, for each piece R , we perform $O(1)$ global-heap operations for boundary vertex of R . So the total number of global-heap operations is $O(n/\sqrt{r})$; each global-heap operation takes $O(\log n)$ time.

Thus, the overall running time of the query phase of FR-Dijkstra is $O((n/\sqrt{r})(\log^2 r + \log n))$. (The final $\log n$ term can be eliminated with more effort.)

Theorem: *After $O(n \log r)$ preprocessing time, we can compute the shortest-path distance between any two vertices in a dense distance graph in $O((n/\sqrt{r})(\log^2 r + \log n))$ time.*

21.4 Back to minimum cut

In the previous lecture, we reduced computing minimum (s, t) -cuts to the following problem. Given a planar map Σ with non-negatively weighted edges, and vertices $s_0, s_1, \dots, s_k, t_k, \dots, t_1, t_0$ in cyclic order on the outer face, compute the shortest path distance $\text{dist}(s_i, t_i)$ for every index i . Reif's algorithm solves this problem in $O(n \log k)$ time by computing the *median* shortest path π_m from s_m to t_m , where $m = \lfloor k/2 \rfloor$, and then recursing on both sides of the sliced map $\Sigma \setminus \pi_m$.

The more efficient algorithm of Italiano et al. follows Reif's divide-and-conquer strategy, in three phases.

- In the *initialization* phase, we construct a nice r -division of Σ , construct its dense distance graph by running MSSP in each piece, and initialize the range-minimum trees needed to support FR-Dijkstra. This phase runs in $O(n \log r)$ time.
- Let $\lambda = \lfloor \log_2 k \rfloor$. In the *coarse* divide-and-conquer phase, we compute shortest paths from $s_{i\lambda}$ to $t_{i\lambda}$ for all indices $0 \leq i \leq \lfloor i/\lambda \rfloor$, using Reif's divide-and-conquer strategy, using FR-Dijkstra to compute each shortest path.
- Finally, in the *fine* divide-and-conquer phase, we run Reif's algorithm within each of the $O(k/\lambda)$ slabs left by the previous phase, using the linear-time shortest path algorithm to compute each shortest path. Since each slab has only $\lambda = O(\log k)$ terminal pairs on its boundary, the total time for this phase is $O(n \log \log k)$.

Crudely, the coarse divide-and-conquer phase stops after $O(\log(k/\lambda)) = O(\log n)$ levels of recursion, and the total time spent at each level is $O((n/\sqrt{r})(\log^2 r + \log n))$ time at each level. It follows that the overall time for this phase is $O((n/\sqrt{r})(\log^2 r + \log n) \log k) = O((n/\sqrt{r}) \log^3 n)$, and thus the overall running time of the overall algorithm is

$$O\left(n \log r + \frac{n}{\sqrt{r}} \log^3 n + n \log \log k\right).$$

Setting $r = \log^6 n$ gives us a final running time of $O(n \log \log n)$. (With more effort, this time bound can be reduced to $O(n \log \log k)$.)

21.4.1 Technical Details

The previous high-level description and analysis overlooks several technical details which are crucial for the efficiency of the algorithm. Here I'll give only a brief sketch of the most significant outstanding issues and how to resolve them.

Arguably the most significant detail is that the pieces of the r -division do not respect the slab boundaries. The the running time of the query phase of FR-Dijkstra within any slab depends on the *total* size of all pieces that intersect that slab, and a single piece could intersect several (or even *all*) slabs at any level of recursion. To avoid blowing up the running time, we must slice pieces (and their underlying collections of Monge arrays) along the shortest paths we compute. **This can be done.**

Just as in Reif's algorithm, we stop the course recursion early whenever any vertex of the dense-distance graph appears on both the “floor” and “ceiling” paths of a slab. All s_i -to- t_i distances through that slab will be computed in $O(n)$ time in the fine phase of the algorithm. If we ignore these *collapsed* slabs, then at every level of recursion, each boundary vertex appears in at most two slabs, so the sum over all sub-pieces of the number of boundary nodes in that sub-piece is in fact $O(n/\sqrt{r})$.

Another important technical detail is that after the coarse phase ends, we need to translate the shortest paths in the dense-distance graph into explicit shortest paths in Σ . In particular, we need to translate each boundary-to-boundary *distance* within a single piece, as computed by MSSP, into an explicit boundary-to-boundary *path*. If we record the execution of the MSSP algorithm as a persistent data structure, we can extract the last edge of the shortest path from any boundary

node s to any internal node v in $O(\log \log \deg(v))$ time. Thus, a shortest path consisting of ℓ edges can be extracted in $O(\ell \log \log n)$ time. If we assume (as Italiano et al. do) that

These $O(k/\log k)$ shortest paths in Σ can overlap; in the worst case, the sum of their complexities is $\Omega(nk/\log k)$. The union of these $O(k/\log k)$ shortest paths is a forest F ; Italiano et al. describe how to compute F in $O(n \log \log n)$ time.

Finally, at the beginning of the fine phase of the algorithm, suppose the floor α and ceiling β of some slab coincide. We can compute the endpoints x and y of the shared path $\alpha \cap \beta$ by performing least-common-ancestor queries in the forest F . Then every s_i -to- t_i shortest path in that slab consists of the shortest path from s_i to x , the unique path in F from x to y , and the shortest path from y to t_i . Thus, we can compute all s_i -to- t_i distances in that slab in linear time, by computing shortest path trees at x and y .

21.5 Aptly Named Sir Not

- Faster global minimum cuts (dual to shortest weighted cycle)

Chapter 22

Distributive Flow Lattices \emptyset

Status: Unwritten

22.1 Pseudoflows and Circulations

Let Σ be a planar map. A *pseudoflow* in Σ is an antisymmetric function $\phi : D(\Sigma) \rightarrow \mathbb{R}$ from the darts of Σ to the reals; here antisymmetry means $\phi(d) = -\phi(\text{rev}(d))$ for every dart d .¹ Pseudoflows in Σ define a real vector space $C_1(\Sigma)$, unimaginatively called the *chain space* of Σ , whose dimension is equal to the number of *edges* of Σ . If we arbitrarily fix a *reference dart* e^+ for every edge e , then we can specify a unique 1-chain by assigning arbitrary values to the reference darts.

A *circulation* is a pseudoflow that obeys *Kirchhoff's current law*: For every vertex v , the values assigned to darts into v sum to zero. (We previously called circulations *closed discrete 1-forms*) More generally, the *boundary* $\partial\phi$ of any pseudoflow is the function $\partial\phi : V(\Sigma) \rightarrow \mathbb{R}$ defined by

$$\partial\phi(v) = \sum_{u \rightarrow v} \phi(u \rightarrow v) = \sum_{d : \text{head}(d)=v} \phi(v).$$

(At the risk of confusing the reader, I will use the first summation notation even when Σ has parallel edges.)

Fix a tree-cotree decomposition (T, C) of Σ . For any non-tree edge $e \in C$, the *fundamental cycle* $\text{cycle}_T(e^+)$ is the directed cycle consisting of the reference dart e^+ and the directed path in T from $\text{head}(e^+)$ to $\text{tail}(e^+)$.

Lemma: Fix an arbitrary planar map Σ and an arbitrary tree-cotree decomposition (T, C) of Σ . Every circulation ϕ in Σ satisfies the identity

$$\phi = \sum_{e \in C} \phi(e^+) \cdot \text{cycle}_T(e^+)$$

22.2 Aptly Named Sir Not

¹In the lecture on the Maxwell-Cremona correspondence, we used exactly the same definition for *discrete 1-forms* or *1-cochains*, but topologists should really think of pseudoflows as *1-chains*.

Chapter 23

Maximum Flow \emptyset/α

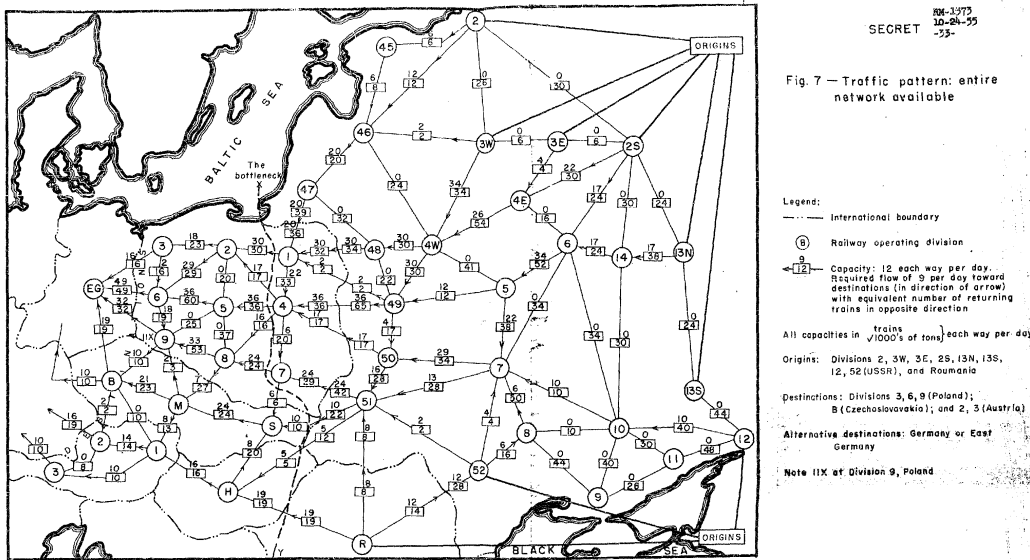


Figure 23.1: Harris and Ross's map of the Warsaw-Pact railway network.

23.1 Background

Here I'll provide a brief overview of standard definitions related to the maximum flow problem. For a more thorough and gentler introduction, see chapters 10 and 11 in my algorithms textbook.

Pseudoflows, flows, and circulations

Recall that a *pseudoflow* (or *1-chain*, or *discrete 1-form*) in a graph G is any function $\phi : D(G) \rightarrow \mathbb{R}$ on the darts of G that is antisymmetric, meaning $\phi(d) = -\phi(\text{rev}(d))$ for every dart d . Intuitively, the value $\phi(u \rightarrow v)$ represents the rate of flow of some divisible substance like water, train cars, or network packets from u to v along the undirected edge uv . In particular, a negative value indicates that the substance is flowing backward from v to u .¹

¹A more common textbook definition of (pseudo)flow is any function $\phi : D(G) \rightarrow \mathbb{R}$ such that for every dart d , we have $\phi(d) \geq 0$ and either $\phi(d) = 0$ or $\phi(\text{rev}(d)) = 0$. That is, for each edge, instead of choosing an arbitrary values

The *boundary* $\partial \phi : V(G) \rightarrow \mathbb{R}$ of a pseudoflow ϕ that intuitively describes the total net flow into each vertex v :

$$\partial \phi(v) := \sum_u \phi(u \rightarrow v).$$

A *circulation* is a pseudoflow ϕ whose boundary $\partial \phi$ is identically zero. Intuitively, circulations are pseudoflows that respect conservation of mass; any positive flow into v must be balanced by negative flow into v (that is, positive flow out of v).

For two fixed vertices s and t , an (s, t) -flow is a pseudoflow f such that $\partial f(v) = 0$ for all v except possibly s and t . The *value* of an (s, t) -flow ϕ is the total net flow into t or out of s :

$$|\phi| := \partial \phi(t) = -\partial \phi(s).$$

Intuitively, (s, t) -flows model some substance being injected into a network of pipes at s and being extracted at t , with conservation at every other vertex. Every circulation is an (s, t) -flow with value 0.

Lemma: *For any two (s, t) -flows ϕ and ψ in the same graph G and any two real numbers α and β , the function $\alpha\phi + \beta\psi$ is an (s, t) -flow in G with value $\alpha|\phi| + \beta|\psi|$. In particular, if ϕ and ψ are circulations, then $\alpha\phi + \beta\psi$ is also a circulation. Thus, circulations and (s, t) -flows in any graph G define vector spaces.*

We can regard any directed cycle γ as a circulation:

$$\gamma(d) = \begin{cases} 1 & \text{if } d \in \gamma \\ -1 & \text{if } \text{rev}(d) \in \gamma \\ 0 & \text{otherwise} \end{cases}$$

Similarly, we can regard any directed path π from s to t as an (s, t) -flow:

$$\pi(d) = \begin{cases} 1 & \text{if } d \in \pi \\ -1 & \text{if } \text{rev}(d) \in \pi \\ 0 & \text{otherwise} \end{cases}$$

Lemma: *Every circulation is a weighted sum of simple directed cycles. Every (s, t) -flow is a weighted sum of simple directed (s, t) -paths and simple directed cycles.*

Capacities and residual graphs

A *capacity* function for a graph G is any function $c : D(G) \rightarrow \mathbb{R}$ from the darts to the reals. Capacities are not necessary either symmetric, antisymmetric, or non-negative. A *flow network* is a graph G together with a capacity function c .

A pseudoflow (or circulation or (s, t) -flow) ϕ is *feasible* with respect to c if and only if $\phi(d) \leq c(d)$ for every dart d . In particular, we allow the capacity of a dart to be negative; a negative dart capacity is equivalent to a positive *lower bound* on the amount of flow through the reversal of the dart. The zero flow $\phi \equiv 0$ is feasible if and only if every dart has non-negative capacity.

for the darts that sum to 0, we choose both a direction and a non-negative value for the edge. Converting between the antisymmetric formulation and the non-negative formulation is straightforward.

Given a graph G , capacity function c , and two vertices s and t as input, the maximum flow problem asks for a feasible (s, t) -flow in G with the largest possible value.

Fix a graph G and a capacity function c . Any pseudoflow ϕ in G induces a *residual capacity* function $c_\phi : D(G) \rightarrow \mathbb{R}$, defined simply as $c_\phi(d) = c(d) - \phi(d)$. A pseudoflow ϕ is feasible if and only if every dart has non-negative residual capacity. The *residual graph* G_ϕ is just the original graph G but with the new capacity function c_ϕ . A *residual path* (respectively, *residual cycle*) is a directed path (respectively, directed cycle) in G_ϕ in which every dart has *positive* residual capacity.

The standard textbook algorithm for maximum flows, proposed by Lester Ford and Delbert Fulkerson in 1953, is the *augmenting path* method. The method starts by finding an initial feasible (s, t) -flow ϕ ; typically all capacities are non-negative, so we can start with the zero flow $\phi \equiv 0$. Then we repeatedly *augment* the flow ϕ by *pushing* more flow along paths from s to t . Specifically, at each iteration, we find a residual path π and augment the flow by setting $\phi' \leftarrow \phi + \min_{d \in \pi} c_\phi(d) \cdot \pi$; here I'm treating π both as a sequence of darts and as an (s, t) -flow. Straightforward definition-chasing implies that if the original flow ϕ is feasible, then the augmented flow ϕ' is also feasible. When G_ϕ contains no more residual paths, ϕ is a maximum (s, t) -flow. More generally:

Lemma: Let ϕ and ϕ' be any (not necessarily feasible) (s, t) -flows in G .

- (a) ϕ' is a feasible (s, t) -flow in G if and only if $\phi' - \phi$ is a feasible (s, t) -flow in the residual graph G_ϕ .
- (b) In particular, if $|\phi| = |\phi'|$, then ϕ' is a feasible (s, t) -flow in G if and only if $\phi' - \phi$ is a feasible **circulation** in G_ϕ .
- (c) In particular, ϕ' is a **maximum** (s, t) -flow in G if and only if $\phi' - \phi$ is a **maximum** (s, t) -flow in G_ϕ .

23.2 Planar Circulations

Flows and circulations have particularly nice structure in planar graphs, or more accurately, in planar *maps*.

Fix an arbitrary circulation ϕ in an arbitrary planar map Σ , with a distinguished outer face o . The *winding number* of ϕ around each face f of Σ , denoted $\text{wind}(\phi, f)$ can be defined by extending the definition of the Alexander numbering of a curve:

- $\text{wind}(\phi, o) = 0$
- For every dart d , we have $\text{wind}(\phi, \text{left}(d)) = \phi(d) + \text{wind}(\phi, \text{right}(d))$.

Conservation at each vertex v implies that this set of constraints has a unique solution. Equivalently, for any path (in fact, any *walk*) π in the dual map Σ^* from dual of the outer face o^* to the dual vertex f^* , we have

$$\text{wind}(\phi, f) = \sum_{d^* \in \pi} \phi(d).$$

The second definition is independent of the choice of dual path π , again by conservation. A third equivalent definition uses the fact that ϕ is a weighted sum of simple cycles:

$$\phi = \sum_i \alpha_i \cdot \gamma_i \implies \text{wind}(\phi, f) = \sum_i \alpha_i \cdot \text{wind}(\gamma_i, f);$$

This definition is independent of the chosen decomposition of ϕ into cycles $\gamma_1, \gamma_2, \dots$.

Alexander numbering is an example of a *face potential* (or 2-chain); more generally, a face potential in Σ is any function $\alpha: F(\Sigma) \rightarrow \mathbb{R}$ assigning a real number to each face of Σ . The *boundary* of a face potential α is the circulation $\partial\alpha: D(\Sigma) \rightarrow \mathbb{R}$ defined by setting

$$\partial\alpha(d) = \alpha(\text{left}(d)) - \alpha(\text{right}(d))$$

for every dart d . It should be easy to verify that $\partial\alpha$ is indeed a circulation. Moreover, the boundary operator ∂ is linear; for all face potentials α and β and real numbers a and b , we have $\partial(a \cdot \alpha + b \cdot \beta) = a \cdot \partial\alpha + b \cdot \partial\beta$.

The following lemma is a natural generalization (and consequence) of the Jordan Curve Theorem.

Lemma: *Every circulation in a planar map is a boundary circulation.*

Proof: For any circulation ϕ , routine definition-chasing implies $\phi = \partial(\text{wind}(\phi))$. That is, $\phi = \partial\alpha$, where $\alpha(f) = \text{wind}(\alpha, f)$ for every face f . \square

Corollary: *The difference between any two (s, t) -flows with the same value in the same planar map Σ is a boundary circulation in Σ .*

23.3 Feasible Planar Circulations and Shortest Paths

Now suppose we endow our planar map Σ with a capacity function $c: D(\Sigma) \rightarrow \mathbb{R}$. Every dart d^* in the dual map Σ^* has a *cost* or *length* $c(d^*)$ equal to the capacity of the corresponding primal dart d ; in short, we have $c(d^*) = c(d)$.

Lemma [Venkatesan]: *Let Σ be any planar map, and let $c: D(\Sigma) \rightarrow \mathbb{R}$ be any capacity function for Σ . There is a feasible circulation in Σ if and only if the dual map Σ^* has no negative cycles.*

Proof: First, consider an arbitrary circulation ϕ in Σ and an arbitrary cycle λ^* in the dual map Σ^* with negative total cost. Without loss of generality, assume λ^* is simple and oriented counterclockwise. Whitney's duality theorem implies that the set λ of primal darts whose duals lie in λ^* define a *directed edge cut*. Specifically, let A denote the vertices of Σ whose corresponding dual faces lie inside λ^* . Then λ is the set of all darts in Σ such that $\text{head}(d) \in A$ and $\text{tail}(d) \notin A$. Straightforward calculation implies

$$\begin{aligned} \sum_{d \in \lambda} \phi(d) &= \sum_{\text{head}(d) \in A} \phi(d) && \text{because } \phi(d) = -\phi(\text{rev}(d)) \\ &= \sum_{v \in A} \sum_{\text{head}(d)=v} \phi(d) \\ &= \sum_{v \in A} \partial\phi(v) && \text{by definition of } \partial \\ &= \sum_{v \in A} 0 && \text{because } \phi \text{ is a circulation} \\ &= 0 \\ &> \sum_{d \in \lambda} c(d). \end{aligned}$$

(In the first step, we are adding $\phi(d)$ for all darts with both endpoints in A .) We conclude that $\phi(d) > c(d)$ for at least one dart $d \in \lambda$; in short, ϕ is not feasible.

On the other hand, suppose shortest-path distances are well-defined in Σ^* . For any dual vertex p , let $\text{dist}(p)$ denote the shortest-path distance from the outer face o to p . We can interpret the function dist as a face potential function for Σ . I claim that the boundary circulation ∂dist is feasible. For any dart d , we have

$$\phi(d) = \text{dist}(\text{left}(d)^*) - \text{dist}(\text{right}(d)^*)$$

Now define the *slack* of every dart d as

$$\begin{aligned} \text{slack}(d) &:= c(d) - \phi(d) \\ &= c(d) - \text{dist}(\text{left}(d)^*) + \text{dist}(\text{right}(d)^*) \\ &= \text{dist}(\text{tail}(d^*)) + c(d^*) - \text{dist}(\text{head}(d^*)) \end{aligned}$$

The definition of shortest paths implies that $\text{slack}(d) \geq 0$ for every dart d , and thus $\phi(d) \leq c(d)$ for every dart d . We conclude that ϕ is feasible.

Corollary: *Given a planar map Σ with n vertices and arbitrary dart capacities, we can compute either a feasible circulation in Σ or a negative-cost cycle in Σ^* in $O(n \log^2 n)$ time.*

Proof: Run the shortest-path algorithm of Klein, Mozes, and Weimann, starting at the vertex o^* dual to the outer face o . If shortest-path distances in Σ^* are well-defined, set $\phi(d) = \text{dist}(\text{left}(d)^*) - \text{dist}(\text{right}(d)^*)$ for every dart d . Otherwise, the algorithm finds a negative cycle in Σ^* . In both cases, the algorithm runs in $O(n \log^2 n)$ time.

23.4 Our First Planar Max-flow Algorithm

The previous lemma can also be used to find feasible (s, t) -flows with particular values. Fix two vertices s and t in G .

Corollary: *Let ϕ be an arbitrary (not necessarily feasible) (s, t) -flow in Σ . There is a feasible (s, t) -flow in G with value $|\phi|$ if and only if the dual residual map Σ_ϕ^* has no negative cycles.*

Corollary: *Given a planar map Σ with n vertices, arbitrary dart capacities, and a real number λ , we can either compute a feasible (s, t) -flow in Σ with value λ , or correctly report that no such flow exists, in $O(n \log^2 n)$ time.*

Proof: Let π be any path from s to t in Σ with value λ , and let ϕ be the flow $\lambda \cdot \pi$. Then ϕ' is a feasible (s, t) -flow with value λ if and only if $\phi' - \phi$ is a feasible circulation in the residual map Σ_ϕ^* . \square

Corollary: *Given a planar map Σ with n vertices, non-negative **integer** dart capacities $c(d)$, we can compute a maximum (s, t) -flow in Σ in $O(n \log^2 n \log(nU))$ time, where $U = \max_d c(d)$.*

Proof: Suppose every dart in Σ has an integer capacity between 0 and U . Because all capacities are non-negative, we know that the zero circulation is a feasible flow with value 0, and the upper bound on individual capacities implies that every feasible flow has value at most nU . If there is a feasible flow with any value λ , we can scale it down to a feasible flow with any value smaller than λ . Finally, Ford and Fulkerson's augmenting-path algorithm implies by induction that the maximum flow in a network with integer capacities has integer value. Thus, we can compute a maximum flow in Σ by performing a binary search over the nU possible flow values, running the $O(n \log^2 n)$ -time decision algorithm at each iteration. \square

I find this algorithm deeply unsatisfying, in part because it requires integer capacities, but it does at least serve as a proof of concept. Hassin and Johnson proved that for *undirected* planar graphs, where every dart has the same capacity as its reversal, we can compute a maximum (s, t) -flow by first running Reif's minimum-cut algorithm and then running Dijkstra's algorithm in a modified dual graph. Using Reif's original algorithm, this approach funds maximum flows in $(n \log^2 n)$ time; this running time can be improved to $O(n \log n)$ using either the linear-time shortest-path algorithm of Henzinger et al inside Reif's algorithm, or by replacing Reif's algorithm with multiple-source shortest paths.

Unfortunately, this approach does not extend to directed planar graphs, because we do not have a similar divide-and-conquer minimum-cut algorithm in that setting. In 1997, Karsten Weihe described an algorithm to compute maximum flows in directed planar graphs in $O(n \log n)$ time, generalizing his earlier $O(n)$ -time algorithm for undirected unit-capacity planar graphs. However, his algorithm assumes that every dart in the input graph appears in at least one simple path from s to t . Darts that do not satisfy this criterion can be safely removed from the input graph, but an efficient algorithm to find all such “useless” darts was only found in 2017, by Jittat Fakcharoenphol, Bundit Laekhanukit, and Pattara Sukprasert.

Meanwhile, in 2006, Glencora Borradaile and Philip Klein discovered a much cleaner algorithm to compute planar maximum flows in $O(n \log n)$ time. In the rest of this lecture note I will describe a reformulation of their algorithm that I published in 2010.

23.5 Parametric Shortest Paths

We formulate the planar maximum-flow problem as a *parametric shortest-path* problem, similar to our first multiple-source shortest-path problem. Fix an arbitrary path π from s to t . We are trying to find the largest value λ such that Σ supports and (s, t) -flow with value λ . Equivalently, by the arguments in the last two sections, we are looking for the largest value λ such that the dual residual map $\Sigma_{\lambda, \pi}^*$ does not contain a negative cycle. The algorithm maintains a shortest-path tree in the dual residual map $\Sigma_{\lambda, \pi}^*$ as the parameter λ continuously increases from 0. At critical values of λ , darts $p \rightarrow q$ in Σ^* become tense and pivot into the shortest-path tree, replacing earlier darts $p' \rightarrow q$. The algorithm halts when a pivot introduces a cycle into the shortest-path tree, which would become negative if we increased λ any further. (That cycle is dual to the minimum cut!)

Again, we fix an arbitrary path π from s to t ; we treat this path as a flow with value 1:

$$\pi(d) = \begin{cases} 1 & \text{if } d \in \pi \\ -1 & \text{if } \text{rev}(d) \in \pi \\ 0 & \text{otherwise} \end{cases}$$

We also fix a vertex o in the dual map Σ^* . Let's establish some notation.

- Σ_λ is just shorthand for the residual graph $\Sigma_{\lambda, \pi}$.
- $c(\lambda, d) = c(\lambda, d^*) = c(d) - \lambda \cdot \pi(d)$ is the capacity of d in the residual graph Σ , and therefore the cost of d^* in the dual residual map Σ_λ^* .
- T_λ is the single-source shortest-path rooted at o in Σ_λ^* .
- $\text{dist}(\lambda, p)$ is the shortest-path distance from o to p in Σ_λ^* .
- $\text{path}(\lambda, p)$ is the shortest path from o to p in Σ_λ^* .

- $\text{pred}(\lambda, p)$ is the second-to-last vertex of $\text{path}(\lambda, p)$.
- $\text{slack}(\lambda, p \rightarrow q) = \text{dist}(\lambda, p) + c(\lambda, p \rightarrow q) - \text{dist}(\lambda, q)$
- $\text{cycle}(\lambda, p \rightarrow q)$ is the closed walk obtained by concatenating $\text{path}(\lambda, p)$, $p \rightarrow q$, and $\text{rev}(\text{path}(\lambda, q))$.
- A dart d of Σ_λ is *tense* if $\text{slack}(\lambda, d^*) = 0$.
- An edge e of Σ_λ is *loose* if neither of its darts is tense.
- L_λ is the subgraph of all loose edges in Σ_λ .
- A dart d in Σ_λ is *active* if $\text{slack}(\lambda, d^*)$ is decreasing at λ .
- LP_λ is the set of all active darts in Σ_λ .

Except at critical values of λ , subgraph L_λ is a spanning tree of Σ_λ , and in fact (L_λ, T_λ) is a tree-cotree decomposition of Σ .

Lemma: LP_λ is the unique path from s to t in L_λ .

Lemma: LP_λ is the set of all active darts in Σ_λ .

23.6 Active Darts

23.7 Fast Pivots

23.8 Universal Cover Analysis

23.9 References

1. Therese C. Biedl, Broná Brejová, and Tomáš Vinař. Simplifying flow networks. *Proc. 25th Symp. Math. Found. Comput. Sci.*, 192–201, 2000. Lecture Notes Comput. Sci. 1893, Springer-Verlag.
2. Glencora Borradaile and Anna Harutyunyan. Maximum st-flow in directed planar graphs via shortest paths. *Proc. 24th Int. Workshop Combin. Algorithms*, 423–427, 2013. Lecture Notes Comput. Sci. 8288, Springer. arXiv:1305.5823.
3. Glencora Borradaile and Philip Klein. An $O(n \log n)$ algorithm for maximum st-flow in a directed planar graph. *J. ACM* 56(2):1–9:1–30, 2009.
4. David Eppstein and Kevin A. Wortman. Optimal embedding into star metrics. *Proc. 11th Algorithms Data Struct. Symp. (WADS)*, 290–301, 2009. Lecture Notes Comput. Sci. 5664, Springer. Another application of parametric shortest paths.
5. Jeff Erickson. Parametric shortest paths and maximum flows in planar graphs. *Proc. 21st Ann. ACM-SIAM Symp. Discrete Algorithms*, 794–804, 2010.
6. Jittat Fakcharoenphol, Bundit Laekhanukit, and Pattara Sukprasert. Finding all useless arcs in directed planar graphs. Preprint, May 2018. arXiv:1702.04786.
7. Lester R. Ford and Delbert R. Fulkerson. Maximal flow through a network. *Canad. J. Math.* 8(399–404), 1956. First published as Research Memorandum RM-1400, The RAND Corporation, Santa Monica, California, November 19, 1954.

8. Lester R. Ford and Delbert R. Fulkerson. *Flows in Networks*. Princeton University Press, 1962. First published as Research Memorandum R-375-PR, The RAND Corporation, Santa Monica, California, August 1962.
9. Theodore E. Harris and Frank S. Ross. Fundamentals of a method for evaluating rail net capacities. Research Memorandum RM-1573, The RAND Corporation, Santa Monica, California, October 24, 1955. Declassified May 13, 1999.
10. Refael Hassin and Donald B. Johnson. An $O(n \log^2 n)$ algorithm for maximum flow in undirected planar networks. *SIAM J. Comput.* 14(3):612–624, 1985.
11. Samir Khuller, Joseph (Seffi) Naor, and Philip Klein. The lattice structure of flow in planar graphs. *SIAM J. Discrete Math.* 477–490, 1993. Removing clockwise residual cycles.
12. Karl Menger. Zur allgemeinen Kurventheorie. *Fund. Math.* 10:96–115, 1927.
13. Shankar M. Venkatesan. *Algorithms for network flows*. Ph.D. thesis, The Pennsylvania State University, 1983.
14. Karsten Weihe. Edge-disjoint (s, t) -paths in undirected planar graphs in linear time. *J. Algorithms* 23(1):121–138, 1997.
15. Karsten Weihe. Maximum (s, t) -flows in planar networks in $O(|V| \log |V|)$ time. *J. Comput. Syst. Sci.* 55(3):454–476, 1997.

23.10 Aptly Not

Chapter 24

Surface Maps $^\beta$

Recall that a *planar map* is the decomposition of the plane (or by standard abuse of terminology, the sphere) induced by an embedding of a graph in the plane. Any planar map can be represented by a *rotation system* $\Sigma = (D, \text{rev}, \text{succ})$ where D is the set of darts of the embedded graph, rev is the reversal involution for those darts, and succ is a permutation of the darts whose orbits describe the darts into each vertex of the embedded graph in clockwise order. The orbits of the permutation $\text{rev}(\text{succ})$ describe the counterclockwise order of darts around the boundary of each face. A rotation system with n vertices, m edges, and f faces is *planar* if and only if $n - m + f = 2$.

But what if $n - m + f \neq 2$? In that case, Σ represents a map on a more complex surface.

24.1 Surfaces, Polygonal Schemata, and Cellular Embeddings

A *surface* (or *2-manifold*) is a (compact, second-countable, Hausdorff) topological space that is *locally homeomorphic* to the plane. That is, every point lies in an open subset of the space that is homeomorphic to \mathbb{R}^2 . (Later we will also consider *surfaces with boundary*, spaces where every point lies in an open neighborhood homeomorphic to either the plane or a closed halfplane.)

The simplest method to construct surfaces is to glue disks together along their boundary segments. A *polygonal schema* is a finite set of polygons with labeled edges, where each label appears exactly twice. We can construct a surface by identifying every pair of edges with the same label; specifically, if the edges of each polygon are oriented counterclockwise around its interior, we identify each edge with the *reversal* of the other edge with the same label. The vertices and edges of the polygons become the vertices and edges of a graph; the interiors of the polygons become the faces of the resulting embedding.

Formally, an (abstract) polygonal schema is a triple $(D, \text{rev}, \text{succ}^*)$, where D is a set of darts (representing the sides of the polygons), rev is an involution of those darts (representing pairs of sides with matching labels), and succ^* is a permutation describing the counterclockwise order of darts around each face/polygon. Hopefully it's clear that “abstract polygonal schema” is just a synonym for “dual rotation system”.

To transform an abstract polygonal schema Π into a topological space, let F denote a set of disjoint closed disks in the plane, one for each orbit of succ^* . For each orbit of length d , we subdivide the counterclockwise boundary of the corresponding disk into d paths. We identify

those paths with the darts, so that $\text{succ}^*(d)(0) = d(1)$ for every dart/path d . Then the space $\mathcal{S}(\Pi)$ is the quotient space $\bigsqcup F / \sim$, where $d(t) \sim \text{rev}(d)(1-t)$ for every dart/path d and $t \in [0, 1]$. In other words, we identify each dart with the reversal of its reversal! It is not hard to verify that the space $\mathcal{S}(\Pi)$ is always a 2-manifold; the vertices, edges, and faces constitute a map $\Sigma(\Pi)$ of this surface.¹

Moving in the other direction, recall that an *embedding* of a graph $G = (V, \text{rev}, \text{head})$ on a surface S is a continuous injective function from G (as a topological graph) into S . The components of the complement of the image of the embedding are the *faces* of the embedding. An embedding is *cellular* if every face is homeomorphic to an open disk. The vertices, edges, and faces of an embedding define a surface map if and only if the embedding is cellular; in particular, the embedded graph must be connected.

24.2 Orientability

Any discussion of rotation systems or polygonal schemata for surface maps assumes *a priori* that the underlying surface is *orientable*, meaning it is possible to consistently define “clockwise” and “counterclockwise” everyone on the surface. As we’ll prove in the next lecture, every orientable surface can be constructed from the sphere by attaching one or more “handles”; the number of handles is called the *genus* of the surface. More formally, the genus of a surface S is the maximum number of closed curves $\gamma_1, \dots, \gamma_g$ in S whose complement $S \setminus (\gamma_1 \cup \dots \cup \gamma_g)$ is connected.

However, not all 2-manifolds are orientable. The simplest example of a non-orientable surface (with boundary) is the *Möbius band*, which can be constructed from a strip of paper by gluing opposite ends with a half-twist. More formally, the Möbius band is the quotient space $[0, 1]^2 / \sim$ where $(0, t) \sim (1, 1-t)$ for all $t \in [0, 1]$. In fact, Möbius bands are the *only* obstruction to orientability; a surface is orientable if and only if it does not contain (a subspace homeomorphic to) a Möbius band.

In one of Lewis Carroll’s lesser-known works, one character explains to another how to sew three square handkerchiefs into “Fortunatus’s Purse” (so called because “Whatever is *inside* that Purse, is *outside* it; and whatever is *outside* it, is *inside* it. So you have all the wealth of the world in that leetle Purse!”). His instructions can be interpreted as a signed polygonal schema for a non-orientable surface map of genus 1.

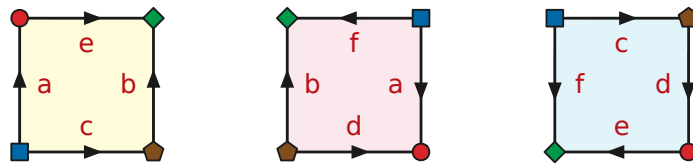


Figure 24.1: Mein Herr’s instructions for sewing Fortunatus’s Purse. Sewing the first two squares along edges a and b yields a Möbius band; so does sewing the last two squares along f and d , or sewing the first and last square along c and e .

We can’t represent non-orientable surface maps using rotation systems, so we need a different combinatorial representation. It is possible to define signed versions of both rotation systems and polygonal schemata, but their navigation requires awkward bookkeeping and case analysis.

¹This construction breaks down when $D = \emptyset$; in this case, the space $\mathcal{S}(\Pi)$ is the sphere and $\Sigma(\Pi)$ is the trivial map with one vertex, one face, and no edges.

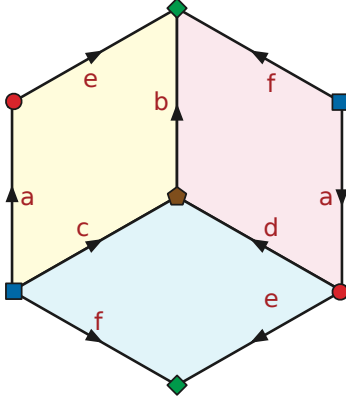


Figure 24.2: Another signed polygonal schema for Fortunatus’s Purse.

Instead we consider a more elegant but slightly more verbose combinatorial representation that works for both orientable and non-orientable surfaces.

24.3 Band Decompositions

Let $\Sigma = (V, E, F)$ be an arbitrary map of some surface S , which may or may not be orientable. We construct a related surface map Σ^\square , called a *band decomposition*, intuitively by shrinking each face of Σ slightly, expanding each vertex of Σ into a small closed disk, and replacing each edge of Σ with a closed quadrilateral “band”.

- Each vertex of Σ^\square correspond to a *blade* in Σ , which is an edge with a chosen direction (specifying its head) and an *independent* orientation (specifying its “left” shore).
- There are three types of edges in Σ^\square , corresponding to the sides, corners, and darts of Σ .
- There are three types of faces in Σ^\square , corresponding to the vertices, edges, and faces of Σ .
- Every vertex of Σ^\square is incident to exactly one edge and one face of each type.

If a surface map Σ has n vertices, m edges, and f faces, then its band decomposition Σ^\square has $4m$ vertices, $6m$ edges (2 m of each type), and $n + m + f$ faces.

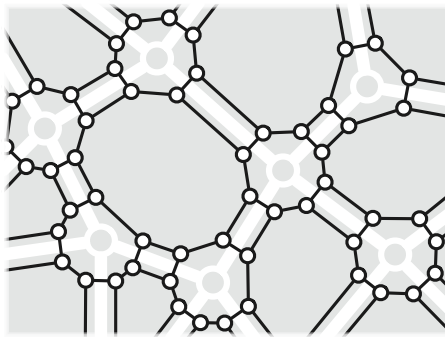


Figure 24.3: A band decomposition (black) of a surface map (white).

Lemma: *A surface map Σ is orientable if and only if the graph of its band decomposition Σ^\square is bipartite.*

24.4 Reflection Systems

Band decompositions immediately suggest the following combinatorial representation of surface maps. A *reflection system*² is a quadruple $\Xi = (\Phi, a, b, c)$ with the following components:

- Φ is a finite set of abstract objects called *blades* or *flags*.
- $a : \Phi \rightarrow \Phi$ is an involution of Φ , whose orbits are called *sides*.
- $b : \Phi \rightarrow \Phi$ is an involution of Φ , whose orbits are called *corners*.
- $c : \Phi \rightarrow \Phi$ is an involution of Φ , whose orbits are called *darts*.
- The involutions a and c commute, and their product $ac = ca$ is an involution

To simplify notation, I'll use concatenation to denote compositions of the involutions a , b , and c ; thus, for example, ac is shorthand for the permutation $a \circ c$, and $abc(\phi)$ is shorthand for $a(b(c(\phi)))$.

Each blade in Σ can be associated with a triple (v, e, f) , where e is an edge of Σ , v is one of e 's endpoints, and f is one of e 's shores. Intuitively, each of the involutions a , b , c , changes one of the components of this triple: a changes the vertex (or *apex*); b changes the edge (or *border*); c changes the face (of *chamber*). More formally, the orbits of the permutation group $\langle b, c \rangle$ are the *vertices* of the reflection system; the orbits of $\langle a, c \rangle$ are its *edges*; and the orbits of $\langle a, b \rangle$ are its *faces*.

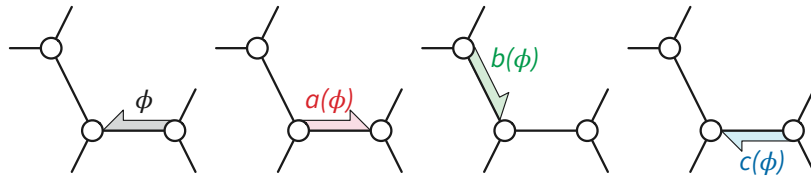


Figure 24.4: Operations on blades in a reflection system.

Every reflection system represents a unique surface map with corresponding blades, sides, corners, darts, vertices, edges, and faces. (In particular, the trivial reflection system with $\Phi = \emptyset$ represents the trivial map.) Conversely, every surface map is represented by a *unique* reflection system.

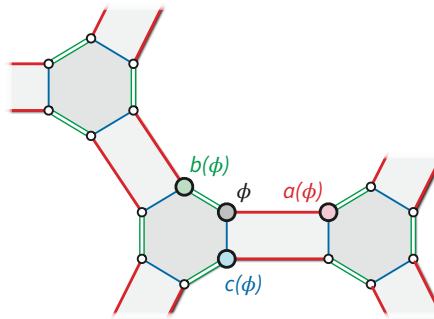


Figure 24.5: Corresponding vertices and edges in the band decomposition.

Just as rotation systems are mathematical abstractions of incidence lists, reflection systems can also be encoded as a simple data structure for surface maps, which has one record for every

²The term “reflection system” is non-standard, but I think it's both sufficiently evocative and sufficiently similar to “rotation system” to justify its use. Reflection systems are also called *graph-encoded maps* or *graph-encoded manifolds* or *gems* (Lins 1983), but the most common term seems to be “combinatorial map” (or just “map”). Yeah.

blade ϕ , each containing the index of its head and pointers to its neighboring blades $a(\phi)$, $b(\phi)$, $c(\phi)$, along with an array indexed by vertices pointing to an arbitrary blade into each vertex. (It may also be convenient to store the index of each blade's "left" shore, and a face-indexed array pointing one blade for each face.)

A particularly simple implementation represents blades by integers from 0 to $4m - 1$, such that for any blade ϕ , the neighboring blades $a(\phi)$ and $c(\phi)$ are obtained by flipping the two least significant bits, for example, by defining $a(\phi) = \phi \oplus 2$ and $c(\phi) = \phi \oplus 1$. Thus, edge e consists of blades $4e, 4e + 1, 4e + 2, 4e + 3$, and blade ϕ belongs to edge $[\phi/4]$. Then any static surface map can be represented using five arrays:

- $vany[0..n]$ storing an arbitrary blade for each vertex;
- $fany[0..f]$ storing an arbitrary blade for each face;
- $vert[0..4m - 1]$ storing the "head" vertex of each blade;
- $face[0..4m - 1]$ storing the "left" face of each blade;
- $B[0..4m - 1]$ storing the involution b .

Notice that $vert(\phi) = vert(c(\phi)) = vert(\phi \oplus 1)$ and $face(\phi) = face(a(\phi)) = face(\phi \oplus 2)$, so in principle, exactly half of the $vert$ and $face$ arrays are redundant.

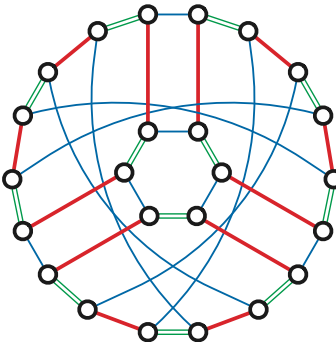


Figure 24.6: A reflection system for Fortunatus's Purse.

24.5 Equivalence

Transforming a rotation system of a surface map into an equivalent reflection system or vice versa (if the map is orientable) is straightforward.

Let $\Sigma = (D, \text{rev}, \text{succ})$ be a rotation system. Then setting $\Phi := D \times \{-1, +1\}$ and defining the involutions as follows gives us an equivalent reflection system:

$$\begin{aligned} a((d, +1)) &:= (\text{rev}(d), -1) & a((d, -1)) &:= (\text{rev}(d), +1) \\ b((d, +1)) &:= (\text{succ}(d), -1) & b((d, -1)) &:= (\text{succ}^{-1}(d), +1) \\ c((d, +1)) &:= (d, -1) & c((d, -1)) &:= (d, +1) \end{aligned}$$

Conversely, let $\Xi = (\Phi, a, b, c)$ be an orientable reflection system. Because Ξ is orientable, we can partition Φ into two subsets Φ^+ and Φ^- , so that each of the involutions a, b, c is a bijection between the two subsets. We can construct a rotation system equivalent to Ξ by setting $D := \Phi^+$ and $\text{rev} := a \circ c$ and $\text{succ} := b \circ c$.

24.6 Duality

Duality generalizes naturally from planar maps to surface maps. Two surface maps Σ and Σ^* of the same underlying surface are *duals* if (up to homeomorphism) each face of Σ contains exactly one vertex of Σ^* , each face of Σ^* contains exactly one vertex of Σ , and each edge of Σ crosses exactly one edge of Σ^* .

Just as in the planar setting, the dual of a rotation system $\Sigma = (D, \text{rev}, \text{succ})$ is obtained by replacing the successor permutation succ with $\text{succ}^* := \text{rev}(\text{succ})$; that is, $\Sigma^* = (D, \text{rev}, \text{rev}(\text{succ}))$. Thus, the darts in any *orientable* surface map Σ are dual to (or more formally, *are*) the darts in the dual map Σ^* .

Duality for reflection systems is similarly straightforward. Suppose $\Xi = (\Phi, a, b, c)$ is the reflection system for a surface map Σ ; exchanging the involutions a and c , gives us the dual reflection system $\Xi^* = (\Phi, c, b, a)$, which is the reflection system of its dual map Σ^* . (As a mnemonic device, we could refer to the vertices, edges, and faces of the dual map Σ^* as *areas*, *borders*, and *centroids*, respectively.) In this representation, darts in a surface map are dual to (or more formally, *are*) *sides* in its dual map, rather than darts.

Lemma: *Every surface map Σ and its dual Σ^* have the same band decomposition: $\Sigma^\square = (\Sigma^*)^\square$.*

For *orientable* surface maps, we have exactly the same correspondences between features in primal and dual rotation systems as we do for planar maps.

Table 24.1: A (partial) duality dictionary for rotation systems of orientable surface maps

Primal Σ	Dual Σ^*	Primal Σ	Dual Σ^*
vertex v	face v^*	head(d)	left(d^*)
dart d	dart d^*	tail(d)	right(d^*)
edge e	edge e^*	left(d)	head(d^*)
face f	vertex f^*	right(d)	tail(d^*)
succ	$\text{rev} \circ \text{succ}$	clockwise	counterclockwise
rev	rev		

There is a similar but slightly more complex correspondence between primal and dual *reflection* systems. In particular, the dual of a *directed* map (where every edge has a preferred “head” vertex) on a non-orientable surface is not another directed graph, but rather an *sided* map (where every edge has a preferred *face*).

Table 24.2: A (partial) duality dictionary for reflection systems

Primal Σ	Dual Σ^*	Primal Σ	Dual Σ^*
vertex v	face v^*	a	c
blade ϕ	blade ϕ^*	b	b
dart d	side d^*	c	a
side σ	dart σ^*	$\text{vert}(\phi)$	$\text{face}(\phi^*)$
edge e	edge e^*	$\text{face}(\phi)$	$\text{vert}(\phi^*)$
face f	vertex f^*		

24.7 Loops and Isthmuses; Deletion and Contraction

Recall that a *loop* in a graph is an edge that is incident to only one vertex, and a *bridge* is an edge whose deletion disconnects the graph. An *isthmus* in a surface map is an edge that is incident to only one face. As in planar maps, every bridge in a surface map is also an isthmus. The Jordan curve theorem implies that every isthmus in a *planar* map is also a bridge, but because the Jordan curve theorem does not extend to maps on other surfaces, an isthmus in a surface map is *not* necessarily a bridge. Moreover, unlike in planar graphs, the same edge in a surface map can be *both* a loop and an isthmus.

Let $\Sigma = (V, E, F)$ be an arbitrary surface map. Deleting any edge e that is not an isthmus yields a simpler map $\Sigma \setminus e$ of the same surface with the same vertices, one less edge, and with the two faces on either side of e replaced with their union. Similarly, contracting any edge e that is not a loop yields a simpler map Σ / e of the same surface with the endpoints of e merged into a single vertex, one less edge, and the same number of faces.

Contraction and deletion modify the rotation system of an orientable surface map exactly as they do in planar maps:

$$(succ \setminus e)(d) = \begin{cases} succ(succ(succ(d))) & \text{if } succ(d) \in e \text{ and } succ(succ(d)) \in e, \\ succ(succ(d)) & \text{if } succ(d) \in e, \\ succ(d) & \text{otherwise.} \end{cases}$$

$$(succ / e)(d) = \begin{cases} succ(succ^*(succ^*(d))) & \text{if } succ(d) \in e \text{ and } succ^*(succ(d)) \in e, \\ succ(succ^*(d)) & \text{if } succ(d) \in e, \\ succ(d) & \text{otherwise.} \end{cases}$$

The first deletion case occurs when the deleted edge is an empty loop; the first contraction case occurs when one endpoint of the contracted edge is a *leaf* (has degree 1).

Deletion and contraction can be similarly implemented in reflection systems, even in non-orientable maps. If we equate e with the corresponding set of four flags in Φ , then the reflection systems $\Xi \setminus e = (\Phi \setminus e, a, b \setminus e, c)$ and $\Xi / e = (\Phi \setminus e, a, b / e, c)$, which respectively represent the maps $\Sigma \setminus e$ and Σ / e , can be defined as follows, for all $\phi \in \Phi \setminus e$:

$$(b \setminus e)(\phi) := \begin{cases} bcb(\phi) & \text{if } b(\phi) \in e \text{ and } bcb(\phi) \in e \\ bcb(\phi) & \text{if } b(\phi) \in e \\ b(\phi) & \text{otherwise} \end{cases}$$

$$(b / e)(\phi) := \begin{cases} babab(\phi) & \text{if } b(\phi) \in e \text{ and } babab(\phi) \in e \\ bab(\phi) & \text{if } b(\phi) \in e \\ b(\phi) & \text{otherwise} \end{cases}$$

Again, the complicated first cases correspond to the only edge incident to a vertex or an edge. We emphasize the involutions a and c from the original reflection system Ξ appear verbatim (except for their smaller domains) in $\Xi \setminus e$ and Ξ / e .

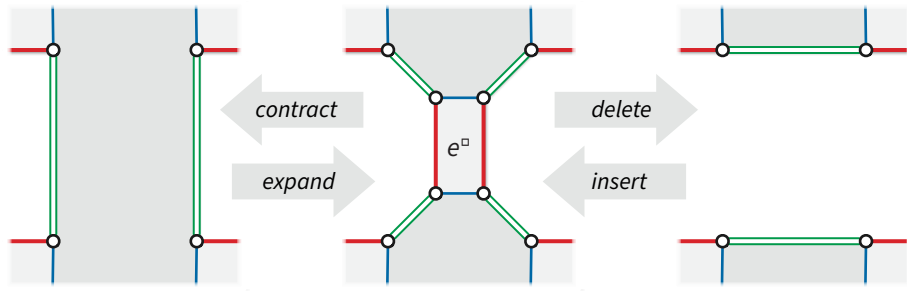


Figure 24.7: Typical contraction, expansion, deletion, and insertion in the band decomposition.

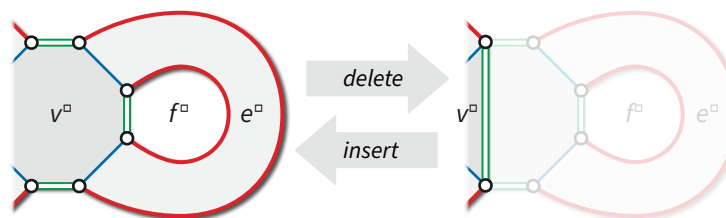


Figure 24.8: Deleting or inserting an empty loop.

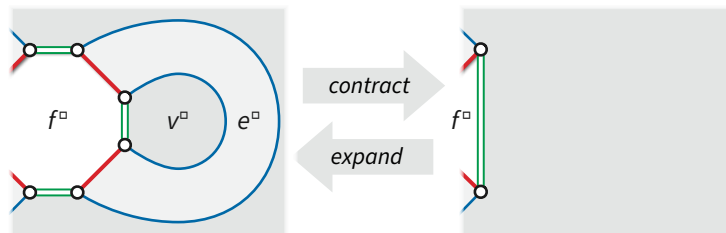


Figure 24.9: Contracting or expanding a leaf.

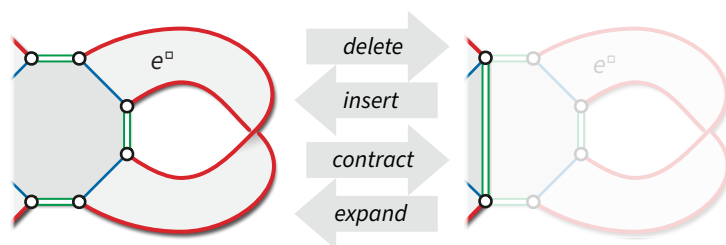


Figure 24.10: Deleting or contracting a twisted loop/isthmus.

24.8 References

1. Lewis Carroll. *Sylvie and Bruno Concluded*. Illustrated by Henry Furniss. Macmillan and Co., 1893.
2. Sóstenes Lins. Graph-encoded maps. *J. Comb. Theory Ser. B* 32:171–181, 1982.

24.9 Sir Not Appearing

- Henry Slade and the “Afghan Bands”



Figure 24.11: Mein Herr explains to Lady Muriel how to sew Fortunatus’ Purse.

Chapter 25

Surface Classification^β

In this lecture, we will prove that up to homeomorphism, surfaces are uniquely identified by two pieces of data: their *genus* and their *orientability*.

- The *genus* of a surface \mathcal{S} is the maximum number of simple disjoint cycles that can be deleted without disconnecting the surface.
- A surface \mathcal{S} is *orientable* if it does not contain a subspace homeomorphic to a Möbius band.

A difficult theorem of Kerékjártó (1923) and Rado (1925) states that every compact 2-manifold is the underlying surface of some map.¹ In light of this result, it suffices to consider an arbitrary surface *map* Σ , represented by a reflection system, and argue that the underlying surface of Σ is determined by its genus and orientability. By assumption all surface maps are connected.

For any vertex v , edge e , or face f of Σ , let v^\square , e^\square , or f^\square denote the corresponding face of the band decomposition Σ^\square .

25.1 Tree-Cotree Decompositions and Systems of Loops

A *tree-cotree decomposition* of a surface map Σ is a partition of the edges $E = T \sqcup L \sqcup C$, where T is a spanning tree of Σ , C^* is a spanning tree of the dual map Σ^* , and $L = E \setminus (C \cup T)$ is the set of *leftover* edges.

Because Σ is connected, Σ has a spanning tree T , and we can contract all edges in T to obtain a single-vertex map Σ / T . The dual map $(\Sigma / T)^*$ is also connected, so it has a spanning tree C ; we can delete the corresponding primal edges C^* to obtain a map $\Sigma / T \setminus C$ that has one vertex, one face, and zero or more edges. Thus, every surface map has a tree-cotree decomposition.

When Σ is a planar (or spherical) map, every tree-cotree decomposition has $L = \emptyset$. Tree-cotree decompositions were first studied for orientable surface maps by Norman Biggs and for arbitrary surface maps by Bruce Richter and Herbert Shank; however, David Eppstein was apparently the first to call the three-way edge partition (T, L, C) a “tree-cotree decomposition”.

We call any map with a single vertex and a single face a *system of loops*. Trivially, every edge in a system of loops is both a loop (incident to only one vertex) and an isthmus (incident to

¹This claim may seem obvious; in fact it was considered obvious until the early 20th century. The same claim is false for 4-dimensional manifolds!

only one face). Because contraction and deletion do not change the underlying surface of a map, the Kerékjártó-Rado theorem implies that every surface supports a system of loops. Thus, for purposes of proving the surface classification theorem, we can assume without loss of generality that **the original map Σ is a system of loops**.

For any edge e in a system of loops, the union $e^\square \cup v^\square$ is either a Möbius band or an annulus. If $e^\square \cup v^\square$ is a Möbius band, we call e a *one-sided* loop; otherwise, e is a *two-sided* loop.

25.2 Handles

A *handle* in a surface S is an annulus A whose complement $S \setminus A$ is connected. The Jordan curve theorem implies that the sphere has no handles, but this theorem does not extend to other surfaces. To detach the handle, we delete it from S and glue disks to the two resulting boundary circles, as shown in the figure below.

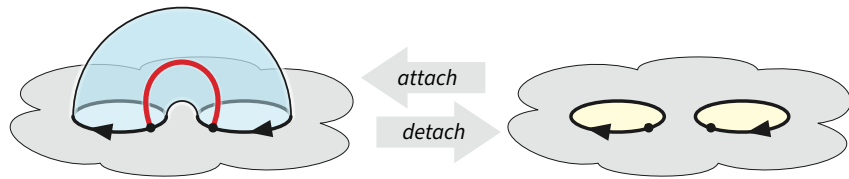


Figure 25.1: Detaching or attaching a handle.

Now suppose our system of loops Σ is orientable, or equivalently, that every loop in Σ is two-sided. Let e be any loop in Σ , and let v be its only vertex. Then the band decomposition Σ^\square contains a handle H_e , composed of e^\square and the rectangle in v^\square connecting the four vertices of e^\square ; see Figure 2 below.

The two endpoints of e cannot be adjacent around v , because then e would be the boundary of an empty loop on one side and another face on the other, contradicting the facet that Σ has only one face.

Normally, we are not allowed to contract loops, but for the sake of argument, consider the map Σ / e obtained by contracting e using the usual formula for contraction in a reflection system. If (Φ, a, b, c) is a reflection system for Σ , then $(\Phi \setminus e, a, b / e, c)$ is a reflection system for Σ / e , where for any dart $\phi \in \Phi \setminus e$,

$$(b / e)(\phi) := \begin{cases} babab(\phi) & \text{if } b(\phi) \in e \text{ and } bcb(\phi) \in e \\ bab(\phi) & \text{if } b(\phi) \in e \\ b(\phi) & \text{otherwise} \end{cases}$$

Combinatorially, contracting e splits its sole endpoint v of e into two vertices, each incident to the darts that enter v from one side or the other of e . (This counterintuitive behavior is exactly why we normally forbid contracting loops.) Topologically, the contraction detaches the handle H_e . The resulting map Σ / e has two vertices but still only one face.

Symmetrically, because e is also an isthmus, *deleting* e also detaches a handle in the band decomposition, this time consisting of e^\square and a rectangle inside f^\square . The resulting map $\Sigma \setminus e$ has two faces but still only one vertex.

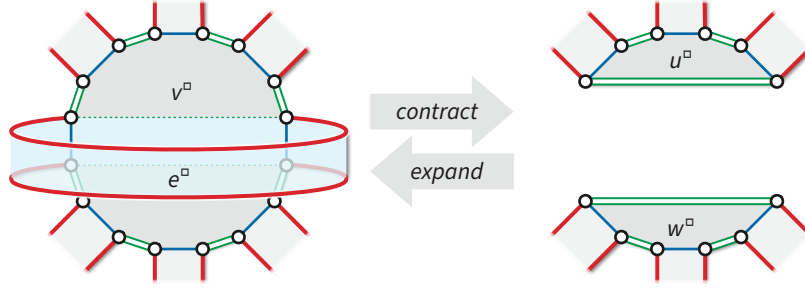


Figure 25.2: Detaching a handle by contracting a two-sided loop.

Theorem: Every orientable surface can be reduced to a sphere by detaching zero or more handles.

Proof: Let Σ be any system of loops on an orientable surface S . If Σ has no edges, then S is the sphere. Otherwise, let e be any loop in Σ . Contracting e detaches a handle from S and leaves a map Σ / e with two vertices and one face. Σ / e must contain an edge e' between its two vertices; otherwise, Σ / e would be disconnected and thus have more than one face. The map $\Sigma / e \setminus e'$ is a smaller system of loops. By the inductive hypothesis, the underlying surface of $\Sigma / e \setminus e'$ can be reduced to a sphere by detaching handles. \square .

This theorem is more commonly stated in terms of *attaching* handles. For any integer $g \geq 0$, let $S(g, 0)$ denote the surface obtained from the sphere by attaching g handles. For example, $S(0, 0)$ is the sphere and $S(1, 0)$ is the torus. Up to homeomorphism, it does not matter where or in what order the handles are attached, as long as they are attached in a way that preserves the orientability of the surface (as shown in Figure 1).

Theorem: Every orientable surface is homeomorphic to $S(g, 0)$ for some integer $g \geq 0$.

The integer g is called the *genus* of the surface $S(g, 0)$, or the genus of any map on that surface.

25.3 Twists

A *twist* in a surface S is any subspace $M \subset S$ homeomorphic to a Möbius band. Because M has only one boundary edge, the complement $S \setminus M$ is always connected. To detach the twist, we delete it from S and glue a disk to the resulting boundary circle, as shown in the figure below. (Here I am drawing the Möbius band as a self-intersecting surface called a *cross-cap*, whose boundary is a standard circle, instead of the usual embedding as a twisted paper strip.)

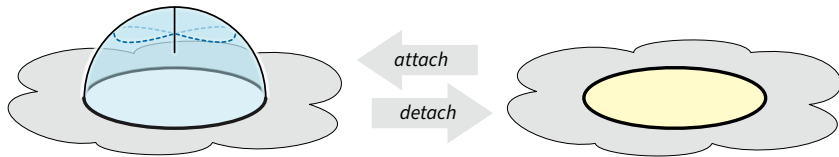


Figure 25.3: Detaching or attaching a twist.

Now suppose our system of loops Σ is non-orientable, or equivalently, that Σ contains at least one one-sided loop. Let e be any one-sided loop in Σ . Then the band decomposition Σ^\square contains a twist M_e , composed of e^\square and the rectangle in v^\square connecting the four vertices of e^\square ; see Figure 4 below. In this case, the two endpoints of e can be adjacent around v .

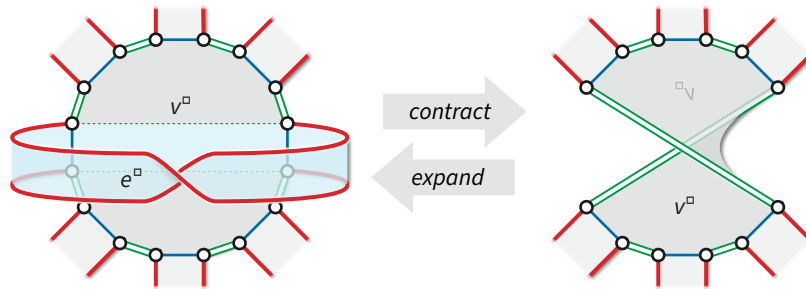


Figure 25.4: Detaching a handle by contracting a one-sided loop.

Once again, consider the map $\Sigma \setminus e$ obtained by contracting e using the usual formula for contraction in a reflection system. Combinatorially, contracting e reverses the cyclic order of the incoming darts on one side of e . (If the darts of e are adjacent around v , then all other darts into v are on the same side of e , so nothing gets reversed.) Topologically, the contraction detaches the twist M_e . The resulting map Σ / e is still a system of loops.

Symmetrically, because e is also an isthmus, *deleting* e also detaches a twist in the band decomposition, this time consisting of e^\square and a rectangle inside f^\square . The resulting map $\Sigma \setminus e$ is actually isomorphic (not just homeomorphic!) to Σ / e .

Theorem: *Every surface can be reduced to a sphere by detaching zero or more twists, and then detaching zero or more handles.*

For any integers $g \geq 0$ and $h \geq 0$, let $S(g, h)$ denote the surface obtained from the sphere by attaching g handles and h twists. Up to homeomorphism, it does not matter where or in what order the handles and twists are attached. In particular, if $h > 0$, we can even attach *disorienting* handles that destroy the orientability of the surface. The surface $S(g, h)$ is orientable if and only if $h = 0$.

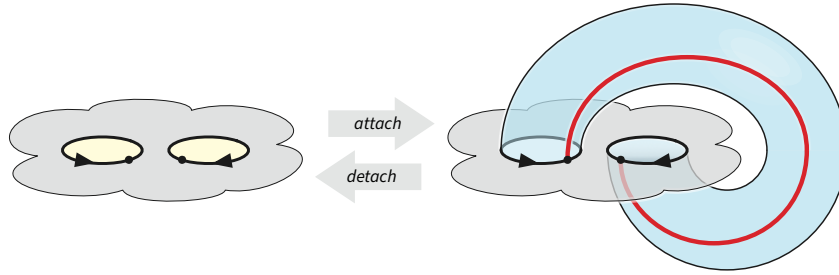


Figure 25.5: Detaching or attaching a disorienting handle.

Theorem: *Every non-orientable surface is homeomorphic to $S(g, h)$ for some integers $g \geq 0$ and $h > 0$.*

25.4 Dyck's Surface

Our classification of surfaces into classes $S(g, h)$ is not yet complete, because the same non-orientable surface can have multiple classifications, depending on the order in which we contract one-sided loops.

Consider the following example, called *Dyck's surface* after its discoverer Walter von Dyck (1888).² Let Σ be a system of three one-sided loops x, y, z incident to the unique vertex in the order x, y, x, z, y, z . Contracting y gives us an orientable system of loops on the torus $S(1, 0)$, implying that $|\Sigma| = S(1, 1)$. On the other hand, contracting either x or z yields a non-orientable system of loops on the Klein bottle $S(0, 2)$, implying that $|\Sigma| = S(0, 3)$. We conclude that $S(1, 1)$ and $S(0, 3)$ are actually the same surface.

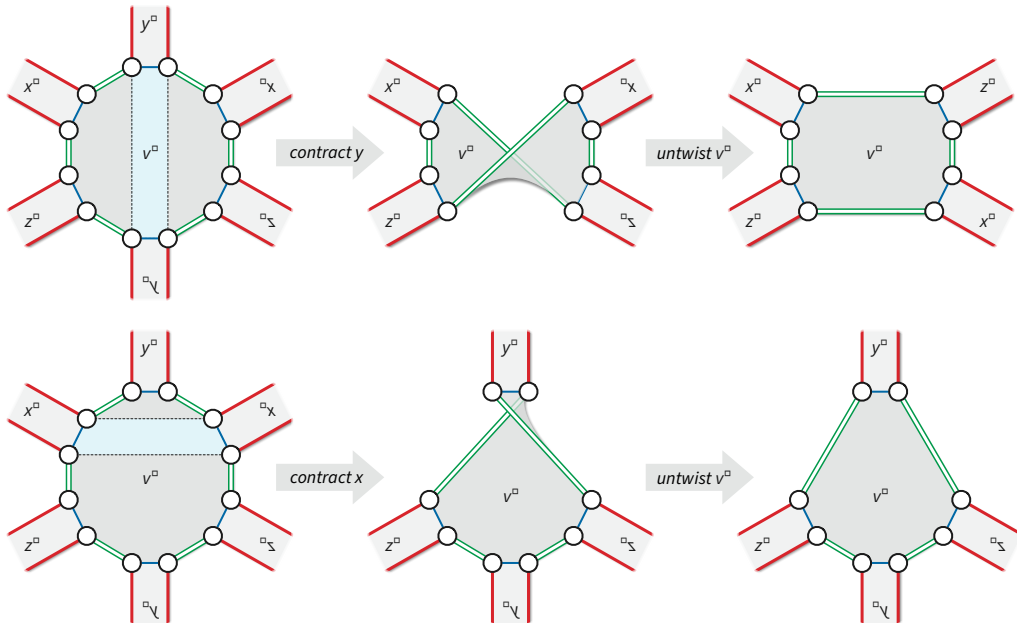


Figure 25.6: Contracting different one-sided loops on Dyck's surface yields either a torus (top) or a Klein bottle (bottom).

A straightforward inductive argument now implies the following more general equivalence, which in turn implies a simpler classification of non-orientable surfaces.

Lemma (Dyck): $S(g, h) = S(0, h + 2g)$ for all positive integers g and h .

Theorem: Every non-orientable surface is homeomorphic to $S(0, g)$ for some positive integer $g > 0$.

Again, the integer g is called the *genus* of the surface $S(0, g)$, or of any map on that surface.

25.5 Canonical Polygonal Schemata

Write this

25.6 “Oiler’s” Formula

The *Euler characteristic* $\chi(\Sigma)$ of a surface map $\Sigma = (V, E, F)$ is the integer $|V| - |E| + |F|$. Euler's formula states that every planar map has Euler characteristic 2. The following generalization,

²Dyck may be better known to computer scientists for proposing the *Dyck language*, which is the language of all properly balanced strings of brackets [and]. The Dyck language is also the set of all possible crossing sequence of a closed curve with winding number 0 around the origin with an arbitrary ray from the origin.

first proposed³ by the French mathematician Simon Antoine Jean l'Huilier in 1811, implies that the Euler characteristic is actually an invariant of the underlying surface.

Theorem: *Every map on the surface $\mathcal{S}(g, h)$ has Euler characteristic $2 - 2g - h$.*

Proof: Contraction and deletion preserve both the underlying surface and the Euler characteristic, so it suffices to consider a system of loops Σ . There are three cases to consider:

The trivial map (with one vertex, one face, and no edges) on the sphere $\mathcal{S}(0, 0)$ clearly has Euler characteristic 2.

Suppose Σ is orientable but not planar. Let e be any loop in Σ , and let e' be any edge between the two vertices of Σ / e . The system of loops $\Sigma / e \setminus e'$ has two fewer loops than Σ , and therefore has Euler characteristic $\chi(\Sigma) + 2$. It follows by induction that $\chi(\mathcal{S}(g, 0)) = 2 - 2g$.

Finally, suppose Σ is non-orientable. Let e be any one-sided loop in Σ . The system of loops Σ / e has one fewer loops than Σ , and therefore has Euler characteristic $\chi(\Sigma) + 1$. It follows by induction that $\chi(\mathcal{S}(g, h)) = \chi(\mathcal{S}(g, 0)) - h = 2 - 2g - h$. \square

Corollary: *Two surface maps lie on the same underlying 2-manifold if and only if (1) they are either both orientable or both non-orientable and (2) their Euler characteristics (or their genera) are equal.*

Corollary: *For any tree-cotree decomposition (T, L, C) of any surface map Σ , we have $|L| = 2 - \chi(\Sigma)$. Thus, $|L| = 2g$ if Σ is orientable, and $|L| = g$ if Σ is not orientable.*

In contexts where both orientable and non-orientable surface maps are being discussed, it is often convenient to use the *Euler genus* \bar{g} instead of the standard genus g . The Euler genus of a map Σ is equal to the number of leftover edges in any tree-cotree decomposition of Σ :

$$\bar{g} := |L| = 2 - \chi = \begin{cases} 2g & \text{if } \Sigma \text{ is orientable} \\ g & \text{if } \Sigma \text{ is not orientable} \end{cases}$$

The Combinatorial Gauss-Bonnet theorem also immediately generalizes from planar maps to surface maps. Let Σ be any surface map. Assign an arbitrary real value \angle_c to each corner c of a planar map Σ , called the *exterior angle* at c . Recall that *combinatorial curvature* of a face f or a vertex v , with respect to this angle assignment, is defined as follows:

$$\kappa(f) := 1 - \sum_{c \in f} \angle_c \quad \kappa(v) := 1 - \frac{1}{2} \deg(v) + \sum_{c \in v} \angle_c$$

The Combinatorial Gauss-Bonnet Theorem: *For any surface map $\Sigma = (V, E, F)$ and for any assignment of angles to the corners of Σ , we have $\sum_{v \in V} \kappa(v) + \sum_{f \in F} \kappa(f) = \chi(\Sigma)$.*

Proof: We immediately have $\sum_f \kappa(f) = |F| - \sum_c \angle_c$ and $\sum_v \kappa(v) = |V| - |E| + \sum_c \angle_c$, which implies that $\sum_v \kappa(v) + \sum_f \kappa(f) = |V| - |E| + |F| = \chi(\Sigma)$ by definition. \square .

³Actually, l'Huilier only proposed this formula for the special (orientable) case of polyhedra with disjoint prismatic tunnels. The full classification theorem is arguably due to August Möbius (1863), but was not properly formalized until the early 20th century, after the proof of the Jordan Curve Theorem.

25.7 References

1. Norman Biggs. Spanning trees of dual graphs. *J. Comb. Theory Ser. B* 11:127–131, 1971.
2. David Eppstein. Dynamic generators of topologically embedded graphs. *Proc. 14th Ann. ACM-SIAM Symp. Discrete Algorithms*, 599–608, 2003. arXiv:cs/0207082.
3. R. Bruce Richter and Herbert Shank. The cycle space of an embedded graph. *J. Graph Theory* 8:365–369, 1984.

25.8 Aptly Named Sir

Chapter 26

Homotopy in Surface Maps^α

There's not a lot in this section about *algorithms*, but there is a lot of important *structure*. Everything described in this note is based on *tree-cotree* decompositions.

Recall from the previous lecture that a *tree-cotree decomposition* of a surface map Σ is a partition of the edges E into three disjoint subsets $T \sqcup L \sqcup C$, where

- T is a spanning tree of Σ ,
- C^* is a spanning tree of the dual map Σ^* , and
- $L = E \setminus (C \cup T)$ is the set of *leftover edges*.

Every surface map has a tree-cotree decomposition (T, L, C) . In fact, we can choose either the spanning tree T or the complementary dual spanning tree C arbitrarily, just as we did for tree-cotree decompositions of planar maps.

More generally, suppose we modify a map Σ by repeatedly either (1) contracting an arbitrary non-loop edge or (2) deleting an arbitrary non-isthmus edge, until every edge is both a loop and an isthmus. Let T be the set of contracted edges, let V be the set of deleted edges, and let L be the final set of isthmus-loops (loop-isthmuses?). Then (T, L, C) is a tree-cotree decomposition of the original map Σ .

Equivalently, suppose we color the edges of Σ red, green, or blue in arbitrary order so that (1) every cycle contains at least one blue edge, (2) every edge cut contains at least one red edge, and (3) an edge is green if and only if it cannot be colored either red or blue. Then the red, green, and blue edges respectively define the spanning tree, leftover edges, and spanning cotree of a tree-cotree decomposition.

[[[Figure! Running example on a genus-2 map?]]]

26.1 Cut Graphs

A *cut graph* of a map Σ on surface S is any subgraph X of Σ such that $S \setminus X$ is an open topological disk. (Let me emphasize that here \setminus means to remove the points from the space, not merely deleting the edges from the map.)

Alternatively, we can define cut graphs in terms of a generalization of the *slicing* operation we already saw in the context of separators and minimum cuts. Slicing a map Σ along a subgraph X

produces a new map $\Sigma \setminus\! X$ which contains $\deg_X(v)$ copies of every vertex v of X , two copies of every edge of X , and at least one new face in addition to the faces of Σ . By convention, we think of the faces of $\Sigma \setminus\! X$ that are not faces of Σ as *holes* that are missing from the surface; thus, $\Sigma \setminus\! X$ is always a map of a surface *with boundary*. At least intuitively, $\Sigma \setminus\! X$ is the map obtained by gluing together the faces of Σ along every edge that is *not* in X . Then a cut graph of Σ is any subgraph X such that $\Sigma \setminus\! X$ is a closed disk.

[[[Figure]]]

For any tree-cotree decomposition (T, L, C) of Σ , the subgraph $T \cup L$ is a cut graph of Σ . Typically the cut graph $X = T \cup L$ will contain several vertices with degree 1; removing any such vertex from X yields a smaller cut graph. A *reduced* cut graph is a cut graph with no degree-1 vertices at all; equivalently, a reduced cut graph is a *minimal* subgraph X such that $\Sigma \setminus\! X$ is a disk. We can *reduce* any cut graph by repeatedly removing degree-1 vertices until none are left.¹

In any surface map with Euler genus $\bar{g} = 2 - \chi > 1$, every reduced cut graph can be further decomposed into at most $2\bar{g} - 2$ *cut paths* between at most $3\bar{g} - 3$ vertices with degree at least 3, called *branch points*. In particular, if every branch point has degree exactly 3, there are exactly $3\bar{g} - 3$ branch points and $2\bar{g} - 2$ cut paths. (The only two exceptional surfaces are the projective plane (non-orientable genus 1), where every reduced cut graph is a single one-sided cycle, and the sphere (orientable genus 0), where by convention every reduced cut graph is a single vertex.)

[[[Figure!]]]

26.2 Systems of Loops and Homotopy

Fix an arbitrary vertex x , called the *basepoint*. For each vertex v , let $\text{path}(v)$ denote the unique directed path in the spanning tree T from x to v . For every dart d , let $\text{loop}(d)$ denote the following directed closed walk:

$$\text{loop}(d) := \text{path}(\text{tail}(d)) \cdot d \cdot \text{rev}(\text{path}(\text{head}(d))).$$

Notice that $\text{loop}(\text{rev}(d)) = \text{rev}(\text{loop}(d))$.

Finally, let $\mathcal{L} = \{\text{loop}(e^+) \mid e \in L\}$, where e^+ denotes an arbitrary *reference* dart for edge e . The set \mathcal{L} is called a *system of loops* for Σ .

Recall that two closed curves in some space X are (*freely*) *homotopic* if one curve can be continuously deformed into the other on X . Similarly, two paths in X with the same endpoints are *homotopic* if one path can be continuously deformed into the other while keeping the endpoints fixed. A system of loops gives us the necessary structure to decide whether two curves are homotopic, similarly to the “fences” in our planar homotopy-testing algorithm.

26.3 What’s a “curve”?

But before we can start talking concretely about algorithms, we have to nail down the phrase “given two curves” and “given a surface”. Our planar homotopy algorithm assumes that input curves are given as *polygons*, specified as a sequence of vertex coordinates; while it is possible

¹A few papers refer to degree-vertices in a cut graph as *hair* and the reduction process as *shaving* the cut graph.

to impose coordinates on surfaces that would permit a natural generalization of “polygons”, imposing geometry is almost always both wasteful and unnecessary.²

It is usually simpler and more efficient to treat curves on surfaces purely combinatorially, representing surfaces as *maps* (using rotation systems or reflection systems), and representing curves using one of two natural combinatorial models:

- *Traversal*: We consider only curves that are walks in the graph of Σ ; curves cannot intersect faces, and if a curve intersects an edge, it must traverse that edge monotonically from one end to the other. We can represent any such curve as an alternating sequence of vertices and darts (directed edges). If the edges of Σ are weighted, the *length* of a curve α is the sum of the weights of the edges that α traverses, counted with appropriate multiplicity.
- *Crossing*: We consider only curves that intersect the edges of Σ transversely, away from the vertices, and whose intersection with each face of Σ is simple (injective). We can represent any such curve as an alternating sequence of faces and knives (oriented edges). If the edges of Σ are weighted, the *length* of a curve α is the sum of the weights of the edges that α crosses, counted with appropriate multiplicity.

These two models are clearly dual to each other; a crossing curve in Σ is equivalent to—or more formally, **IS**—a traversing curve in the dual map Σ^* , and vice versa. Which curve model we choose is strictly a matter of convenience. For the rest of this lecture, I'll use the traversal model.

26.4 Spur and Face Moves

Even though we do not allow the *input* curves to intersect the interiors of faces, we cannot impose the same restriction on *homotopies*. Recall that we can think of any homotopy as a continuously deforming curve. Even though the deforming curve starts and ends on the vertices and edges of Σ , it may pass through faces in some or all intermediate stages.

However, just as with generic curves in the plane, it turns out that any homotopy between traversal curves in surface maps can be decomposed into a finite sequence of combinatorial *moves*, of two types:

- A *spur* move either inserts or deletes a subpath consisting of a dart followed by its reversal; we call such a subpath a *spur* (or sometimes a *spike*).
- A *face* move replaces a subpath of the boundary of some face f with the complementary subpath on the boundary of f .

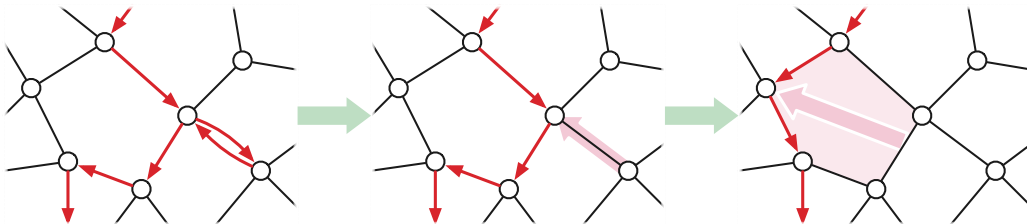


Figure 26.1: Traversal homotopy moves: A spur move followed by a face move.

²One natural exception to this rule is the *flat torus*, which is the metric space obtained by gluing opposite sides of the unit square (or any other parallelogram) in the plane. Homotopy testing on the flat torus is nearly trivial.

Thus, asking whether a closed walk W in some map Σ is contractible is a purely combinatorial problem: Is there a sequence of spur and face moves that transforms W into a trivial walk?

There is a dual pair of homotopy moves for crossing curves. The dual of a spur move, called a *bigon* move, deforms the curve to either insert or remove two consecutive crossings of the same edge. The dual of a face move, called a *vertex* move, deforms the curve across one vertex.

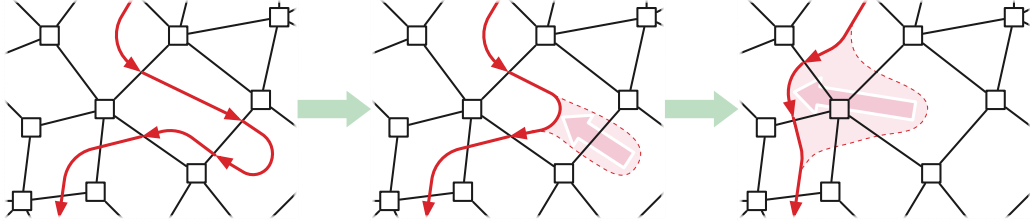


Figure 26.2: Crossing homotopy moves: A bigon move followed by a vertex move.

26.5 Characterizing Homotopy

Lemma: Let (T, L, C) be an arbitrary tree-cotree decomposition of a surface map Σ , and let x be a vertex of Σ . Every directed walk from x to x in Σ is homotopic to a directed walk from x to x in the cut graph $T \cup L$.

Proof: It suffices to prove that any dart d in C (or more formally, any dart whose edge is in C) is homotopic to a walk in $T \cup L$ from $\text{tail}(d)$ to $\text{head}(d)$.

Consider the fundamental domain $\Delta = \Sigma \setminus (T \cup L)$. The dart d is a boundary-to-boundary chord through the interior of Δ . Using a sequence of face moves, we can deform d to a path π around the boundary of Δ from $\text{tail}_\Delta(d)$ to $\text{head}_\Delta(d)$. This boundary path π projects to a walk in the cut graph $T \cup L$ from $\text{tail}_\Sigma(d)$ to $\text{head}_\Sigma(d)$. \square

Let \mathcal{L}^* denote the set of all loops formed by concatenating a finite sequence of loops in \mathcal{L} and their reversals. That is, $\ell \in \mathcal{L}^*$ if and only if one of the following recursive conditions is satisfied:

- ℓ is the empty loop
- $\ell = \text{loop}(e^+) \cdot \ell'$ for some edge $e \in L$ and some loop $\ell' \in \mathcal{L}^*$.
- $\ell = \text{loop}(e^-) \cdot \ell'$ for some edge $e \in L$ and some loop $\ell' \in \mathcal{L}^*$.

Lemma: Let (T, L, C) be an arbitrary tree-cotree decomposition of a surface map Σ , and let x be a vertex of Σ . Every directed walk from x to x in Σ is homotopic to a loop in \mathcal{L}^* .

Proof: In light of the previous lemma, it suffices to consider only walks in the cut graph $T \cup L$.

Consider the closed walk $w = v_0 \rightarrow v_1 \rightarrow v_2 \rightarrow \dots \rightarrow v_L$, where $v_0 = v_L = x$. We easily observe that w is homotopic to the concatenation of paths

$$\begin{aligned} & \text{path}(v_0) \cdot v_0 \rightarrow v_1 \cdot \text{rev}(\text{path}(v_1)) \cdot \text{path}(v_1) \cdot v_1 \rightarrow v_2 \cdot \text{rev}(\text{path}(v_2)) \cdots \\ & \quad \cdots \text{path}(v_{i-1}) \cdot v_{i-1} \rightarrow v_i \cdot \text{rev}(\text{path}(v_i)) \cdots \\ & \quad \cdots \text{path}(v_{L-1}) \cdot v_{L-1} \rightarrow v_L \cdot \text{rev}(\text{path}(v_L)) \\ & = \text{loop}(v_0 \rightarrow v_1) \cdot \text{loop}(v_1 \rightarrow v_2) \cdots \text{loop}(v_{i-1} \rightarrow v_i) \cdots \text{loop}(v_{L-1} \rightarrow v_L) \end{aligned}$$

because the initial path $\text{path}(v_0)$ and final path $\text{rev}(\text{path}(v_L))$ are both empty, and every intermediate path through T is immediately followed by its reversal.

Thus, it suffices to argue that every fundamental loop $\text{loop}(d)$ is homotopic to a loop in \mathcal{L}^* . Again, in light of the previous lemma, there are only two cases to consider:

- If $|d| \in L$, then by definition either $\text{loop}(d) \in \mathcal{L}$ or $\text{rev}(\text{loop}(d)) = \text{loop}(\text{rev}(d)) \in \mathcal{L}$.
- Suppose $|d| \in T$. Then $\text{loop}(d) = \text{path}(v) \cdot \text{rev}(\text{path}(v))$, where v is one of the endpoints of d , so we can deform $\text{loop}(d)$ to the empty loop, through a finite sequence of spur moves. \square

[[[Figure!]]]

This lemma does not *uniquely* characterize homotopy classes of loops; in fact, every loop based at x is homotopic to *infinitely* many loops in \mathcal{L}^* . In the next lecture, we'll develop an efficient algorithm to decide whether two loops are homotopic, in effect by defining a *canonical* loop in \mathcal{L}^* for each homotopy class.

26.6 References

26.7 Aptly Named Sir

- Pants decompositions (except possibly in passing)

Chapter 27

Planarization and Separation ^{α/β}

In this note I'll describe how to generalize several results about planar separators to more complex surface maps. These generalizations imply reductions from several problems on arbitrary surface maps to related (or even identical) problems on planar graphs, possibly with larger complexity.

The first step in any such reduction is to either delete or slice a subgraph of the input map to remove any interesting topology. We've already seen one example of such a subgraph: A *cut graph* in a surface map Σ is a subgraph X such that the sliced surface $\Sigma \setminus X$ is a disk. Unfortunately, it is easy to construct surface maps in which every cut graph uses a constant fraction of the edges, and we need sublinear complexity to support efficient reductions.

So instead we consider a weaker structure. A *planarizing* or *degenerating*¹ *subgraph* of Σ is any subgraph X such that the sliced surface $\Sigma \setminus X$ has genus 0, but possibly with more than one boundary cycle. Once we have planarizing subgraphs with sublinear complexity, we can use standard planar-separator techniques to balanced separators with sublinear complexity.

Throughout this note, we fix a surface *triangulation* Σ with n vertices and Euler genus $\bar{g} = o(n)$. (Surface maps with Euler genus $\Omega(n)$ do not have small planarizing subgraphs or small separators.) Euler's formula implies that Σ has exactly $3n - 6 + 3\bar{g} < 6n$ edges and $2n - 4 + 2\bar{g} < 4n$ faces.

27.1 Multiple Short Cycles

Lemma: *Let σ and τ be cycles in a surface map Σ . If either σ or τ is a separating cycle, then σ and τ cross an even number of times. Equivalently, if σ and τ cross an odd number of times, both σ and τ are nonseparating.*

Lemma [Albertson and Hutchinson]: *Every orientable surface triangulation contains a nonseparating cycle of length at most $2\sqrt{n}$.*

Proof: Let Σ be an orientable surface triangulation, and let σ be the shortest nonseparating cycle in Σ . Let σ^\flat and σ^\sharp denote the two copies of σ in the sliced map $\Sigma \setminus \sigma$, and let m denote the number of vertices in σ .

¹...because it removes all the genus.

Let S be the smallest subset of vertices of $\Sigma \setminus\!\!/\sigma$ that separates σ^\flat and σ^\sharp . The subgraph of Σ induced by S must contain (and therefore must be) a cycle τ that is homologous with σ and therefore nonseparating. Thus, τ has at least m vertices. Menger's Theorem now immediately implies that there are at least m vertex-disjoint paths from σ^\flat to σ^\sharp in $\Sigma \setminus\!\!/\sigma$.

On the other hand, let π be the shortest path in $\Sigma \setminus\!\!/\sigma$ from a node in σ^\flat to its clone in σ^\sharp . The edges of π comprise a cycle in Σ that crosses σ once and thus is nonseparating. It follows that π has length at least m . At most $m/2$ edges in π lie in either σ^\flat or σ^\sharp . Thus, every path from σ^\flat to σ^\sharp has at least $m/2$ edges.

We conclude that $n \geq m^2/2$. \square

Alberston and Hutchinson's proof requires orientability. If σ is a one-sided cycle in a nonorientable surface map Σ , the sliced map $\Sigma \setminus\!\!/\sigma$ has a single boundary cycle that covers σ twice. However, a similar result can be proved for nonorientable surface maps by considering the oriented double cover Σ^2 .

Corollary [Gilbert, Hutchinson, and Tarjan]: *Any surface map Σ with n vertices and genus g can be transformed into a genus-0 map by slicing along g cycles of total length $O(g\sqrt{n})$.*

Proof: Let Σ be an orientable surface map with genus g . Without loss of generality, we can assume that Σ is a simple triangulation; otherwise, remove all loops, remove all but one edge in every family of homotopic parallel edges, and triangulate every face with more than three sides. If $g = 0$, there is nothing to do, so assume otherwise. Let σ be the shortest noncontractible cycle in Σ . The map $\Sigma' = \Sigma \setminus\!\!/\sigma$ has at most $n + 2\sqrt{n}$ edges has genus $g - 1$. The result now follows by induction. \square

Hutchinson proved that every orientable surface triangulation contains a noncontractible cycle of length $O(\sqrt{n/g} \log g)$; the same inductive argument implies that we can planarize any orientable surface map by slicing along g cycles of total length $O(\sqrt{ng} \log g)$. Colin de Verdière, Hubbard, and Lazarus proved that there are surface maps in which every noncontractible cycle has length at least $\Omega(\sqrt{n/g} \log g)$; so Hutchinson's bound is tight in the worst case. Nevertheless it is possible to compute (slightly) smaller planarizing subgraphs.

27.2 Slabification

The following construction of a smaller planarizing subgraph is based on results of David Eppstein, which refines an earlier construction of Aleksandrov and Djidjev; similar techniques were also described by Hutchinson and Miller. Eppstein's construction uses the same notion of *depth contours* as Miller's planar cycle-separator algorithm, which we saw in Chapter 12.

Without loss of generality, assume that Σ is a simple triangulation. We start by building a tree-cotree decomposition (T, L, C) , where T is a breadth-first spanning tree rooted at an arbitrary source vertex s . For any vertex v , let $\text{depth}(v)$ denote the unweighted shortest-path distance from s to v , and define the depth of an edge or face to be the maximum depth of its vertices.

For any index j , the j th *depth contour* D_j of Σ is the subgraph induced by edges incident to both a face with depth j and a face with depth $j + 1$.

For any integers $i < j$, let $\Sigma[i, j]$ denote the subcomplex of Σ containing all faces f such that $i < \text{depth}(f) \leq j$, along with their incident edges and vertices; notice that the range of face-depths excludes the lower index i . We refer to $\Sigma[i, j]$ as a *slab* of Σ . In particular, $\Sigma[0, j]$ is the

subcomplex of vertices, edges, and faces with depth at most j , or equivalently, the component of $\Sigma \setminus\setminus D_j$ containing s . The boundary of $\Sigma[i, j]$ naturally partitions into its *upper* boundary D_{i-1} and its *lower* boundary D_j .

For any subset $L' \subseteq L$, let $Q(L') = \bigcup \{\text{loop}_T(\ell) \mid \ell \in L'\}$. In particular, $Q(L)$ is a (possibly unreduced) Qut graph of Σ , and $Q(\emptyset)$ is the empty subgraph.

Finally, for all indices $i < j$, let $L[i, j] = L \cap \Sigma[i, j]$ and $Q[i, j] = \Sigma[i, j] \cap Q(L[i, j])$. Each subgraph $Q[i, j]$ contains all edges $\ell \in L[i, j]$, along with shortest paths (through T) from the endpoints of ℓ “up” to the depth contour D_{i-1} .

Lemma: *For all indices $i < j$, $Q[i, j]$ is a planarizing subgraph of $\Sigma[i, j]$.*

Proof: Every submap of a genus-0 map has genus 0, so it suffices to consider the spacial case $i = 0$. Let Σ' be the surface map obtained from $\Sigma[0, j]$ by gluing a disk to each boundary cycle.

The intersection $T' = T \cap \Sigma'$ is a breadth-first spanning tree of $\Sigma[0, j]$, consisting of the first j levels of the global breadth-first spanning tree T .

The intersection $C \cap \Sigma'$ defines a forest in the dual map $(\Sigma')^*$, which spans every face except the caps. We can extend this coforest to a spanning cotree C' by adding edges that are not in T' (in fact, only edges on the boundary of $\Sigma[0, j]$).

Thus, we have a tree-cotree decomposition (T', L', C') of Σ' , where $L' = E(\Sigma') \setminus (C' \cup T') \subseteq L[0, j]$. It follows that $Q' = Q(L')$ is a cut graph for Σ' . On the other hand, Q' is a subgraph of $Q[0, j]$. \square

For any integers $0 \leq i < k$, let $D(i, k) = \bigcup \{D_j \mid j \bmod k = i\}$. Slicing Σ along these depth contours partitions it into several slabs:

$$\Sigma \setminus\setminus D(i, k) = \bigcup_a \Sigma[ak + i, (a+1)k + i].$$

Let $Q(i, k)$ denote the corresponding subgraph of the cut graph $Q(L)$:

$$Q(i, k) = \bigcup_a Q[ak + i, (a+1)k + i].$$

Finally, let $P(i, k) = D(i, k) \cup Q(i, k)$. The previous lemma implies that $P(i, k)$ is a planarizing subgraph of Σ , for all indices i and k .

Lemma: *For some integers i and k , the subgraph $P(i, k)$ has at most $2\sqrt{\bar{g}n}$ vertices.*

Proof: For each endpoint v of each edge in L , the subgraph $Q(i, k)$ contains the shortest path from v to its nearest ancestor in T that lies on the depth contour $D(i, k)$. This path has length $(\text{depth}(v) - i) \bmod k$. Moreover, $Q(i, k)$ is the union of all \bar{g} such subpaths with L . It follows that for any fixed k , we have

$$\sum_{i=0}^{k-1} |V(Q(i, k))| \leq \sum_{v \in V(L)} \sum_{i=0}^{k-1} (\text{depth}(v) - i) \bmod k = \bar{g}k(k-1) < \bar{g}k^2.$$

Each vertex and edge of Σ belongs to at most one depth contour D_i , so

$$\sum_{i=0}^{k-1} |V(D(i, k))| \leq n.$$

We conclude that

$$\sum_{i=0}^{k-1} |V(P(i, k))| \leq \bar{g}k^2 + n$$

which implies that for some index i , the subgraph $P(i, k)$ has at most $\bar{g}k + n/k$ vertices. In particular, some subgraph $P(i, \sqrt{n/\bar{g}})$ has at most $2\sqrt{\bar{g}n}$ vertices.² \square

Let $k^* = \sqrt{n/\bar{g}}$, and let i^* be the index i that minimizes the number of vertices in $P(i, k^*)$. Euler's formula implies that $P(i^*, k^*)$ has at most $12\sqrt{\bar{g}n}$ edges.

Theorem: *Every surface triangulation Σ with n vertices and Euler genus $\bar{g} < n$ has a planarizing subgraph $P(i^*, k^*)$ with $O(\sqrt{\bar{g}n})$ vertices and edges, which can be computed in $O(n)$ time.*

Proof: We can compute the breadth-first spanning tree T and the depths of every vertex, edge, and face of Σ in $O(n)$ time via (surprise, surprise) breadth-first search. Computing the depth contours D_j , the number of vertices in each subgraph $D(i, k^*)$, and the optimal index i^* in $O(n)$ time is straightforward. Then for each endpoint v of each edge in L , we walk upward in T marking edges, until we encounter either a marked edge or a vertex in $D(i^*, k^*)$. Because each edge of Σ is marked at most once, the total time to find the marked edges is their number plus $O(\bar{g})$, which is $O(n)$. The marked edges and L comprise the subgraph $Q(i^*, k^*)$. \square

Corollary: *Every surface triangulation Σ with n vertices and Euler genus $\bar{g} < n$ has a $(3/4)$ -separator with $O(\sqrt{\bar{g}n})$ vertices and edges, which can be computed in $O(n)$ time.*

Proof: The sliced surface $\Sigma \setminus\setminus P(i^*, k^*)$ has at most one component with more than $3/4$ of the faces of Σ . If there is such a component, apply the planar separator theorem within that component. \square .

27.3 Nice r -divisions

A *nice r -division* of a surface map Σ is a subdivision of Σ into subcomplexes called *pieces* with the following properties:

- Every face of Σ lies in exactly one piece.
- There are $O(n/r)$ pieces.
- Each piece has $O(r)$ vertices.
- Each piece has $O(\sqrt{r})$ boundary vertices.
- Each piece has $O(1)$ holes (boundary cycles).
- Each piece has genus 0.

This definition is identical to our definition of nice r -divisions of planar maps, except for the last condition, which is obviously redundant if Σ has genus 0. The definition implies that any nice r -division has a total of $O(n/\sqrt{r})$ boundary vertices.

Now suppose we wanted to extend our planarizing subgraph $P(i^*, k^*)$ to obtain a nice r -division. The number of vertices in $P(i^*, k^*)$ suggests we should try $r = O(n/\bar{g})$. Unfortunately, the partition $\Sigma \setminus\setminus P(i^*, k^*)$ has $\Theta(\sqrt{\bar{g}n})$ face-connected components, which is more than the $O(\bar{g})$ pieces we need for a nice $O(n/\bar{g})$ -division. Moreover, we have no control over the number of vertices, boundary vertices, and holes in each individual piece of $\Sigma \setminus\setminus P(i^*, k^*)$.

²More careful analysis implies the upper bound $\sqrt{\bar{g}n} = \sqrt{2gn}$ when Σ is orientable.

We can modify $P(i^*, k^*)$ to obtain a nice r -division, first by removing redundant cycles, and then by adding cycles to make the pieces nice.

First, consider the face-connected fragments of the map $\Sigma \setminus\setminus D(i^*, k^*)$ obtained by slicing only along the short depth contours $D(i^*, k^*)$. We call each fragment *interesting* if it contains at least one path through T from an endpoint of an edge in L to the upper boundary of that fragment. There are clearly at most $2\bar{g}$ interesting fragments. Let $U(i^*, k^*)$ denote the Union of the Upper boundaries of the interesting fragments, and let $P'(i^*, k^*) = U(i^*, k^*) \cup Q(i^*, k^*)$.

Lemma: $P'(i^*, k^*)$ is a planarizing subgraph of Σ with $O(\sqrt{\bar{g}n})$ vertices and edges. Moreover, $\Sigma \setminus\setminus P'(i^*, k^*)$ consists of $O(\bar{g})$ face-connected fragments.

The subgraph $P'(i^*, k^*)$ induces a partition \mathcal{P} of Σ into $O(\bar{g})$ genus-0 pieces, with a total of $O(\sqrt{\bar{g}n})$ boundary vertices and $O(\bar{g})$ holes. But the vertices, boundary vertices, and holes are not distributed evenly among the pieces, so we do not yet have a nice $O(n/\bar{g})$ -division. We apply a variant of the algorithm of Klein, Mozes, and Sommer to construct a nice $O(n/\text{barg})$ -division of each face-connected fragment of $\Sigma \setminus\setminus P'(i^*, k^*)$ in three phases.

- We repeatedly split pieces with more than n/\bar{g} vertices using balanced cycle separators, until every piece has at most n/barg vertices. This phase requires at most $O(\bar{g})$ splits. Naively, if we compute each cycle separator independently, the total time for this phase of the algorithm is $O(n \log g)$, but the time reduces to $O(n)$ if we use the faster Klein-Mozes-Sommer algorithm. The total number of boundary vertices at the end of this phase is $O(\sqrt{\bar{g}n})$.
- Next, we repeatedly split pieces whose boundary has more than $\sqrt{n/\bar{g}}$ vertices until no such pieces remain. We split each piece by giving each boundary vertex weight 1 and each interior vertex weight 0, and then computing a balanced cycle separator. Finding a cycle separator in a piece with $O(n/\bar{g})$ vertices takes $O(n/\bar{g})$ time. This phase requires at most $O(\bar{g})$ splits to evenly partition the $O(\sqrt{\bar{g}n})$ boundary vertices, so the total time for this phase is $O(n)$, even if we compute each cycle separator independently.
- Finally, we repeatedly split pieces that have more than (say) 20 boundary cycles until no such pieces remain. We split each piece by triangulating each hole with one additional vertex, giving the added vertices weight 1 and all other vertices weight 0, and then computing a balanced cycle separator. Finding a cycle separator in a piece with $O(n/\bar{g})$ vertices takes $O(n/\bar{g})$ time. This phase requires at most $O(\bar{g})$ splits to evenly partition the $O(\bar{g})$ holes, so the total time for this phase is $O(n)$.

Theorem: Given a surface map Σ with n vertices and Euler genus $\bar{g} = o(n)$, we can compute a nice (n/\bar{g}) -division of Σ in $O(n)$ time.

We can now compute r -divisions for smaller values of r , or even hierarchies of such divisions, by applying planar algorithms to the individual pieces of this (n/\bar{g}) -division.

Corollary: Given a surface map Σ with n vertices and Euler genus $\bar{g} = o(n)$, and any integer $r < n/\bar{g}$, we can compute a nice r -division of Σ in $O(n)$ time.

Corollary: Given a planar triangulation Σ with n vertices, and any exponentially decreasing vector $\vec{r} = (r_1, r_2, \dots, r_t)$ with $r_1 < n/\bar{g}$, we can construct a good \vec{r} -division of Σ in $O(n)$ time.

27.4 Applications

This construction allows us to extend several algorithms for planar maps to surface maps with no change in the running time, provided the genus is sufficiently small. For example, using the planar algorithms described earlier in these notes, we obtain the following:

Corollary: *Given a surface map Σ with n vertices and genus $g = o(n/\log^2 n)$, with non-negatively weighted darts, we can compute a single-source shortest path tree in Σ in $O(n \log \log n)$ time.*

(This time bound can be improved to $O(n)$.)

Corollary: *Given a surface map Σ with n vertices and genus $g = o(n/\log^2 n)$, with arbitrarily weighted darts, we can compute either a single-source shortest path tree or a negative cycle in Σ in $O(n \log^2 n / \log \log n)$ time.*

The only significant subtlety in generalizing the planar algorithms is some pieces in the relevant r -divisions can be adjacent to themselves across one of the paths in $Q(i^*, k^*)$. Thus, “boundary vertex” does not mean “vertex that belongs to more than one piece”; rather, pieces are defined by slicing the surface map along certain paths and cycles, and “boundary vertex” means a vertex on one of these slicing curves. The dense-distance graph of a piece is defined by shortest boundary-to-boundary paths *within* the piece, even though there may be shorter paths that use only vertices and edges of the piece but that cross the boundary of the piece.

27.5 References

1. Lyudmil Aleksandrov and Hristo Djidjev. Linear algorithms for partitioning embedded graphs of bounded genus. *SIAM J. Discrete Math.* 9(1):129–150, 1996.
2. Éric Colin de Verdière, Alfredo Hubard, and Arnaud de Mesmay. Discrete systolic inequalities and decompositions of triangulated surfaces. *Discrete Comput. Geom.* 53(3):587–620, 2015.
3. Hristo N. Djidjev. A separator theorem. *C. R. Acad. Bulg. Sci.* 34:643–645, 1981.
4. David Eppstein. Dynamic generators of topologically embedded graphs. *Proc. 14th Ann. ACM-SIAM Symp. Discrete Algorithms*, 599–608, 2003. arXiv:cs/0207082.
5. John R. Gilbert, Joan P. Hutchinson, and Robert Endre Tarjan. A separator theorem for graphs of bounded genus. *J. Algorithms* 5(3):391–407, 1984.
6. Joan P. Hutchinson. On short noncontractible cycles in embedded graphs. *SIAM J. Discrete Math.* 1(2):185–192, 1988.
7. Joan P. Hutchinson and Gary L. Miller. Deleting vertices to make graphs of positive genus planar. *Discrete Algorithms and Complexity Theory, Proc. Japan-US Joint Seminar, Kyoto, Japan*, 81–98, 1987. Academic Press.

27.6 Aptly Named Sir

- Local approximation (Baker-Eppstein)

Chapter 28

Homotopy Testing on Surface Maps $^{\beta}$

Let's return to one of the earliest problems we saw this semester: Given two curves in the same surface, decide whether they are *homotopic*, meaning one can be continuously deformed into the other. Here I'll describe a linear-time algorithm that slightly improves a classical algorithm of Max Dehn (1911).

To keep things simple, I'll focus on the following special case: Given a *closed* curve γ in some surface S , is γ *contractible* in S ? That is, can γ be continuously deformed on the surface S to a single point?

This question is obviously trivial in the plane or the sphere, and it turns out to be easy on the projective plane, torus, or Klein bottle, so without loss of generality, I will assume that the underlying surface has negative Euler characteristic $\chi < 0$. Let $\bar{g} = 2 - \chi$ denote the *Euler genus* of the input surface; recall that the Euler genus is equal to the standard genus if the surface is non-orientable, and twice the standard genus otherwise.

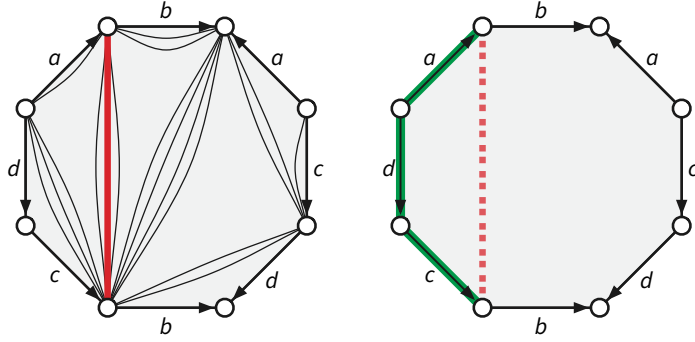
28.1 Reducing to a System of Loops

Let W be a given closed walk through some surface map Σ . Like every other surface-map algorithm, we begin by computing an arbitrary tree-cotree decomposition (T, L, C) of Σ . We then reduce Σ to a system of \bar{g} loops $\Lambda = \Sigma / T \setminus C$ by contracting every edge in T and then deleting every edge in C , simultaneously modifying the closed walk W as follows:

- When we contract edges in T , we simply remove any darts of T from W . After all edges in T are contracted, all remaining edges are loops.
- Then when we delete edges in C , we replace each dart in W whose edge is in C with a walk around the boundary of the unique face of Λ , as shown in the figure below.

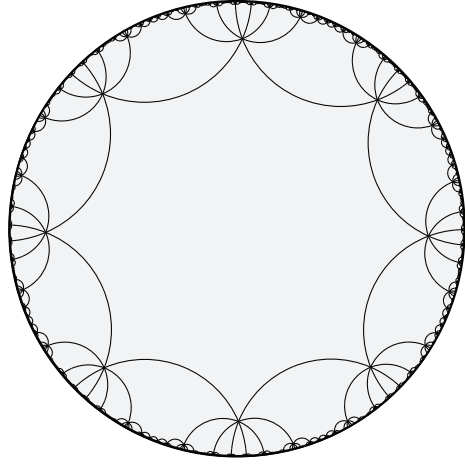
The reduction takes $O(n + \ell') = O(n + \bar{g}\ell)$ time to compute, where n is the complexity of the input map Σ , ℓ is the length of the input walk W in Σ , and ℓ' is the length of the transformed walk W' in Λ . (Later I'll remove the factor of \bar{g} by reducing to a slightly different map.)

We have now reached the special case of the homotopy problem that Dehn actually solved in 1911: Given a closed walk in a system of loops, is there a sequence of spur and face moves that reduce it to a trivial walk?

**Figure 28.1:** Reducing to a system of loops.

28.2 Universal Cover

The *universal cover* $\tilde{\Lambda}$ of Λ is an infinite planar map obtained by gluing an infinite lattice of copies of the single face of Λ along corresponding edges. Combinatorially, $\tilde{\Lambda}$ is isomorphic to a regular tiling of the *hyperbolic* plane by regular $2\bar{g}$ -gons meeting $2\bar{g}$ at each vertex. For example, if the input map Σ is an orientable map with genus 2, and therefore Euler genus 4, we reduce Σ to a system of loops Λ containing four loops. The universal cover $\tilde{\Lambda}$ of Λ is an 8-regular hyperbolic tiling by octagons.

**Figure 28.2:** The universal cover of an orientable system of loops with genus 2.

Formally, a *covering map* is a continuous surjection $\pi: \Sigma' \rightarrow \Sigma$ between topological spaces, such that each point $x \in \Sigma$ lies in an open neighborhood $U \subset \Sigma$ whose preimage $\pi^{-1}(U)$ is the disjoint union of open sets $\bigsqcup_{i \in I} U_i$, where the restriction of π to each set U_i is a homeomorphism to U . Space Σ' is called a *covering space* of Σ if there is a covering map from Σ' to Σ . By convention, covering spaces are assumed to be connected.

Covering maps can also be formulated combinatorially as follows. A *map-covering map* is a surjective function $\pi: \Sigma' \rightarrow \Sigma$ between *surface maps* that sends vertices to vertices, darts to darts, and faces to faces, and that preserves degrees of vertices and faces. For example, if the maps Σ' and Σ are represented rotation systems $(D', \text{rev}', \text{succ}')$ and $(D, \text{rev}, \text{succ})$, a covering map is a function $\pi: D' \rightarrow D$ such that $\text{rev} \circ \pi = \pi \circ \text{rev}'$ and $\text{succ} \circ \pi = \pi \circ \text{succ}'$, and π sends every orbit of succ' or $\text{rev}'(\text{succ})'$ bijectively to an orbit of succ or $\text{rev}(\text{succ})$, respectively. There is a similar

combinatorial formulation for reflection systems.

A *lift* of any vertex v of Σ to a covering space Σ' is a vertex v' of Σ' such that $\pi(v') = v$. Lifts of darts, edges, and faces are defined similarly. Locally, it is impossible to distinguish between a feature of Σ and any of its lifts in Σ' .

The *universal cover* of a space X is the unique (connected) covering space \tilde{X} that is *simply connected*, meaning all closed curves are contractible. The universal cover \tilde{X} is also the “largest” (connected) covering space of X , meaning \tilde{X} is a covering space of every (connected) covering space of X . For almost all surfaces, the universal cover is homeomorphic to the plane. (The only exceptions are the sphere, which is its own universal cover, and the projective plane, whose universal cover is the sphere.) Similarly, universal cover of any surface *map* Σ is a spherical map if Σ lies on the sphere or the projective plane, and an *infinite* planar map otherwise.

Lemma: *A closed walk W in a surface map Σ is contractible if and only if W is the projection of a closed walk \tilde{W} in the universal cover $\tilde{\Sigma}$.*

Proof: Let $\pi: \tilde{\Sigma} \rightarrow \Sigma$ denote the universal covering map.

First, let \tilde{W} be any closed walk in $\tilde{\Sigma}$, and let $W = \pi(\tilde{W})$. Because $\tilde{\Sigma}$ is simply connected, \tilde{W} must be contractible. Consider any sequence of spur moves and face moves $\tilde{W}_0 \rightarrow \tilde{W}_1 \rightarrow \tilde{W}_2 \rightarrow \dots \rightarrow \tilde{W}_N$ that reduces $\tilde{W} = \tilde{W}_0$ to a trivial closed walk \tilde{W}_N . For each index i , let $W_i = \pi(\tilde{W}_i)$. Then $W_0 \rightarrow W_1 \rightarrow W_2 \rightarrow \dots \rightarrow W_N$ is also a sequence of spur moves and face moves that reduces $W = W_0$ to a trivial walk W_N . Specifically, if $\tilde{W}_{i-1} \rightarrow \tilde{W}_i$ is a spur move on some edge \tilde{e} , then $W_{i-1} \rightarrow W_i$ is a spur move on the edge $\pi(\tilde{e})$, and if $\tilde{W}_{i-1} \rightarrow \tilde{W}_i$ is a face move on some edge \tilde{f} , then $W_{i-1} \rightarrow W_i$ is a face move on the edge $\pi(\tilde{f})$. We conclude that W is contractible.

Conversely, let W be any closed walk in Σ . Formally, W is an alternating sequence $v_0, d_1, v_1, d_2, \dots, d_\ell, v_\ell$ of vertices and darts, where $v_\ell = v_0$ and for each index i , we have $v_{i-1} = \text{tail}(d_i)$ and $v_i = \text{head}(d_i)$. We can iteratively lift W to a (not necessarily closed) walk \tilde{W} as follows. First, let \tilde{v}_0 be any lift of v_0 , and then for each index $i > 0$, let \tilde{d}_i be the unique lift of d_i whose tail is \tilde{v}_{i-1} , and let $\tilde{v}_i = \text{head}(\tilde{d}_i)$.

Now suppose W is contractible. Then there is a sequence $W_0 \rightarrow W_1 \rightarrow W_2 \rightarrow \dots \rightarrow W_N$ of spur and face moves transforming some trivial walk W_0 into $W_N = W$. (Yes, we are expanding here rather than contracting.) Fix an arbitrary lift \tilde{W}_0 of W_0 . Then for each index j , let \tilde{W}_j be the closed walk in $\tilde{\Sigma}$ obtained from \tilde{W}_{j-1} by lifting the move $W_{j-1} \rightarrow W_j$. Specifically, if $W_{j-1} \rightarrow W_j$ inserts a spur $v_i \rightarrow w \rightarrow v_i$ into W_{j-1} at its i th vertex v_i , then \tilde{W}_j is obtained by inserting a spur $\tilde{v}_i \rightarrow \tilde{w} \rightarrow \tilde{v}_i$ into \tilde{W}_{j-1} at its i th vertex \tilde{v}_i , where $\tilde{v}_i \rightarrow \tilde{w}$ is the unique lift of dart $v_i \rightarrow w$ whose tail is \tilde{v}_i . Face moves can be lifted similarly. By induction, each of the resulting walks \tilde{W}_j is closed, and therefore the final walk \tilde{W}_N is a closed walk such that $\pi(\tilde{W}_N) = W$. \square

With this lemma in hand, we can now phrase the contractibility problem in the form that Dehn' considered it. *Given a closed walk W in some system of loops Λ , is W the projection of a closed walk in the universal cover $\tilde{\Lambda}$?*

28.3 Dehn's Lemma

We use a version of the combinatorial Gauss-Bonnet theorem for surfaces with boundary (some faces marked as missing). Here curvature is defined as

$$\kappa(f) = 1 - \sum_{c \in f} \angle c \quad \kappa(v) = 1 - \frac{1}{2} \deg(v) + \sum_{c \in v} \angle c$$

where $\deg(v)$ is the number of *darts* incident to v , not the number of corners. Then as usual we have $\sum_v \kappa(v) + \sum_f \kappa(f) = \chi$. In our application, we will always set $\angle c = 1/4$, so

$$\kappa(f) = 1 - \frac{1}{4} \deg(f) \quad \kappa(v) = 1 - \frac{1}{2} \deg(v) + \frac{1}{4} \deg_2(v)$$

where $\deg_2(v)$ is the number of *corners* incident to v .

Lemma: *Every nontrivial closed walk \tilde{W} in $\tilde{\Lambda}$ contains either a spur or at least $2\bar{g} - 2$ consecutive edges on the boundary of some face.*

Proof: First consider the special case where \tilde{W} is a nontrivial *simple* closed walk; in particular, \tilde{W} has no spurs. Let $\Delta = (V, E, F)$ denote the map of the *disk* consisting of faces inside \tilde{W} . Assign every corner of Δ the angle $1/4$.

- For any face f , we have $\kappa(f) = 1 - \deg(f)/4 = 1 - \bar{g}/2 < 0$.
- For any interior vertex v , we have $\deg_2(v) = \deg(v)$ and therefore $\kappa(v) = 1 - \deg(v)/4 = 1 - \bar{g}/2 < 0$.
- For any boundary vertex v , we have $\deg_2(v) = \deg(v) - 1$ and therefore $\kappa(v) = 3/4 - \deg(v)$.

Call a boundary vertex of Δ *convex* if it is incident to exactly one face of Δ . Every convex boundary vertex has degree 2 in Δ and therefore has curvature $1/4$; all other vertices of Δ have curvature at most 0.

The combinatorial Gauss-Bonnet theorem implies that $\sum_v \kappa(v) + \sum_f \kappa(f) = 1$, which implies that

$$\left(1 - \frac{\bar{g}}{2}\right)|F| + \frac{1}{4}|V_+| \geq 1 \implies |V_+| \geq (2\bar{g} - 4)|F| + 4$$

where V_+ is the set of convex vertices. It follows that some face f is incident to $2\bar{g} - 3$ convex boundary vertices. These must be consecutive around the boundary of f . We conclude that f has $2\bar{g} - 2$ consecutive edges on the boundary of Δ . In fact, there must be at least two such faces, unless Δ consists of a single face.

Now suppose \tilde{W} is a non-simple closed walk in $\tilde{\Lambda}$. If \tilde{W} contains a spur, we are done, so assume otherwise. Let \tilde{x} be the first vertex to appear more than once along \tilde{W} , and let \tilde{X} be subwalk of \tilde{W} from the first occurrence of \tilde{x} to the second. If \tilde{X} is the boundary of a single face f , then \tilde{W} contains $2\bar{g}$ consecutive boundary edges of f . Otherwise, there are at least two faces f such that \tilde{X} contains at least $2\bar{g} - 2$ consecutive edges on the boundary of f . These two subpaths are disjoint, so at most one of them contains x , so at least one of them is a subpath of \tilde{W} . \square

Projection back to the system of loops immediately gives us the following corollary.

Corollary: Every nontrivial contractible closed walk W in Λ contains either a spur or at least $2\bar{g} - 2$ edges on the boundary of some face.

28.4 Dehn's algorithm!

Finally, Dehn's algorithm uses a simple greedy improvement strategy: Repeatedly remove spurs (using spur moves) and long boundary subpaths (using face moves) from W' until no more remain, and then return true if and only if the remaining walk is trivial. Correctness follows immediately from Dehn's lemma.

To find long boundary subpaths efficiently, we assign a unique label to each dart and represent W as a (circular) string of dart labels, sorted in a circular linked list. Then we slide a window of length $2\bar{g} - 2$ over the string, checking each of the $O(\bar{g})$ possible long boundary subpaths at each position. Using brute force string comparisons, this check takes $O(\bar{g}^2)$ time per position. We can improve this to $O(1)$ time per position by building a DFA that matches all long boundary subpaths; building this DFA adds $O(\bar{g}^2)$ time to preprocessing.

Whenever we find a long boundary subpath, we replace it with its complement (of length 2) and move the window back $2\bar{g}$ steps; we charge both the deletion and the time to find the long boundary subpath to the decrease in string length. Similarly, whenever we notice a spur, we can remove it in $O(1)$ time. The algorithm ends after $O(\ell')$ iterations.

Thus, the overall running time of Dehn's algorithm, starting with an arbitrary surface map Σ with complexity n and Euler genus \bar{g} , is $O(n + \bar{g}^2 + \bar{g}\ell)$.

28.5 System of quads

To remove the dependence on \bar{g} in the running time, we reduce to a different elementary map called a *system of quads*.

For any surface map $\Sigma = (V, E, F)$, the *radial map* $\Sigma^\diamond = (V^\diamond, E^\diamond, F^\diamond)$ is defined as follows:

- $V^\diamond = V \cup F^*$, where F^* is the set of vertices of the dual map Σ^* .
- Edges in E^\diamond correspond to corners in Σ . Any primal vertex v and dual vertex f^* are connected by one radial edge for each incidence between v and f .
- Faces in F^\diamond correspond to edges in Σ . Every face $e^\diamond \in F^\diamond$ has degree 4; its vertices are the endpoints of e and the endpoints of the dual edge e^* .

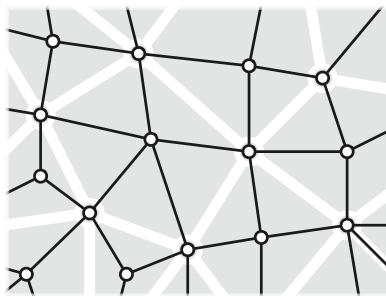


Figure 28.3: The radial map (black) of a surface map (white).

A system of quads is the radial map of a system of loops: $Q = \Lambda^\diamond$. This map has exactly 2 vertices, $2\bar{g}$ edges, and \bar{g} quadrilateral faces.

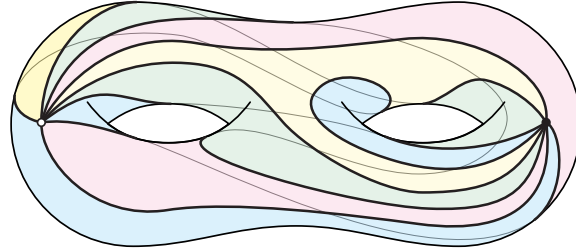


Figure 28.4: A system of quads on an orientable surface of genus 2 (and thus Euler genus 4). Each face has a unique color.

We can reduce an arbitrary closed walk W in an arbitrary map Σ to a homotopic closed walk W' in a system of quads Q by modifying our earlier reduction to a system of loops. Fix an arbitrary tree-cotree decomposition (T, L, C) , and contract the edges in the spanning tree T . Let v and f respectively denote the only vertex and the only face of the system of loops $\Lambda = \Sigma \setminus T / C$. Each edge e of $\Sigma \setminus T$ can be considered (or perturbed into) a path through f from one corner to another. We replace each such edge with the corresponding path of length 2 in $Q = \Lambda^\diamond$, from v to f^* to v . The resulting walk W' in Q has length at most 2ℓ , and the reduction requires $O(n + \ell)$ time.

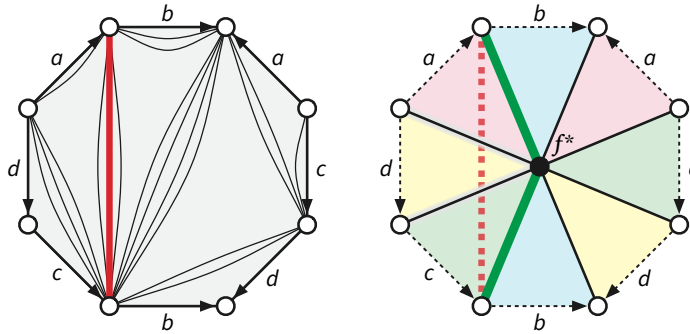


Figure 28.5: Reducing to a system of quads. (Pairs of triangles with the same color comprise faces.)

The universal cover of Q is a hyperbolic tiling by squares meeting $2\bar{g}$ at each vertex. Our earlier arguments imply that W' (and therefore W) is contractible if and only if W' is the projection of a closed walk in the universal cover \tilde{Q} .

28.6 Brackets

Dehn's lemma still applies to the infinite hyperbolic tiling \tilde{Q} —Every closed walk in \tilde{Q} contains either a spur of a subpath that covers all but two edges of some face. But now the complement of a “long” boundary subpath also has length 2; a single face move does not necessarily decrease the length of the walk. We need to find larger moves that are still simple enough to find and execute quickly, but that are guaranteed to shrink any closed walk.

To make this easier, we encode the walk W' as a *turn sequence*. The *turn* of any subwalk $u \rightarrow v \rightarrow w$ of W is the number of corners at the middle vertex v to the left of that subpath, modulo \bar{g} . Thus, for example, a *spur* is any subpath of W with turn 0. The regularity of the tiling \tilde{Q} implies that

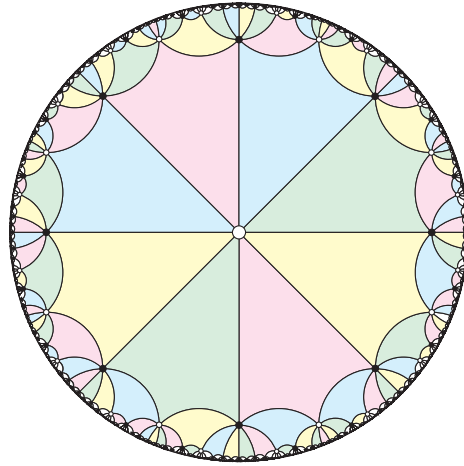


Figure 28.6: The universal cover of an orientable system of quads with genus 2.

the contractibility of any closed walk depends only on its (cyclic) turn sequence. Moreover, we can easily compute the turn sequence of any walk in time proportional to its length.

A *right bracket* is any subpath whose turn sequence consists of 1, followed by zero or more 2s, followed by 1. A *left bracket* is any subpath whose turn sequence has the form $-1, -2, \dots, -2, -1$, for any number of -2 s. (In the interest of readability, from now on I will indicate negation with a bar instead of a minus sign; for example, $\bar{2} = -2$.)

Bracket figure

Lemma: *Every nontrivial contractible closed walk in Q contains a spur or a bracket.*

Proof: [Combinatorial Gauss-Bonnet again.]

The previous lemma implies that we can reduce any nontrivial contractible closed walk in Q either using a spur move or by “sliding” a bracket. Both of these moves can be performed entirely by modifying the turn sequence. For example, removing a spur preceded by turn x and followed by turn y leaves a single turn with value $x + y$. (All turn arithmetic is implicitly performed modulo \bar{g} .)

$$\begin{aligned} x, 0, y &\rightsquigarrow x + y \\ x, 1, 2^k, 1, y &\rightsquigarrow x - 1, \bar{2}^k, y - 1 \\ x, \bar{1}, \bar{2}^k, \bar{1}, y &\rightsquigarrow x + 1, 2^k, y + 1 \end{aligned}$$

Here superscripts represent repetition, not exponentiation.

[[bracket slide figure]]

28.7 Reduction algorithm

To make detecting and sliding brackets easier, we actually store and manipulate a *run-length encoding* of the turn sequence. Instead of recording repeated turns explicitly, we store a sequence of pairs $((\tau_0, r_0), (\tau_1, r_1), \dots)$ to represent r_0 repetitions of turn τ_0 , followed by r_1 repetitions of τ_1 , and so on. Thus, any bracket turn sequence overlaps at most five runs. (In fact, it suffices to encode only runs of 2s and $\bar{2}$ s.)

We now proceed as in Dehn’s classical algorithm. We slide a window of width 5 over the run-length-encoded turn sequence; whenever the window contains a spur or a bracket, we modify the runs within the window to perform a spur move or bracket move, and then move the window back five steps. At each window position, we need $O(1)$ time to detect spurs and brackets, and $O(1)$ time to perform each spur or bracket move. The algorithm iterates until we have made a complete scan with no reductions, in which case we are done, or at most five runs remain in the run sequence, in which case we can complete the algorithm in $O(1)$ additional time. Standard amortisation arguments imply that the reduction algorithm runs in $O(\ell)$ time.

Thus, the overall running time of Dehn’s algorithm, starting with an arbitrary surface map Σ with complexity n , is $O(n + \ell)$, with no hidden dependence on the surface genus.

28.8 References

1. Max Dehn. Über unendliche diskontinuierliche Gruppen. *Math. Ann.* 71(1):116–144, 1911.
2. Max Dehn. Transformation der Kurven auf zweiseitigen Flächen. *Math. Ann.* 72(3):413–421, 1912.
3. Tamal K. Dey and Sumanta Guha. Transforming curves on surfaces. *J. Comput. Syst. Sci.* 58:297–325, 1999.
4. Jeff Erickson and Kim Whittlesey. Transforming curves on surfaces redux. *Proc. 24th Ann. ACM-SIAM Symp. Discrete Algorithms*, 1646–1655, 2013.
5. Francis Lazarus and Julien Rivaud. On the homotopy test on surfaces. *Proc. 53rd Ann. IEEE Symp. Found. Comput. Sci.*, 440–449, 2012. arXiv:1110.4573.

28.9 Sir Not

- surfaces with boundary
- projective plane, torus, and Klein bottle
- testing free homotopy between cycles
- isotopy testing for graph embeddings [Ladegaillerie 74] [Colin de Verdière and De Mesmay 14]

Chapter 29

Systems of Cycles and Homology^α

Homology is a natural equivalence relation between cycles, similar to but both simpler and coarser than homotopy; where homotopy treats cycles as *sequences* of darts, homology treats cycles as *sets of edges* (or more generally, *linear combinations* of darts). Homology can be defined with respect to any “coefficient ring”, but to keep the presentation simple, I’ll describe only the simplest special case (\mathbb{Z}_2 -homology) in this section, and return to a slightly more complicated special case (\mathbb{R} -homology) in a later note.

29.1 Cycles and Boundaries

Fix a surface map $\Sigma = (V, E, F)$ with Euler genus \bar{g} .

\mathbb{Z}_2 -homology is an equivalence relation between certain *subgraphs* of Σ , formally represented as subsets of E .

An even subgraph of Σ is a subgraph H such that $\deg_H(v)$ is even for every vertex $v \in V(\Sigma)$. The empty subgraph is an even subgraph, as is every simple cycle. Every even subgraph is the union (or symmetric difference) of simple edge-disjoint cycles.

For every edge $e \notin T$, let $\text{cycle}_T(e)$ denote the unique simple undirected cycle in the graph $T + e$; we call $\text{cycle}_T(e)$ a *fundamental cycle* with respect to T . Let $\mathcal{C} = \{\text{cycle}_T(e) \mid e \in L\}$. The set \mathcal{C} is called a *system of cycles* for the map Σ .

Fundamental Cycle Lemma: *Let T be an arbitrary spanning tree of an arbitrary graph G (sic). For every even subgraph H of G , we have*

$$H = \bigoplus_{e \in H \setminus T} \text{cycle}_T(e).$$

Thus, even subgraphs are symmetric differences of fundamental cycles.

Proof: Let H be an arbitrary even subgraph of G , and let $H' = \bigoplus_{e \in H \setminus T} \text{cycle}_T(e)$. The symmetric difference of any two even subgraphs is even, so $H \oplus H'$ is an even subgraph and therefore the union of edge-disjoint cycles. On the other hand, $H \oplus H'$ is a subgraph of T and therefore acyclic. We conclude that $H \oplus H'$ is empty, or equivalently, $H = H'$. \square

Mnemonically, any even subgraph can be *named* by listing its edges in $C \cup L$.

Let Z be a subset of the faces of Σ . The *boundary* of Z , denoted ∂Z , is the subgraph of Σ containing every edge that is incident to both a face in Z and a face in $F \setminus Z$. A *boundary subgraph* is any subgraph that is the boundary of a subset of faces. Every boundary subgraph is an even subgraph. Conversely, if Σ is a planar map, the Jordan curve theorem implies that every even subgraph is a boundary subgraph, but this equivalence does not extend to more complex surfaces.

Fundamental Boundary Lemma: *Let (T, L, C) be an arbitrary tree-cotree decomposition of a surface map Σ . For every boundary subgraph B of Σ , we have*

$$B = \bigoplus_{e \in B \cap C} \text{bdry}_C(e).$$

Thus, boundary subgraphs are symmetric differences of fundamental boundaries.

Proof: We mirror the proof of the Fundamental Cycle lemma. Let B be any boundary subgraph, and let $B' = \bigoplus_{e \in B \cap C} \text{bdry}_C(e)$. The boundary space is closed under symmetric difference, so $B' \oplus B$ is a boundary subgraph. On the other hand, $B \oplus B'$ has no edges in C , so $B \oplus B'$ is a subgraph of the cut graph $T \cup L$. We conclude that $B \oplus B'$ is empty, or equivalently, $B = B'$. \square .

Mnemonically, any boundary subgraph can be *named* by listing its edges in C .

29.2 Homology

Finally, two subgraphs A and B of Σ are (\mathbb{Z}_2) -homologous if their symmetric difference $A \oplus B$ is a boundary subgraph of Σ . For example, every boundary subgraph is homologous with the empty subgraph, which is why boundary subgraphs are also called *null-homologous* subgraphs. Straightforward definition-chasing implies that (\mathbb{Z}_2) -homology is an equivalence relation, whose equivalence classes are obviously called (\mathbb{Z}_2) -homology classes. We usually omit “ \mathbb{Z}_2 ” if the type of homology is clear from context.

Lemma: *Let (T, L, C) be an arbitrary tree-cotree decomposition of a surface map Σ . The only boundary subgraph of the cut graph $T \cup L$ is the empty graph.*

Proof: Let H be a non-empty cut graph in Σ ; H must be the boundary of a non-empty proper subset Z of the faces in Σ . Consider the fundamental domain $\Delta = \Sigma \setminus (T \cup L)$. Because both Z and its complement are non-empty, some interior edge e of Δ separates a face in Z from a face not in Z . But the interior edges of Δ are precisely the edges in C . \square

Lemma: *Let (T, L, C) be an arbitrary tree-cotree decomposition of a surface map Σ . Every even subgraph in Σ is homologous with an even subgraph of the cut graph $T \cup L$.*

Proof: It suffices to prove that every edge $e \in C$ is homologous with a subgraph of $T \cup L$ that has even degree everywhere except the endpoints of e .

Consider the fundamental domain $\Delta = \Sigma \setminus (T \cup L)$. Every edge $e \in C$ appears in Δ as a boundary-to-boundary chord, which partitions the faces of Δ into two disjoint subsets $Y \sqcup Z$. (Recall that no edge in C can be an isthmus!) Every face of Δ is a face of the original map Σ and vice versa; let β denote the boundary of Y (or equivalently, the boundary of Z) in Σ . Because β is a boundary subgraph in Σ , e is homologous with $\beta \oplus e$. Finally, every edge in $\beta \oplus e$ is an edge in the cut graph $T \cup L$. \square

Lemma: Let (T, L, C) be an arbitrary tree-cotree decomposition of a surface map Σ . Every subgraph of Σ is homologous with a symmetric difference of cycles in \mathcal{C} .

Proof: By the previous lemma, it suffices to consider only even subgraphs of the cur graph $T \cup L$.

Every even subgraph of $T \cup L$ is the symmetric difference of simple cycles in $T \cup L$. The simple cycles in $T \cup L$ are precisely the cycles in \mathcal{C} . \square

Homology Basis Theorem: Let (T, L, C) be an arbitrary tree-cotree decomposition of a surface map Σ . For every even subgraph H of Σ , we have

$$H = \left(\bigoplus_{i \in I(H)} \text{cycle}_T(\ell_i) \right) \oplus \left(\bigoplus_{e \in H \cap C} \text{bdry}_T(e) \right)$$

for some subset $I(H) \subseteq \{1, 2, \dots, \bar{g}\}$. Thus, every even subgraph is homologous with the symmetric difference of a **unique** subset of cycles in \mathcal{C} , which is nonempty if and only if H is a boundary subgraph.

The Homology Basis Theorem immediately implies an algorithm to decide if two even subgraphs H and H' are homologous: Compute their canonical decompositions into fundamental cycles and boundaries, with respect to the same tree-cotree decomposition, and then compare the index sets $I(H)$ and $I'(H)$. A careful implementation of this algorithm runs in $O(\bar{g}n)$ time; details are left as an exercise (because we're about to describe simpler algorithms).

29.3 Relax, it's just linear algebra!

Unlike our earlier characterization of homotopy, our characterization of homology is unique; every even subgraph is homologous with the symmetric difference of *exactly one* subset of cycles in \mathcal{C} . The easiest way to prove this fact is to observe that subgraphs, even subgraphs, boundary subgraphs, and homology classes all define vector spaces over the finite field $\mathbb{Z}_2 = (\{0, 1\}, \oplus, \cdot)$. In particular, homology can be viewed as a linear map between vector spaces.

Subgraphs (subsets of E) comprise the **edge space** (or *first chain space*) $C_1(\Sigma) = \mathbb{Z}_2^{|E|}$. The (indicator vectors of) individual edges in Σ comprise a basis of the edge space.

Even subgraphs of Σ comprise a subspace of $C_1(\Sigma)$ called the **cycle space** $Z_1(\Sigma)$. The Fundamental Cycle Lemma implies that the fundamental cycles $\text{cycle}_T(e)$, for all $e \notin T$, define a basis for the cycle space. The number of fundamental cycles is equal to the number of edges not in T , which is $|E| - (|V| - 1)$. Thus, $Z_1(\Sigma) = \mathbb{Z}_2^{|E| - |V| + 1}$.

Boundary subgraphs of Σ comprise a subspace of $Z_1(\Sigma)$ called the **boundary space** $B_1(\Sigma)$. The Fundamental Boundary lemma implies that the fundamental boundaries $\text{bdry}_C(e)$, for all $e \in C$, define a basis for the boundary space. The number of fundamental boundaries is equal to the number of edges of C , which is $|F| - 1$. Thus, $B_1(\Sigma) = \mathbb{Z}_2^{|F| - 1}$.

Finally, the set of homology classes of even subgraphs of Σ comprise the (*first*) **homology space**, which is the quotient space

$$\begin{aligned} H_1(\Sigma) &:= Z_1(\Sigma)/B_1(\Sigma) \\ &= \mathbb{Z}_2^{|E| - |V| + 1}/\mathbb{Z}_2^{|F| - 1} \\ &\cong \mathbb{Z}_2^{|E| - (|V| - 1) - (|F| - 1)} \\ &= \mathbb{Z}_2^{|E| - |T| - |C|} = \mathbb{Z}_2^{|L|} = \mathbb{Z}_2^{\bar{g}}. \end{aligned}$$

(Hey look, we proved Euler's formula again!) The Homology Basis Theorem implies that homology classes of fundamental cycles $\text{cycle}_T(e)$, for all $e \in L$, define a basis for the homology space. In particular, there are exactly $2^{\bar{g}}$ distinct homology classes.

29.4 Crossing Numbers

Another way to characterize the homology class of an even subgraph H is to determine which cycles in a system of cycles *cross* H . The definition of “cross” is rather subtle, but mirrors the intuition of transverse intersection.

Consider two distinct simple cycles α and β , and let π be one of the components of the intersection $\alpha \cap \beta$. (Because $\alpha \neq \beta$, the intersection π must be either a single vertex or a common subpath.) We call π a *crossing* between α and β (or we say that α and β *cross at* π) if, after contracting the path π to a point p , the contracted curves α/π and β/π intersect transversely at p .

Equivalently, α and β cross at π if, no matter how we perturb the two curves within a small neighborhood of π , the two perturbed curves $\tilde{\alpha}$ and $\tilde{\beta}$ intersect. By convention, no two-sided cycle crosses itself (because we can perturb two copies of a two-sided cycle so that they are disjoint), but every one-sided cycle crosses itself once (because we cannot).

For any simple cycles α and β , the *crossing number* $\text{cr}(\alpha, \beta)$ is the number of crossings between α and β , modulo 2. In particular, $\text{cr}(\alpha, \alpha) = 0$ if for every two-sided cycle α , and $\text{cr}(\beta, \beta) = 1$ for every one-sided cycle β .

We can extend this definition of crossing number to even subgraphs by linearity: $\text{cr}(\alpha \oplus \beta, \gamma) = \text{cr}(\alpha, \gamma) \oplus \text{cr}(\beta, \gamma)$. Although one can express any even subgraph as a symmetric difference of cycles in many different ways, crossing numbers are the same for every such decomposition.

For any face f and any cycle γ , we have $\text{cr}(\partial f, \gamma) = 0$. It follows by linearity that if either γ or δ is a boundary subgraph, then $\text{cr}(\delta, \gamma) = 0$. More generally, it follows that crossing numbers are a *homology invariant*: if α and β are homologous even subgraphs, then $\text{cr}(\alpha, \gamma) = \text{cr}(\beta, \gamma)$ for every cycle γ , because $\alpha \oplus \beta$ is the symmetric difference of face boundaries.

Lemma: *For any even subgraphs H and H' , if $\text{cr}(H, H') = 1$, then neither H nor H' is a boundary subgraph.*

Proof: If (say) H is a boundary subgraph, then H is the symmetric difference of face boundaries, and therefore $\text{cr}(H, H') = 0$ by linearity. \square

Lemma: *Let σ be a simple cycle and let $\mathcal{C} = \{\gamma_1, \gamma_2, \dots, \gamma_{\bar{g}}\}$ be a system of cycles in a surface map Σ . Then σ is boundary cycle if and only if $\text{cr}(\sigma, \gamma_i) = 0$ for every cycle $\gamma_i \in \mathcal{C}$.*

Proof: If σ is a boundary cycle, homology invariance immediately implies $\text{cr}(\sigma, \gamma_i) = \text{cr}(\emptyset, \gamma_i) = 0$.

Suppose on the other hand that σ is not a boundary cycle. Then by definition the sliced surface $\Sigma \setminus \sigma$ is connected. Let v be a vertex of σ , and let π be any path from v^+ to v^- in $\Sigma \setminus \sigma$. This path π appears in Σ as a closed walk that crosses σ exactly once, so $\text{cr}(\pi, \sigma) = 1$. It follows from the previous lemma that π is not a boundary cycle. Thus, by the Homology Basis theorem, π is homologous with $\bigoplus_{i \in I} \gamma_i$ for some non-empty subset $I \subseteq \{1, 2, \dots, \bar{g}\}$. Finally, homology invariance implies $\text{cr}(\pi, \sigma) = \bigoplus_{i \in I} \text{cr}(\gamma_i, \sigma) = 1$, so we

must have $\text{cr}(\gamma_i, \sigma) = 1$ for an odd number of indices $i \in I$, and therefore for at least one such index. \square

Corollary: Let \mathcal{C} be a system of cycles in a surface map Σ . An even subgraph H of Σ is a boundary subgraph if and only if $\text{cr}(H, \gamma_i) = 0$ for every cycle $\gamma_i \in \mathcal{C}$. Two even subgraphs H and H' of Σ are homologous if and only if $\text{cr}(H, \gamma_i) = \text{cr}(H', \gamma_i)$ for every cycle $\gamma_i \in \mathcal{C}$.

29.5 Systems of Cocycles and Cohomology

Cohomology is the dual of homology. While homology is an equivalence relation between subgraphs of maps, cohomology is an equivalence relation between subgraphs of *dual* maps. In fact, it's the *dual* equivalence relation between subgraphs of dual maps. Two subgraphs A and B of Σ are *cohomologous* if and only if the corresponding dual subgraphs A^* and B^* of Σ^* are homologous.

I'll adopt the convenient convention of adding the prefix “co” to indicate the dual of a structure in the dual map. Mnemonically, a cosnarfle in Σ is the dual of snarfle in Σ^* .

- We've already defined a *spanning co-tree* of Σ is a subset of edges whose corresponding dual edges comprise a spanning tree of Σ^* . Less formally, a spanning cotree of Σ is the dual of a spanning tree of Σ^* .
- A *cocycle* in Σ is the dual of a cycle in Σ^* . (In planar graphs, every cocycle is a minimal edge cut, but that equivalence does not extend to more complex surfaces.)
- A *co-even subgraph* of Σ is the dual of an even subgraph of Σ^* . That is, a subgraph H of Σ is co-even if every face of Σ has an even number of incidences with H . No edge in a co-even subgraph is a loop, because loops are co-isthmuses.
- The *coboundary* if a subset X of vertices of Σ , denoted δX , is the dual of the boundary of the corresponding subset X^* of faces of Σ^* . That is, δX is the subset of edges with one endpoint in X and one endpoint not in X . A *coboundary* subgraph is the coboundary of some subset of vertices. Every coboundary subgraph is co-even.
- Finally, two co-even subgraphs are cohomologous if their symmetric difference is a coboundary subgraph.

As usual, fix a tree-cotree decomposition (T, L, C) of a surface map Σ . For every edge $e \in T \cup L$, let $\text{cocycle}_C(e)$ denote the subgraph of Σ dual to the fundamental cycle $\text{cycle}_{c^*}(e^*)$ in the dual map Σ^* . Finally, let $\mathcal{K} = \{\text{cocycle}_C(e) \mid e \in T\}$. The following lemmas follow immediately from our earlier characterization of homology.

Lemma: Let (T, L, C) be an arbitrary tree-cotree decomposition of a surface map Σ . Every co-even subgraph of Σ a symmetric difference of fundamental cocycles $\text{cocycle}_C(e)$ where $e \notin C$.

Lemma: Let (T, L, C) be an arbitrary tree-cotree decomposition of a surface map Σ . Every co-even subgraph of Σ is cohomologous with a co-even subgraph of the cocut graph $C \cup L$.

Lemma: Let (T, L, C) be an arbitrary tree-cotree decomposition of a surface map Σ . Every co-even subgraph of Σ is cohomologous with a symmetric difference of cocycles in \mathcal{K} .

29.6 Homology Signatures

More importantly, however, cohomology offers us a **COnvenient** method to efficiently **CO**mpute homology classes of even subgraphs of the primal map Σ , by assigning a **CO**ordinate system to the first homology space. Index the leftover edges in L as $\ell_1, \ell_2, \dots, \ell_{\bar{g}}$.¹ For every edge e in Σ , the *homology signature* $[e]$ is the \bar{g} -bit vector indicating which cocycles in \mathcal{K} contain e . Specifically:

$$[e]_i = 1 \iff e \in \text{cocycle}_C(\ell_i).$$

Finally, the homology signature $[H]$ of any subgraph H is the bitwise exclusive-or of the homology signatures of its edges.

The function $H \mapsto [H]$ is a *linear* function from the cycle space $Z_1(\Sigma)$ to the vector space $\mathbb{Z}_2^{\bar{g}}$ of homology signatures. In particular:

Linearity Lemma: *For any two even subgraphs H and H' of Σ , we have $[H \oplus H'] = [H] \oplus [H']$.*

Basis Lemma: *For all indices i and j , we have $[\text{cycle}_T(\ell_i)]_j = 1$ if and only if $i = j$.*

Proof: The only edge in any fundamental cycle $T(e)$ that is *not* in T is the determining edge e . Similarly, the only edge in any fundamental cocycle $C(e)$ that is *not* in C is the determining edge e . Thus, $\text{cycle}_T(\ell_i) \cap \text{cocycle}_C(\ell_j) = \emptyset$ whenever $i \neq j$, and $\text{cycle}_T(\ell_i) \cap \text{cocycle}_C(\ell_i) = \ell_i$ for every index i . \square

Theorem: *Two even subgraphs H and H' of Σ are homologous if and only if $[H] = [H']$.*

Proof: By the Linearity Lemma, it suffices to prove that an even subgraph H is a boundary subgraph if and only if $[H] = 0$.

Let f be any face of Σ , and let λ be any cocycle in Σ . The boundary of f either contains no edges of λ or exactly two edges of λ , depending on whether the dual cycle λ^* contains the dual vertex f^* . It follows that $[\partial f] = 0$ for every face f . The Linearity Lemma implies that $[H] = 0$ for every boundary subgraph H .

Conversely, suppose H is not null-homologous. Then we can write

$$H = \left(\bigoplus_{i \in I} \text{cycle}_T(\ell_i) \right) \oplus \left(\bigoplus_{e \in H \cap C} \text{bdry}_T(e) \right)$$

for some nonempty subset $I \subseteq \{1, 2, \dots, \bar{g}\}$. The Linearity and Basis lemmas imply that

$$[H] = \left(\bigoplus_{i \in I} [\text{cycle}_T(\ell_i)] \right)$$

and therefore $[H]_i = 1$ if and only if $i \in I$. Because I is non-empty, $[H] \neq 0$. \square

29.7 Separating Cycles

Lemma: *Let γ be a simple cycle in a surface map Σ . The sliced map $\Sigma \setminus \gamma$ is disconnected if and only if $[\gamma] = 0$*

¹Here I'm using ℓ as a mnemonic for "leftover edge" instead of "loop". We have a lot of other e 's flying around, so I don't want to use e_i to denote the i th edge in L .

29.8 References

29.9 Aptly Named Sir

- Pants decompositions (except possibly in passing)

Chapter 30

Shortest Interesting Cycles^α

In this lecture, I'll describe algorithms to find the shortest cycle in a surface map that is topologically interesting. I'll specifically consider two different definitions of "interesting":

- A cycle is *noncontractible* if it cannot be continuously deformed to a single point; noncontractible cycles are *homotopically* nontrivial.
- A cycle is *nonseparating* if slicing along the cycle does not disconnect the surface; nonseparating cycles are *homologically* nontrivial.

The input to our algorithms is a surface map Σ with positively weighted edges.¹ I will assume throughout this presentation that there is a unique shortest path between any pair of vertices; this assumption can be enforced with standard perturbation schemes. Crucially, we will treat the underlying graph of Σ as a continuous topologically space; any edge with weight ℓ is isometric to the interval $[0, \ell]$ on the real line. Thus, we can reasonably consider shortest paths between points that lie in the interior of edges.

30.1 Properties of Shortest Nontrivial Cycles

It is unfortunately common for papers on surface-map algorithms to use the word "cycle" in two different senses. For topologists, a *cycle* is the continuous image of the circle S^1 , but for graph theorists, a *cycle* is a closed walk with no repeated vertices. That is, graph theorists assume that cycles are *simple* (or *injective*), but topologists do not. Fortunately for us, shortest nontrivial cycles are the same for both tribes.

Lemma: *The shortest noncontractible (or nonseparating) closed walk in a positively edge-weighted surface map is a simple cycle.*

Proof: For the sake of argument, suppose the shortest noncontractible closed walk W is *not* simple. We can decompose W into two closed walks $X \cdot Y$ at any vertex that W visits more than once. X and Y are both shorter than W , so they must both be contractible. The concatenation of two contractible closed walks is contractible. So W is contractible, contradicting its definition. Essentially the same argument applies to the shortest nonseparating closed walk. \square

¹With more effort, these algorithms can be generalized to *directed* surface maps with asymmetrically weighted *darts*.

3-Path Condition (Carsten Thomassen): Let x and y be two points (either at vertices or in edge interiors) in a surface map Σ , and let α, β, γ be paths in Σ from x to y . If the cycles $\alpha \cdot \text{rev}(\beta)$ and $\beta \cdot \text{rev}(\gamma)$ are contractible (resp. separating), then the cycle $\alpha \cdot \text{rev}(\gamma)$ is also contractible (resp. separating).

Proof: The concatenation of any two contractible closed walks is contractible.

The symmetric difference of any two separating cycles is separating. \square

Antipodality Condition (Carsten Thomassen): Let σ be the shortest noncontractible (resp. nonseparating) cycle in a surface map Σ . Any pair of antipodal points partition σ into two equal-length shortest paths.

Proof: Fix a pair x and \bar{x} of antipodal points in σ . These points clearly partition σ into two equal-length paths; call these paths α and β . Suppose α and β are not shortest paths, and let γ be a shortest path from x to \bar{x} . The cycles $\alpha \cdot \text{rev}(\gamma)$ and $\beta \cdot \text{rev}(\gamma)$ are both shorter than $\alpha \cdot \text{rev}(\beta) = \sigma$ and thus are contractible (resp. separating). But then the 3-path property implies that σ is contractible (resp. separating), contradicting its definition. \square

Crossing Condition: Any shortest path crosses the shortest noncontractible (resp. nonseparating) cycle at most once.

Proof: Let π be a shortest path and let σ be a simple noncontractible (resp. separating) cycle, and suppose the intersection $\pi \cap \sigma$ is disconnected. Then we can decompose π into three subpaths $\pi^- \cdot \pi^\circ \cdot \pi^+$, where π° starts and ends at vertices of σ but is otherwise disjoint from σ . Because π is a shortest path, its subpath π° is also a shortest path. Similarly, we can decompose σ into two paths α and β at the endpoints of π° . The 3-path condition implies that at least one of the cycles $\alpha \cdot \text{rev}(\pi^\circ)$ and $\beta \cdot \text{rev}(\pi^\circ)$ is noncontractible (resp. nonseparating). Because vertex-to-vertex shortest paths are unique, both of these cycles are shorter than σ . \square

30.2 A polynomial-time algorithm

Thomassen's 3-path condition implies the following algorithm to find the shortest noncontractible cycle σ . The antipodality condition implies that σ must consist of a shortest path from a vertex x to another vertex y , the edge yz , and the shortest path from z back to x . (Uniqueness of vertex-to-vertex shortest paths implies that the antipodal point \bar{x} lies in the interior of the edge yz .) There are only $O(n^2)$ loops of this form. We compute the distance between every pair of vertices in $O(n^2 \log n)$ time by running Dijkstra's algorithm n times, after which we can compute the length of each candidate cycle in $O(1)$ time. Finally, for each candidate loop γ , we test whether γ is contractible in $O(n)$ time, using Dehn's algorithm. Finally, we return the shortest candidate cycle that is noncontractible.

Theorem [Thomassen]: Given any edge-weighted surface map Σ with complexity n , we can compute the shortest noncontractible cycle in Σ in $O(n^3)$ time.

In fact, Dehn's algorithm is overkill for testing the contractibility of simple cycles. Instead we can rely on the classical lemma:

Lemma [David Epstein²]: A nontrivial simple cycle σ on any surface S is contractible if and only if

²David Epstein-with-one-p is a curly-haired English mathematician who was born in South Africa. David Eppstein-with-two-p's is a curly-haired American mathematician (and computer scientist) who was born in England. It's a

if $\mathcal{S} \setminus \sigma$ is disconnected and at least one component is an open disk.

We can test whether a simple cycle σ is the boundary of a disk as follows. First, we perform a whatever-first search in the dual map Σ^* to determine whether the sliced map $\Sigma \setminus \sigma$ (or alternatively, the contracted map Σ/σ) is connected. If $\Sigma \setminus \sigma$ is connected, then σ is noncontractible. Otherwise, we compute the Euler characteristics and orientability of both components in $O(n)$ time. If either component is orientable with genus 1, that component is a disk and σ is contractible; otherwise, σ is non-contractible.

We can find the shortest *nonseparating* cycle in the same time bound, using a slightly *simpler* algorithm. A given simple cycle σ is non-separating if and only if $\Sigma \setminus \sigma$ is connected; we can test this condition in $O(n)$ time using whatever-first search in the dual map Σ^* . Otherwise, the algorithm is the same.

Theorem [Thomassen]: *Given any edge-weighted surface map Σ with complexity n , we can compute the shortest nonseparating cycle in Σ in $O(n^3)$ time.*

30.3 Near-quadratic time

- Build a tree-cotree decomposition (T, L, C) where T is a shortest-path tree, in $O(n \log n)$ time, using Dijkstra's algorithm.
- Let X^* be the *dual cut graph* $(C \cup L)^*$. A fundamental loop $\text{loop}(x, yz)$ is separating if and only if $(yz)^*$ is a bridge of X^* , and contractible if and only if at least one component of $X^* \setminus (yz)^*$ is a tree.
- We can classify every edge of X^* as hair, bridge, or neither in $O(n)$ time. So we can find shortest noncontractible and nonseparating loops based at x in $O(n \log n)$ time.
- Try all basepoints $\Rightarrow O(n^2 \log n)$ time.

The high-level approach of this algorithm is due to Sariel Har-Peled and me, but we used a much more complicated algorithm to find shortest interesting loops, which interleaves Dijkstra steps and brute-force traversal of the dual map. Replacing Dijkstra's algorithm with a linear-time shortest-path algorithm reduces the overall running time to $O(n^2)$.

This is the fastest algorithm known for arbitrary genus. However, Martin Kutz proved that for any *constant* genus g , it is possible to computer shortest nontrivial cycles in only $O(n \log n)$ time, by a reduction to the planar minimum-cut problem (or more properly, to the dual problem of finding the shortest generating cycle in an annulus). The running time of Kutz's algorithm depends exponentially on the genus. Later work by Sergio Cabello and Erin Chambers reduced the dependence on g to a small polynomial.

30.4 Multiple-Source Shortest Paths

We can significantly improve Thomassen's algorithm using a generalization of either of the multiple-source shortest path algorithms that we saw earlier for planar maps.

[The rest of this section is only an outline.]

minor miracle that they have never been coauthors.

Parametric

Grove decomposition of the dual cut graph $T \cup L$ into $O(g)$ trees, each with a central cut path. Each pivot requires $O(g)$ dynamic-forest operations, and thus takes $O(g \log n)$ amortised time. Each dart pivots into the shortest path tree T at most $O(g)$ times. Total time is $O(g^2 n \log n)$, assuming generic edge weights. This can be improved to $O(gn \log n)$ time with more careful data structures and analysis.

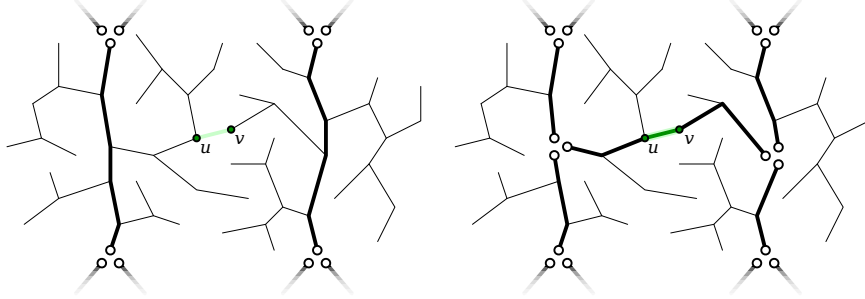


Figure 30.1: Pivoting one edge into a grove decomposition.

Surface-Tree Lemma: Let T be any tree embedded on a surface with exactly one boundary cycle B ; call any vertex in $T \cap B$ a boundary vertex. Let e be any edge of T , and let U and W be the components of $T \setminus e$. Either U contains every boundary vertex, or boundary vertices in U induce at most $g + 1$ paths in B .

Proof(?): Let Σ be the surface map induced by $T \cup B$, and let o be the face of Σ bounded by B . Let (T, L, C) be any tree-cotree decomposition of Σ with the given spanning tree T .

Consider the subgraph $X^* = C^* \cup L^* \cup \{e^*\}$ of the dual map Σ^* . The induced embedding of X^* has exactly two faces, each containing (the faces of Σ^* dual to vertices of) one component of $T \setminus e$. Let Y^* be the boundary subgraph comprised of the non-isthmus edges of X^* . This boundary subgraph can be decomposed into at most $g + 1$ simple non-crossing cycles. (Recall the the *definition* of the genus G is the maximum number of disjoint cycles whose deletion does not disconnect the surface.) Each of these cycles crosses B at most twice. Thus, either X^* does not cross B at all, or X^* splits B into at most $2g + 2$ intervals, which alternate between vertices of U and vertices of W . \square

Recursive

Precompute homology annotations (via a system of cocycles) once at the start. Compute shortest-path trees T_i and T_j in $O(n \log n)$ time. Compute homology signatures of all shortest paths from s_i and s_k in $O(gn)$ time. Dart $u \rightarrow v$ is properly shared by T_i and T_k if it satisfies the following conditions:

- $\text{pred}_i(v) = \text{pred}_k(v) = u$
- $[\text{path}_i(u)] = [\text{path}_k(u)]$ — **This condition is new!**
- If $t = \text{pred}_i(u) = \text{pred}_k(u)$, then $t \rightarrow u$ is properly shared by T_i and T_k .
- Otherwise, darts $\text{pred}_i(u) \rightarrow u$ and $v \rightarrow u$ and $\text{pred}_k(u) \rightarrow u$ are oriented clockwise around u .

The second condition holds if and only if these two shortest paths define a separating arc from s_i through u to s_k .

Finding and contracting all properly shared darts takes $O(gn)$ time. Each vertex has $O(g \deg(v))$ interesting sources, so the total size of all maps at each level of recursion is $O(gn)$. The total preprocessing time is $O(gn \log n + g^2n)$; the query time is still $O(\log n)$. It's unclear whether $O(gn \log n)$ time can be achieved with this approach.

30.5 Shortest Nonseparating Cycles in Near-Linear Time

Lemma [Cabello Mohar]: *The shortest nonseparating cycle in any surface map Σ crosses at least one cycle in a greedy system of cycles for Σ exactly once.*

Proof: [[[to be written. The usual exchange argument implies 3 crossings is impossible, and every nonseparating cycle crosses some basis cycle an odd number of times]]]

Lemma: *For any cycle γ , the shortest cycle that crosses γ exactly once can be computed in $O(\bar{g}^2n \log n)$ time.*

Proof: Let $\Sigma' = \Sigma \setminus\!\!/\gamma$. If γ is two-sided, then Σ' has two boundary cycles γ^- and γ^+ , each of which is a copy of γ . If γ is one-sided, then Σ' has a single boundary cycle γ^\pm that covers γ twice. In either case, Σ' contains two copies v^- and v^+ of every vertex v of γ .

Now let σ be the shortest cycle in Σ that crosses γ once. This cycle appears in Σ' as a shortest path from v^- to v^+ for some vertex v of Σ . We can compute all such shortest paths in $O(\bar{g}^2n \log n)$ time using either MSSP algorithm, using either γ^+ or γ^\pm as the “outer” face.

□

Theorem: *The shortest nonseparating cycle in a surface map with Euler genus \bar{g} and complexity n can be computed in $O(\bar{g}^3n \log n)$ time.*

Proof: Let (T, L, C) be a tree-cotree decomposition of Σ where T is a shortest-path tree. Let Q be the reduced cur graph obtained by removing degree-1 vertices from $T \cup L$, and let $\mathcal{C} = \{\gamma_1, \gamma_2, \dots, \gamma_{\bar{g}}\}$ be the system of cycles induced by T and L .

For each cycle γ_i , we compute the shortest cycle in Σ that crosses γ_i exactly once, in $O(\bar{g}n \log n)$ time, by running a multiple-source shortest-path algorithm in $\Sigma \setminus\!\!/\gamma_i$. The shortest of these \bar{g} cycles is the shortest nonseparating cycle. □

30.6 Shortest Noncontractible Cycles in Near-Linear Time (sketch)

This one is a bit more complicated.

Lemma: *Every noncontractible cycle in any surface map Σ crosses any cut graph of Σ at least once.*

The following lemma distills a more complex argument of Cabello, Chambers, and Erickson. [[[Take this with a grain of salt until I wrote down a complete proof.]]]

Lemma: *Let σ be the shortest noncontractible cycle in some surface map Σ . Let (T, L, C) be a tree-cotree decomposition of Σ where T is a shortest path tree and C is a maximum spanning tree. Let \mathcal{C} denote the corresponding system of cycles.*

- (a) σ crosses each cycle in \mathcal{C} at most once.
- (b) σ is a nonseparating cycle if and only if σ crosses some cycle in \mathcal{C} at least once.
- (c) If σ is a separating cycle, then σ is also the shortest non-contractible cycle in $\Sigma' = \Sigma \setminus\!\!/\mathcal{C}$.

Proof: [[[To be written. Notice that (a) is a stronger claim than the nonseparating crossing lemma!]]]

Lemma: Let σ be the shortest noncontractible cycle in some surface map Σ' with genus 0 and at least two boundaries. Let π be the shortest path between any two boundaries of Σ' . Either (a) σ crosses π exactly once, or (b) σ does not cross π and σ is the shortest noncontractible cycle in $\Sigma' \setminus \pi$.

Proof: [[[Mostly follows from the Crossing Condition.]]]

Theorem: The shortest noncontractible cycle in a surface map with Euler genus \bar{g} and complexity n can be computed in $O(\bar{g}^3 n \log n)$.

Proof: Let (T, L, C) be a tree-cotree decomposition of Σ where T is a shortest-path tree and C is a maximum spanning tree. Let $\mathcal{C} = \{\gamma_1, \gamma_2, \dots, \gamma_{\bar{g}}\}$ be the system of cycles induced by T and L .

First, for each cycle γ_i , we compute the shortest cycle in Σ that crosses γ_i exactly once, in $O(\bar{g}^2 n \log n)$ time, by running a multiple-source shortest-path algorithm in $\Sigma \setminus \gamma_i$. The shortest of these \bar{g} cycles is the shortest nonseparating cycle. Thus, if the shortest noncontractible cycle is nonseparating, then the shortest of these \bar{g} cycles is the shortest noncontractible cycle. Otherwise, we need to compute the shortest noncontractible cycle in the sliced surface $\Sigma' = \Sigma \setminus \mathcal{C}$.

The surface Σ' has genus 0 and b boundary cycles, for some $1 \leq b \leq \bar{g}$. If $b = 1$, then Σ' is a disk, so every cycle in Σ' is contractible. Otherwise, we compute a shortest path π between any two boundary cycles, compute the shortest cycle σ^\times in Σ' that crosses π exactly once via multiple-source shortest paths, and recursively search $\Sigma' \setminus \pi$. The algorithm halts after computing $b - 1$ cycles; the shortest of these is the shortest noncontractible cycle in Σ' .

Altogether the algorithm runs multiple-source shortest paths $\bar{g} + b = O(\bar{g})$ times, each on a surface map with complexity $O(n)$ and genus less than \bar{g} . So the overall running time is $O(\bar{g}^3 n \log n)$, as claimed. \square

30.7 References

1. Sergio Cabello, Erin W. Chambers, and Jeff Erickson. Multiple-source shortest paths in embedded graphs. *SIAM J. Comput.* 42(4):1542–1571, 2013. arXiv:1202.0314.
2. Sergio Cabello and Bojan Mohar. Finding shortest non-separating and non-contractible cycles for topologically embedded graphs. *Discrete Comput. Geom.* 37(2):213–235, 2007.
3. David B. A. Epstein. Curves on 2-manifolds and isotopies. *Acta Math.* 115:83–107, 1966.
4. Jeff Erickson. Shortest non-trivial cycles in directed surface graphs. *Proc. 27th Ann. Symp. Comput. Geom.*, 236–243, 2011.
5. Jeff Erickson, Emily Kyle Fox, and Luvsandondov Lkhamsuren. Holiest minimum-cost paths and flows in surface graphs. *Proc. 50th Ann. ACM Symp. Theory Comput.*, 1319–1332, 2018. arXiv:1804.01045.
6. Jeff Erickson and Sariel Har-Peled. Optimally cutting a surface into a disk. *Discrete Comput. Geom.* 31(1):37–59, 2004. arXiv:cs/0207004.

7. Emily Kyle Fox. Shortest non-trivial cycles in directed and undirected surface graphs. *Proc. 24th Ann. ACM-SIAM Symp. Discrete Algorithms*, 352–364, 2013. arXiv:1111.6990.
8. Martin Kutz. Computing shortest non-trivial cycles on orientable surfaces of bounded genus in almost linear time. *Proc. 22nd Ann. Symp. Comput. Geom.*, 430–438, 2006. arXiv:cs/0512064.
9. Carsten Thomassen. Embeddings of graphs with no short noncontractible cycles. *J. Comb. Theory Ser. B* 48(2):155–177, 1990.

30.8 Aptly Named Sir

- Enforcing shortest-path and optimal-cycle uniqueness
- Tight cycles
- Directed graphs
- Shortest systems of loops, arcs, or cycles
- Shortest homotopic paths, cycles, systems of loops, pants decompositions

Chapter 31

Surfaces with Boundary \emptyset

31.1 Arcs and Slicing

31.2 Forest-Cotree Decompositions

31.3 Cut Graphs and Systems of Arcs

31.4 Tree-Coforest Decompositions and Systems of Coarcs

31.5 References

31.6 Aptly Named Sir

- Pants decompositions (except possibly in passing)

Chapter 32

Minimum Cuts in Surface Graphs \emptyset

Only describe the homology-cover algorithm. Mention the crossing sequence algorithm in passing, if at all. (But remember that the homology cover algorithm still needs some simple crossing arguments to enable MSSP!)

32.1 Duality with Even Subgraphs

32.2 \mathbb{Z}_2 -Homology Cover

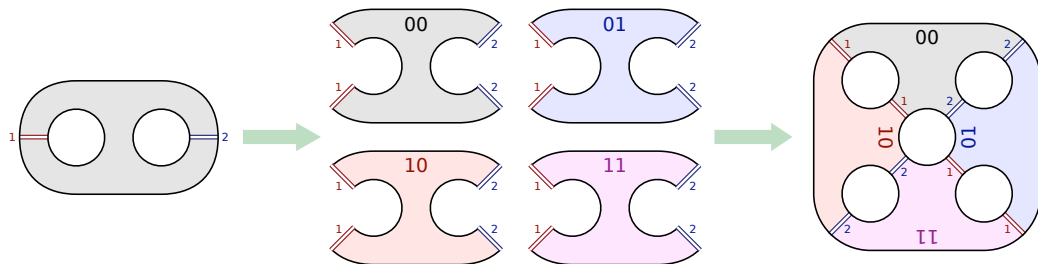


Figure 32.1: Building the homology cover of a pair of pants

32.3 \mathbb{Z}_2 -Minimal Cycles

Build the homology cover. Also lift greedy primal system of arcs.

32.4 \mathbb{Z}_2 -Minimal Even Subgraphs

Dynamic programming!

32.5 NP-hardness (??)

32.6 References

1. Chambers Erickson Fox Nayyeri

2. Kutz

32.7 Aptly Named Sir

- Crossing-bound/homotopy algorithm
- Global mincut

Chapter 33

Maximum Flows in Surface Graphs \emptyset

33.1 Real Homology

33.2 Homologous Feasible Flows

33.3 Shortest Paths with Negative Edges

$O(n \log^2 n / \log \log n)$ time (Real RAM)

- ***[[[Move to planarization chapter?]]]]\$\$\$

33.4 Ellipsoid Method (Sketch)

33.5 Summary

To simplify notation, assume $C = n^{O(1)}$ and (because off-the-shelf algorithms are faster otherwise) $g = o(n^{1/4})$.

- # iterations $N = O(d \log \Delta)$
- Dimension $d = O(g)$
- Aspect ratio $\Delta = C^{O(g)}$
- So $N = O(g^2 \log C)$
- Oracle time $T_s = O(n \log^2 n)$
- Iteration time $O(T_s + d^2)$ arithmetic operations
- k th iteration requires $O(k)$ bits of precision
- So k th iteration takes $O(T_s A(k) + d^2 M(k))$ time
- Total time is $O(N A(N) T_s + d^2 N M(N))$

- Real RAM *without* square roots: $A(N) = O(1)$ and $M(N) = O(\log \log N)$ (for square roots)

$$\begin{aligned}
O(NA(N)T_s + d^2N M(N)) &= O(N T_s + d^2 N \log \log N) \\
&= O(g^2 \log C) \cdot O(n \log^2 n) + O(g^2) \cdot O(g^2 \log C \log \log(g \log C)) \\
&= O(g^2 n \log^2 n \log^2 C) + O(g^4 \log C \log \log(g \log C)) \\
&= O(g^2 n \log^4 n)
\end{aligned}$$

- Bit RAM, grade school arithmetic: $A(N) = O(N)$ and $M(N) = O(N^2)$

$$\begin{aligned}
O(NA(N)T_s + d^2N M(N)) &= O(N^2 T_s + N^3 d^2) \\
&= O(g^4 \log^2 C) \cdot O(n \log^2 n) + O(g^6 \log^3 C) \cdot O(g^2) \\
&= O(g^4 n \log^2 n \log^2 C) + O(g^8 \log^3 C) \\
&= O(g^4 n \log^4 n) + O(g^8 \log^3 n)
\end{aligned}$$

First term dominates because $g = O((n \log n)^{1/4})$.

- Fast bit RAM: $A(N) = O(N)$ and $M(N) = O(N \log N)$

$$\begin{aligned}
O(NA(N)T_s + d^2N M(N)) &= O(N^2 T_s + d^2 N^2 \log N) \\
&= O(g^4 \log^2 C) \cdot O(n \log^2 n) \\
&\quad + O(g^2) \cdot O(g^4 \log^2 C \log(g \log C)) \\
&= O(g^4 n \log^2 n \log^2 C) + O(g^6 \log^2 C \log(g \log C)) \\
&= O(g^4 n \log^4 n)
\end{aligned}$$

First term dominates because $g = o(\sqrt{n \log n})$.

- Fast word RAM: $A(N) = M(N) = O(N)$ — Need to verify square root time

$$\begin{aligned}
O(NA(N)T_s + d^2N M(N)) &= O(N^2 T_s + d^2 N^2) \\
&= O(g^4 \log^2 C) \cdot O(n \log^2 n) + O(g^2) \cdot O(g^4 \log^2 C) \\
&= O(g^4 n \log^2 n \log^2 C) + O(g^6 \log^2 C) \\
&= O(g^4 n \log^4 n)
\end{aligned}$$

... because $g = o(\sqrt{n})$

Theorem: Let Σ be a surface map with n vertices, genus $g = o(\sqrt{n \log n})$, positive integer edge capacities less than $n^{O(1)}$, and two vertices s and t . We can compute the maximum (s, t) -flow in Σ in $O(g^4 n \log^4 n)$ time.

33.6 References

1. Alt JACM 1988
2. Brent JACM 1976
3. Chambers Erickson Nayyeri
4. fast integer multiplication
5. Fürer arXiv:1402.1811

33.7 Aptly Named Sir

- Directed graphs
- Non-orientable surfaces(?)
- Multi-dimensional parametric search
- Min-cost homologous circulations
- Spectral min-cost-flow algorithms, scaling

Chapter 34

Geodesic Embeddings \varnothing

This is by far the least developed chapter, even in my head.

34.1 Flat Torus

34.1.1 Spring Embeddings

34.2 Spring Embeddings on Other Surfaces

Colin de Verdière, Hass: simplicial complexes, negative curvature

Ideally: essentially (strongly) 3-connected, homotopic to embedding \implies strictly convex embedding.

34.3 Circle Packing on Other Surfaces

Algorithms: Colin de Verdière, Mohar (Rivin, Bobenko/Springborn, Stephenson?)

34.4 References

34.5 Named Sir Not

Chapter 35

Closing the Loop \varnothing

We covered several topics related to *planar* curves and maps early in the course, which we did not revisit in the context of more complex surfaces. For some topics, I decided not to cover the surface generalization because the results are considerably more technical. For others, I didn't cover the surface generalization because little or nothing is known. In this final chapter, I'll walk through each of the early planar topics and describe the state of the art for the surface generalization.

35.1 Simple Polygons

As we've already seen, the Jordan curve theorem does not generalize to surfaces with positive genus. Indeed, the *definition* of the genus of a surface S is the maximum number of disjoint simple closed curves in S whose complement is connected. Nevertheless, some of our most basic results on simple polygons do generalize to “polygons” on more complex surfaces.

To properly generalize *polygons* in the plane to more complex surfaces, we need an appropriate generalization of *line segments*, which in turn relies on appropriate generalizations of *lengths* and *angles*.

Theorem: *Any geodesic embedding of a graph on any surface with constant non-negative Gaussian curvature can be extended to a geodesic triangulation without adding vertices.*

The restriction to non-positive curvature is necessary; this theorem does *not* extend to geodesic graphs or even geodesic *polygons* on the sphere! The least restricted analogue of this theorem is due to Brehm and Kühnel. Let P be a spherical geodesic polygon whose edges all have length less than π , no three of whose three vertices lie on a common great circle. Treating P as a spherical map, let S be any face that does not contain a great circle; there must be at least one such face. Using a natural spherical extension of ear-cutting, Brehm and Kühnel prove that S can be triangulated without additional vertices, again using only geodesics of length less than π . Halperin observed that both sides of P can be triangulated with short geodesics using at most one additional vertex, most likely using a generalization of trapezoidal decompositions. Brehm and Kühnel's theorem does not extend to spherical polygons with edges of length greater than π ; O'Rourke describes several counterexamples.

35.2 Winding Numbers

These are only well-defined for null-homologous curves; these are sometimes called *lacets*. For non-orientable surfaces, winding numbers are only defined modulo 2; for orientable surfaces, they can be defined either as integers or a residues with respect to any integer modulus.

35.3 Curve Homotopy

Homotopy moves; Dehn's algorithm

35.4 Shortest Homotopic Paths and Cycles

Algorithms for traversal/crossing curves with respect to any edge-weighted surface map. Given a walk W with hop-length k in a surface map with complexity n and genus g , we can find the minimum-length walk homotopic to W (with fixed endpoints) in $O(gnk)$ time. If W is a closed walk, we can find the shortest closed walk homotopic to W in $O(gnk \log nk)$ time.

Shortest homotopic systems of loops, pants decompositions, graph embeddings

35.5 Gauss codes

Unsigned Gauss codes are well-defined for any (multi)curve on any surface; signed Gauss codes require the underlying surface to be orientable.

A signed Gauss code of length n can be interpreted as a rotation system for a 4-regular graph with n vertices, and thus represents a unique curve (up to homeomorphism) on a unique orientable surface.

In principle, given an unsigned Gauss code x and a surface S (specified by orientability and genus), we can determine whether x is consistent with a curve on S in time $g^{O(g)}n$ as follows.

1. Construct the Nagy graph $G(X)$.
2. Compute any Euler tour of $G(X)$.
3. Construct the Dehn *diagram* $D(X)$ of this Euler tour (not just the Dehn *code*).
4. Finally, check whether the Dehn diagram $D(X)$ can be embedded on S . This, of course, is the hard part.

35.6 Curve Invariants and Simplification

35.7 Geodesic Embeddings

Inductive

Tutte

Koebe

Schnyder

35.8 Maxwell–Cremona

Non-planar Frameworks in the Plane

Let Σ be an orientable surface map—that is, a graph G together with a rotation system succ —with positive genus. (The underlying graph G might be planar!) Any position function $p: V(\Sigma) \rightarrow \mathbb{R}^2$ induces a straight-line drawing of G in the plane. I will call the pair (G, p) a *framework* and (for lack of better standard terminology) the pair (Σ, p) an *ordered framework*. The *displacement* of any dart $u \rightarrow v$ in G with respect to p is the vector $\Delta(u \rightarrow v) = p(v) - p(u)$. The dual graph G^* is the underlying graph of the dual surface map Σ^* .

The definitions of non-zero, strict, and equilibrium stresses and closed and exact 1-forms all generalize directly from the setting where Σ is a planar map.

However, closed discrete 1-forms on positive-genus maps are not necessarily exact. Consider, for example, the 1-form defined on a toroidal grid, where all “upward” darts have value 1, and all “horizontal” darts have value 0; this discrete 1-form is closed but not exact.

The difference between closed and exact 1-forms is captured by *cohomology* on the surface map Σ . Closed 1-forms are duals of circulations; exact 1-forms are duals of boundary circulations; thus, two closed 1-forms are cohomologous if and only if their difference is an exact 1-form.

Not every equilibrium stress on a framework induces a reciprocal framework. First, the definition of “reciprocal” requires a rotation system to define the dual graph G^* ; only *ordered* frameworks have reciprocals. But even with a fixed rotation system, the dual displacement function $\Delta^*(d^*) := \omega(d) \cdot \Delta(d)^\perp$ is not necessarily an exact 1-form on the dual graph G^* (although it is always closed). I will call a stress ω *reciprocal* for an ordered framework (Σ, p) if the dual displacement function Δ^* is a closed 1-form on G^* .

Theorem: *An equilibrium stress ω for an ordered framework (Σ, p) induces a reciprocal framework (Σ^*, p^*) if and only if ω is a reciprocal stress for (Σ, p) . Conversely, any reciprocal framework (Σ^*, p^*) defines a unique reciprocal stress ω for (Σ, p) .*

Let me emphasize this theorem describes restrictions on both the stress ω and the rotation system defining Σ . The same stress ω can be reciprocal for some rotation systems but not others.

Polyhedral Lifts of Non-planar Frameworks

The theory of polyhedral lifts was recently extended to non-planar frameworks by Cooperband, Ghrist, and Hansen (using the language of sheaves and cosheaves) and by Karpenkov, Servatius, and Servatius. Specifically, Cooperband, Ghrist, and Hansen prove that an ordered framework

with n vertices, m edges, and genus g admits a reciprocal stress if and only if $m - 2n + 3 > 4g$, and admits a polyhedral lift into \mathbb{R}^3 if and only if $m - 2n + 3 > 6g$. (Here $m - 2n + 3$ is the dimension of the vector space of equilibrium stresses.) Karpenkov, Servatius, and Servatius extend these results, using more combinatorial language, to frameworks defined by projecting *nonorientable* surface maps into the plane.

Toroidal Frameworks

35.9 References

1. Ulrich Brehm and Wolfgang Kühnel. Smooth approximation of polyhedral surfaces regarding curvatures. *Geom. Dedicata* 12:435–461, 1982.
2. Zoe Cooperband, Robert Ghrist, Jakob Hansen. A cosheaf theory of reciprocal figures: Planar and higher genus graphic statics. Preprint, November 2003. arXiv:2311.12946.
3. Oleg Karpenkov, Brigitte Servatius, and Herman Servatius. Liftings of surfaces in the plane. Preprint, May 2025. arXiv:2505.18841.
4. Joseph O'Rourke. Computational geometry column 51. *SIGACT News* 39(3):58–62, 2008.